

METHOD DEVELOPMENT FOR DETERMINATION OF β -AGONISTS USING COLORIMETRIC
AND ELECTROCHEMICAL SENSORS



A Dissertation Submitted in Partial Fulfillment of the Requirements
for the Degree of Doctor of Philosophy in Chemistry

Department of Chemistry

FACULTY OF SCIENCE

Chulalongkorn University

Academic Year 2019

Copyright of Chulalongkorn University

การพัฒนาวิธีการตรวจวัดสารกลุ่มบีตาแอกโทนิสต์โดยใช้ตัวรับรู้เชิงสีและเชิงเคมีไฟฟ้า



วิทยานิพนธ์นี้เป็นส่วนหนึ่งของการศึกษาตามหลักสูตรปริญญาวิทยาศาสตรดุษฎีบัณฑิต

สาขาวิชาเคมี ภาควิชาเคมี

คณะวิทยาศาสตร์ จุฬาลงกรณ์มหาวิทยาลัย

ปีการศึกษา 2562

ลิขสิทธิ์ของจุฬาลงกรณ์มหาวิทยาลัย

อัจฉรา ลอแม : การพัฒนาวิธีการตรวจวัดสารกลุ่มบีตาแอกอนิสต์โดยใช้ตัวรับรู้เชิงสีและเชิงเคมีไฟฟ้า. (METHOD DEVELOPMENT FOR DETERMINATION OF β -AGONISTS USING COLORIMETRIC AND ELECTROCHEMICAL SENSORS) อ.ที่ปรึกษาหลัก : อ. ดร.เจนจิรา ปานชมพู, อ.ที่ปรึกษาร่วม : ศ. ดร.อรรพรรณ ชัยลาภกุล,รศ. ดร.วิณา เสียงเพชร

วิทยานิพนธ์ฉบับนี้มุ่งเน้นการพัฒนาเซ็นเซอร์ในการตรวจวิเคราะห์ปริมาณของสารสำคัญ ได้แก่ สารกลุ่มบีตาแอกอนิสต์ และสารสื่อประสาท ซึ่งเป็นสารบ่งชี้ที่สำคัญในการควบคุมการปนเปื้อนของอาหาร การใช้สารต้องห้ามในนักกีฬา รวมถึงการวินิจฉัยโรคทางการแพทย์ ในปัจจุบันนี้วิธีการตรวจวัดเชิงสีและการตรวจวัดเชิงเคมีไฟฟ้าถือเป็นสองวิธีการตรวจวัดที่สำคัญและถูกใช้อย่างแพร่หลายในการพัฒนาเซ็นเซอร์ตรวจวัด เนื่องจากการใช้งานและการอ่านผลที่ง่าย การตรวจวัดที่รวดเร็ว สามารถนำไปบูรณาการร่วมกับเทคนิคอื่น ๆ ได้ และสามารถสร้างให้เครื่องตรวจวัดมีขนาดเล็กเพื่อนำไปใช้งานในภาคสนามได้ จากคุณสมบัติที่น่าสนใจของรูปแบบการตรวจวัดทั้งสองวิธีนี้ ทำให้นักศึกษาในวิทยานิพนธ์นี้แบ่งออกเป็นสองส่วนประกอบหลัก คือ (1) การพัฒนาเซ็นเซอร์ตรวจวิเคราะห์แบบบูรณาการโดยใช้เทคนิคการตรวจวัดเชิงสี และ (2) การพัฒนาเซ็นเซอร์ตรวจวิเคราะห์แบบบูรณาการโดยใช้เทคนิคการตรวจวัดเชิงเคมีไฟฟ้า โดยการศึกษาในส่วนแรก มุ่งเน้นการพัฒนาเซ็นเซอร์ตรวจวัดฐานแผ่นใสร่วมกับเทคนิคการตรวจวัดเชิงสีสำหรับการตรวจวัดสารซัลบูทามอล โดยอาศัยการเปลี่ยนแปลงสีจากปฏิกิริยารีดอกซ์ ร่วมกับการใช้กล้องถ่ายภาพในการติดตามการเปลี่ยนแปลงสีที่เกิดขึ้นจากปฏิกิริยาออกซิเดชันของซัลบูทามอลด้วยโพแทสเซียมเปอร์แมงกาเนตซึ่งเป็นตัวออกซิไดซ์ที่ดี สำหรับวิทยานิพนธ์ในส่วนที่สอง กล่าวถึงการพัฒนาเซ็นเซอร์ทางเคมีไฟฟ้าอย่างจำเพาะ โดยจำแนกออกเป็น 3 งานวิจัยย่อย ดังนี้ ในส่วนงานวิจัยย่อยที่ 1 มุ่งเน้นการพัฒนาขั้วไฟฟ้าโดมอนด์เจือโบรอนที่ผ่านการดัดแปรขั้วไฟฟ้าด้วยอนุภาคพลาสมาเพียงขนาดนาโนเมตรร่วมกับโครมาโทกราฟีของเหลวสมรรถนะสูงเพื่อใช้ในการตรวจวัดสารประกอบบีตาแอกอนิสต์ทั้งสี่ชนิดในเวลาเดียวกัน ผลการวิจัยพบว่าระบบการตรวจวัดที่พัฒนาขึ้นมีประสิทธิภาพในการตรวจวิเคราะห์สารได้อย่างรวดเร็ว รวมทั้งเพิ่มประสิทธิภาพในการลดการเกาะติดผิวของกลุ่มสารตัวอย่างที่ผิวหน้าขั้วได้อย่างโดดเด่น งานวิจัยย่อยที่ 2 มุ่งเน้นพัฒนาความสามารถในการตรวจวัดอย่างจำเพาะสำหรับสารบีตาแอกอนิสต์ด้วยพอลิเมอร์ที่มีรอยประทับโมเลกุลร่วมกับขั้วไฟฟ้ากราฟีนที่ผสมคาร์บอนที่ผ่านการดัดแปรผิวหน้าขั้วไฟฟ้าด้วยพอลิเมอร์นำไฟฟ้าอย่าง พอลิอะนิลีน ผลการวิจัยพบว่าเซ็นเซอร์ตรวจวิเคราะห์ที่พัฒนาขึ้นมีความจำเพาะสูงต่อการตรวจวัดสารที่สนใจ สำหรับงานวิจัยย่อยที่ 3 มุ่งเน้นการพัฒนาขั้วไฟฟ้ากราฟีนที่ผสมคาร์บอนที่มีคุณสมบัติโดดเด่นในการเป็นตัวเร่งปฏิกิริยาทางเคมีไฟฟ้าแบบเสริมกันของอนุภาคนาโนของสารประกอบโลหะสามชนิดได้แก่ ทองแดง นิกเกิล และทอง สำหรับใช้ในการตรวจวัดสารสื่อประสาท ได้แก่ เซโรโทนินและนอร์อิพิเนฟรินที่มีศักยภาพไฟฟ้าในการเกิดปฏิกิริยาออกซิเดชันที่ซ้อนทับกัน ผลการวิจัยพบว่าเซ็นเซอร์ตรวจวัดที่พัฒนาขึ้นสามารถนำไปประยุกต์ใช้ในการวิเคราะห์สารสื่อประสาทที่สนใจทั้งสองชนิดในเวลาเดียวกัน อีกทั้งยังสามารถเพิ่มประสิทธิภาพของการวิเคราะห์ทางด้านความไวและความจำเพาะในการตรวจวัด โดยสรุปแล้วเซ็นเซอร์ตรวจวัดเชิงสีและเชิงเคมีไฟฟ้าที่พัฒนาขึ้นในงานวิจัยนี้ ให้ความไวและความจำเพาะในการวิเคราะห์สูงขึ้น ราคาข้อมเยาเข้าถึงได้ง่าย ใช้งานง่าย และสามารถวิเคราะห์สารได้อย่างรวดเร็ว นอกจากนี้ยังสามารถนำเซ็นเซอร์ดังกล่าวนี้มาพัฒนาต่อยอดให้มีประสิทธิภาพเพิ่มมากขึ้นเพื่อนำไปใช้ในการตรวจวิเคราะห์นอกสถานที่ได้อย่างง่าย

สาขาวิชา เคมี
ปีการศึกษา 2562

ลายมือชื่อนิสิต
ลายมือชื่อ อ.ที่ปรึกษาหลัก
ลายมือชื่อ อ.ที่ปรึกษาร่วม
ลายมือชื่อ อ.ที่ปรึกษาร่วม

5772216123 : MAJOR CHEMISTRY

KEYWORD: Colorimetric sensor Transparency-based device Boron-doped diamond (BDD) Pd nanoparticles (PdNPs) Electrochemical sensor Ultra-high performance liquid chromatography (UHPLC) Ternary CuNiAu alloy Trimetallic catalyst Electrocatalytic activity Synergistic effect Molecularly imprinted polymer (MIP) Polyaniline (PANI) β -agonists Salbutamol (SAL) Neurotransmitter Serotonin (5-hydroxytryptamine or 5-HT) Norepinephrine (NE)

Atchara Lomae : METHOD DEVELOPMENT FOR DETERMINATION OF β -AGONISTS USING COLORIMETRIC AND ELECTROCHEMICAL SENSORS. Advisor: Dr. JANJIRA PANCHOMPOO Co-advisor: Prof. Dr. ORAWON CHAILAPAKUL, Assoc. Prof. Dr. Weena Siangproh

This dissertation focused on the development of analytical sensors for quantitative analysis of various electroactive compounds such as β -agonists and neurotransmitters, which could be considered as important indicators for food-safety monitoring, drug doping control in sports, clinical testing, and health care inspection. Up to date, colorimetry and electrochemistry are the two attractive approaches that have extensively been employed as analytical sensing tools, due to their simple operation and interpretation, fast analysis time, good ability of coupling with other techniques, and high capability of miniaturization. With these two detection platforms, this dissertation would then be divided into two main parts: (1) The development of integrated platforms for the colorimetric sensor and its application; and (2) The development of integrated platforms for the electrochemical sensor and its application. In the first section, the transparency-based colorimetric sensor for salbutamol determination relying on the redox reaction was developed. Digital camera was used as the optical readout, and the noticeable color change, induced through the oxidation of salbutamol by strongly oxidizing permanganate (KMnO_4), could then be monitored. In the second part, the selective electrochemical sensors were developed and classified into three sub-sections. For the first sub-section, the anti-fouling PdNPs-modified BDD electrode was combined with UHPLC separation system for the simultaneous determination of four β -agonists. The remarkable improvement in analytical efficiency regarding fast analysis and fouling resistance capability was attained. In the second sub-section, the molecularly imprinted polymer (MIP) with selective recognition of salbutamol was electrochemically synthesized and immobilized onto the polyaniline (PANI)-modified screen-printed graphene electrode. A great enhancement in selectivity of the proposed sensing system towards the oxidation of the target analyte (Salbutamol ; SAL), could be obtained. Lastly, in the third sub-section, the synergistically electrocatalytic activity and the selectivity improvement of the trimetallic CuNiAu alloy towards the oxidation of monoamine neurotransmitters were first examined. The corresponding trimetallic CuNiAu composite was modified onto the screen-printed graphene electrode, and the developed electrochemical sensor was subsequently used for the simultaneous determination of serotonin (5-HT) and norepinephrine (NE). The enhanced analytical performance regarding the sensitivity and selectivity of this sensor could be achieved. Conclusively, the developed colorimetric and electrochemical sensors thoroughly studied in this dissertation could offer good sensitivity, high selectivity, affordability, simplification, and high-throughput analysis with great potential to be further developed for on-site applications.

Field of Study: Chemistry

Academic Year: 2019

Student's Signature

Advisor's Signature

Co-advisor's Signature

Co-advisor's Signature

ACKNOWLEDGEMENTS

First and foremost, it is a genuine pleasure to express my deepest appreciation of gratitude to my advisor, Dr. Janjira Panchompoo who provided advice and support throughout my Ph.D. research. She continually and convincingly conveyed a spirit of adventure regarding research and excitement, especially her timely guidance and meticulous scrutiny. Without her suggestion and persistent assistance, this dissertation would not have been accomplished. It has been an honor to be her Ph.D. student.

I would also like to show my gratitude to my co-advisors, Professor Dr. Orawon Chailapakul, and Associate Professor Dr. Weena Siangproh, for their insightful guidance and support throughout this research. Without their encouragement, this research would not have come this far.

My deepest acknowledgment goes to Associate Professor Takeshi Kondo from Tokyo University of Science, Japan, and Professor Peter Lieberzeit from the University of Vienna, Austria, for giving me the great internship opportunities in their research groups, leading me to confront in diverse challenge projects. I appreciate all insightful guidance and support over these past 3 weeks in Japan and 7 months in Austria.

Additionally, I would also like to extend my sincerely grateful to my thesis committees: Associate Professor Dr. Vudhichai Parasuk, Associate Professor Dr. Nattaya Ngamrojanavanich, Associate Professor Dr. Suchada Chuanuwatanakul and Assistant Professor Dr. Amara Apilux, for sacrificial time, meaningfully academic comments and suggestion.

I truly acknowledge the Science Achievement Scholarship of Thailand (SAST) that made my project possible by support and funding throughout my Ph.D. research.

Also, I would like to thank all wholehearted support from members of Electrochemistry and Optical Spectroscopy Center of Excellence (EOSCE). They had always encouraged me during the good and difficult times leading me to endure frequent disappointment.

Lastly, I would like to pay high regard to my family for their unconditional love, sincere encouragement, and endless patience. Having them beside me in my life can drive and motivate me to get myself moving forward. I realized that anything in this work would not have been achieved without them.

Atchara Lomae

TABLE OF CONTENTS

	Page
ABSTRACT (THAI).....	iii
ABSTRACT (ENGLISH).....	iv
ACKNOWLEDGEMENTS.....	v
TABLE OF CONTENTS.....	vi
LIST OF TABLES.....	xiv
LIST OF FIGURES.....	xv
CHAPTER 1.....	1
INTRODUCTION.....	1
1.1 Introduction.....	1
1.2 Research objectives.....	5
1.3 Scope of this research.....	6
CHAPTER 2.....	7
THEORY.....	7
2.1 Sensor fabrication.....	7
2.2 Colorimetric detection.....	9
2.3 Electrochemical detection.....	10
2.3.1 Faradaic and non-faradaic process.....	10
2.3.2 Mass transfer.....	11
2.3.3 Electrochemical techniques.....	12
2.3.3.1 Voltammetry.....	13
2.3.3.1.1 Cyclic Voltammetry.....	14

2.3.3.1.2 Differential-pulse voltammetry.....	16
2.3.3.1.3 Square-wave voltammetry (SWV).....	17
2.3.3.2 Amperometry.....	18
2.3.3.3 Electrochemical Impedance Spectroscopy (EIS)	19
2.3.4 Electrochemical cell / instrumentation	20
2.3.4.1 Working electrode (WE).....	21
2.3.4.1.1 Boron-doped diamond electrode (BDD).....	21
2.3.4.1.2 Screen-printed graphene electrode (SPGE).....	22
2.3.4.1.3 Modified electrodes	23
2.3.4.1.3.1 Noble metal nanoparticle modified electrode	23
2.3.4.1.3.2 Polymer-based modified electrode.....	24
2.3.4.2 Reference electrode (RE)	24
2.3.4.3 Counter electrode (CE).....	25
2.4 Chromatography technique.....	25
2.4.1 Principle of high-performance liquid chromatography (HPLC)	25
2.4.1.1 Capacity Factor.....	26
2.4.1.2 Column selectivity.....	26
2.4.1.3 Column efficiency.....	26
2.4.1.4 Resolution.....	27
2.4.1.5 Band Broadening	27
2.4.2 Instrumentation of HPLC	27
2.4.2.1 Solvent reservoir	28
2.4.2.2 Sample injection system.....	28

2.4.2.3 Pump	28
2.4.2.4 Column.....	28
2.4.2.5 Detector	29
2.4.2.6 Ultra-high-performance liquid chromatography (UHPLC).....	30
CHAPTER 3.....	31
THE DEVELOPMENT OF INTEGRATED PLATFORMS FOR COLORIMETRIC SENSOR AND ITS APPLICATION.....	31
3.1 Development of transparency-based analytical device for facile colorimetric determination of salbutamol.....	32
Abstract.....	33
3.1.1 Introduction	34
3.1.2 Experimental.....	36
3.1.2.1 Chemicals and materials.....	36
3.1.2.2 Design and fabrication of TADs.....	37
3.1.2.3 Colorimetric detection of SAL on the TAD	37
3.1.2.4 Analysis of SAL in pharmaceutical samples	38
3.1.3 Results and discussion	38
3.1.3.1 Colorimetric determination of SAL on the TAD.....	38
3.1.3.2 Optimization of colorimetric detection conditions for SAL analysis	41
3.1.3.2.1 Effects of acid type.....	41
3.1.3.2.2 Effects of sulfuric acid concentration.....	42
3.1.3.2.3 Effects of permanganate concentration	43
3.1.3.2.4 Effects of reaction time and temperature	44

3.1.3.3 Performance study of the proposed colorimetric method on the TAD	45
3.1.3.4 Colorimetric determination of SAL in real samples.....	47
3.1.4 Conclusion	49
CHAPTER 4.....	50
THE DEVELOPMENT OF INTEGRATED PLATFORMS FOR ELECTROCHEMICAL SENSOR AND ITS APPLICATION	50
4.1 Simultaneous determination of β -agonists by UHPLC coupled with electrochemical detection based on palladium nanoparticles modified BDD electrode	51
Abstract	52
4.1.1. Introduction	53
4.1.2 Materials and methods	57
4.1.2.1 Chemicals and reagents	57
4.1.2.2 Fabrication and modification of PdNPs modified BDD electrode..	58
4.1.2.3 UHPLC-ECD and apparatus	58
4.1.2.4. Sample preparation.....	59
4.1.3 Results and discussion	60
4.1.3.1 Influence of electrodeposition parameter.....	60
4.1.3.2 Characterization of PdNPs deposition onto BDD electrode	61
4.1.3.3 Electrochemical responses of β -agonists at PdNPs modified BDD electrode	64
4.1.3.4. UHPLC separation of four β -agonists.....	66
4.1.3.4.1 Effects of the proportion of MeOH.....	66
4.1.3.4.2 Effects of injection volume.....	68

4.1.3.4.3 Effects of buffer pH	70
4.1.3.4.4 Effects of detection potential	70
4.1.3.4.5 Electrode fouling during the analysis of β -agonist compounds at PdNPs modified electrode	72
4.1.3.5 Method Validation	74
4.1.3.6 Analytical applications	76
4.1.4 Conclusion	80
4.2 A ready-to-use electrochemical origami-like sensor based on molecular imprinting for selective detection of SAL	81
Abstract	82
4.2.1 Introduction	83
4.2.2. Experimental	86
4.2.2.1 Materials and equipment	86
4.2.2.2 Preparation of polyaniline modified screen-printed graphene electrode (PANI/SPGE)	87
4.2.2.3 Preparation of imprinted and non-imprinted electrode	87
4.2.2.4 Fabrication of the origami-ePAD	87
4.2.2.5 Measurement of SAL using the origami-like electrochemical paper- based analytical device (origami-ePAD)	90
4.2.2.6 Preparation of real sample	90
4.2.3. Results and discussion	90
4.2.3.1 Characterization of the MIP modified PANI/SPGE	90
4.2.3.2 Optimization of influence parameters for SAL determination using the MIP/PANI/SPGE	94
4.2.3.2.1 Effect of aniline concentration on PANI thickness	94

4.2.3.2.2 Effect of MIP-template formation	95
4.2.3.2.3 Effect of MIP thickness.....	96
4.2.3.3 Optimization of influent parameters for electrochemically SAL detection using sliding PADs based MIP/PAN/SPGE.....	99
4.2.3.3.1 Influence of incubation time for SAL detection using sliding PADs based MIP/PAN/SPGE.....	100
4.2.3.3.2 Influence of $\text{Fe}(\text{CN})_6^{3-/4-}$ concentration for SAL detection using sliding PADs based MIP/PAN/SPGE.	101
4.2.3.4 Analytical figures of merit	102
4.2.3.5 Reproducibility, Selectivity and Stability of the sliding-PADs based electrochemical detection.....	103
4.2.3.6 Determination of SAL in urine sample.....	106
4.2.4 Conclusion	107
4.3 Synergistically catalytic activity of trimetallic CuNiAu alloy modified screen- printed graphene-based electrochemical sensor towards simultaneous determination of norepinephrine and serotonin	108
Abstract.....	109
4.3.1 Introduction	110
4.3.2 Experimental methods.....	112
4.3.2.1 Material and apparatus.....	112
4.3.2.2 Fabrication of the trimetallic CuNiAu modified screen-printed graphene electrode.	113
4.3.2.3 Characterization of CuNiAu modified SPGE surface	114
4.3.2.3.1 Electrochemical characterization.....	114
4.3.2.3.2 Morphological characterization.....	114
4.3.2.3.4 Electrochemical measurement.....	115

4.3.2.3.5 Sample analysis.....	115
4.3.3. Results and discussion	115
4.3.3.1 Characterization of trimetallic CuNiAu/SPGE and bare SPGE	115
4.3.3.2 Electrochemical performance of the modified electrodes	119
4.3.3.3 Electrocatalytic activity toward the oxidation of NE and 5-HT at CuNiAu/SPGE.....	122
4.3.3.4 Optimization of parameters	124
4.3.3.4.1 Effect of electrodeposition parameters.....	125
4.3.3.4.2 The effect of ion precursor ratio	129
4.3.3.4.3. The effect of pH on the separated oxidation peak of NE and 5-HT	131
4.3.3.4.4 The effect of SWV parameter	132
4.3.3.5 Analytical figure of merit.....	134
4.3.3.5.1. Individual determination of NE and 5-HT using CuNiAu/SPGE	134
4.3.3.5.2 Simultaneous determination of NE and 5-HT using CuNiAu/SPGE	135
4.3.3.6 Interference study	138
4.3.3.7 Simultaneous determination of NE and 5-HT in the artificial serum	141
4.3.4 Conclusion	142
CHAPTER 5.....	144
CONCLUSIONS AND FUTURE PERSPECTIVE	144
5.1 Future Perspective.....	145
REFERENCES	146

VITA.....177



จุฬาลงกรณ์มหาวิทยาลัย
CHULALONGKORN UNIVERSITY

LIST OF TABLES

	Page
Table 2.1 The comparison between HPLC and UHPLC ⁹⁷	30
Table 3.1 Colorimetric determination of SAL in real drug samples using permanganate as oxidizing agent at the transparent PET-based sensor.....	47
Table 3.2 Recovery study for SAL determination in the spiked drug samples (n=3)...	48
Table 4.1.1 Regression equations, linearities, the limits of detection (LODs) and the limits of quantification (LOQs) of UHPLC-ECD for the analysis of four β -agonists ^a (n=3).....	75
Table 4.1.2 Previous literature using other electrodes for the UHPLC combined with electrochemical detection of β -agonist compounds.....	75
Table 4.1.3 Repeatability of intra- and inter-day and recoveries of the UHPLC-ECD method (n=3).	78
Table 4.1.4 The recoveries of spiked samples reported using the developed UHPLC-ECD and UHPLC-UV methods.	79
Table 4.2.1 The R_{ct} and K_{et} values of different electrodes.....	93
Table 4.2.2 The comparison the analytical performance for SAL determination using different electrode.	103
Table 4.2.3 Determination of SAL in urine sample. The recovery and RSD were obtained from the mean of three measurements.....	106
Table 4.3.1 Comparison of the linear range and detection sample obtained at the CuNiAu/SPGE for simultaneous determination of NE and 5-HT with others.....	138

LIST OF FIGURES

	Page
Figure 2. 1 The transparency-based colorimetric sensor for Ca(II) ion determination ⁴⁰	8
Figure 2. 2 The electrochemical sensors based on polymeric substrate.....	8
Figure 2. 3 Wax printing process.	9
Figure 2. 4 (a) The changing color of various concentrations of NO ₃ ⁻ in the presence of Griess reagent ⁴⁷ . (b) The colorimetric performance of I ⁻ determination in the presence of Au ³⁺ ion ⁴⁸	10
Figure 2. 5 The family tree of interfacial electrochemical techniques ⁵¹	13
Figure 2.6 (a) Potential-time excitation signal in cyclic voltammetric experiment ⁵⁶ (b) typical cyclic voltammogram for a reversible process ⁵²	16
Figure 2.7 (a) Excitation signal for differential-pulse voltammetry ⁵⁸ . (b) Differential pulse voltammogram.....	17
Figure 2.8 (a) The potential modulation in square-wave voltammetry. (b) single potential cycle in square-wave voltammetry and (c) typical square-wave voltammogram ⁶⁰	18
Figure 2.9 (a) The excitation waveform (b) the resulting current-time response under static condition (c) the resulting current-time after integrated with flow system.	19
Figure 2.10 The Nyquist plot from simple Randles equivalent circuit for an electrochemical cell including the solution resistance (R _s), double layer charging at the electrode surface (C _{dl}), charge transfer resistance (R _{ct}), and the Warburg Element (Z _w) ⁶⁵	20
Figure 2.11 (a) Freestanding BDD electrode ⁶⁹ (b) Commercial BDD electrode ⁷⁰	22
Figure 2.12 Preparative HPLC system.....	29
Figure 3.1 TAD with the reaction solution of 0.15 mM KMnO ₄ in 0.5 mM H ₂ SO ₄ in the absence (a) and presence (b) of 10 ppm SAL, and the color change from light pink (a) to pale orange (b) could be clearly observed on the TAD.....	39

Figure 3.2 PAD with the reaction solution of 0.15 mM KMnO_4 in 0.5 mM H_2SO_4 in the absence (a) and presence (b) of 10 ppm SAL, where the color change could not be clearly observed on the PAD.....	41
Figure 3.3 Effects of acid type on the colorimetric determination of SAL using permanganate in acidic medium as reagent.....	42
Figure 3.4 Plots showing the effects of experimental parameters, including (a) concentration of H_2SO_4 , and (b) concentration of KMnO_4 on the colorimetric determination of SAL.....	44
Figure 3.5 Effects of reaction time (studied within 20 min) and temperature at (a) 25 °C, (b) 30 °C, (c) 40 °C and (d) 50 °C on the colorimetric detection of SAL.....	45
Figure 3.6 (a) Corresponding images of the colorimetric detection of SAL at various concentrations ranging from 0 – 40 ppm on the TAD colorimetric sensor, and (b) Plot of linear regression analysis with the SAL concentrations of 0.5 – 40.0 ppm in a log scale. Inset: Plot of the average color change intensity against the concentration of SAL in a range of 0.5 – 40.0 ppm.	46
Figure 4.1.1 Structures of terbutaline (TER), salbutamol (SAL), ractopamine (RAC) and clenbuterol (CLB).....	54
Figure 4.1.2 Effects of (A) Pd (II) concentration, (B) scan rate, and (C) number of cycles on the PdNPs modification on BDD electrodes.	61
Figure 4.1.3 The SEM image (a) and the EDS elemental Pd map (b) of bare BDD electrode. The SEM images (c),(e),(g) and the EDS elemental Pd maps (d),(f),(h) of different deposition CV scans in PdNPs modification step.....	63
Figure 4.1.4 (a,e,i) EDS elemental Pd on BDD map, (b,f,j) EDS elemental C map , (c,j,k) EDS elemental Pd map and (d, h, l) EDX results of 3, 7 and 15 repetitive cycles of PdNPs modified BDD electrode, respectively.....	64
Figure 4.1.5 Cyclic voltammograms of 10 mM (a) TER, (b) SAL, (c) RAC and (d) CLB in MeOH: PBS (50:50; v/v) with a potential scanned from 0.0 to 1.6 V vs Ag/AgCl at a bare BDD electrode (black line) and a PdNPs-modified electrode (orange line) with a scan	

rate of 100 mV s^{-1} , as well as a column chart (e) comparing oxidation current responses of four β -agonists at bare BDD and PdNPs-modified BDD electrode. 66

Figure 4.1.6 UHPLC-ECD chromatogram of $10 \mu\text{g mL}^{-1}$ of (a) TER, (b) SAL, (c) RAC, and (d) CLB at PdNPs modified BDD electrode in a (0.05 M phosphate buffer solution (pH 7): MeOH) mobile phase with the detection potential of 1.0 V vs Ag/AgCl; the injection volume of $10 \mu\text{L}$; and the flow rate of 1 mL min^{-1} . This chromatogram was a representative of three independent repetitions. 68

Figure 4.1.7 (A) Amperometric chromatograms of different injection volumes at PdNPs modified BDD for a $10 \mu\text{g mL}^{-1}$ of (a) TER, (b) SAL, (c) RAC, and (d) CLB. (B) Current responses of (○) TER, (□) SAL, (◇) RAC, and (△) CLB in a mobile phase solution of 0.05 M phosphate buffer solution (pH 7): MeOH, with the detection potential of 1.0 V vs Ag/AgCl, and the flow rate of 1 mL min^{-1} . Each data point represents the average current of three repetitive experiments. 69

Figure 4.1.8 Effect of (a) pH and (b) detection potential on (○) TER, (□) SAL, (◇) RAC, and (△) CLB with injection volume of $8 \mu\text{L}$, and the flow rate of 1 mL min^{-1} using PdNPs-modified BDD electrode coupled with UHPLC. Each data point represents the average of three repetitive experiments. 71

Figure 4.1.9 Plots between amperometric normalized current of $10 \mu\text{g mL}^{-1}$ (a) TER, (b) SAL, (c) RAC and (d) CLB and number of successive measurements using SPCE (black line) and PdNPs-modified BDD electrode (orange line). All parameters were performed under optimal conditions. Note that the first peak current measured in each case has been normalized to 100%. 73

Figure 4.1.10 The amperometric chromatograms of (a) TER, (b) SAL, (c) RAC, and (d) CLB in the concentration range of $0.2 - 20 \mu\text{g mL}^{-1}$ at PdNPs modified BDD electrode after being separated by UHPLC and the corresponding calibration plots (inset). The experiments were performed under optimal conditions. 76

Figure 4.2.1 Schematic illustration of the fabrication of the origami-ePAD based MIP/PANI/SPGE device as follows: (a) the small holes were created around WE, (b) the holed double-side adhesive tape was stuck over the electrode. (c) the constructed

electrode was then attached onto the holding PADs. For sliding-PADs manufacture, (d) the holding PADs was firstly placed beneath sliding PADs. Then (e) the sensing channel contained MIP modified electrode was flipped over the sliding PADs, followed by the fold of upper-side of sliding-PAD over electrode sensor. After that, the (f) the holding channel was flipped again over the sliding PADs. The established device was shown in (g). Finally, (h) the attained device was sandwiched between two acrylic plates and tightened by the magnet.....89

Figure 4.2.2 The characterization of MIP/PANI/SPGE sensor in the step-by-step modification for the SAL determination by (a) EIS technique and its data was obtained for the equivalent circuit including solution resistance (R_1), charge transfer resistance (R_2), constant Phase Element (Q) and warburg element (W), and (b) CV of 10 mM $[\text{Fe}(\text{CN})_6]^{3-/4-}$ in absent and present of $10 \mu\text{g mL}^{-1}$ of SAL with potential scan from -0.8 – 1.0 V vs Ag/AgCl and scan rate of 100 mVs^{-1} 93

Figure 4.2.3 The effects of (a) aniline concentration, (b) number of CV scans in aniline polymerization step, (c) the molar ratio between monomer and target analyte, (d) the molar ratio between monomer and cross-linker and (e) number of CV scans in MIP polymerization step, these parameters were investigated using EIS techniques for determination of $10 \mu\text{g mL}^{-1}$ SAL. All experimental results were obtained from the mean of three repetitive measurements..... 98

Figure 4.2.4 Schematic illustration of sequential sliding-step for SAL determination. 100

Figure 4.2.5 (a) The Cyclic voltammogram of 10 mM $\text{Fe}(\text{CN})_6^{3-/4-}$ with scan rate 100 mV s^{-1} and continuous four repetitive measurements. The changing ΔR_{ct} response of $10 \mu\text{g mL}^{-1}$ with (b) varied rebinding time in the range of 1 to 15 min and (c) different electroactive species concentration from 0.5 to 10 mM..... 101

Figure 4.2.6 (a) The R_{ct} response of various SAL concentration in the range of 0.05 to $20 \mu\text{g mL}^{-1}$ using MIP/PANI/SPGE accompanying with sliding PADs. (b) The linear calibration plot of SAL concentration (inset picture) and its logarithm against the changing ΔR_{ct} response. 102

Figure 4.2.7 The selectivity test of other structurally related to SAL including TER, RAC and PHE by comparison of MIP and NIP based electrochemical sensor.	105
Figure 4.2.8 The storage stability of the sliding PADs based MIP/PANI/SPGE.	105
Figure 4.3.1 Schematic illustration of designed electrode and wax barrier platform on PVC substrate.....	114
Figure 4.3.2 FE-SEM image with 20,000 magnification of (a) bare graphene, (b) CuNiAu/SPGE and FE-SEM image with 40,000 magnification of (c) Ni/SPGE, (d) Cu/SPGE, (e) Au/SPGE and (f) CuNiAu/SPGE, orderly. XPS spectra of (g) Au, (h) Cu and (i) graphene, respectively. EDS element analysis of CuNiAu/SPGE (j-k) EDS element analysis.	118
Figure 4.3.3 The CV of (a) CuNiAu (molar ratio 2:100:2), (b) 5 mM of Cu(II), (c) 5 mM of Au (III) and (d) 5 mM of Ni(II) in 0.2 M Na ₂ SO ₄ on SPGE was scan from 0.0 V to 1.0 V vs Ag/AgCl at 100 mVs ⁻¹ of scan rate. The inset figure; the zooming in figure of CV of 5 mM Ni (II).....	119
Figure 4.3.4 (A) The CV of 5 mM [Fe(CN) ₆] ^{3-/4-} in 0.1 M KCl solution at different electrode as follows Ni/SPGE (a; green line), SPGE (b; black line), Au/SPGE (c; yellow line), CuNiAu/SPGE (d; light orange line) and Cu/SPGE (e; red line) was performed from -1.0 V to 1.0 V vs Ag/AgCl at 100 mVs ⁻¹ of scan rate. (B) Nyquist plot of Ni/SPGE (a; green line), Cu/SPGE (b; red line), Au/SPGE (c; yellow line), CuNiAu/SPGE (d; light orange line), and SPGE (e; black line) in the present of 5 mM [Fe(CN) ₆] ^{3-/4-} in 0.1 M KCl solution. Inset: equivalent circuit applied to model EIS data, R ₁ : the electrolyte solution resistance; C ₁ : the capacitance phase angle element; R ₂ : the interfacial electron transfer resistance; W ₁ : the Warburg impedance introduced by diffusion of ions.....	121
Figure 4.3.5 The CV of 25 μM NE and 50 μM 5-HT in 0.1 M PBS buffer pH 7.4 at different modified electrode as follows (a) SPGE, (b) Cu/SPGE, (c) Ni/SPGE, (d) Au/SPGE, (e) NiAu/SPGE, (f) CuAu/SPGE, (g) CuNi/SPGE, (h) CuNiAu/SPGE, (i) Au/Cu/Ni/SPGE, (j) Ni/Cu/Au/SPGE, (k) Cu/Au/Ni/SPGE, (l) Au/Ni/Cu/SPGE, (m) Ni/Au/Cu/SPGE and (n) Cu/Ni/Au/SPGE was scan from 0.0 V to 1.0 V vs Ag/AgCl at 100 mVs ⁻¹ of scan rate. (o) The comparing bar chart of NE and 5-HT current response at CuAu/SPGE and CuNiAu/SPGE.....	124

Figure 4.3.6 (a) The SWV voltammogram of 25 μM NE and 50 μM 5-HT at the different electrodeposition potential performed from 0.0 V to 0.6 V vs Ag/AgCl with E_{step} of 0.4 mV, amplitude of 50 mV and frequency of 35 Hz. (b) The relative plot between current response of 25 μM NE and 50 μM 5-HT and electrodeposition potential. (c) The SWV voltammogram of 25 μM NE and 50 μM 5-HT at the different electrodeposition time scanned from 0.0 V to 0.6 V vs Ag/AgCl with E_{step} of 0.4 mV, amplitude of 50 mV and frequency of 35 Hz. (e) The relative plot between current response of 25 μM NE and 50 μM 5-HT and electrodeposition time. The SWV voltammogram and current response values are representative of three measurements. 127

Figure 4.3.7 SEM image of 40,000 magnification of different electrodeposition potential of modified electrode procedure at (a) -0.8 V, (b) -1.0 V and (c) -1.2 V vs Ag/AgCl and various electrodeposition time of (d) 60 s, (e) 200 s and (f) 400 s. Additionally, SEM image of various molar ratio of Cu:Ni:Au was investigated for morphology study of (g) 1:100:1, (h) 1:100:2 and (i) 2:100:2 128

Figure 4.3.8 Molar ratio of metal precursors effect accompanied with the SWV voltammogram of (a and d) various molar ratio of Ni was studied at 10, 50, 100, 200 and 300 fold comparing with molar ratio of Cu and Au (fixed at 1-fold of molar ratio), (b and e) different molar ratio of Au was examined from 1, 2, 3, 4, 5, and 6 fold while the molar ratio of Ni and Cu was kept at 100 and 1, orderly, of molar ratio, (c and f) the molar ratio of Cu was varied from 1, 2, 3, 4, 5, and 6 fold, meanwhile the molar ratio of Ni and Au was kept at 100 and 2 fold, orderly, of molar ratio..... 130

Figure 4.3.9 (a) The SWV voltammograms of 25 μM NE and 50 μM 5-HT at the pH range 6.0 to 9.0 were performed from 0.0 V to 0.6 V vs Ag/AgCl with E_{step} of 0.4 mV, amplitude of 50 mV and frequency of 35 Hz. (b) The relationship between S/N and pH. The SWV voltammograms are representative of three repeated measurements. 132

Figure 4.3.10 The plot of SWV parameters between S/N and (a) E_{step} , (b) amplitude, (c) frequency of 25 μM NE and 50 μM 5-HT in 0.1 M PBS buffer pH 7.4. The SWV voltammogram of various (d) E_{step} , (e) amplitude and (f) frequency against with potential. The SWV voltammograms are representative of three repetition..... 134

Figure 4.3.11 Individual test for (a) different concentration of 5-HT in the presence of 25 μM of NE in 0.1M PBS buffer (pH 7.4). 5-HT concentration are: 2.5, 5, 10, 20, 30, 40, 50, 60 and 70 μM , (b) different concentration of NE in the presence of 30 μM of 5-HT in 0.1M PBS buffer (pH 7.4). NE concentration are: 0.1, 1, 2.5, 5, 10, 20, 25, 30 and 40 μM and (c) different concentration of NE and 5-HT in 0.1M PBS buffer (pH 7.4). NE concentration are: 1, 2.5, 5, 10, 20, 25, 30 and 40 μM . Meanwhile 5-HT concentration are 5, 10, 20, 30, 40, 50, 60, and 70. Inset picture: the relationship between concentration of the target analyte and the current response coexisting with the linear regressive equation. 137

Figure 4.3.12 The common interfering species in serum were studied by mixed various interference with standard solution of 25 μM NE and 50 μM 5-HT in 0.1 M PBS buffer pH 7.4. The interfering species as follows 0.05 M of Cl^- , K^+ and Mg^{2+} , 1 mM of glucose, L-glycine and tyrosine, and 0.1 mM of ascorbic acid (AA) and uric acid (UA) were investigated. 140

Figure 4.3.13 The SWV voltammograms of sequentially eliminated AA. All SWV voltammograms are representative of three repetitive experiments. 141

LIST OF ABBREVIATIONS

ΔE_p	Peak separation
ΔI	Intensity difference
ΔR_{ct}	The difference of charge transfer resistance
5-HT	5-hydroxytryptamine or serotonin
μg	Microgram
μL	Microliter
μm	Micrometer
μPAD	Paper-based analytical device
$^{\circ}\text{C}$	Degree Celsius
A	Electrode surface area
A	Ampere
Ag/AgCl	Silver-silver chloride electrode
Au (III)	Gold ion
AuNPs	Gold nanoparticles
APB	3-aminophenylboronic acid
BDD	Boron-doped diamond
C	Concentration
C_1	The capacitance
CE	Counter electrode
CLB	Clenbuterol
CV	Cyclic Voltammetry
Cu (II)	Copper ion
CuNPs	Copper nanoparticles
D	Diffusion coefficient (in $\text{cm}^2 \text{s}^{-1}$)
E°	Standard reduction potential
E_p	Potential
$E_{p,a}$	Anodic peak potential
$E_{p,c}$	Cathodic peak potential
ECD	Electrochemical detector
EDS	Energy dispersive x-ray spectra

ePAD	Electrochemical paper-based analytical device
EIS	Electrochemical impedance spectroscopy
F	The faraday constant
Hz	Hertz
i	Current
i_f	Forward pulse
i_r	End of reverse pulse
KMnO_4	Potassium permanganess
K_{et}	The electron transfer rate
L	Column length
L	Liter
LOD	Limit of detection
LOQ	Limit of quantitation
M	Molar
min	Minute
mL	Milliliter
mm	Millimeter
mM	Millimolar
MIP	Molecularly imprinted polymer
n	Number of electrons
n	Number of repetitions
N	Theoretical plates number
ng	Nanogram
nm	Nanometer
NE	Norepinephrine
Ni (II)	Nickel ion
NiNPs	Nickel nanoparticles
o-PD	o-phenylenediamine
PANI	Polyaniline
PB	Phosphate buffer
PBS	Phosphate buffer saline

PdNPs	Palladium nanoparticles
POC	Point-of-care
ppm	Parts per million
psi	Pounds per square inch
R	The ideal gas constant ($\text{JK}^{-1} \text{mol}^{-1}$)
R^2	Correlation coefficient
R_s	Electrolyte resistance
R_s	Resolution
R_{ct}	Charge transfer resistance
RAC	Ractopamine
RE	Reference electrode
RSD	Relative standard deviation
s	Second
S/cm	Siemens per centimeter
S/N	Signal-to-noise ratio
SAL	Salbutamol
SD	Standard deviation
SEM	Scanning electron microscope
SPGE	Screen-printed graphene electrode
SWV	Square wave voltammetry
T	Temperature (K)
TAD	Transparency-based analytical device
TER	Terbutaline
t_m	Void time
t_r	Retention time
UHPLC	Ultra-high-performance liquid chromatography
UV-Vis	UV-Visible spectrophotometry
V	Volt
W	Peak width
W_1	Warburg impedance
WADA	World anti-doping agency

WE	Working electrode
XPS	X-ray photoelectron spectroscopy
Z	Impedance
α	Column selectivity
α	Transfer coefficient
Ω	Ohm
ν	Scan rate (Vs^{-1})



CHAPTER 1

INTRODUCTION

1.1 Introduction

In this globalized era, the demands of high sensitivity, good accuracy, facileness, and fast response of analytical approaches accompanying with scalably small and portable devices for various sensing applications have been readily rising on account of the research breakthrough and the advanced technology. Basically, the numerous sensors have been developed for different aspects of use, including industrial, agricultural, environmental and clinical application, in order to mainly facilitate human health and well-being, leading to better quality of life. For example, various sensing devices have been developed and potentially employed for quality control¹⁻³, point of care testing^{4, 5} and environmental monitoring⁶. As extensively reported in the literature, the colorimetric and electrochemical techniques have attracted significant attention for sensing application as their detection platforms could be affordable, rapid, and user-friendly^{6, 7}. In addition, the colorimetric and electrochemical sensor could be capable of miniaturization offering favorable advantages of reducing cost, decreasing chemical consumption and being portable for on-site application⁷⁻⁹.

As for colorimetric analysis, it possesses real-time detection capabilities relying on the color change which could be clearly observed by the naked eye, and the color test could be simply conducted with no sophisticated and expensive instruments needed. Typically the color change observed could occur based on several strategies, including ion-exchange¹⁰, complexation^{11, 12}, and redox reaction¹³⁻¹⁶. Among these mechanisms, the redox reaction, consisting of oxidation and reduction, is a simple and well-known method which involves the change in the oxidation number of a participating molecule, atom or ion through either gaining or losing electrons. Herein, the colorimetric approach, based on redox reaction, has been developed in this work for quantification of salbutamol (SAL) in pharmaceutical drugs which could be potentially applied in the quality control process. Generally, salbutamol (SAL), classified as one of the β -agonist compounds, and typically used in medication for

asthma treatment, was selected as the representative analyte used to assess the developed detection method. In this work, the colorimetric sensor was fabricated using the transparency-based substrate providing vivid color change which could be easily seen as well as having mechanically robust, chemically inert and hydrophobic characteristics. The motivation and details of the developed transparency-based colorimetric devices are described in Chapter 3. Although, the detection of SAL by colorimetry gave quite decent results, showing a potential application for SAL measurement in asthma medication real samples, the execution of this colorimetric sensor in complex media containing some interferences such as human fluids and food samples still not applicable due to the low detection limit and unspecific or side reaction of color change.

Thus, electrochemical detection could be considered as the prime method used to fabricate a sensing platform suitable for complex samples, which could be then overcome those colorimetric limitations. Basically, the electrochemical approach processes many advantages, including high sensitivity and selectivity, fast analysis, facileness, affordability, small-volume of sample consumption, and compatibility with microfabrication technologies^{7, 17}. However, the operation of electrochemical technique for simultaneous determination of various β -agonists, which have almost the same oxidation potentials, still remains challenging due to their overlapping peak, lading to non or pretty low selectivity in detection. To overcome this drawback, coupling of various separation techniques such as high-performance liquid chromatography (HPLC) and ultrahigh-performance liquid chromatography (UHPLC) prior to the electrochemical detection (ECD) has been widely reported in the literature^{18, 19}. The sample preparation and separation could then be pursued using these chromatographic separation approaches before the individual analyte chromatographically separated could be detected selectively by the electrochemical sensor. However, there has been another issue regarding the electrode fouling during electrolysis of phenolic compounds, widely reported in the literature^{20, 21}. Typically, the fouling resulting from the oxidation of these phenolic compounds has been well-

known to be due to formation of dimeric or polymeric film, adsorbing onto the electrode surface via π - π interaction^{22, 23}, and subsequently resulting in passivation of electrode surface where no electrochemical response could be further obtained. Several studies have attempted to solve this electrode fouling problem, and one simple way to do so has been reported to be using the boron-doped diamond (BDD) as an alternative electrode material, offering the high resistance to electrode fouling due to the inert H terminated group and a little π -electron density on its structure^{24, 25}. Another obstacle in the electrochemical detection of β -agonist compounds that has been previously reported is the low sensitivity of signal response. This has then brought about the modification of BDD surface by catalytic palladium nanoparticles (PdNPs) which could remarkably increase the sensitivity of the electrochemistry-based systems. Therefore, in this work, the electrochemical sensor based on PdNPs modified BDD integrating with UHPLC for simultaneous determination of four β -agonist compounds including terbutaline (TER), salbutamol (SAL), ractopamine (RAC) and clenbuterol (CLB) has been developed, and the proposed UHPLC-coupled ECD sensor has been subsequently applied in biological and food samples. The procedures of chromatographic separation and surface modification of BDD sensing electrode, as well as the simultaneous detection of four- β -agonists are described in detail in Chapter 4.1. Though the selectivity of the electrochemical determination of β -agonists could successfully be enhance by coupling the chromatographic separation unit with the electrochemical detection platform, the separation method itself seem to have some drawback, including tediousness, high instrumental expenses, and sophisticated equipment with professional training needed. Hence, the development of a highly selective analytical method for the determination of β -agonists has become of great interest for future investigation.

Throughout the past decade, the molecularly imprinted polymers (MIPs) have been attracting the attention of many researchers as they could be tailor-made with specific recognition sites for the target analyte, improving the selectivity of the

detection. Basically, the characteristic of MIPs has relied on a molecular recognition and specific interaction, mimicking antibody-like features with strong binding affinities toward the target analyte. The synthesis of MIPs could be simply performed by copolymerization of functional monomers, crosslinkers, and template molecules to form a polymer. Afterwards the template molecules would be removed to generate the polymer with specific cavities that could particularly match the target analytes with specific shape, size, and functional groups^{26, 27}. Moreover, the polymeric film thickness and the MIP morphology could be deliberately controlled during the synthesis to generate the most suitable MIP mold^{26, 28}. The obtained MIP with binding cavities complementary to the target analyte has been reported to possess unique properties, including high selectivity, long stability, great physical and chemical resistance, cost efficiency, and capability of modifying the electrode surface or being used as electrode material^{26, 28}. Thereby in this work, the MIP with specific recognition site toward SAL could be synthesized simply by electro-polymerization to obtain the imprinted polymer sticking onto the working electrode surface, creating a MIP-based electrochemical sensor for selective determination of SAL. The experimental parameters regarding the MIP synthesis, the electrode surface modification, and the selective determination of SAL in complex biological media using the proposed electrochemical sensor have been thoroughly investigated and discussed in more detail in Chapter 4.2.

Beside MIP technology, metal nanoparticles possessing comparatively high surface area and high catalytic capability have truly become the promising materials widely used as electrocatalysts in several electrochemistry-based applications, especially ones involving a range of organic compounds which generally have more or less the same oxidation potentials, resulting in the overlapping peaks and making them quite difficult to be electrochemically detected²⁹. Recently, it has been reported in the literature that the catalytic activities of metal nano-catalysts could be greatly enhanced if using either bimetallic or trimetallic nanoparticles, compared to the monometallic counterparts that showed the least catalytic performance³⁰⁻³⁴. Literally,

the enhanced catalytic activities of these multicomponent metallic nanoparticles could be attributed to the excellent synergistic effects of metal nanoparticles with diverse intrinsic properties. In this work, the trimetallic nanoparticles, consisting of Au, Cu and Ni, have been electrochemically synthesized and modified onto the surface of a screen-printed graphene electrode (SPGE). The obtained trimetallic CuNiAu modified SPGE synergistically showed the catalytic activity toward the electrochemical detection of biomarker, including serotonin (5-HT) and norepinephrine (NE), with completed separation of the two adjacent peaks located at potentials pretty close to each other. The scope of this study and the synergistically catalytic capability of the developed trimetallic nanoparticle modified SPGE sensor towards the oxidation of these biomolecules were described in detail in Chapter 4.3.

1.2 Research objectives

The main aims of this research are comprised of three achieving goals for the development of sensing devices with enhanced detection performance, as follows:

1. To develop the analytical sensing tools (both colorimetric and electrochemical sensors) for the sensitive and selective determination of β -agonists (e.g. SAL) in pharmaceutical, biological and food samples.
2. To improve the specification and performance of the electrochemical sensors for SAL determination using a wide range of electrode materials and modifiers, such as metal nanoparticles, BDD, and MIP.
3. To enhance the selectivity and sensitivity of the electrochemical sensor using the trimetallic composite-modified electrode with increased electrocatalytic activity towards the oxidation of organic compounds. The developed sensing device showed the synergistic behaviors of trimetallic catalyst's properties and could be applied for simultaneously measuring the biomarkers, including 5-HT and NE.

1.3 Scope of this research

To develop the highly sensitive and selective sensors with detection platforms based on colorimetric and electrochemical approaches, as follows:

1. Both colorimetric and electrochemical sensors were developed with miniaturized feature and portable design, being user-friendly and compatible to the on-site applications.
2. The colorimetric sensing device for SAL detection was simply fabricated, and the color change should be easily and clearly observed by the naked eye. In addition, the color change intensity should be measured and processed accurately using ImageJ.
3. To enhance the selectivity of the electrochemical sensors towards the detection of β -agonists, several procedures, involving either the use of UHPLC separation unit coupled with the ECD sensor, or the modification of electrode surface with MIP having SAL recognition sites, were thoroughly studied.

There are five chapters in this dissertation. Chapter 1 is the introduction demonstrating the aspect and scope of this research. Chapter 2 is the theory comprising the detection methods (including colorimetric and electrochemical detection) and the fabrication of sensing devices. The development of the colorimetric sensor for SAL is then addressed in detail in Chapter 3. Meanwhile the electrochemical sensor established a significant advance toward the selectivity was reported in Chapter 4. Lastly, Chapter 5 is the conclusion and future perspectives for this dissertation.

CHAPTER 2

THEORY

2.1 Sensor fabrication

Nowadays, the demand for miniaturized sensing development has grown substantially throughout the years offered the portability, inexpensive and less sample and reagent requirement. With this perspective, the paper-based and polymer-based (e.g. polyvinylchloride (PVC) either opaque or transparent) materials have been extensively employed as valuable substrates for the development of sensors. The beneficial advantages including their affordability, biocompatibility, biodegradability, robustness, and easiness of miniaturization make these materials the first ranked-choice for sensor substrates. Both papers and polymers have been reported to be broadly employed in diverse applications presented in numerous publications³⁵⁻³⁹. As for detection approach, the colorimetric and electrochemical techniques, offering rapid analysis, facile operation, and inherent miniaturization, have been widely used in many sensing devices. For example, as reported by Duenchay et.al⁴⁰, they presented the utilization of polymer-based transparent sheet for colorimetric determination of Ca(II) ion. The remarkable color change was obtained when comparing between before and after Ca (II) ion addition using the developed transparency-based sheet (Figure 2.1). Additionally, the polymeric substrate could be employed for electrochemical sensor fabricated by screen-printing method as shown in Figure 2.2. Herein, the colorimetric transparency-based, and the electrochemistry-based sensors were fabricated and used in various applications, as described in Chapter 3 and 4.

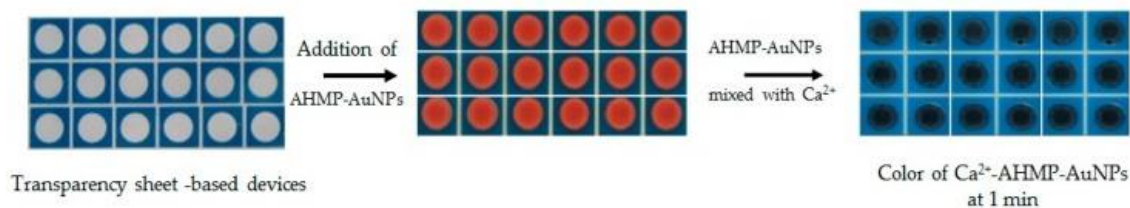


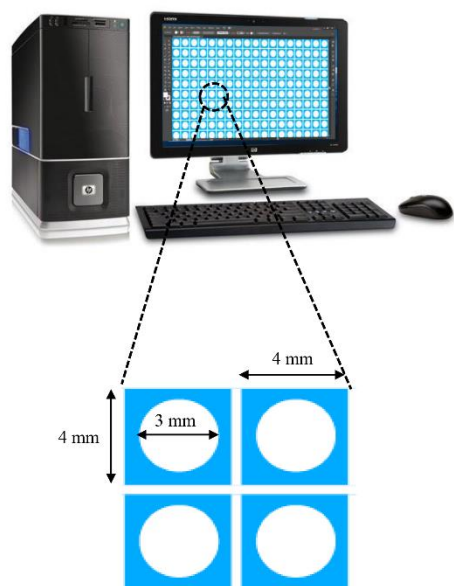
Figure 2.1 The transparency-based colorimetric sensor for Ca(II) ion determination ⁴⁰



Figure 2.2 The electrochemical sensors based on polymeric substrate.

For the sensor fabrication, the hydrophobic barriers which could guard the reaction zone on polymeric substrate, could be fabricated by numerous methods including wax printing⁴¹, photolithography⁴², and direct printing of hydrophobic polymer^{43, 44}. Due to the ease of hydrophobic barrier production, the wax printing has been employed to generate the wax-based hydrophobic barriers in this dissertation. This process consisted of only two steps as follows; (1) the design of wax pattern easily created by Adobe illustrator software, (2) the wax pattern printed onto polymeric substrate surface using Xerox colorcube (wax printer) (Figure 2.3).

1. Designed wax pattern



2. Print wax

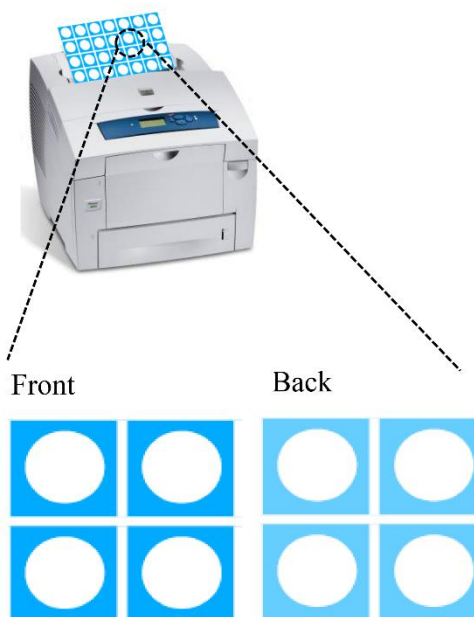


Figure 2.3 Wax printing process.

2.2 Colorimetric detection

Presently, the colorimetric approach has attracted much attention due to its simple operation and observable visual interpretation. The colorimetric method has typically relied on the direct measurement of color change in a variety of reactions such as redox reaction^{13, 14, 36}, enzymatic assay⁴⁵, and complexation⁴⁶. Among these reactions, an oxidation-reduction (redox) reaction, which is a spontaneous chemical reaction relating to the transfer of electrons between two species, was selected in this dissertation. The common examples of redox reactions involving in sensing systems are nitrate (NO_3^-) sensing involving the reduction of NO_3^- to NO_2 by Griess reaction⁴⁷ and the iodide ions (I^-) determination principally based on the oxidation reaction of I^- in the presence of Au(III) ion⁴⁸. The colorimetric response has typically been obtained using spectrophotometer. However, it still suffers from complicated instrument and training requirement, restricting its uses only in the laboratory. Currently, the color intensity analysis software such as ImageJ and color assist have been developed

throughout the year, offering several convenient alternative methods for on-site applications.

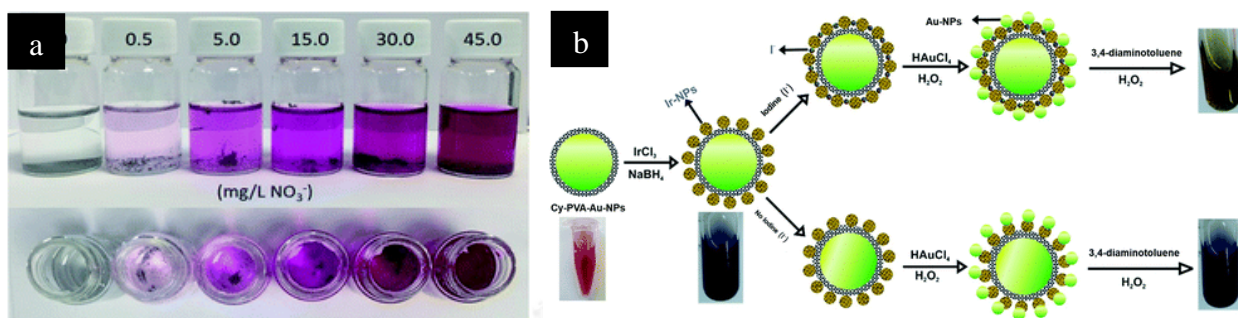


Figure 2.4 (a) The changing color of various concentrations of NO_3^- in the presence of Griess reagent⁴⁷. (b) The colorimetric performance of I^- determination in the presence of Au^{3+} ion⁴⁸.

2.3 Electrochemical detection

The electrochemical detection is often be the first choice used for the miniaturized sensing platforms, popularly applied in various applications. The unique characteristic of electrochemistry is fast analysis, high sensitivity, compact size, and low power requirement. The electrochemical technique relies on the electrical quantity such as current, potential and charge measurement, occurring from the electron transfer of the interest analyte at the electrode/electrolyte interface. Basically, the electrochemical measurement is based on the investigation of charge-transfer or electron transfer process at the electrode surface, where the potential is applied, and the corresponding current is then measured.

2.3.1 Faradaic and non-faradaic process

Basically, the interfacial electrode process consists of two main process. The first process, which involves the movement of electrons across the interfacial boundary of electrode/electrolyte by oxidation and/or reduction reactions that obey Faraday's law (stating that the attained current flowing through an electrode/electrolyte interface

is proportionally driven by the amount of chemical change at an electrode-electrolyte boundary), is called faradaic process. The second one does not rely on the charge-transfer process but the external current which flows through the electrode-electrolyte boundary occurring from the adsorption and desorption process, known as non-faradaic processes. The non-faradaic current is termed as background current motif in electrochemical technique⁴⁹.

2.3.2 Mass transfer

For electrochemical process, the molecules of interest need to be transported from the bulk solution toward the electrode surface for redox reaction occurring at electrode boundary. This driving force is called mass transfer process which critically affects the rate of the electrochemical process, along with the electron-transfer kinetic. Theoretically, there are three types of mass transport behavior as follows:

1. Migration is the movement of charged species under the influence of an electric field. With this relevant condition, the positive ion species will transport toward the negative charge whereas the negative ion species will transport toward the opposite direction. The ion mobility is influenced by the potential at electrode surface. To eradicate the ion migration, the high concentration of the electrolyte is typically employed.

2. Diffusion is the movement of species under the influence of a concentration gradient by moving from a region of high concentration toward the region of low concentration.

3. Convection is the movement of species under stirring or hydrodynamic condition. The fluid flow is generally driven by the density gradients, known as natural convection, and force convection which can be characterized by stagnant regions, laminar flow, and turbulent flow.

Mass transfer to an electrode is governed by the Nernst-Planck equation⁵⁰, written for one-dimensional mass transfer along the x-axis as

$$J_i(x) = -D_i \frac{\partial C_i}{\partial x} - \frac{z_i}{RT} D_i C_i \frac{\partial \phi(x)}{\partial x} + C_i v(x) \quad (2.1)$$

Where $J_i(x)$ is the flux of species i ($\text{mol s}^{-1} \text{cm}^{-2}$) at distance x from the surface, D_i is the diffusion coefficient ($\text{cm}^2 \text{s}$), $\partial C_i(x)/\partial(x)$ is the concentration gradient at distance x , $\partial \phi(x)/\partial(x)$ is the potential gradient, z_i and C_i are the charge (dimensionless) and concentration (mol cm^{-3}) of species i , respectively, and $v(x)$ is the velocity (cm s^{-1}) which a volume element in solution moves along the axis. The three terms on the right-hand side represent the contributions of diffusion, migration, and convection, respectively, to the flux.

2.3.3 Electrochemical techniques

The electrochemical technique can be classified according to the property of electrical measurement in terms of potential, charge, or current for quantitative analysis of the interested analytes. In brief, there are 4 main electrochemical techniques consisting potentiometry, coulometry, amperometry, and voltammetry (Figure 2.5).

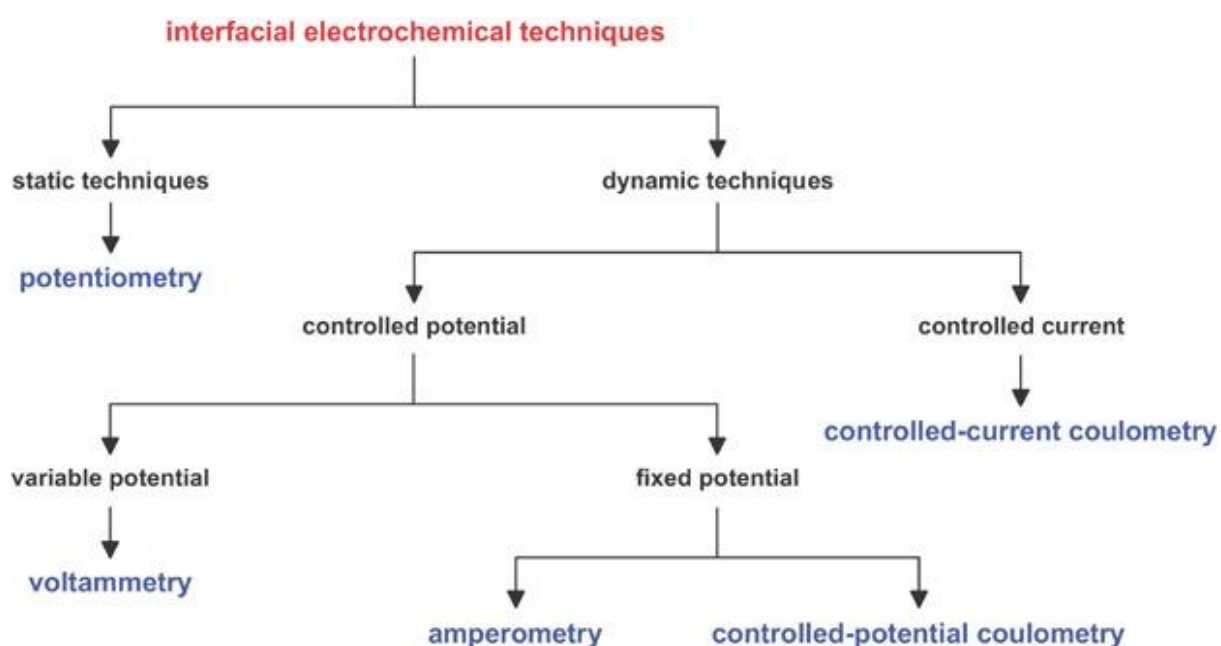


Figure 2.5 The family tree of interfacial electrochemical techniques⁵¹.

In this research, voltammetry and amperometry were used as electrochemical detection methods. Therefore, an overview of these two techniques will be described in this chapter.

2.3.3.1 Voltammetry

The voltammetry is categorized in the class of electroanalytical techniques, relying on the measurement of current at the electrode surface by scanning potential. The plot of resulting current against potential is called a voltammogram. Voltammetry can be employed for studying electrochemical behavior of electroactive species that can be oxidized or reduced at the working electrode. The controlled potential of electrode causes the oxidation-reduction (redox) reaction of the electroactive species to occur. When the potential of electrode is controlled toward more negative direction, it causes the reduction reaction of electroactive species to occur at electrode

interface. In contrast when the potential of electrode is applied toward more positive direction, it causes the oxidation reaction of electroactive species to occur at electrode interface. Voltammetry can be classified as numerous types such as linear sweep voltammetry, polarography, cyclic voltammetry, staircase voltammetry, normal pulse voltammetry, differential pulse voltammetry, square wave voltammetry, anodic stripping voltammetry, cathodic stripping voltammetry, and adsorptive stripping voltammetry.

Herein, the voltammetric technique, employed in this dissertation including the cyclic voltammetry, differential pulse voltammetry and square wave voltammetry are also described.

2.3.3.1.1 Cyclic Voltammetry

Cyclic voltammetry (CV) is the most common technique utilized to initially study the electrochemical behavior of the electroactive species and the developed electrochemical system in terms of kinetic parameter, the redox potentials of the electroactive species, a number of intermediates, a number of reaction steps, and the stability of the product from the electrochemical reaction.

In this method, the potential of working electrode is scanned as a function of time as a triangular potential waveform (Figure 2.6a.). The potential is firstly scanned linearly from an initial value toward a set value, known as the switching potential, and then the potential of working electrode is scanned toward the opposite direction in order to return to the initial potential. As the potential is being scanned, the result is measured by the potentiostat. The resulting cyclic voltammogram created from the plot of the current against the potential is attained.

The acquired cyclic voltammogram of reversible redox couple during a single potential cycle is illustrated in Figure 2.6b. It is assumed that there is only the reduced form (R) in the initial solution. The potential is scanned to a positive direction in the first half-cycle, indicating no oxidation occurring at starting potential. After the formal

potential (E^0) for redox process is reached, the increased anodic current generated by the oxidation of reduced form (R) to oxidized form (O) and the signal then reached the top as a peak. With subsequent decreases in the current at excess reduction potential indicates a decrease in the analyte concentration near the electrode surface due to the accumulation of the product molecule. After the applied potential returns toward the initial potential, the O molecules are oxidized back to R form and the cathodic peak is observed⁵²⁻⁵⁴.

For reversible system, at 25 °C, the concentration of the electroactive species is related to peak current governed by the Randles-Sevcik equation.

$$i_p = (2.69 \times 10^5) n^{3/2} A C D^{1/2} \nu^{1/2} \quad (2.2)$$

where n is the number of electrons, A is the electrode area (cm^2), C is the concentration (mol cm^{-3}), D is the diffusion coefficient ($\text{cm}^2 \text{s}^{-1}$), and ν is the scan rate (V s^{-1}).

For a reversible system, the peak position on the potential axis (E_p) depends on the formal potential of the redox reaction, which is centered between $E_{p,a}$ and $E_{p,c}$:

$$E^0 = \frac{E_{p,a} + E_{p,c}}{2} \quad (2.3)$$

The separation between the peak potentials is governed by:

$$\Delta E_p = E_{p,a} - E_{p,c} = \frac{0.059}{n} \nu \quad (2.4)$$

Therefore, the number of electron transfer in the redox reaction can be entirely calculated by equation 2.4. For example, a redox reaction involving one electron transfer provided ΔE_p of about 59 mV. Additionally, E_p is independent of scan rate for

reversible wave. When the current is proportional to the square root of the scan rate, this demonstrates the diffusion-controlled electrochemical process⁵⁵.

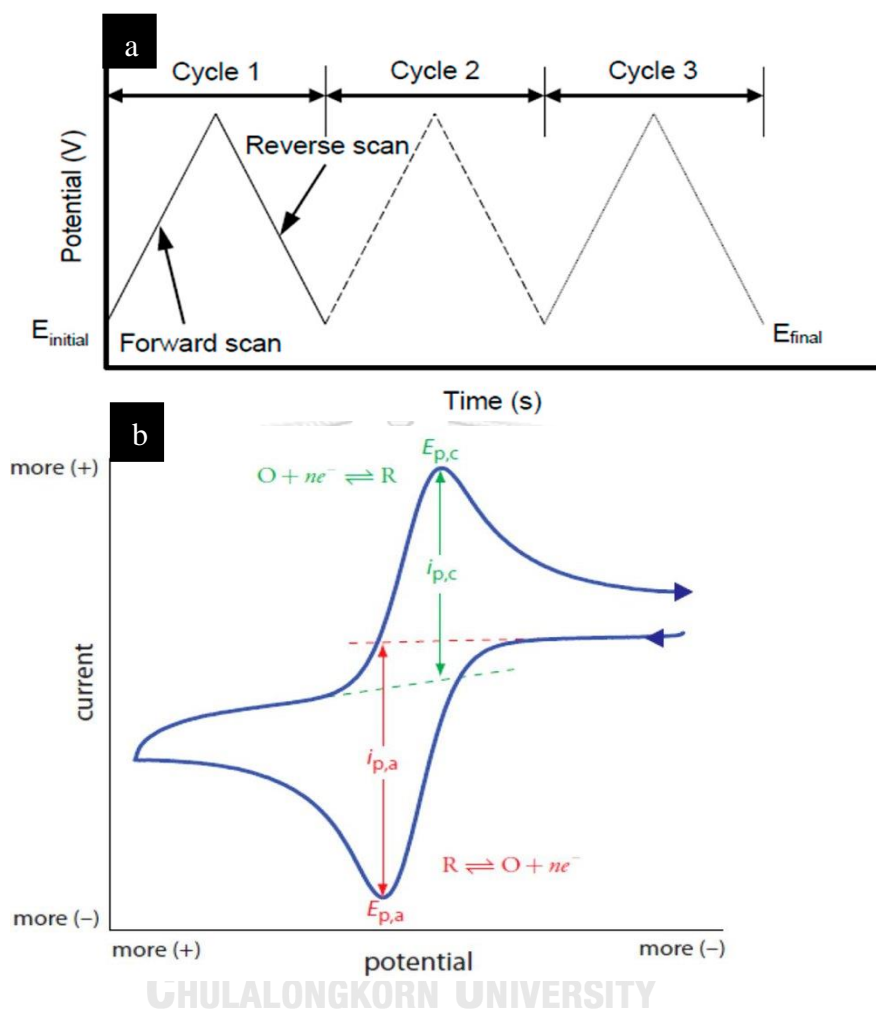


Figure 2.6 (a) Potential-time excitation signal in cyclic voltammetric experiment⁵⁶ (b) typical cyclic voltammogram for a reversible process⁵².

2.3.3.1.2 Differential-pulse voltammetry

Differential-pulse voltammetry (DPV) is a powerful technique with an increased discrimination of Faradaic currents, derived by the electron-transfer at interfacial electrode. The DPV technique depends on the fixed-magnitude pulses, superimposing on a staircase waveform as shown in Figure 2.7a. The current difference at two points

between the point before the pulse application (t_1) and at the end of the pulse (t_2) is recorded. This current difference ($\Delta i = i_1 - i_2$) of these points for each pulse is measured and plotted versus the base potential, the plot is known as differential pulse voltammogram as shown in Figure 2.7b. Additionally, the peak height is directly proportional to the concentration of the corresponding analytes involving the redox reaction occurring at working electrode⁵⁷.

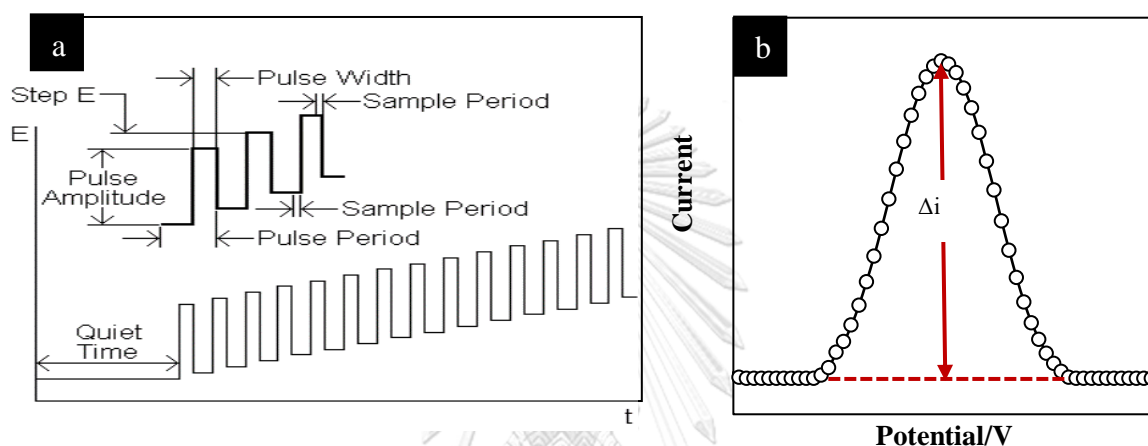


Figure 2.7 (a) Excitation signal for differential-pulse voltammetry⁵⁸. (b) Differential pulse voltammogram.

2.3.3.1.3 Square-wave voltammetry (SWV)

Square-wave voltammetry (SWV) is the fastest and the most sensitive of pulse voltammetry. With the characteristic of this technique, it enables the evaluation of the kinetics and mechanism of the electrode process. The symmetrical SWV waveform is derived from the application of potentials of height pulse amplitude (ΔE), which superimposed on a staircase potential step (E_{step}) as shown in Figure 2.8a. The difference in current is measured at the end of the forward pulse (t_f) and the end of the reverse pulse (t_r). Due to the opposite direction of the staircase scan in forward and reverse pulse, a difference current (Δi) is calculated from $i_f - (-i_r)$. With the opposite signs current, the higher net current is obtained, resulting in an extreme sensitivity of this technique. The shape of the square wave voltammogram is derived from the plot of current difference versus the base potential as shown in Figure 2.8c.^{57, 59, 60}

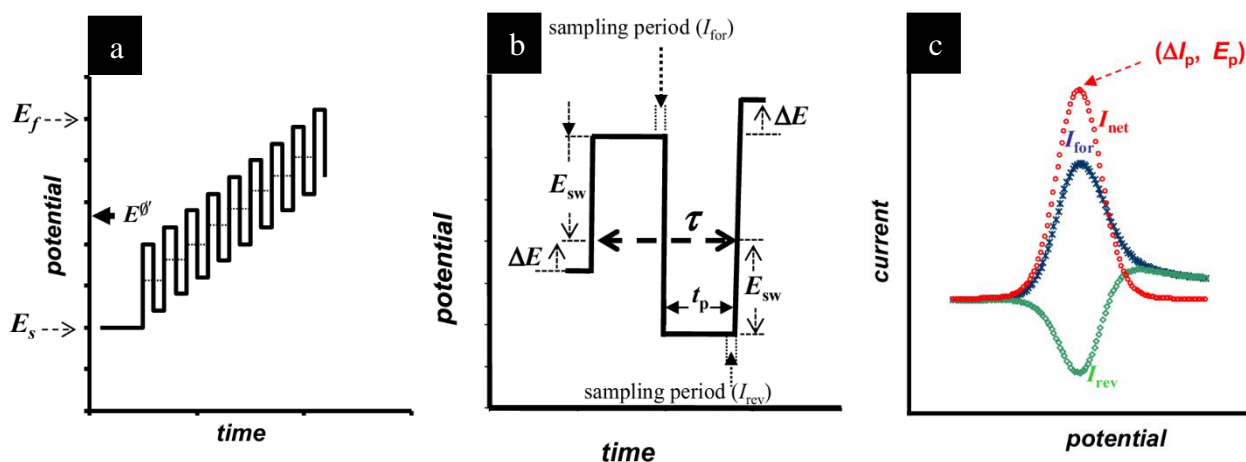


Figure 2.8 (a) The potential modulation in square-wave voltammetry. (b) single potential cycle in square-wave voltammetry and (c) typical square-wave voltammogram⁶⁰.

2.3.3.2 Amperometry

Amperometry is one of the most extensively employed detection methods. The resulting current is directly monitored as a function of constant potential applied to the working electrode with respect to the reference electrode⁶¹. With this feature, the amperometric technique is a useful tool to integrate with flow system such as flow injection analysis (FIA)^{62, 63} and high-performance liquid chromatography (HPLC)^{18, 64}. Typically, the magnitude of the resulting current is directly proportional to the concentration of the interested analyst which are reduced or oxidized at electrode surface.

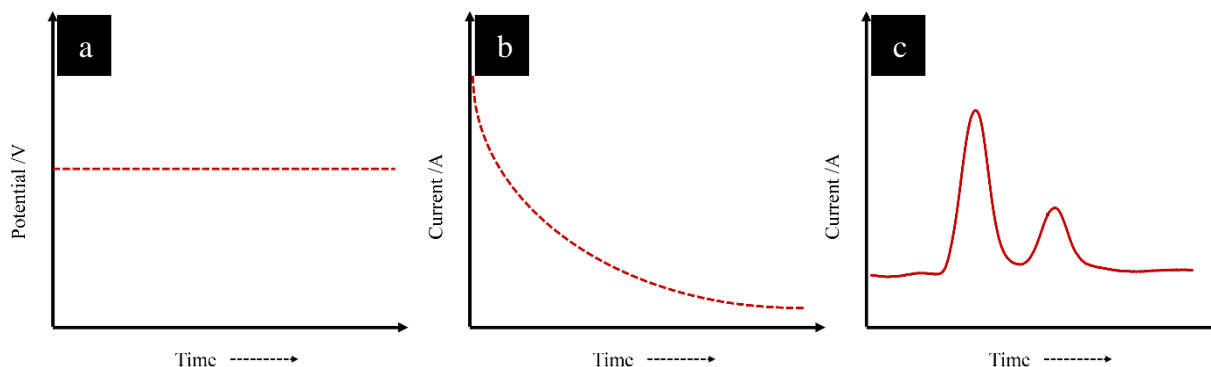


Figure 2.9 (a) The excitation waveform (b) the resulting current-time response under static condition (c) the resulting current-time after integrated with flow system.

2.3.3.3 Electrochemical Impedance Spectroscopy (EIS)

Electrochemical impedance spectroscopy (EIS) is one of the most complex techniques, measuring the resistance capability of electrons flowing through the working electrode. Unlike resistance, the impedance is observed in alternative current (AC) circuits which disobey the Ohm's law. For EIS measurement, a sinusoidal voltage is applied across the three-electrode system and the change in frequency of an input sinusoidal signal is monitored^{57, 65}. With the common knowledge about calculation of the frequency shift to complex numbers in impedance, it can be described in term of the real part of impedance Z' , referring to the resistance, and imaginary part Z'' , standing for capacitance". The equation of complex number in impedance toward the Z' and Z'' parameters is presented below.

$$Z(\omega) = \frac{E}{i} = Z_0 \exp(i\phi) = Z_0 \exp(\cos\phi - j\sin\phi) = Z'(\omega) - Z''(\omega) \quad (2.5)$$

Where Z is the impedance, Z_0 is the impedance, which is expressed in term of a magnitude, E is the potential, I is the response signal, ϕ is the phase shift and ω is the radial frequency.

The plot of Z' and Z'' is called Nyquist plots (Figure 2.10). With this relevant feature, the EIS is normally used as surface sensitive tool for studying the morphology of electrode surface after modification. Additionally, the EIS technique is extensively applied for biosensors and other label-free assays.

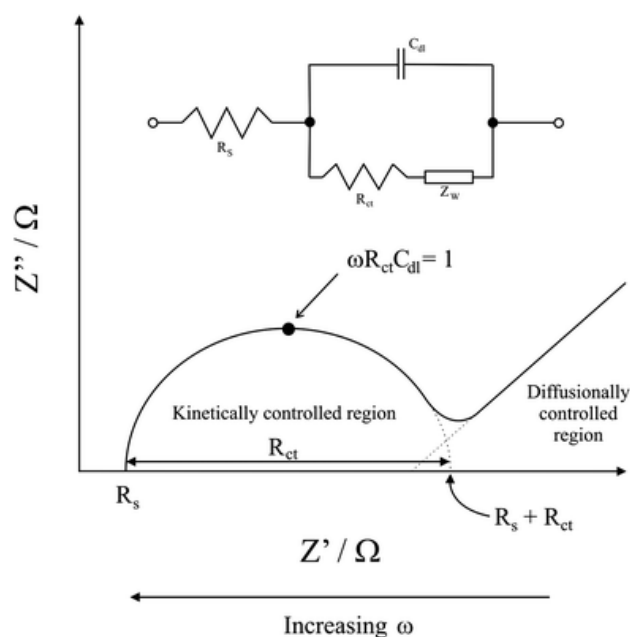


Figure 2.10 The Nyquist plot from simple Randles equivalent circuit for an electrochemical cell including the solution resistance (R_s), double layer charging at the electrode surface (C_{dl}), charge transfer resistance (R_{ct}), and the Warburg Element (Z_w)

65.

CHULALONGKORN UNIVERSITY

2.3.4 Electrochemical cell / instrumentation

In electrochemical process, the electron flow through the electrode/electrolyte interface is considered. For electrolyte phase, the charge species are moved under influence of electric field. This movement of ionic species in electrolyte phase can eliminate the migration of the interested analyte as addressed in Chapter 2.3.2. The liquid aqueous phase containing ionic species such as H^+ , Na^+ , K^+ and Cl^- are frequently employed as electrolyte in the electrochemical system. As for the electrodes, the electrochemical cell basically consists of three electrodes which

are working electrode (WE), reference electrode (RE) and auxiliary/ counter electrode (CE) which are described below⁶⁶.

2.3.4.1 Working electrode (WE)

A working electrode (WE) is the most crucial electrode at which the redox reaction (oxidation or reduction) of the interested analyte is occurring. An oxidation reaction is driven by the application of positive potential toward WE. In contrast, the reduction reaction is driven by the application of the negative potential toward WE⁶⁷. Thus, the WE should have wide potential range suitable for monitoring an oxidation/reduction reaction. Additionally, it must be stable toward the corrosion attributing to the electrochemical process. With this perspective, the carbon-based material such as boron-doped diamond, screen-printed graphene electrode has been attractive used to make the WE. However, the carbon-based material still suffers from poor sensitivity and selectivity of some organic molecule. To improve these factors, the modifiers, in particular metal nanoparticles and polymers, are extensively used for the electrode modification. The property of carbon-based and other modified electrodes used in this dissertation is discussed below.

2.3.4.1.1 Boron-doped diamond electrode (BDD)

A boron-doped diamond electrode (BDD) has found wide-spread use for electrochemical oxidation of various organic compounds due to its excellent physical and chemical property⁶⁸. The characteristic of BDD is wide solvent window, low background (low capacitance), high fouling resistance, stable at high temperature and pressures or in challenging environments, and biocompatibility^{25, 69}. For BDD preparation, it is frequently produced by a chemical vapor deposition (CVD) technique at low pressure. Firstly, the diamond is synthetically grown onto silicon substrate by CVD. It relies on the generated carbon radical and the disassociated hydrogen (H) of gas phase carbon source at high temperatures, typically greater than 700 degree Celsius ($^{\circ}\text{C}$). Due to the wide band gap semiconductor of around 5.47 eV at 300 K ⁶⁹, it makes diamond useless in electrochemical process. Thereby, the dopant impurities will be

added to improve the conducting property of diamond electrode. Because of its high replacement capability toward displaced carbon atoms position with a relatively small activation energy (0.37 eV), the boron is employed as the preferred dopant for improving electrical property of diamond, produced by CVD technique using diborane (B_2H_6) or trimethyl borate ($B(OCH_3)_3$) as the boron source. Although, the BDD offers several advantages as mentioned above, it still suffers from the low electrocatalytic activity. This drawback can be improved by modifying the BDD surface with metal nanoparticles, as described in detail later in Chapter 2.3.4.1.3.

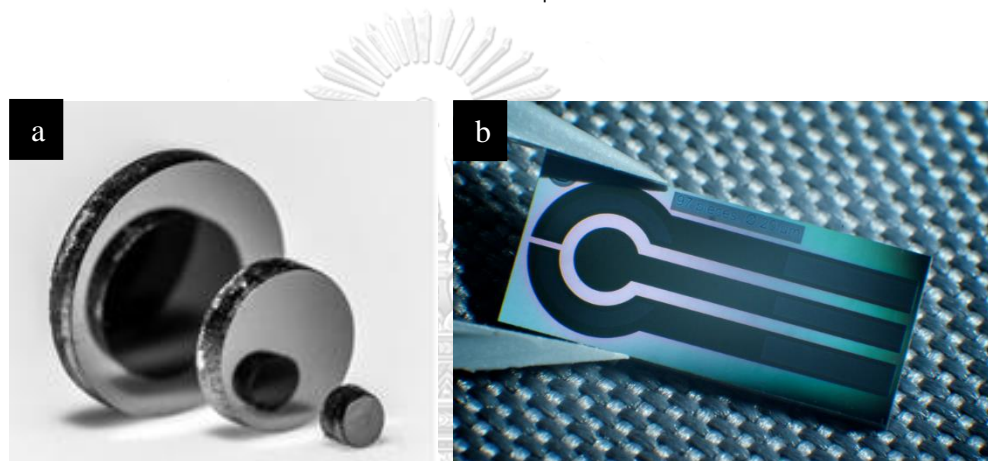


Figure 2.11 (a) Freestanding BDD electrode⁶⁹ (b) Commercial BDD electrode⁷⁰.

2.3.4.1.2 Screen-printed graphene electrode (SPGE)

Graphene is a one-atom-thick sp^2 -bonded carbon sheet exhibiting a high electron conductivity, fast heterogeneous electron-transfer rate at edges and basal-plane defect sites of graphene sheet and good biocompatibility. For the graphene-based electrochemical sensor, there are numerous fabrication methods such as drop-coating⁷¹, ink-Jet printing⁷², and screen-printing method^{35, 71}. Among these fabrication methods, the screen-printing offers the inherent superiority of its manufacturing process, consisting of the inexpensiveness, high throughput, facileness and good reproducibility^{73, 74}. Therefore, the graphene-based screen-printing method has been applied for diverse applications throughout the year. Nevertheless, it still has the low

electrocatalytic activity and lacks selectivity toward the oxidation of some organic compounds. To handle these drawbacks, the nanomaterials and polymeric modifiers are required for the modification of electrode surface, as described below.

2.3.4.1.3 Modified electrodes

For further improvement of the electrocatalytic property (in terms of sensitivity and selectivity), the noble metals and diverse supporting materials including polymer, carbon black, graphene oxide and reduced graphene oxide have been used for the modification of electrode surface. The noble metal nanoparticles and polymers, employed as electrode modifiers in this dissertation, are described below.

2.3.4.1.3.1 Noble metal nanoparticle modified electrode

Up to date, the nanostructured metal (such as platinum; Pt, Gold; Au, palladium; Pd) and copper; Cu) is the most promising modifier for electrode modification, due to their unique properties of high catalytic activity toward, high surface area and excellent sensitivity improvement. Among these noble metals, gold nanoparticle (AuNP) is extensively used for electrode modification for electrochemical determination of pesticide^{18, 75} and phenolic compound⁷⁶ attributing to their high catalytic activity toward the oxidation of hydroxy (-OH) and sulfur (-SH) containing substances⁷⁷. In addition to AuNPs, the palladium nanoparticle (PdNP) is the most interesting modifier toward the oxidation of phenolic compound. PdNPs are able to enhance the electron transfer rate of phenolic compound at electrode interface resulting in the increase in sensitivity of the electrochemical detector⁷⁸. The monometallic modified electrode suffers from poor durability and high cost of modifier. Furthermore, the bimetallic and trimetallic modified electrodes have been developed through many researchers' attempt. These combinations of metal elements such as PtAu³⁴, PtFeNi⁷⁹, PtPdRu⁸⁰, PtPdCu⁸¹ and NiPtPd⁸², exhibited superior catalytic activity compared to the monometallic material. Additionally, the synergistic property of flexible and tunable composition can satisfy the varied demands for the decent electrochemical sensors.

2.3.4.1.3.2 Polymer-based modified electrode

The use of conducting polymer-based materials, especially polyaniline (PANI) and poly(3,4-ethylenedioxythiophene) : poly(styrenesulfonate) (PEDOT:PSS), for improving the sensitivity of electrochemical sensor are broadened. These polymeric modifier exhibits the environmental stability⁸³, good electrical conductivity^{84, 85}, facile modification⁸³ and biocompatibility⁸⁶, making their use beneficial for several application such as super-capacitor⁸⁷ and electroanalytical sensor^{83, 86, 88}. Beside the sensitivity improvement, the polymeric film-based recognition system known as molecularly imprinted polymer (MIP) has been attracted attention for selectivity enhancement in electrochemical sensor. The MIP is identified as “the synthetic polymer”, exhibiting selective recognition sites of its cavities to the functionality and shape of the target molecule^{89, 90}. For MIP polymerization, the desired geometrical and chemical match of MIP cavities can be easily tailored through the polymerization process using necessary component as follows: (i) The template is the interested molecule including complex or a molecular, ionic or macromolecular assembly, and micro-organisms, (ii) the monomer is the substance that can strongly bind with the template and form a specific complex with the template before polymerization, (iii) the cross-linker is considerable factor, used to fix the monomer-template formation and formed highly cross-linked rigid MIP polymer⁹¹. Once template is removed, the vacated recognition cavities are generated complementary to the template species. The MIP technique offers advantages of straightforward preparation, high physical stability, noticeable robustness, making it attractive in many fields, especially in electrochemical analysis^{26, 28}.

2.3.4.2 Reference electrode (RE)

A reference electrode (RE) should have the constant and well-known potential unaffected by the environmental system. The RE is employed to provide a standard potential for electrochemical process by controlling the applied potential toward WE. The most common one typically used as the primary reference electrode is Ag/AgCl electrode. It is constructed by immersing a Ag wire in a saturated solution of Ag and

KCl⁹². Currently, the commercial Ag/AgCl ink has been developed to enable facile fabrication by screen-printed method.

2.3.4.3 Counter electrode (CE)

A counter electrode (CE) permits the flow of current toward WE for completing the circuit without disturbing the potential at RE. Therefore, the inert materials such as carbon and platinum are required for constructing the CE which has the opposite redox reaction against the WE⁹³.

2.4 Chromatography technique

Chromatography is one of the most established technique that employed for separating a mixture of chemical substances to its individual constituent. There are numerous types of chromatography techniques which are high performance liquid chromatography (HPLC), gas chromatography (GC), ion-exchange chromatography and affinity chromatography. Herein, the detailed principle of liquid chromatography (LC) is described below.

2.4.1 Principle of high-performance liquid chromatography (HPLC)

The separation of LC is basically relied on the distribution of the interested analytes between a mobile phase and a stationary phase, contained within the HPLC column. In HPLC measurement, the analyte is introduced into the column and then delivered through the column by the mobile phase. As analyte travel through the column, it can be separated due to the difference of physicochemical interaction with the stationary phase. The hydrophobic interaction is most frequently used in this separation system. Finally, the analyte is eluted in an order according to the strength of its interaction which depends on its properties.

The measurement in HPLC is described in term of four key concepts which are capacity, efficiency, selectivity, and resolution⁹⁴. The detail of these major concepts is explained below.

2.4.1.1 Capacity Factor

The capacity factor (k'_R) is used to define the efficiency of the HPLC column in term of the capacity to retain sample and the separation ability to separate the analyte component. Furthermore, k'_R factor can be determined from the strength of the interaction between the analyte molecule and the packing material within the LC column as expressed in equation 2.6.

$$k'_R = \frac{t_r - t_0}{t_0} = \frac{t'_r}{t_0} \quad (2.6)$$

Where t_r is the retention time of the interested analyte

t_0 is the column's void time

t'_r is the adjusted retention of the interested analyte

2.4.1.2 Column selectivity

The selectivity of the chromatographic system is a term used to describe the separation efficiency of between two components. The separation factor is defined in term of α .

$$\alpha = \frac{t_2 - t_0}{t_1 - t_0} = \frac{k'_2}{k'_1} \quad (2.7)$$

The α value range from 1 which derived by the elution time of component 1 and 2. To improve the selectivity, the significant factors controlling the changing selectivity by the alteration of the analyte and stationary phase interaction, are the mobile phase component and stationary phase type.

2.4.1.3 Column efficiency

Theoretically, the chromatographic column is considered to be composed of numerous individual section, known as "plates", which permit the analyte to equilibrate between the mobile phase and stationary phase. Thus, the greater number of theoretical plates (N), are the more efficient chromatographic column is considered to be. These terms are expressed as follows:

$$N = \frac{L}{H} \quad (2.8)$$

Where L is the length of the column (millimeter, mm)

2.4.1.4 Resolution

The resolution (R_s) is defined as the degree of separation in the proposed chromatographic system. This factor is influenced by capacity, selectivity, and efficiency of the column. The relationship of these factors is expressed below.

$$R_s = \left(\frac{\sqrt{N}}{4}\right) \left(\frac{\alpha-1}{\alpha}\right) \left(\frac{k'_{12}}{1+k'_{12}}\right) \quad (2.9)$$

The R_s value greater than 0.5 is acceptable for quantitative analysis because the peak of two interested analytes are well separated.

2.4.1.5 Band Broadening

The narrow band width of the sample becomes broad after traveling through the column. This phenomenon is actually caused by the transport mechanisms of the analyte through a chromatographic column. There are three powerful mechanisms as follows: (i) the mass transport in mobile phase, (ii) the mass transport in stationary phase and (iii) the longitudinal diffusion. These diffusion factors, contributing to the band broadening phenomena, are considered in terms of the rate theory described by the Van Deemter equation.

$$H = A + \frac{B}{\mu} + (C_s + C_m)\mu \quad (2.10)$$

Where A is the factors relevant to the multipath flows of the analyte in column (called Eddy diffusion), B is referred to the longitudinal diffusion and the C_s and C_m represent to the mass transport resistance in stationary phase and mobile phase, respectively, μ is referred to the velocity⁹⁵.

2.4.2 Instrumentation of HPLC

Figure 2.12 shows the representation of the HPLC system. There are main five components in HPLC system including the solvent reservoir, the sample injection, the pump, chromatographic column, and detector⁹⁶. A brief description of each component is given in this section.

2.4.2.1 Solvent reservoir

The mobile phase in HPLC system is typically a mixture of the polar and non-polar liquid component contained in a glass reservoir. The concentration of mobile phase relating to the composition of the sample is considered. Consequently, the elution method is divided into two methods which are isocratic elution and gradient elution. The isocratic elution is the use of constant mobile concentration throughout the separation process, meanwhile the gradient elution changes mobile phase concentration throughout the separation process. The mobile phase concentration in HPLC system is controlled by solvent programming.

2.4.2.2 Sample injection system

A micro-syringe is frequently used for direct injection of the sample into the column. Recently, the auto sampling device in HPLC system is developed for user convenience. The simplest way of injection is the use of an injection valve. It allows the specific volume of the sample passing through the column. The amount of the injected sample is usually varied in the range of 10 – 100 μL

2.4.2.3 Pump

Pump is typically employed for delivery of the mobile phase throughout the chromatographic column. Since the change in solvent flow rate will affect the retention time in the identification of the analysis. The pump system is important to use for maintaining the constant flow rate during the analysis. The normal operating pressure of the pump system is around 0-4000 psi. The efficiency in separation increases with the increasing flow rate. Therefore, the flow rates are generally operated at high psi.

2.4.2.4 Column

The separation process is performed inside the column, either coated liquid stationary phase, or loaded packing solid particle. The columns normally have an internal diameter (i.d) in the range of 4.5 to 5 mm and the length of 10 to 25 cm. Additionally, the number of theoretical plates (N) is influenced by the length of the column. The longer length provides the higher N resulting the high separation

efficiency. However, it suffers from the long-time analysis. While the shorter column offers rapid analysis, but the N is limited. The analysis time and separation efficiency are compromisingly considered. In addition, the chemical composition of the analyte importantly influences the selection of stationary phase. There are various types of stationary phase encountered inside the column such as silica, styrene-divinylbenzene, polysaccharide or octadecyl chain (C18). Therefore, the stationary types and column length are crucial factor for naturally varied application.

2.4.2.5 Detector

The use of HPLC detector relies on the analyte. The HPLC detector is classified into two types which are universal detector and selective detector. The response of universal detector, such as the refractive index IR and conductometric detector, is derived from the similar structure of the interest molecule, whereas the response of selective detector is obtained by the specific molecular structure of the analyte. The absorbance, fluorescence, and electrochemical detectors are termed selective detectors, popularly utilized for HPLC analysis.

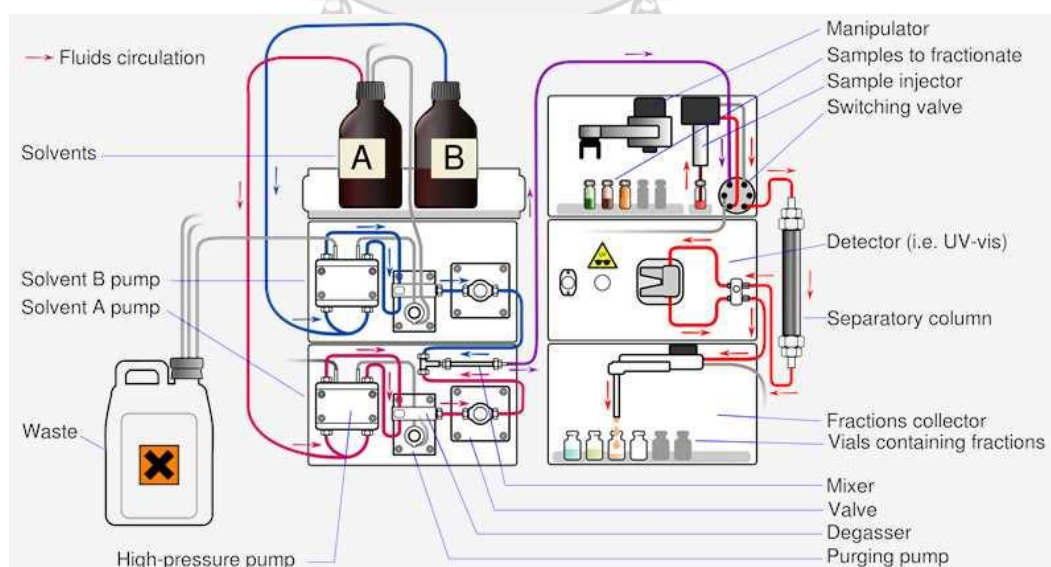


Figure 2.12 Preparative HPLC system.

2.4.2.6 Ultra-high-performance liquid chromatography (UHPLC)

The ultra-high-performance liquid chromatography (UHPLC) is the other type of HPLC relying on similar principles of liquid chromatography. UHPLC is constructed to improve the efficiency and analysis time of the HPLC separation by the development in term of instrumentation. The comparison between HPLC and UHPLC regarding the equipment and separation efficiency is expressed in Table 2.1

Table 2.1 The comparison between HPLC and UHPLC ⁹⁷

Parameter	HPLC	UHPLC
Pressure	6000 psi	100,000 psi
Particle size	5 μm	1.7 μm
Flow rate	mL/min	$\mu\text{L}/\text{min}$
Resolution	Relatively low	Relatively high

The separation efficiency of UHPLC is improved by greatly reducing packing particles and increasing flow rate operation. Thus, the band broadening is reduced, leading to sensitivity enhancement.

CHAPTER 3

THE DEVELOPMENT OF INTEGRATED PLATFORMS FOR COLORIMETRIC SENSOR AND ITS APPLICATION

Colorimetry has been promisingly and powerfully integrated to the miniaturized platforms in the past two decades. This colorimetric detection platform offers portable device, simple operation, affordability and easy-to-use. In this chapter, the transparency-based colorimetric sensor was fabricated for salbutamol (SAL) determination. The detail of this work is reported below.



3.1 Development of transparency-based analytical device for facile colorimetric determination of salbutamol

Atchara Lomae^a , Sudkate Chaiyo^{a,b} , Orawon Chailapakul^a , Weena Siangproh^{c*}, and Janjira Panchompoo^{a**}

^a Electrochemistry and Optical Spectroscopy Center of Excellence, Department of Chemistry, Faculty of Science, Chulalongkorn University, Pathumwan, Bangkok 10330, Thailand

^b The Institute of Biotechnology and Genetic Engineering, Chulalongkorn University, Pathumwan, Bangkok, 10330, Thailand

^c Department of Chemistry, Faculty of Science, Srinakharinwirot University, Sukhumvit 23, Wattana, Bangkok 10110, Thailand



**Corresponding author

*Co-corresponding author

Abstract

The low-cost and portable transparency-based analytical device (TAD) for colorimetric determination of salbutamol (SAL) was first developed. The TAD was simply fabricated by wax-printing onto a transparent polymer-based substrate to create the hydrophobic barriers and the colorimetric reaction zones where the color changes could be easily observed with the naked eye. In this work, potassium permanganate (KMnO_4) was simply used as a colorimetric reagent for SAL. Once SAL reacted with KMnO_4 in the acidified system, it could undergo oxidation and the color of KMnO_4 subsequently changed from light pink to orange. The reaction color could also be recorded using a digital camera and then analyzed by ImageJ for quantitative analysis. Under the optimized conditions, the developed method together with the TAD exhibited high efficiency for SAL determination with a linear calibration ranging from 0.5 to 40 $\text{mg}\cdot\text{L}^{-1}$. Limits of detection (LOD) and quantitation (LOQ) were found to be 0.05 and 0.17 $\text{mg}\cdot\text{L}^{-1}$, respectively. Furthermore, the proposed TAD-based sensor was applied for SAL determination in drug samples with %recovery and %RSD in the ranges of 81.00 to 108.87% and 1.32 to 7.53%, respectively.



Keywords: Salbutamol; Potassium permanganate; Transparency-based analytical device; Colorimetric detection; Redox reaction

3.1.1 Introduction

Salbutamol (SAL), which belongs to a class of β_2 -adrenergic agonists, is commonly used as bronchodilator for the treatment of human chronic obstructive pulmonary disease and asthma^{98,99}. Besides, SAL is generally employed in veterinary medication¹⁰⁰ as it can induce relaxation of smooth muscle and decrease systemic vascular resistance¹⁰¹. However, high doses of SAL have anabolic-like effects (e.g. promoting protein production for muscle build-up and enhancing strength performance) which are sometimes used illegally by athletes in sports. According to the World Anti-Doping Agency (WADA), the concentration of SAL greater than 1000 ng/mL (equal to 3 μ M) found in urine literally indicates the doping behavior in athletes^{22, 102-104}. Moreover, SAL is the most common β_2 -agonist used in animal feed as growth promoter and meat leaner, enhancing the transformation of nutritive body fat to more muscle in livestock⁹⁸⁻¹⁰⁰. However, SAL used in animals for growth promotion would readily accumulate in their tissues and organs and could directly be transferred to humans through the food chain (e.g. consumption of animal products), causing serious effects on human health in numerous symptoms including palpitation, tremors and nervousness^{98,99}. The use of SAL as growth promoter has generally been banned in many countries, especially in China and the European Union^{105, 106}. Therefore, the development of a reliable and sensitive analytical device and method for determination of SAL with quick identification and confirmation is crucially needed to control the drug abuse for both growth promotion and sports-doping.

According to the literature, various analytical techniques have previously been developed for SAL determination, including UHPLC-ECD⁷⁸, HPLC-UV/Vis¹⁰⁷, LC-MS¹⁰⁸, LC-MS/MS¹⁰⁶, UPLC-MS/MS¹⁰², CE^{109, 110} and immunoassay¹¹¹. Although these methods are comparatively precise and sensitive, they inevitably have some disadvantages, such as time-consuming process, complicated procedure, expensive instrumentation, and unsuitable for quick screening test and on-site applications¹¹².

¹¹³. Consequently, colorimetry which has become highly attractive for qualitative and quantitative analysis seems to be the potential method for rapid detection of SAL, due to its simplicity, straightforward signal readout, minimum sample and reagent consumption, and inexpensive apparatus. Considering the colorimetric readout, UV-vis spectrophotometer has been reported to be the traditional tool for colorimetry ^{114, 115}, but the instrument itself is still somewhat sophisticated and unsatisfactory for on-site applications. Hence a digital camera or a camera phone accompanying with the image processing application has been simply used as an alternative device for colorimetric detection with potential applications for point-of-care and on-site testing ¹¹⁶⁻¹¹⁸. Moreover, the microfluidic technology has been currently utilized for miniaturization of various portable devices, making them fitting for field-based testing applications. Generally, papers have been widely used as substrates in this technology, to fabricate various types of “paper-based analytical devices (μ PADs)”. Since first development in 2007, the μ PAD has experienced rapid growth over the past decade because of their affordable, simple and portable properties ^{119, 120}. Other polymer-based materials such as plastic commercial films (both transparent and opaque) which are made of either polyvinyl chloride (PVC) or polyethylene terephthalate (PET) have also become of great interest as substrate materials due to their chemical inertness, physical robustness, excellent flexibility and high resistance to water and moisture, resulting in the long term stability and durability, compared to the μ PADs ¹²¹.

In this work, the transparent polymer-based material, namely PET has been first employed as substrate for the fabrication of a portable gadget, so-called “transparency PET-based analytical device (TAD)” for colorimetric determination of SAL. Unlike the μ PADs, the developed TAD could be simply manufactured by wax printing onto the PET sheet, generating the hydrophobic regions and the transparent colorimetric detection areas where a vivid color change could be obviously seen (owning to the high transparency of PET). The obtained TAD could then be used compactly in

association with a simple colorimetric method in which the acidified potassium permanganate (KMnO_4) was basically employed as reagent for facile colorimetric determination of SAL. Typically, potassium permanganate is a well-known strong oxidizing agent that could quickly oxidize SAL in acidic system, while the permanganate itself would simultaneously undergo reduction, resulting in the color change (from light pink to light orange) which could be clearly observed either by the naked eye for qualitative screening test, or by a digital camera together with an image processing software for quantitative analysis. Subsequently, the proposed colorimetric device and method could be potentially applied for SAL detection in bronchodilator drug samples with comparable results to those labelled on the medicine, demonstrating a proof of concept for quality control in pharmaceutical industry.

3.1.2 Experimental

3.1.2.1 Chemicals and materials

Salbutamol sulfate was purchased from Sigma-Aldrich (Missouri, USA). Potassium permanganate (KMnO_4) used as colorimetric reagent was obtained from Carlo Erba Reagents (Chaussée du Vexin, French). To determine the exact concentration of potassium permanganate solution; once prepared, it was standardized with sodium oxalate ($\text{Na}_2\text{C}_2\text{O}_4$) which was bought from J.T. Baker chemical company (Loughborough, UK). Sulfuric acid (H_2SO_4) was gained from Merck (reagent grade 95-97%, Gernsheim, Germany). Milli-Q water from Millipore ($R \geq 18.2 \text{ M}\Omega \text{ cm}$) was used throughout experiments.

3.1.2.2 Design and fabrication of TADs

A wax-printing technique, which has been reported to be a simple, fast and low-cost method for the fabrication of various μ PADs^{41, 122, 123}, was deliberately used in this work to create the TAD. Generally, the device pattern designing was performed by Adobe illustrator software, and the wax-pattern layout was then printed onto the transparency-based PET sheet (bought from local store in Bangkok, Thailand) using the wax printer (Xerox ColorQube 8570, Japan) in order to create the hydrophobic barrier and the transparent colorimetric reaction zone with diameter of 0.6 cm. Note that the color of hydrophobic wax-pattern was selected to be complementary to the colorimetric reaction region.

3.1.2.3 Colorimetric detection of SAL on the TAD

Potassium permanganate was simply used as a colorimetric reagent for SAL detection. The measurement was performed as follows: 10 μ L of KMnO_4 were directly dropped onto the transparency PET-based device at the transparent reaction zone, following by 20 μ L of H_2SO_4 and 5 μ L of standard SAL (with varying concentrations), respectively. Next, the final volume of solution mixture was adjusted to 40 μ L using Milli-Q water. The color change (from pale pink to varying shades of tinted orange, depending on the concentration of SAL) at the reaction zone could subsequently be observed by the naked eye within the optimized reaction time of 11 min, applicable to qualitative measurement. As for quantitative analysis, the image of the resulting color of the solution mixture on the TAD was thoroughly recorded by a digital camera (Cannon EOS 1000 D1, Japan) in a light-control box, and the color intensity of the sample solution was then measured by ImageJ software. Finally, a calibration curve showing the relationship between color intensity and concentration of SAL could be constructed.

3.1.2.4 Analysis of SAL in pharmaceutical samples

Various brands of pharmaceutical tablets containing SAL (purchased from drug store) were used for validation of the proposed colorimetric method with the developed TAD. Firstly, the tablets were weighed out in order to determine the average weight per tablet, and they were ground using a mortar and pestle. Then, a certain amount of sample powder was weighed once again into a 100-mL volumetric flask. After that, the drug sample was extracted with 50 mL of Milli-Q water for 1 h in a shaker, followed by a sonication in an ultrasonic bath for 10 min. The final volume of sample solution was subsequently adjusted to 100 mL using Milli-Q water. The obtained sample solution would then be filtered through a 0.45 μM polytetrafluoroethylene (PTFE) syringe filter to remove undissolved binder, prior to use in the experiment^{103, 124, 125}.

Regarding the recovery study, it should be noted that the standard SAL was spiked into the sample solution before the extraction in three different concentrations of 2.5, 10.0 and 25.0 ppm, respectively. The percent recovery of SAL added to the drug sample could then be calculated from these spiked samples.

3.1.3 Results and discussion

3.1.3.1 Colorimetric determination of SAL on the TAD

In this work, SAL was first determined using potassium permanganate (KMnO_4), a very common oxidant, as a colorimetric reagent. Once SAL reacted with permanganate in an acidified system at room temperature, the color of permanganate would simply change from light pink to pale orange which could be clearly observed, as shown in Figure 3.1.

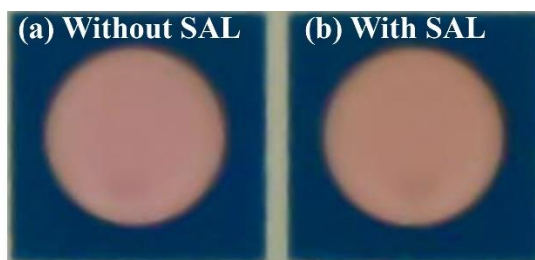
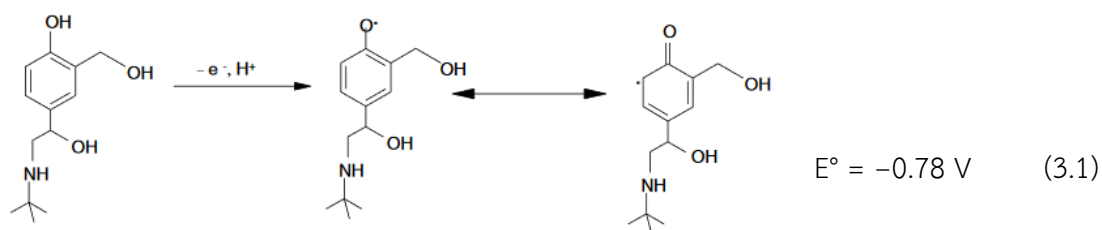


Figure 3.1 TAD with the reaction solution of 0.15 mM KMnO_4 in 0.5 mM H_2SO_4 in the absence (a) and presence (b) of 10 ppm SAL, and the color change from light pink (a) to pale orange (b) could be clearly observed on the TAD.

The reaction of SAL and potassium permanganate which caused the color change could be simply explained by a redox process and the corresponding standard half-cell potentials (E^0) of both half reactions. Typically, permanganate has been very well known to be a powerful oxidizing agent, and the oxidation behaviour of SAL has also been extensively reported in the literature. Therefore, in this colorimetric measurement, SAL which was colorless would get oxidized with its standard half-cell potential of $-0.78 \text{ V vs SHE}^{22}$, as shown in Eq (1), whereas the pale pink permanganate ion would simultaneously undergo reduction in mildly acidic condition with the reported standard reduction potential of $+1.68 \text{ V vs SHE}^{126}$ to form the brownish manganese(IV) oxide (MnO_2), leading to the color change from light pink to orange, as shown in Eq (2). The standard cell potential (E_{cell}^0) of this redox reaction could be calculated and it was found to be $+2.46 \text{ V vs SHE}$, confirming the spontaneous reaction between SAL and permanganate ion.



In addition, the fabrication of the miniaturized colorimetric devices for SAL detection has been thoroughly investigated by wax-printing onto two types of substrates, including paper and PET sheet which resulted in the PAD and the TAD, respectively. The results demonstrated that the TAD seemed to be more compatible with the proposed redox-based colorimetric detecting method, giving more intense and well steady color which could be precisely observed, compared to the PAD, as shown in Fig 2. It can be seen that the pink color of the permanganate itself on the PAD seemed already too faded at the beginning (Figure 3.2a), and when SAL was subsequently added to react with the permanganate reagent, the color change became less intense and unstable (Figure 3.2b). This could be possibly due to the side reaction between the oxidizing permanganate agent and the cellulose-based paper where the cellulose could also get oxidized by permanganate, resulting in the unclear and inconsistent color of the reagent on the PAD¹²⁷. Therefore, the transparent PET sheet was chosen as substrate material for the fabrication of colorimetric TAD sensor as it was chemically inert towards the permanganate ion, and it also provided a vivid color change for SAL determination.

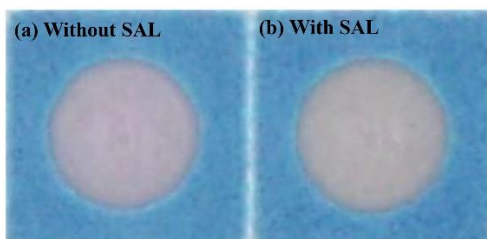


Figure 3.2 PAD with the reaction solution of 0.15 mM KMnO_4 in 0.5 mM H_2SO_4 in the absence (a) and presence (b) of 10 ppm SAL, where the color change could not be clearly observed on the PAD.

3.1.3.2 Optimization of colorimetric detection conditions for SAL analysis

The experimental conditions for the colorimetric determination of SAL on the TAD have been next investigated. Since the colorimetric detection was performed under the acidified system using permanganate as the reagent, the corresponding parameters, including type of acid, concentration of acid, concentration of permanganate reagent, reaction time, and reaction temperature were therefore optimized. In this study, a representative SAL concentration of 10 ppm was used constantly in the optimization as it would cause a well detectable color change, and the color intensity of the reacting solution before and after SAL addition was measured and reported as I_{blank} and I_{sample} , respectively. The intensity value of the color change (ΔI) according to the redox reaction between permanganate and SAL could then be quantitatively calculated by subtracting the blank solution from the sample response ($\Delta I = I_{sample} - I_{blank}$).

3.1.3.2.1 Effects of acid type

The influence of acid type on the colorimetric detection of SAL was first examined using various strong and weak acids, including sulfuric acid (H_2SO_4), hydrochloric acid (HCl), perchloric acid (HClO_4), nitric acid (HNO_3), and acetic acid (CH_3COOH) at the same concentration of 1 mM. Figure 3.3 shows the plots of sample's color intensity change (ΔI) against various types of acid used in this study. As clearly

seen from the results, different types of acid, either strong or weak ones, did not seem to have a significant effect on the color change of permanganate when reacted with SAL. However, it should be noted that the redox reaction between permanganate and SAL had to be done in acidic medium as the reduction process generally required additional protons, as illustrated in Eq (3.1). Therefore, sulfuric acid was chosen as acid species used further in this work, according to the previous study reported by J. Huclová, *et.al.*¹⁰⁴ Moreover, sulfuric acid would dissociate into sulfate ion which was the common ion already present in the system from the dissolution of salbutamol sulfate ($C_{13}H_{21}NO_3 \cdot 0.5H_2SO_4$) used as standard SAL reagent.

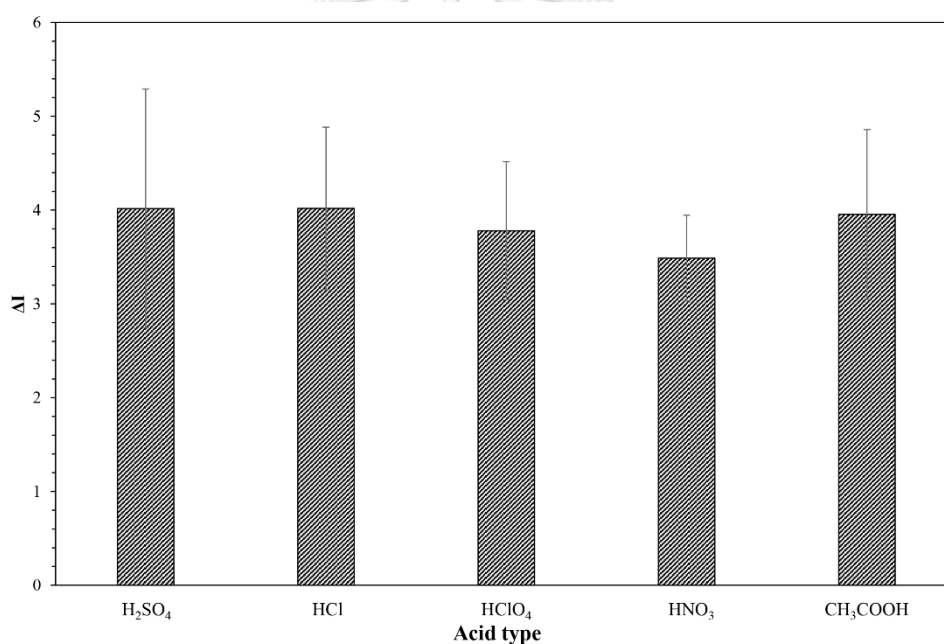


Figure 3.3 Effects of acid type on the colorimetric determination of SAL using permanganate in acidic medium as reagent.

3.1.3.2.2 Effects of sulfuric acid concentration

The concentration of sulfuric acid that might affect the color change intensity in the colorimetric measurement of SAL was next examined over a range of 0.2 – 3.0 mM, and the obtained results were displayed in Figure 3.4a. It could be clearly

observed that the color change intensity (ΔI) of the reacting solution increased with increasing concentration of sulfuric acid from 0.2 to 0.5 mM. After that, the ΔI intensity decreased constantly with increasing concentrations of sulfuric acid up to 3.0 mM. As discussed earlier that the reduction of permanganate would generally occur under slightly acidic condition (*cf.* Eq (3.1) indicating the four-proton-accepting reaction), the mild concentration of sulfuric acid of 0.5 mM likely seemed to be more favored by that redox reaction, showing the highest color change intensity. When high concentrations of sulfuric acid (with several more protons as well) were present in the system, the permanganate ion could further undergo a five-electron and eight-proton transfer reduction to form the colorless Mn^{2+} , leading to the drop in orange-ish color intensity, as observed in this study. Therefore, the optimal concentration of sulfuric acid highly capable of detecting SAL was found to be 0.5 mM.

3.1.3.2.3 Effects of permanganate concentration

The effects of permanganate concentration used as the colorimetric reagent was subsequently investigated in a concentration range of 0.1 – 0.3 mM, and the corresponding results were shown in Figure 3.4b. Typically, the ΔI values increased with increasing concentration of permanganate ion up to 0.15 mM. When the permanganate concentration was above 0.15 mM, the color change intensity got declined instantly. Since high concentration of permanganate would give an intense purple color which could not visibly fade away during the redox reaction, the color change of this intensely purple permanganate could not be clearly observed during the reaction with SAL. Consequently, the concentration of 0.15 mM $KMnO_4$, possessing a pale pink color was selected as an optimal condition for further measurements.

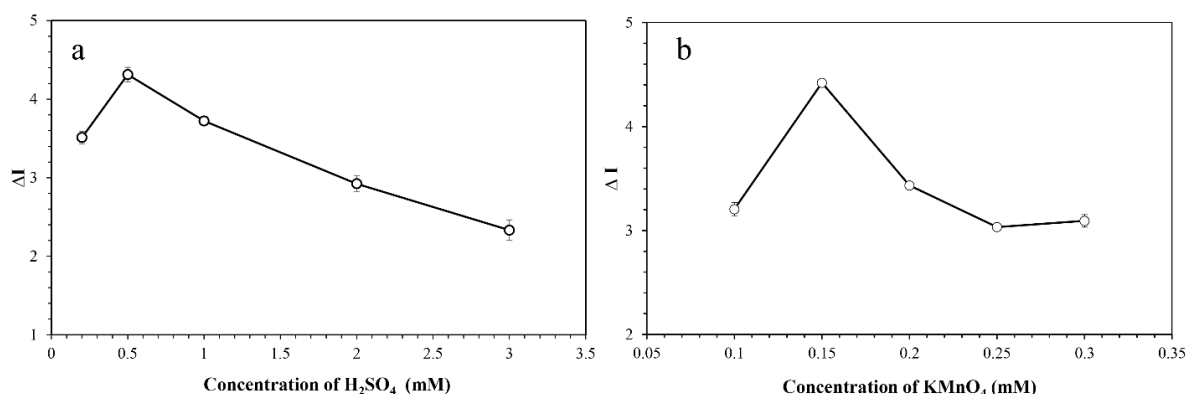


Figure 3.4 Plots showing the effects of experimental parameters, including (a) concentration of H_2SO_4 , and (b) concentration of KMnO_4 on the colorimetric determination of SAL.

3.1.3.2.4 Effects of reaction time and temperature

The reaction time and temperature that would play an important role in the reaction kinetics have been also investigated. Briefly, the effects of reaction time and temperature were studied within 1–20 min at 25 °C, and 1–15 min at 30, 40 and 50 °C, respectively. Figure 3.5 shows the color change intensity (ΔI) observed over a range of time at increasing temperatures. The highest color change intensity could be achieved within 14, 11, 8 and 5 min at 25, 30, 40 and 50 °C, respectively, indicating that the maximum reaction had already developed. The results clearly demonstrated that the reaction rate increased with increasing temperature. However, at the temperatures above 30 °C (*cf.* Figure 3.5c and d), the sample's color intensity observed at the largest values of ΔI got somewhat decreased, resulting in lowering the sensitivity of the detection by *ca.* 18.2% when compared to the highest ΔI obtained at 30 °C. Therefore, the reaction temperature of 30 °C together with the 11 min reaction time were chosen as the optimal conditions for the quick and sensitive determination of SAL.

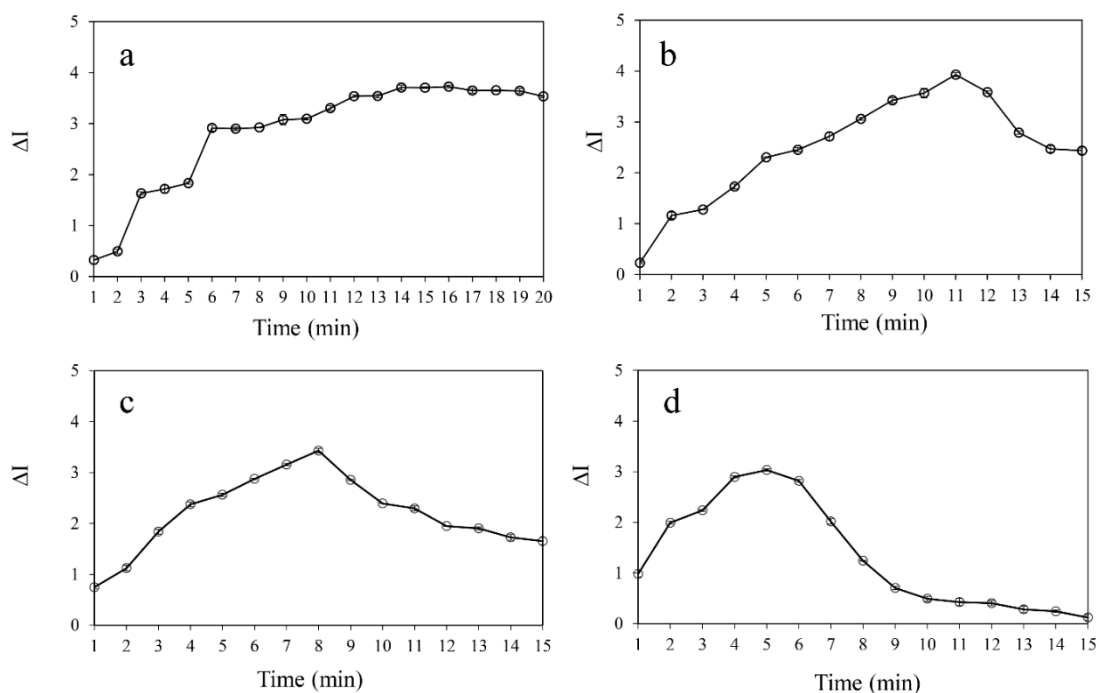


Figure 3.5 Effects of reaction time (studied within 20 min) and temperature at (a) 25 °C, (b) 30 °C, (c) 40 °C and (d) 50 °C on the colorimetric detection of SAL.

3.1.3.3 Performance study of the proposed colorimetric method on the TAD

Under the optimal conditions, the performance of the proposed colorimetric method combined with the TAD was subsequently investigated for quantitative analysis of SAL. Upon the addition of SAL in the concentration ranging from 0–40 ppm, the light pink of permanganate reagent slightly changed to orange-tinted color, as shown in Figure 3.6a. Basically, the experiments were performed in triplicate, and the average color change intensity (ΔI) obtained was then plotted against the SAL concentration, as shown as an inset in Fig 6(b). As clearly seen in Figure 3.6b, the color intensity values of the reacting solution increased steadily but not linearly with the increase of SAL concentration. When the color change intensity (ΔI) was plotted with respect to the log scale of SAL concentration, as shown in Figure 3.6b, a linear response

of SAL detection could be obtained in the range of 0 to 40 ppm under controlling the temperature of reaction at 30 °C with a correlation coefficient of 0.9944. Furthermore, the limits of detection (LOD) and quantification (LOQ) could be calculated using 3σ method (where σ is the standard deviation of the blank solution), and found to be 0.05 and 0.17 ppm, respectively.

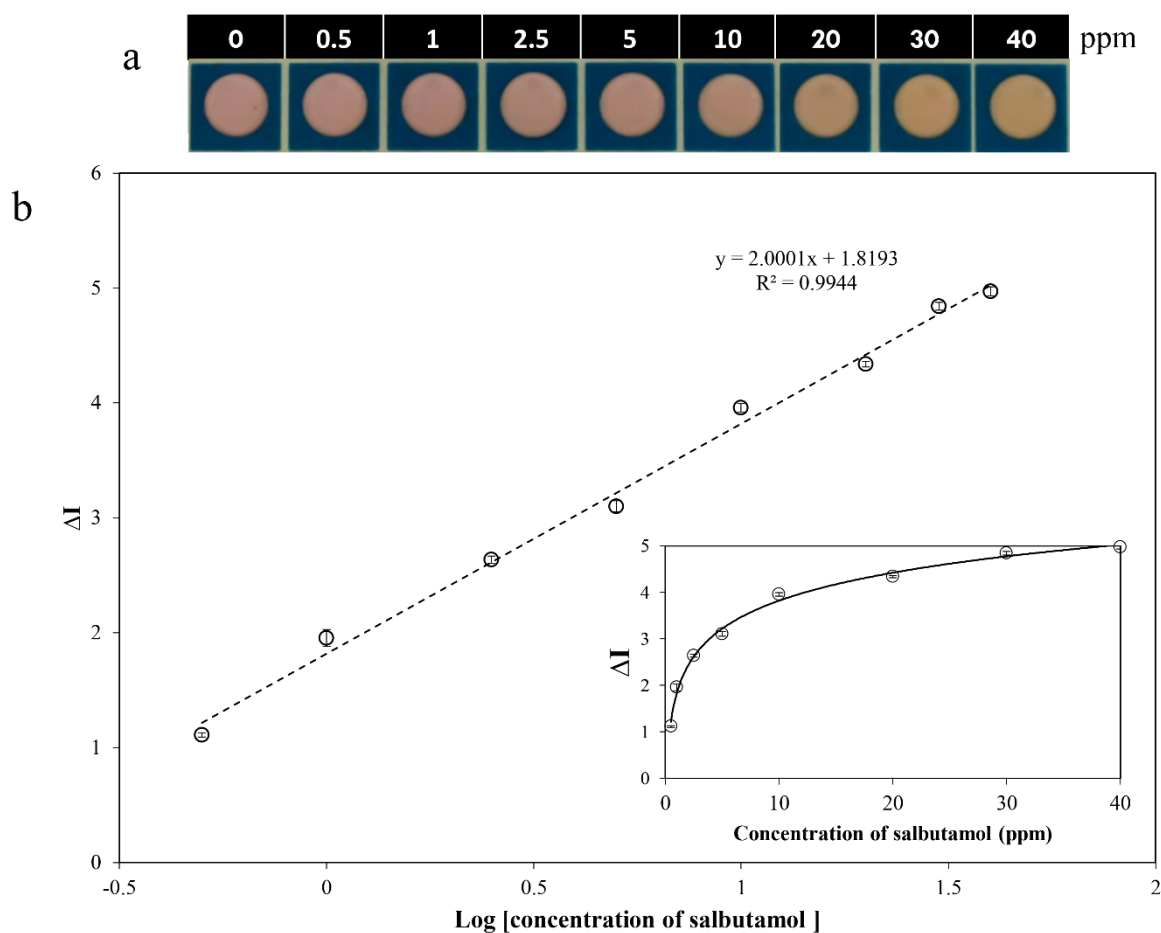


Figure 3.6 (a) Corresponding images of the colorimetric detection of SAL at various concentrations ranging from 0 – 40 ppm on the TAD colorimetric sensor, and (b) Plot of linear regression analysis with the SAL concentrations of 0.5 – 40.0 ppm in a log scale. Inset: Plot of the average color change intensity against the concentration of SAL in a range of 0.5 – 40.0 ppm.

3.1.3.4 Colorimetric determination of SAL in real samples

In order to validate the developed colorimetric method and the corresponding TAD sensor, the determination of SAL in a range of commercially available drug samples has been performed using permanganate as the colorimetric reagent spotting on the proposed transparent PET-based device. A recovery study was also carried out using an external standard method. Generally, it was found that the experimental values for various drug samples were in good agreement with those labelled on the medicine with relative errors less than 8.8%, demonstrating good accuracy for quantitative analysis, as shown in Table 3.1. In addition, the %recoveries and %RSD of the spiked drug samples were found to be in the range of 81.00 – 108.87% and 1.32 – 7.53%, respectively, as presented in Table 3.2. The results typically showed satisfactory recoveries with high precision, as well as indicating a proof of concept of the potential capability of the developed colorimetric method and TAD sensor in pharmaceutical application.

Table 3.1 Colorimetric determination of SAL in real drug samples using permanganate as oxidizing agent at the transparent PET-based sensor.

Samples	Salbutamol content		% Relative error
	Labeled value (mg / tablet)	Contents found (mg / tablet)	
Sample 1	2	2.18 ± 0.06	8.8
Sample 2	2	2.05 ± 0.21	2.7
Sample 3	2	1.85 ± 0.11	7.3
Sample 4	4	4.30 ± 0.36	7.4
Sample 5	4	4.13 ± 0.20	3.3
Sample 6	4	4.19 ± 0.17	4.7

Table 3. 2 Recovery study for SAL determination in the spiked drug samples (n=3).

Sample	Spiked (ppm)	Found (ppm)	Recovery (%)	RSD (%)
		Mean \pm SD	Mean \pm SD	
Sample 1	0	10.89 \pm 0.29	-	-
	2.5	12.98 \pm 0.17	83.60 \pm 6.93	1.33
	10	21.55 \pm 0.57	106.60 \pm 5.72	2.65
	25	35.52 \pm 2.20	98.53 \pm 8.79	6.19
Sample 2	0	10.27 \pm 1.06	-	-
	2.5	12.98 \pm 0.34	108.53 \pm 13.63	2.62
	10	18.76 \pm 0.25	84.93 \pm 2.48	1.32
	25	37.45 \pm 0.99	108.72 \pm 3.95	2.64
Sample 3	0	9.27 \pm 0.53	-	-
	2.5	11.31 \pm 0.15	81.47 \pm 6.00	1.33
	10	18.37 \pm 1.38	81.00 \pm 13.83	7.53
	25	33.68 \pm 2.40	97.64 \pm 9.59	7.12
Sample 4	0	10.74 \pm 0.91	-	-
	2.5	13.39 \pm 0.18	105.87 \pm 7.16	6.67
	10	20.26 \pm 0.27	95.23 \pm 2.71	2.85
	25	37.45 \pm 0.99	106.84 \pm 3.95	3.70
Sample 5	0	10.33 \pm 0.50	-	-
	2.5	12.98 \pm 0.17	106.00 \pm 6.93	6.54
	10	21.22 \pm 0.28	108.87 \pm 2.83	2.60
	25	36.05 \pm 0.99	102.89 \pm 3.97	3.86
Sample 6	0	10.47 \pm 0.42	-	-
	2.5	12.78 \pm 0.17	92.53 \pm 6.70	7.24
	10	19.65 \pm 0.52	91.80 \pm 5.20	5.66
	25	36.90 \pm 1.93	105.73 \pm 7.74	7.32

3.1.4 Conclusion

A transparent PET-based analytical device (TAD), which is inexpensive, portable, and simply manufactured, suitable for colorimetric application was first developed for facile qualitative and quantitative detection of SAL. The TAD was rapidly and easily fabricated by wax-printing method and the colorimetric detection of SAL was simply performed based on the redox reaction of the oxidizing permanganate reagent and the reducing SAL sample. In the presence of SAL, the color of permanganate in acidic medium would visibly change from light pink to pale orange at 30 °C within 11 min reaction time, which could be clearly observed by the naked eye. The proposed colorimetric TAD sensor showed high performance towards SAL measurement with low detection limit of 0.05 ppm. Additionally, this method was successfully applied for determination of SAL in several drug samples where the acceptable relative errors of less than 9%, the satisfied recoveries of 81.00 – 108.87%, and the good RSD of 1.32 – 7.53% could be thoroughly obtained, highlighting that this colorimetric method coupled with the TAD sensor was highly capable of detecting SAL with high accuracy and precision.

CHAPTER 4

THE DEVELOPMENT OF INTEGRATED PLATFORMS FOR ELECTROCHEMICAL SENSOR AND ITS APPLICATION

For a long period of time, the electrochemical techniques have become a promising tool for sensor development attributing to its beneficial property such as cost-effectiveness, high throughput analysis, straightforward operation, and high sensitivity. However, the key challenge confronting high selectivity for the electrochemical detection is the overlapping peaks of the related structural compounds with close redox potentials. To improve the selectivity in the detection, the electrochemical technique is integrated to various platforms, including a separation unit, a recognition system, and a miniaturized device, as described in this chapter. There are three main parts in this chapter as follows:

- Part I (section 4.1) reports on simultaneous determination of β -agonists by UHPLC coupled with electrochemical detection based on palladium nanoparticles modified BDD electrode
- Part II (section 4.2) reports on a ready-to-use electrochemical origami-like sensor based on molecular imprinting for selective detection of SAL
- Part III (section 4.3) reports on synergistically catalytic activity of trimetallic CuNiAu modified SPGE toward distinguishable oxidation of NE and 5-HT.

PART I

4.1 Simultaneous determination of β -agonists by UHPLC coupled with electrochemical detection based on palladium nanoparticles modified BDD electrode

Atchara Lomae^a, Siriwan Nantaphol^a, Takeshi Kondo^d, Orawon Chailapakul^{a,b*},
Weena Siangproh^{c**}, and Janjira Panchompoo^{a***}

^a Electrochemistry and Optical Spectroscopy Center of Excellence (EOSCE), Department of Chemistry, Faculty of Science, Chulalongkorn University, 254 Phayathai Road, Pathumwan, Bangkok 10330, THAILAND

^b Center for Petroleum, Petrochemicals and Advanced Materials, Chulalongkorn University, 254 Phayathai Road, Pathumwan, Bangkok 10330, THAILAND

^c Department of Chemistry, Faculty of Science, Srinakharinwirot University, Sukhumvit, Wattana, Bangkok 10110, THAILAND

^d Department of Pure and Applied Chemistry, Faculty of Science and Technology, Tokyo University of Science, 2641 Yamazaki, Noda 278-8510, JAPAN

CHULALONGKORN UNIVERSITY

*** Corresponding author

** Co-corresponding author

* Co-corresponding author

Abstract

Palladium nanoparticles (PdNPs) modified boron-doped diamond (BDD) electrode was simply fabricated *via* electrodeposition technique for the sensitive electro-analysis of four β -agonist compounds, including terbutaline (TER), salbutamol (SAL), ractopamine (RAC), and clenbuterol (CLB) after a prior separation by ultra-high performance liquid chromatography (UHPLC). The separation was carried out using a reverse phase C18 column with gradient elution of appropriate proportion between methanol and phosphate buffer solution (PBS) pH 7.0 at a flow rate of 1.0 mL⁻¹. The following electrochemical detection (ECD) was accomplished by amperometric method with a detection potential of 1.0 V vs Ag/AgCl. The modified BDD electrode, unlike other carbon-based electrodes used for β -agonists detection, typically showed the superior anti-fouling ability and provided excellent long-term stability, resulting in no complicated cleaning steps needed during each determination. The measurement of β -agonists using the PdNPs modified BDD electrode integrated with UHPLC showed a linear relationship in the range of 0.2 to 200 $\mu\text{g mL}^{-1}$ with detection limits of 0.04, 0.02, and 0.03 $\mu\text{g mL}^{-1}$ for TER, SAL, and RAC, respectively. Meanwhile, CLB displayed linearly in the range of 0.5 to 200 $\mu\text{g mL}^{-1}$ with a detection limit of 0.19 $\mu\text{g mL}^{-1}$. Moreover, this method was successfully applied to detect β -agonists in diverse samples, including swine feed, swine meat, and human urine with satisfied recoveries in the range from 80.5% to 110.0%. Reliability of this developed method was also validated with ultra-high performance liquid chromatography coupled with ultra-violet detection (UHPLC-UV), and the results showed highly quantitative agreement between the two methods. Therefore, the PdNPs modified BDD could be productively utilized as effective electrodes, with good electrocatalytic activity of PdNPs towards β -agonists oxidation and favorable anti-fouling performance of BDD. The simultaneous detection of four β -agonists by UHPLC-ECD exhibited good stability, acceptable reusability, high sensitivity, and rapid analysis.

Keywords: Palladium nanoparticles (PdNPs); Boron-doped diamond (BDD); Anti-fouling; β -agonists; UHPLC-ECD

4.1.1. Introduction

Beta-adrenoceptor agonists (β -agonists) are derivatives of phenylethanolamine with different substituents on aromatic ring and terminal amino group. Terbutaline (TER), salbutamol (SAL), ractopamine (RAC), and clenbuterol (CLB), as shown in Figure 4.1.1, are important β -agonist compounds that have been extensively studied. These compounds have been commonly used as a bronchodilator medicine for the treatment of human chronic obstructive pulmonary disease and asthma^{99, 128, 129}. They typically have ability to induce smooth muscle relaxation in the lung and to decrease systemic vascular resistance¹³⁰. However, TER and SAL have been misused as doping drugs in the athletes to enhance performance due to their ergogenic potentials and anabolic effects^{131, 132}. Besides doping drugs, the forbidden application of β -agonist compounds especially SAL, RAC, and CLB as veterinary drugs has been widely employed in livestock, to enhance the fat level transformation to muscle protein production^{133, 134}. These abuses have caused the poisonous effects to human health *via* the consumption, resulting in various symptomatic expressions such as palpitation, tremors and nervousness^{99, 129}. For this reason, World Anti-Doping Agency (WADA) and European Union (EU) have therefore monitored and controlled these abused substances used as doping agents and growth promoters, respectively. According to the WADA prohibited list, TER is forbidden to present in urine while the presence of SAL in urine higher than 1000 ng mL⁻¹ (or 3 μ M) indicated the intake of performance-enhanced drugs (doping)^{131, 132}. Moreover, all compounds have generally been banned for use as growth promoters in China and the EU^{106, 135}. Therefore, the determination of these four β -agonists is necessary in order to control and monitor the abuse of these substance.

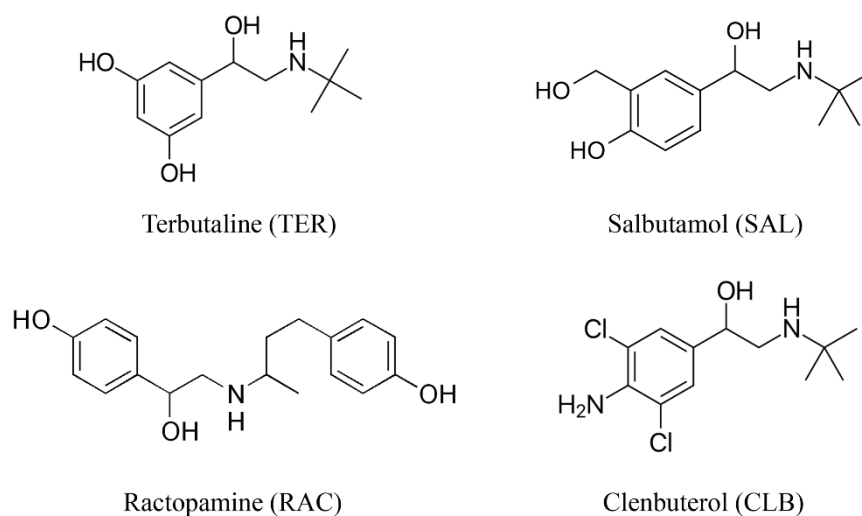


Figure 4.1.1 Structures of terbutaline (TER), salbutamol (SAL), ractopamine (RAC) and clenbuterol (CLB).

Currently, the modern analytical techniques of combined chromatography and mass spectrometry (MS) have been widely used as the standard methods for β -agonists detection^{100, 136, 137}. Although these compounds can be chromatographically separated, and subsequently detected by MS at very low concentration levels with high accuracy and precision, the sophisticated instrument setup and expensive instrumentation of mass spectrometry, as well as the high cost of maintenance are the major limitations of using MS as the detection tool. Ultra-high performance liquid chromatography with electrochemical detection (UHPLC-ECD) is therefore an appealing approach for the quantification of β -agonist compounds. UHPLC offers the higher resolution and efficiency compared to traditional high performance liquid chromatography (HPLC) because it has lower dispersion length of the separated zone and therefore needs lower volume of analyte. As the short column has been used in the solid separation phase, the system can be also operated under high pressure (> 10,000 psi)¹³⁷. ECD exhibits distinct advantages of inexpensive instrument, high sensitivity and simple operation and maintenance. However, the challenge of the

determination of β -agonists by ECD is the strong adsorption of β -agonist compounds on the electrode surface which results in a decrease in sensitivity and the electrode itself is incapable of being used repetitively, unless several cleaning steps are carried out^{131, 138}.

As previously reported in the literature, both SAL and RAC typically possess the phenolic hydroxyl substituents, and their electrochemical behaviors are dominated by the oxidation of these hydroxyl groups on the aromatic ring¹³⁹⁻¹⁴¹, generating some free radical species which could then form the C-C linked dimers that can subsequently adsorb on and passivate the electrode surface^{22, 142}. Similar adsorptive behavior has also been reported for the oxidation of TER which is attributed to the resorcinol group in its molecule^{143, 144}. As for CLB which contains amine-substituted group, the electrochemical response of CLB involves the oxidation of amine functional group, forming the radical cations which could then undergo the “head to tail” coupling, resulting in the formation of dimers that can strongly adsorb onto the electrode surface^{145, 146}. In order to overcome this electrode passivation caused by the oxidation of β -agonists, the use of anti-fouling materials, especially boron doped diamond (BDD), is thought to be an effective way. According to the literature^{24, 147}, the BDD was generally fabricated on Si supports *via* hydrogen plasma chemical vapor deposition (CVD) method, generating H-terminated moiety at the BDD surface which was believed to be a potential functionality for adsorptive inertness. Due to the weak adsorption of polar compounds on their H-terminated surfaces, the BDD electrodes typically offer the anti-fouling ability in electroanalysis. Basically, the fouling resistance capability of BDD electrode has been studied in various applications where the surface fouling was the obstacle to the long-term stability of the electrode. According to the literature, the BDD electrodes could prevent the fouling of their surface during the electrochemical detection of chlorine¹⁴⁸, norepinephrine and serotonin¹⁴⁹, as well as new psychoactive substances *e.g.* 2,5-dimethoxy-N-(2-methoxybenzyl)phenethylamines (NBOMes)¹⁵⁰,

whereas this fouling resistance could not be achieved with such carbon-based electrodes. Additionally, the BDD has many attractive electrochemical properties, as follows: (i) low and stable background current, (ii) wide potential range, and (iii) corrosive resistance owing to the chemically inert behavior of the electrode surface^{151, 152}. With these perspectives, BDD could be considered as an alternative working electrode (WE) used for β -agonists determination.

Besides dealing with the electrode fouling problem, another key issue for β -agonists electrochemical detection is to improve the sensitivity of the electrochemical responses. The modification of electrode surface with nanomaterials has been considered to enhance the sensitivity since they have large specific surface area, excellent conductivity and extraordinary electrocatalytic activity. Various nanomaterials such as gold nanoparticles (AuNPs)²⁹, copper/cuprous oxide nanoparticles (Cu/Cu₂ONPs)¹⁵³, manganese nanoparticles (MnNPs)¹⁵⁴, and silver/palladium (AgPd) bimetallic material¹⁵⁵, have been modified on the electrode for β -agonists determination. Among these nanomaterials, palladium nanoparticles (PdNPs), reported to be able to improve the electron transfer kinetics of phenolic compounds at electrode surface, have been attractively in attention as the catalytic electrode modifiers for enhancing the sensitivity of various phenolic compounds such as dopamine, epinephrine and uric acid¹⁵⁶⁻¹⁵⁹. Since β -agonists typically contain phenolic moieties in their structures, the PdNPs could potentially be modified onto the electrode for the determination of β -agonists.

Herein, we demonstrate the use of PdNPs-modified BDD as an amperometric sensor combined to the UHPLC separation technique for simultaneous determination of four β -agonists. Due to the anti-fouling activity of BDD and the electrocatalytic ability of PdNPs, this proposed system could overcome the limitation of electrode fouling without any cleaning steps during the detection, and the current responses

could be enhanced, resulting in higher sensitivity. Moreover, the combination of UHPLC and electrochemical detection could successfully analyse the target analytes and was prosperously applied in diverse samples including swine feed, swine meat, and urine. The results indicated that this proposed method provided high capability of monitoring and controlling the abuse of these β -agonists as doping agents and growth promoters.

4.1.2 Materials and methods

4.1.2.1 Chemicals and reagents

All chemicals used in this work were of analytical grade, and all solutions were prepared using Milli-Q water from Millipore ($R \geq 18.2 \text{ M}\Omega \text{ cm}$ at $25 \text{ }^\circ\text{C}$). Methanol (HPLC-grade), hydrochloric acid (HCl), and phosphoric acid (H_3PO_4) were obtained from Merck (Darmstadt, Germany). Potassium dihydrogen phosphate (KH_2PO_4), disodium hydrogen phosphate (Na_2HPO_4), potassium chloride (KCl), and sodium hydroxide (NaOH) were purchased from Merck (Darmstadt, Germany). Standard salbutamol, clenbuterol hydrochloride, ractopamine hydrochloride, and terbutaline hydrochloride were obtained from Sigma-Aldrich (St. Louis, MO, USA). Palladium (II) chloride (PdCl_2) was purchased from Wako Pure Chemical Industries (Chuo-Ku, Osaka, Japan).

All of stock standard solutions ($100 \mu\text{g mL}^{-1}$) were prepared by dissolving 1 mg of each standard in methanol. The solutions were then placed in an amber bottle and stored at $4 \text{ }^\circ\text{C}$. As for working standard solutions preparation, the stock standard solution was diluted in suitable proportion of methanol and 0.05 M phosphate buffer solution (50:50; v:v), and the solution was mixed using a vortex mixer. All solutions and solvents were filtered through $0.22 \mu\text{m}$ nylon membranes before analysis by UHPLC-ECD.

4.1.2.2 Fabrication and modification of PdNPs modified BDD electrode

The electrochemical experiments were performed using an CH instrument potentiostat 1232A (CHI Instrument, Inc., USA) at room temperature (25 °C). Boron doped diamond (BDD), silver/ silver chloride (Ag/AgCl), and platinum (Pt) electrodes were used as working, reference, and auxiliary electrodes, respectively. The BDD electrode was prepared by a microwave plasma-assisted chemical vapor deposition system (Astex Corporation). In this study, the BDD electrode was obtained from Associate Prof. Dr. Takeshi Kondo's Laboratory at Tokyo University of Science. To prepare the PdNPs modified BDD electrode using a cyclic voltammetric (CV) technique, the three-electrode system was placed into a cell containing 1 mL of 0.2 mM PdCl₂ in 0.1 M KCl, followed by the electrochemical deposition of palladium onto BDD surface with a repetitive potential scans between 1.2 and -0.25 V vs Ag/AgCl at the scan rate of 10 mV s⁻¹ for seven cycles¹⁶⁰. Then the PdNPs modified BDD was rinsed with distilled water and dried with air-gun before being applied for further electrochemical studies.

4.1.2.3 UHPLC-ECD and apparatus

The UHPLC separation unit consists of a reversed-phase column with an LC-20ADXR solvent deliver unit (Shinadzu Corporation, Japan), an autosampler (SIL-20A) with 0.1-100 mL loop. A Kinetex™ core shell C18 column (50 mm × 4.6 mm i.d. with particle size of 2.6 μm, Phenomenex) was employed for separation of the analytes and was instantly controlled at 37 °C. The mobile phase comprised 40% methanol and 60% phosphate buffer 0.05 M (pH 7) with gradient elution using gradually increased portion of methanol in the range of 5% – 15% at 0 – 7 min. After that the methanol proportion was continuously increased to 40% at 10 min, and kept maintained with methanol 40% at 10 -12 min. The mobile phase was delivered with a constant flow rate of 1 mL min⁻¹ with injection volume of 8 μL.

For electrochemical measurement, the thin-layer flow cell consists of a working PdNPs modified BDD electrode, a Ag/AgCl reference electrode (Bioanalytical system

Inc., USA), and a stainless-steel tube auxiliary electrode. An amperometric technique was executed for an electrochemical detection of β -agonists with no intense chemical cleaning steps required.

4.1.2.4. Sample preparation

Three types of real samples including swine feed, swine meat, and urine were investigated. All feeds and swine meats were obtained from supermarkets and local fresh markets in Thailand. Artificial urine was purchased from Carolina Biological Supply Company (Burlington, USA).

For swine feed, the feed samples were prepared according to the previous literature^{110, 161}. Firstly, 1.0 g of finely ground swine feeds were accurately weighed into 25.0 mL centrifuge tubes, and then feed powder was dissolved in the 3.0 mL mixture of acetone and 1.0 mol L⁻¹ NaOH (9:1; v:v). After that the mixture was sonicated by supersonic vibration for 5 min followed by centrifugation with 10,000 rpm at 5°C for 10 min. The extraction was repeated for four times and the clear supernatants were collected. Later, the combined supernatants were evaporated by nitrogen-blowing. Then, the obtained residues were dissolved in 1 mL of 0.05 M phosphate buffer (pH 7.0), and 1 mL of hexane was subsequently added to remove fats and oils. The resulting solution was centrifuged at 10,000 rpm and 5°C for 5 min, and the water phase was afterward collected for analysis. For the detection, the above extracted solution was diluted with methanol and 0.05 M phosphate buffer (pH 7.0) mixture (50:50; v:v) and the spiked method was performed. Then the estimated recovery percentage was calculated.

The swine meat preparation has been fully described previously in the literature¹¹¹. The meat samples were homogenized by laboratory blender and 4 g of homogenized meat was correctly weighed into the centrifuge tube. The fat digestion was proceeded by addition of 6 mL HCl (0.01 M) with vortex mixing and incubated at

room temperature for 30 min. Next, the mixture was centrifuged with 3000 rpm at 25°C for 10 min and the clear supernatant was collected. The above extracted solution was diluted with the mixture of 50:50 (v:v) methanol and 0.05 M phosphate buffer (pH 7.0) and used for preparation a series of samples by “spiking” the extracted solution with β -agonists standard solution.

For urine preparation, the artificial urine was diluted with the mixture of methanol and 0.05 M phosphate buffer (pH 7) (50:50; v:v). The recoveries of the spiked β -agonists standard solution were thoroughly studies.

4.1.3 Results and discussion

4.1.3.1 Influence of electrodeposition parameter

For the electrode modification using electrodeposition (CV) technique, the parameters including concentration of Pd solution, scan rate, and number of cycles which affected to the size and shape of PdNPs were optimized. To obtain the optimal condition of PdNPs modified BDD, the dependence of all parameters was studied by DPV, and the results were reported in term of the relationship between current response of SAL and studied parameter. The Pd (II) concentrations were studied in the range of 0.01 to 0.5 mM. Figure 4.1.2A displayed the current signal of SAL in 0.05 M phosphate buffer pH 7. The current signal increased when the Pd (II) concentration increased from 0.01 to 0.2 mM, and then peak current decreased with further increased of Pd concentrations from 0.2 to 0.5 mM. Thus 0.2 mM Pd (II) concentration was selected for the modification step. The scan rate of CV was investigated in the range of 5 to 100 mVs^{-1} and showed in Figure 4.1.2B. The current response first significantly increased from 5 to 10 mVs^{-1} and then decreased from 10 to 100 mVs^{-1} . Therefore, scan rate of 10 mVs^{-1} was chosen as optimized condition for the electrodeposition step. The number of cycles in CV was considered as last parameter in range of 3 to 15 cycles as showed in Figure 4.1.2C. The current signal increased as number of cycles

from 3 to 7 cycles and gradually decreased from 7 to 15 cycles. Consequently, 7 cycles were used as the optimal cycles for modification of PdNPs onto BDD surface.

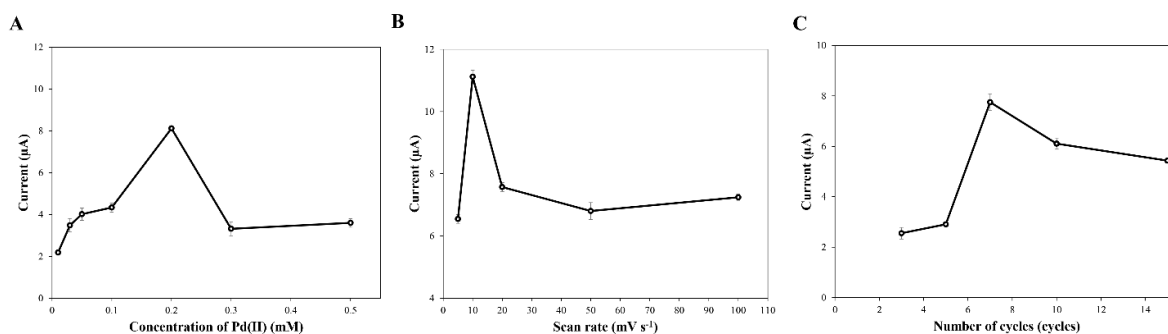
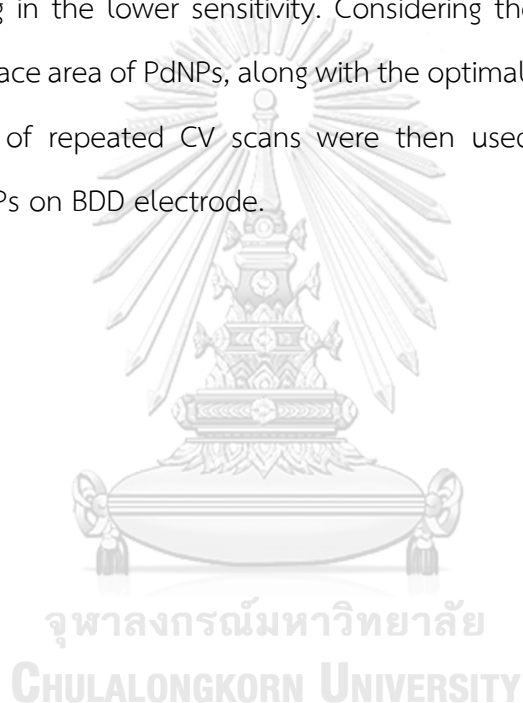


Figure 4.1.2 Effects of (A) Pd (II) concentration, (B) scan rate, and (C) number of cycles on the PdNPs modification on BDD electrodes.

4.1.3.2 Characterization of PdNPs deposition onto BDD electrode

The PdNPs modified BDD electrode was accomplished using electro-deposition method. Generally, the potential was repeatedly scanned between 1.2 V and -0.25 V vs Ag/AgCl in Pd (II) solution by cyclic voltammetry (CV). The surface morphology of the PdNPs modified BDD electrode together with the bare BDD were characterized using a JSM-7610F field emission scanning electron microscopy (FE-SEM) (JEOL Ltd., Japan), as shown in Figure 4.1.3. The smooth surface of the bare BDD electrode with no Pd present could be observed as seen in Figure 4.1.3 (a and b), whereas a wide range of PdNPs distribution on the BDD surface under different numbers of CV-scanned cycles (from 3 to 15 cycles) in PdCl_2 solution could be noticed, as presented in Figure 4.1.3 (c,e and g). The average size and shape of the PdNPs have changed from spherical to flower-like structure, due to the agglomeration of the PdNPs with increasing number of electrodeposition cycles. Experimentally, the amount of PdNPs on BDD surface was found to increase *ca.* 0.14%, 1.19%, and 19.58% with number of CV scans of 3, 7, and 15 cycles, respectively, as shown in EDS elemental Pd map results Figure 4.1.3 (b,d,f and h) and Figure 4.1.4. Obviously, the presence of PdNPs on BDD surface provided

an increase of the electroactive surface area and subsequently enhanced the electrocatalytic oxidation of β -agonist compounds. The large degree of electrocatalytic oxidation of the analytes could be observed at a large amount of PdNPs on BDD surface (e.g. when 15 electrodeposition cycles were carried out). However, the high baseline current was also observed when the large amount of PdNPs was present on the electrode surface. This high capacitive background current was much unbeneficial for the detection due to the increase of signal to background (S/N) response, resulting in the lower sensitivity. Considering the highly catalytic property and the active surface area of PdNPs, along with the optimally low background current, the seven cycles of repeated CV scans were then used for the electrochemical deposition of PdNPs on BDD electrode.



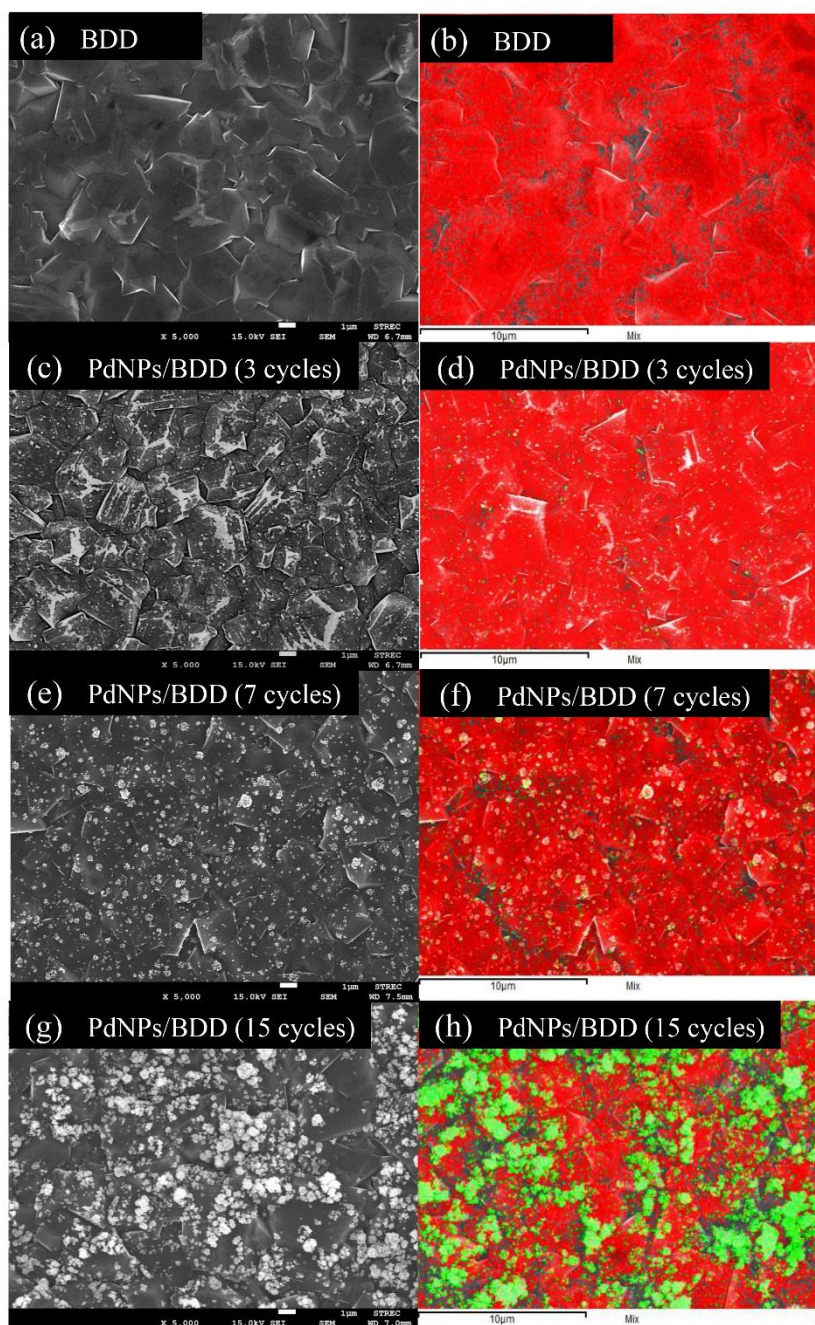


Figure 4.1.3 The SEM image (a) and the EDS elemental Pd map (b) of bare BDD electrode. The SEM images (c),(e),(g) and the EDS elemental Pd maps (d),(f),(h) of different deposition CV scans in PdNPs modification step.

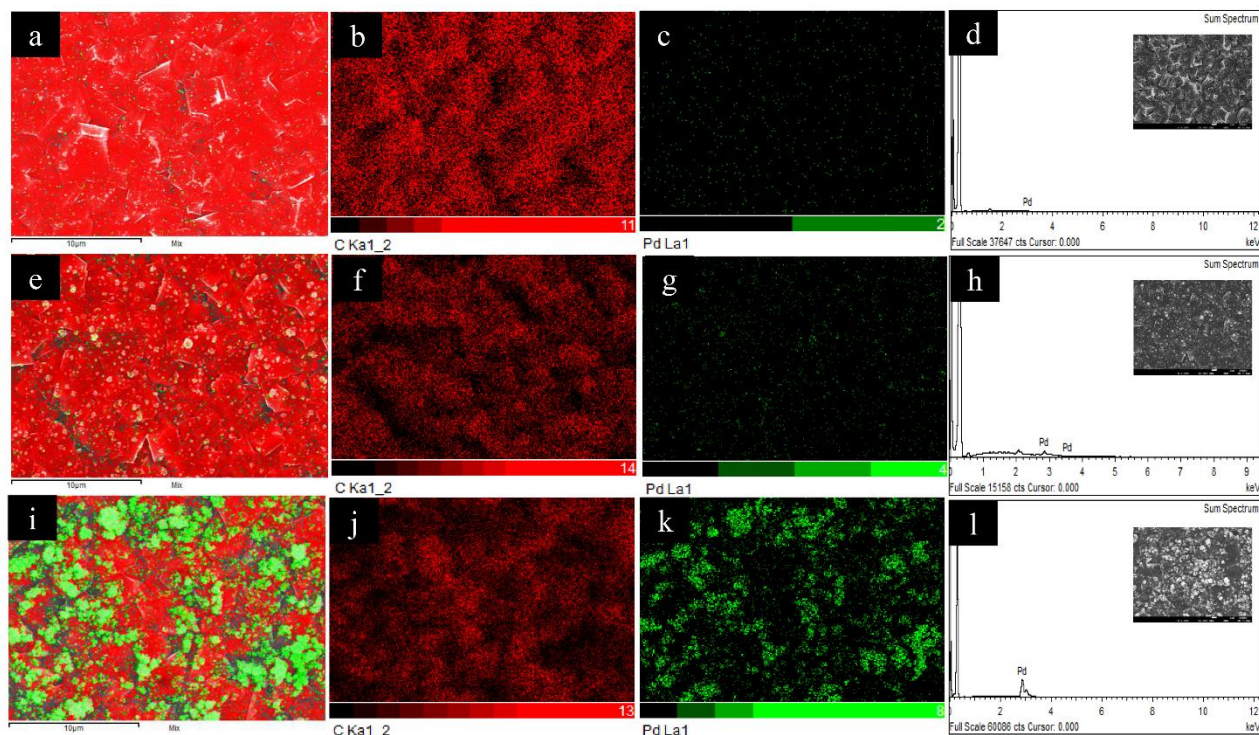


Figure 4.1.4 (a,e,i) EDS elemental Pd on BDD map, (b,f,j) EDS elemental C map, (c,j,k) EDS elemental Pd map and (d, h, l) EDX results of 3, 7 and 15 repetitive cycles of PdNPs modified BDD electrode, respectively.

จุฬาลงกรณ์มหาวิทยาลัย
CHULALONGKORN UNIVERSITY

4.1.3.3 Electrochemical responses of β -agonists at PdNPs modified BDD electrode

In order to study the performance of the PdNPs modified BDD electrode, the electrochemical behaviors and the oxidative current responses of four β -agonists were investigated using cyclic voltammetry (CV) with a scanned potential range of 0.0 V to 1.6 V vs Ag/AgCl at the PdNPs modified BDD electrode, compared with the bare BDD electrode, shown in Figure 4.1.5. It can be clearly seen in Figure 4.1.5(a-d) that these four β -agonists studied, especially SAL and RAC, typically gave an ill-defined oxidation peak with large oxidation overpotential at the unmodified BDD electrode (black line).

On the other hand, a clear increase in the oxidation peak current of could be observed at the PdNPs/BDD electrode (orange line), and the oxidation peak potential slightly shifted towards less positive potentials. In comparison with the bare BDD electrode, the oxidation peak current of TER, SAL, RAC and CLB obtained using the PdNPs modified BDD electrode was found to be significantly higher (ca. three-fold, two-fold, four-fold and fifteen-fold, respectively), as shown in Figure 4.1.5(e), indicating the better electron transfer kinetics at the PdNPs-modified BDD electrode. Moreover, the higher sensitivity of β -agonists observed at the PdNPs-modified BDD electrode could be attributed to the electrocatalytic activity of PdNPs that potentially enhanced the degree of β -agonist oxidation with lower overpotential.



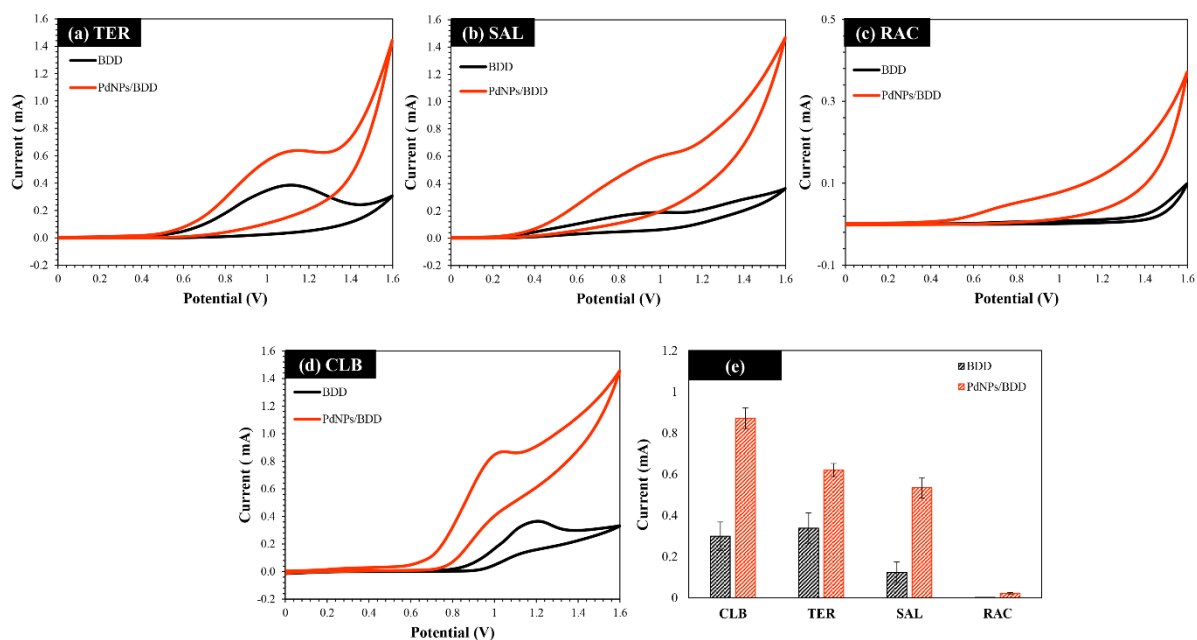


Figure 4.1.5 Cyclic voltammograms of 10 mM (a) TER, (b) SAL, (c) RAC and (d) CLB in MeOH: PBS (50:50; v/v) with a potential scanned from 0.0 to 1.6 V vs Ag/AgCl at a bare BDD electrode (black line) and a PdNPs-modified electrode (orange line) with a scan rate of 100 mV s^{-1} , as well as a column chart (e) comparing oxidation current responses of four β -agonists at bare BDD and PdNPs-modified BDD electrode.

4.1.3.4. UHPLC separation of four β -agonists

4.1.3.4.1 Effects of the proportion of MeOH

In this study, the UHPLC was used to separate TER, SAL, CLB, and RAC prior to the detection with electrochemical sensor (PdNPs-modified BDD electrode). For the separation step, a reverse phase column (C18) was used to separate four β -agonists by gradient elution. The proportion of MeOH in a mobile phase that had an effect on the retention characteristics of the target analytes has been first investigated. When the ratio of MeOH in the mobile phase was lower than 15%, the complete separation of TER and SAL could be observed within 4 min while the separation of RAC and CLB was subsequently observed over 20 min. On the contrary, when the proportion of MeOH was constantly maintained at 40%, the co-eluting of TER and SAL could be

clearly seen. Thus, the gradient elution was necessarily performed to obtain the complete and rapid separation. In this work, the proportion of MeOH was gradually increased from 5% to 15% within 7 min to properly separate SAL and TER. Then, the MeOH ratio was continually increased to 40 % within 10 min and kept maintained at this condition up to 12 min, resulting in the separation of RAC and CLB. Noted that the analysis time for these four β -agonists is relatively rapid when using this gradient elution, and all compounds were completely separated and detected within 11 min. In order to avoid the clogged problem in UHPLC when using high concentration of salt, the 0.05 M phosphate buffer solution (pH 7) was then chosen as aqueous electrolyte in this work. The chromatogram obtained from the separation of standard β -agonists mixture was shown in Figure 4.1.6. The retention times of TER, SAL, RAC and CLB were 3.18, 3.67, 10.0, and 10.69 min, respectively. Retention time in this proposed system was found to have %RSD ranging from 0.1% to 1.5%, indicating the good stability. The peak widths of TER, SAL, RAC and CLB were found to be 27.0, 31.2, 24.0, and 22.8 s, respectively. Therefore, this proposed system presented rapid separation and highly sensitive detection of these four β -agonist compounds.

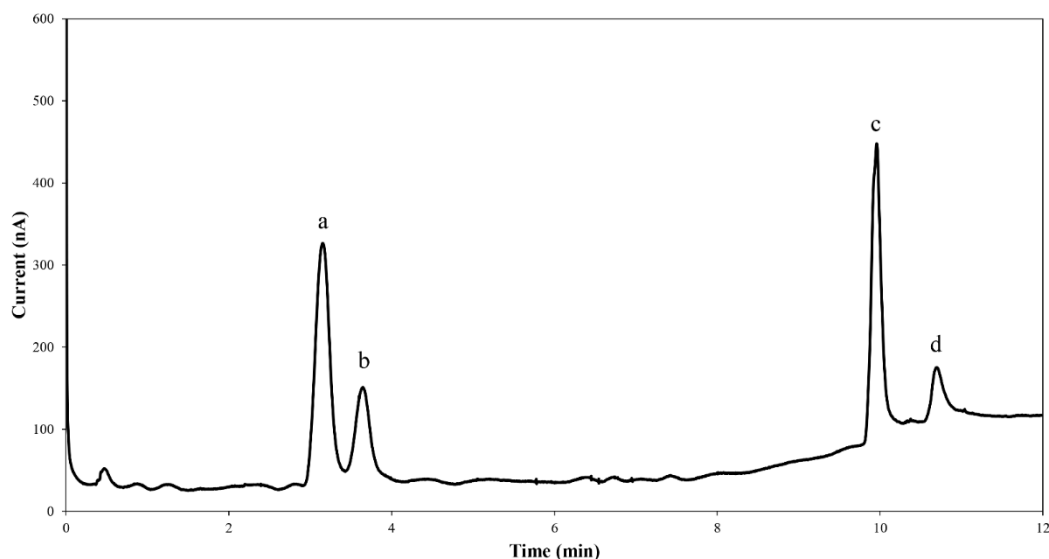


Figure 4.1.6 UHPLC-ECD chromatogram of $10 \mu\text{g mL}^{-1}$ of (a) TER, (b) SAL, (c) RAC, and (d) CLB at PdNPs modified BDD electrode in a (0.05 M phosphate buffer solution (pH 7): MeOH) mobile phase with the detection potential of 1.0 V vs Ag/AgCl; the injection volume of $10 \mu\text{L}$; and the flow rate of 1 mL min^{-1} . This chromatogram was a representative of three independent repetitions.

4.1.3.4.2 Effects of injection volume

Different sample injection volumes were subsequently examined in the range of 2 to $20 \mu\text{L}$. The current responses of the mixed standard β -agonists solution were exhibited in Figure 4.1.7. As seen from the results, the current signals of TER and SAL increased with the injection volume increased from 2 to $12 \mu\text{L}$, and then gradually decreased when the sample was loaded into the system up to 12 to $20 \mu\text{L}$ whereas the current signals of RAC and CLB were in a linear relationship with the injection volume up to $20 \mu\text{L}$. However, the chromatographic peak shape of TER and SAL could be observed to be distorted at high injection volumes ($12 \mu\text{L}$ to $20 \mu\text{L}$) as shown in Figure 4.1.7B. Regarding to the chromatograms shown in Figure 4.1.7A, it can be noticed that the complete separation of RAC and CLB could be observed at all sample injection volumes studied, but the incomplete separation of TER and SAL occurred at

high injection volumes (from 12 μL to 20 μL). Therefore, the resolution (R_s) of TER and SAL was then calculated to evaluate the optimal sample injection volume. R_s of the four analytes injected solution at 2, 5, 8, 10, 12, 15 and 20 μL were 1.84, 1.89, 1.52, 1.45, 1.40, 1.02 and 0.91, respectively. According to HPLC theory, R_s is a quantified peak spacing in liquid chromatography and R_s which is equal to 1.5 is the selected value to indicate the minimum acceptable separation efficiency of the two chromatographic peaks. Considering both R_s and peak current, the sample injection volume of 8 μL was generally chosen as an optimal condition to obtain high sensitivity and well separation of these four β -agonists.

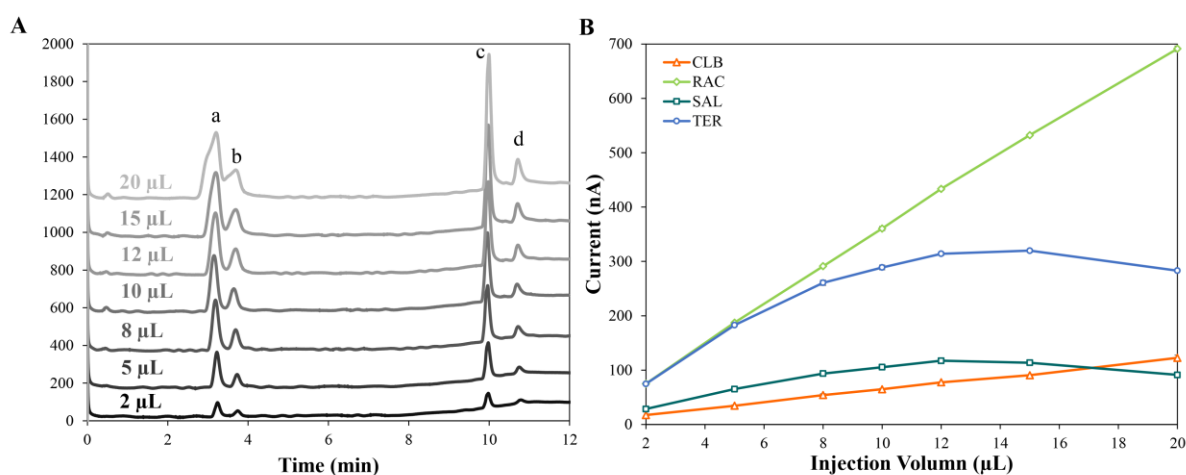


Figure 4.1.7 (A) Amperometric chromatograms of different injection volumes at PdNPs modified BDD for a $10 \mu\text{g mL}^{-1}$ of (a) TER, (b) SAL, (c) RAC, and (d) CLB. (B) Current responses of (\circ) TER, (\square) SAL, (\diamond) RAC, and (Δ) CLB in a mobile phase solution of 0.05 M phosphate buffer solution (pH 7): MeOH, with the detection potential of 1.0 V vs Ag/AgCl, and the flow rate of 1 mL min^{-1} . Each data point represents the average current of three repetitive experiments.

4.1.3.4.3 Effects of buffer pH

pH of buffer solution typically influenced on the charge formation on each β -agonist species that could correspondingly change the interaction between β -agonist and the stationary phase (C18), thereby affecting the chromatographic separation and the amperometric responses. In this work, phosphate buffer solution of pH 4 to 9 was extensively evaluated. The resulting current responses were shown in Figure 4.1.8a. The results demonstrated that the current response of SAL increased with increasing pH while the current responses of RAC, TER, and CLB slightly increased when pH gently rose up to 7, 8 and 8, respectively. The chromatographic dissociation of each compound was literally associated to the analyte/stationary phase (C-18) interaction. The acid dissociation constant (pK_{a1}) values of TER, SAL, RAC, and CLB were 8.8¹⁶², 9.2¹⁶³, 9.4¹⁶⁴ and 9.6¹⁶⁵, respectively. When pH of buffer solution was either lower than 7 (which is close to the pK_{a1} of TER (-OH group)¹⁶²), or lower than 8 (which locates nearby the pK_{a1} of SAL¹⁶³, RAC¹⁶⁴, and CLB(-NH₂ group)¹⁶⁵), the strong attraction between the deprotonated hydrophobic β -agonist compound and the hydrophobic stationary phase was generated, leading to the enhanced separation efficiency and the high current responses of the separated-baselines. Conversely, as pH of buffer solution was higher than 8, the fully protonated β -agonist compound possessed a relatively weak hydrophobic property, resulting in a decrease in the separation efficiency and the current responses, caused by the overlapping baselines. Therefore, the phosphate buffer solution of pH 7 was considered as a suitable pH for working electrolyte to achieve the well-defined amperometric signals.

4.1.3.4.4 Effects of detection potential

The detection potential was also investigated by hydrodynamic voltammetry with the potential ranging from 0.8 V to 1.2 V vs Ag/AgCl using the optimal conditions previously studied, and the results were illustrated in Figure 4.1.8b. It can be obviously seen that the detection potential had an ultimate effect on the oxidation reaction of

β -agonist compounds at electrode surface with direct proportion to the oxidation current. Although the more positive detection potential could give higher oxidation current, the background current also increased, resulting from the MeOH oxidation^{166, 167}. In this case, the results were reported as a net current after background subtraction (S/B). Therefore, the detection potential of 1.0 V vs Ag/AgCl was selected as the optimal potential to obtain the high sensitivity of all β -agonist compounds.

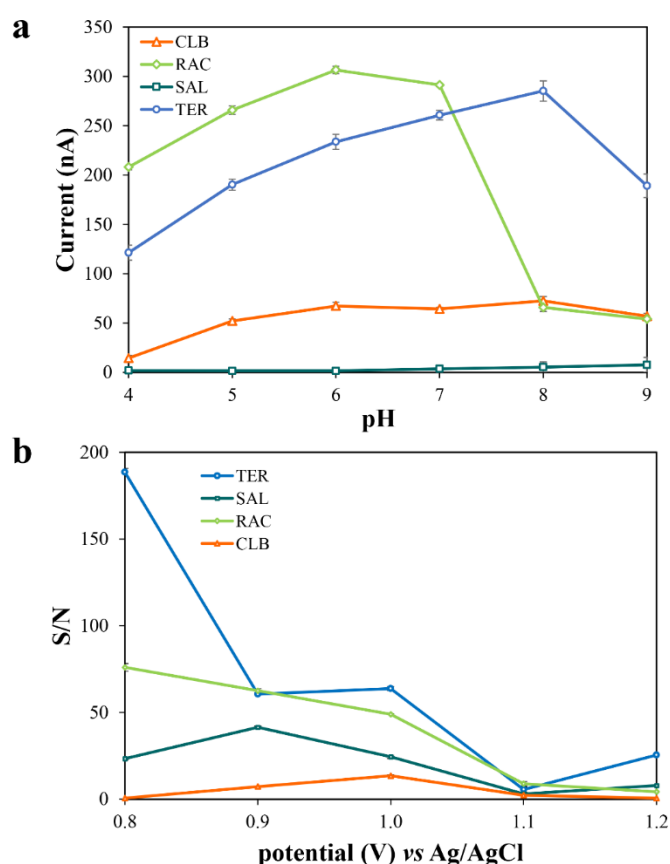


Figure 4.1.8 Effect of (a) pH and (b) detection potential on (○) TER, (□) SAL, (◇) RAC, and (△) CLB with injection volume of 8 μ L, and the flow rate of 1 mL min⁻¹ using PdNPs-modified BDD electrode coupled with UHPLC. Each data point represents the average of three repetitive experiments

4.1.3.4.5 Electrode fouling during the analysis of β -agonist compounds at PdNPs modified electrode

To examine the anti-fouling properties of the PdNPs-modified BDD electrode, the conventional screen-printed carbon electrode (SPCE) was chosen as a comparison. The responses of both electrodes (PdNPs/BDD vs. SPCE) in the detection of four β -agonists were collected using the same electrode surface in each repeated experiment without any cleaning steps. The amperometric peak current of each analyte obtained in the first measurement was identified as 100% normalized current. As exhibited in Figure 4.1.9, the normalized currents of TER, SAL, RAC, and CLB in 10 measurements using the SPCE (black line) instantly increased to 147.5%, 157.2%, 151.5%, and 258.8%, respectively, indicating the high degree of adsorption of polymeric β -agonists film on the electrode surface. According to the literature^{20,22}, the formation of this passivating polymeric β -agonists film continues on two steps. The first step involved the oxidation of phenolic hydroxy group to generate free radical species followed by the combination of two moieties to form dimeric product in the second step. Due to the electroactive species of dimeric β -agonist products adsorbed on the electrode surface, the current response could be instantly increased during repetitive scans which gave the inaccurate results. Therefore, the reuse of SPCE was limited by this electrode fouling characteristic. Meanwhile, the PdNPs modified BDD electrode (orange line) provided the reproducible current response in 10 measurements with a slight increase of normalized current up to only 105.0%. After 10 measurements, the normalized current got instantly increased (to higher than 105%), potentially indicating that the adsorption of the β -agonists' oxidation products could typically occur at the 11th analysis. Therefore, the results implied that the PdNPs modified BDD electrode could be used for the analysis up to 10 times, due to the maximal anti-fouling capability of this BDD electrode. The fouling resistance of BDD literally originated from the extremely weak adsorption of polar compound onto H-terminated BDD, which resulted

in the continuous determination of these powerful adsorbed species without any complicated pre-treatment and cleaning steps^{151, 152, 168}.

Additionally, the proposed electrode proffered excellent repeatability and reproducibility with acceptable relative standard deviation (RSD) values of 3.6%, 1.5%, 4.1% and 5.0% for TER, SAL, RAC and CLB, respectively. The comparing results demonstrated that the PdNPs modified BDD electrode offered the improvement of repeatability and robustness for continuous measurement of these four β -agonists.

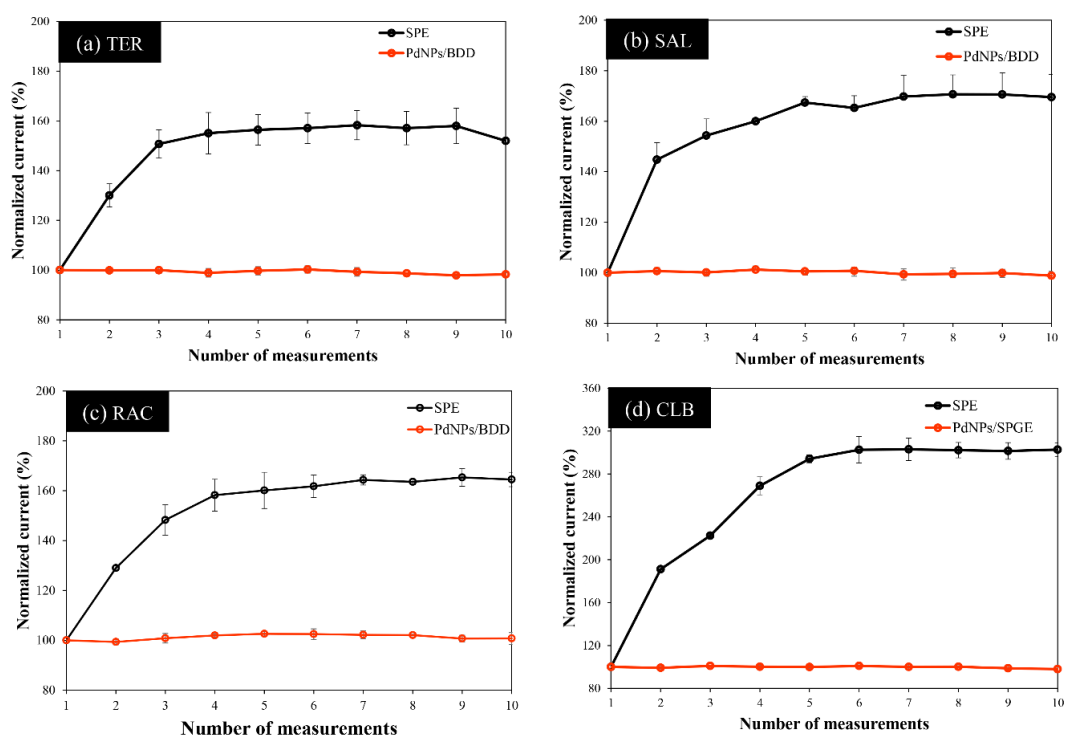


Figure 4.1.9 Plots between amperometric normalized current of $10 \mu\text{g mL}^{-1}$ (a) TER, (b) SAL, (c) RAC and (d) CLB and number of successive measurements using SPCE (black line) and PdNPs-modified BDD electrode (orange line). All parameters were performed under optimal conditions. Note that the first peak current measured in each case has been normalized to 100%.

4.1.3.5 Method Validation

Different concentrations of four β -agonists were measured for constructing calibration curves. All studies were performed using UHPLC-ECD under optimal conditions with three repetitious measurements and the results were reported in Table 4.1.1. The calibration curves of all compounds were displayed in Figure 4.1.10, and it could be clearly seen that all of them exhibited good linearity with correlation coefficients (R^2) in the range of 0.9941-0.9967. The limits of detection (LODs) were determined from the analyte concentration corresponding to the three-time signal-to-noise (3S/N) method, which were found to be 40.0, 20.0, 30.0, and 60.0 ng mL⁻¹ for TER, SAL, RAC, and CLB, respectively. Additionally, the efficiency of PdNPs modified BDD electrode was compared to other electrodes reported previously in the literature for β -agonists determination, as summarized in Table 4.1.2. Although, the proposed PdNPs modified BDD electrode possessed higher LOD than other electrodes, it could potentially be used for the simultaneous determination of four β -agonists without electrode fouling problem which has been reported to be the drawback of those conventional glassy carbon electrodes. It has been highlighted in the literature that the electrode fouling was generally caused by the adsorption of the analytes onto the electrode surface and typically made the detection method more complicated and time-consuming due to several steps of electrode cleaning. Therefore, this proposed BDD electrode feasibly showed good anti-fouling property, with good sensitivity and rapid analysis for β -agonist compounds.

Table 4.1.1 Regression equations, linearities, the limits of detection (LODs) and the limits of quantification (LOQs) of UHPLC-ECD for the analysis of four β -agonists^a (n = 3).

β -agonist Compound	Regression Equation ^b	R ²	Linear range ($\mu\text{g mL}^{-1}$)	LOD (ng mL^{-1})	LOQ ($\mu\text{g mL}^{-1}$)
TER	$y = 27.2x + 0.492$	0.997	0.2 - 20	40.0	0.12
SAL	$y = 10.1x + 1.42$	0.996	0.2 - 20	20.0	0.10
RAC	$y = 29.5x + 5.50$	0.994	0.2 - 20	30.0	0.10
CLB	$y = 5.34x + 5.08$	0.996	0.5 - 20	60.0	0.20

^a The same experimental condition as in Fig.6.

^b y is peak current (nA) of electrochemical detection; x: concentration of analytes ($\mu\text{g mL}^{-1}$).

Table 4.1.2 Previous literature using other electrodes for the UHPLC combined with electrochemical detection of β -agonist compounds.

Electrode	Detection Method	Analyte	Linearity range (ng mL^{-1})	LOD (ng mL^{-1})	Real Samples	Ref.
Glassy carbon electrode (GCE)	Amperometry	CLB	1 - 25	0.5	Calf urine	131
Glassy carbon electrode (GCE)	Pulse amperometry	CLB	5 - 100	5	Bovine tissue	138
PdNPs modified BDD electrode	Amperometry	TER	200 - 2000	40	Swine feed Swine meat Urine	This work
		SAL	200 - 2000	20		
		RAC	200 - 2000	30		
		CLB	500 - 2000	60		

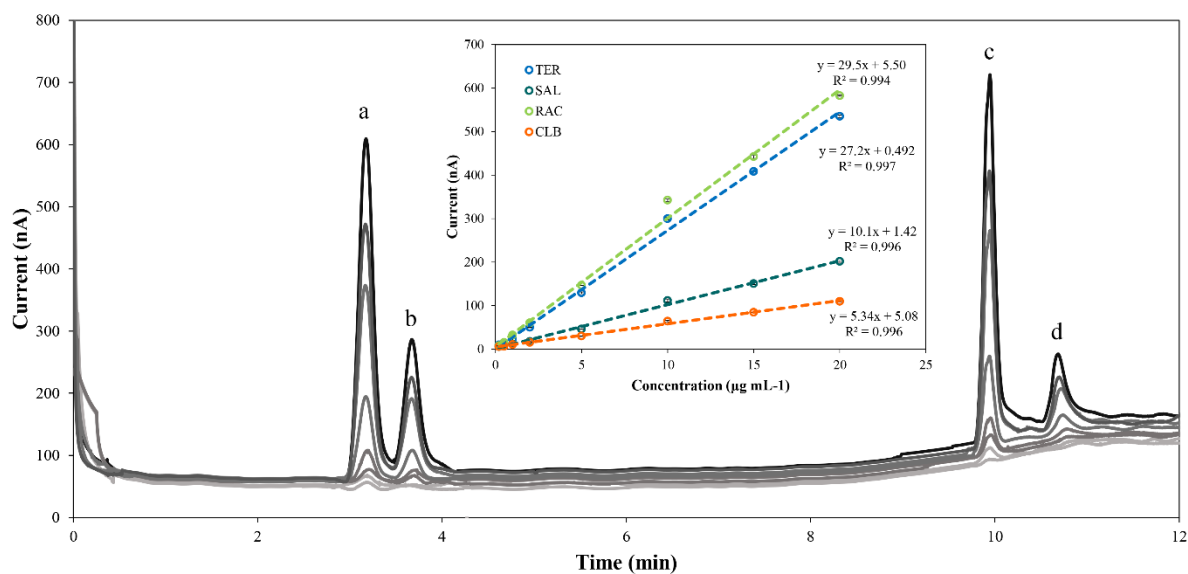


Figure 4.1.10 The amperometric chromatograms of (a) TER, (b) SAL, (c) RAC, and (d) CLB in the concentration range of $0.2 - 20 \mu\text{g mL}^{-1}$ at PdNPs modified BDD electrode after being separated by UHPLC and the corresponding calibration plots (inset). The experiments were performed under optimal conditions.

4.1.3.6 Analytical applications

The applicability of the proposed UHPLC-ECD system for the simultaneous determination of four β -agonists in various samples was evaluated. In this work, feed, meat, and urine samples were used in the quantitative analysis. The feed and meat samples were purchased from supermarket and local fresh market in Thailand. The artificial urine was used as real urine replacement. The different concentrations of β -agonists standard solution were spiked into the extracted samples, and then the spiked samples solution was diluted 20 times with MeOH: 0.05 M phosphate buffer (50:50; v:v). The repeatability of this proposed system was estimated through inter-day and intra-day spiked samples under optimal conditions. The results were summarized in Table 4.2.3. The recoveries of inter-day experiments were obtained in the range of 80.5% – 110% with RSDs ranging from 0.10% to 8.2%, and intra-day recoveries were found to be in the range of 80.3% – 108% with RSDs ranging from 0.10% to 7.3%. It

was indicating that this proposed UHPLC-ECD method had great precision for simultaneous detection of four β -agonists in real samples.

After examining the precision of the UHPLC coupled with ECD (PdNPs/BDD), the acceptability and reliability of this proposed method were tested, and the response was then compared with the validated method (UHPLC-UV). The paired *t*-test at 95% confidence was used to compare the obtained data from UHPLC-UV and UHPLC-ECD. The comparable results were described in Table 4.1.4. The calculated *t*-values of three concentrations in the spiked samples (0.50, 5.0, and 15 $\mu\text{g mL}^{-1}$ of analytes represent the low, medium, and high levels of β -agonists, respectively) were found in the range of 0.252 to 2.315 which was significantly lower than critical *t*-value (2.447). This could imply that the results from UHPLC-ECD method has similar accuracy to those obtained from UHPLC-UV method. As the result, The PdNPs modified BDD electrode coupled with UHPLC is acceptable of simultaneous determination of four β -agonists in various type of samples with high sensitivity and reproducibility.

Table 4.1.1.3 Repeatability of intra- and inter-day and recoveries of the UHPLC-ECD method (n=3).

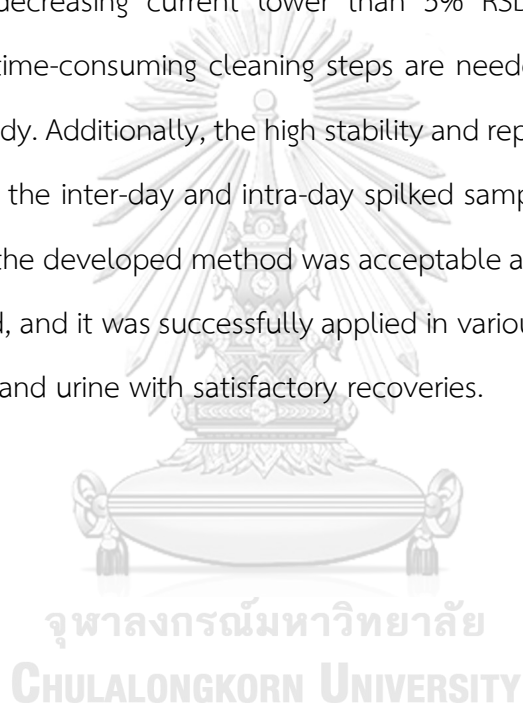
Samples	Spike level ($\mu\text{g g}^{-1}$)	Intra-day						Inter-day									
		Recovery (%)			RSD (%)			Recovery (%)			RSD (%)						
		TER	SAL	RAC	CLB	TER	SAL	RAC	CLB	TER	SAL	RAC	CLB				
1	0.50	83.1	81.7	82.9	107	1.70	5.40	5.30	8.80	95.2	95.7	80.3	99.1	6.80	4.40	6.20	3.50
	5.00	86.4	84.6	94.9	93.0	1.70	0.100	4.00	5.70	89.0	89.2	99.7	89.6	2.90	4.80	2.30	7.70
	15.0	91.1	98.3	98.9	97.9	0.800	1.10	1.30	2.50	90.3	94.9	96.5	94.9	1.00	3.30	3.20	5.80
Swine feed	0.50	95.2	94.1	89.4	80.5	2.80	5.70	3.40	5.80	87.1	90.0	86.3	98.1	3.10	4.90	5.70	7.30
	5.00	95.2	95.6	102	83.2	0.800	5.50	1.10	2.10	93.3	98.0	109	86.6	0.80	4.90	5.20	3.00
	15.0	94.3	96.8	104	95.5	1.50	0.900	1.00	1.00	95.3	93.9	103	91.6	4.60	1.50	2.90	4.70
3	0.50	97.5	88.4	88.5	99.6	4.80	6.20	2.30	6.50	86.0	81.2	87.2	96.5	5.20	4.80	6.70	5.80
	5.00	92.6	94.6	102	92.0	4.10	1.10	3.30	1.80	88.7	89.1	99.4	89.3	5.70	4.90	2.80	5.60
	15.0	94.2	102	101	94.7	1.80	1.40	0.80	1.50	92.1	81.2	99.0	97.7	0.100	4.80	2.30	3.90
1	0.50	101	104	99.0	95.1	5.50	2.60	1.30	6.50	106	96.4	100	93.8	4.50	1.60	1.10	3.20
	5.00	93.8	93.2	102	94.8	4.30	3.20	2.40	4.50	102	92.3	101	99.8	5.50	1.10	4.30	5.70
	15.0	97.4	98.1	101	102	1.30	1.00	1.90	0.40	103	99.7	101	99.9	4.40	7.00	5.00	1.60
Swine meat	0.50	93.0	94.8	100	95.4	5.10	5.00	4.40	8.20	94.2	93.7	101	99.2	5.60	4.60	1.50	5.80
	5.00	95.0	97.1	105	102	0.800	0.400	0.700	2.90	99.5	96.7	98.6	102	3.90	1.00	5.80	2.30
	15.0	101	90.6	103	106	1.30	2.50	2.50	2.90	105	92.7	99.7	101	3.10	2.00	5.60	3.70
3	0.50	94.8	108	106	109	1.50	2.10	7.00	5.80	90.3	104	104	106	4.30	5.40	1.70	4.00
	5.00	104	105	102	109	1.30	1.60	3.40	1.90	105	104	103	105	1.30	0.800	1.10	3.40
	15.0	107	105	100	99.7	1.40	1.60	2.10	4.60	108	106	102	98.9	1.10	0.300	2.10	1.90
Artificial urine	0.50	108	101	88.8	107	3.50	2.30	4.30	3.80	105	97.0	94.3	100	4.80	5.50	5.60	6.70
	5.00	100	109	100	89.5	2.10	2.30	4.30	5.20	96.9	103	102	96.0	3.50	6.20	2.60	6.30
	15.0	105	110	103	96.2	1.70	2.30	2.40	3.50	103	103	102	100	2.50	6.70	0.60	3.70

Table 4.1.4 The recoveries of spiked samples reported using the developed UHPLC-ECD and UHPLC-UV methods.

Sample	Spiked level ($\mu\text{g/g}$)	Amount found ($\mu\text{g ml}^{-1}$) ($n \pm \text{SD}$)												% Recovery			
		UHPLC-ECD				UHPLC-UV				UHPLC-ECD				UHPLC-UV			
		TER	SAL	RAC	CLB	TER	SAL	RAC	CLB	TER	SAL	RAC	CLB	TER	SAL	RAC	CLB
1	0.00	ND ^a	ND	ND	ND	ND	ND	ND	ND	ND	ND	ND	ND	ND	ND	ND	ND
	0.50	0.590 ± 0.1	0.480 ± 0.1	0.440 ± 0.1	0.710 ± 0.1	0.510 ± 0.1	0.520 ± 0.1	0.710 ± 0.1	0.610 ± 0.1	0.520 ± 0.1	0.520 ± 0.1	0.710 ± 0.1	83.1	81.7	82.9	107	89.9
	5.00	4.49 ± 0.1	4.50 ± 0.1	4.78 ± 0.2	4.71 ± 0.3	4.69 ± 0.1	5.14 ± 0.1	5.16 ± 0.1	4.80 ± 0.1	5.14 ± 0.1	5.14 ± 0.1	5.16 ± 0.1	86.4	84.6	94.9	93.0	92.7
	15.0	13.7 ± 0.1	14.8 ± 0.2	14.8 ± 0.2	14.7 ± 0.4	13.7 ± 0.1	15.1 ± 0.1	16.5 ± 0.1	14.2 ± 0.1	15.1 ± 0.1	15.1 ± 0.1	16.5 ± 0.1	91.1	98.3	98.9	97.9	91.4
	0.00	ND	LLOQ ^b	ND	ND	ND	LLOQ	ND	LLOQ	ND	ND	ND	-	-	-	-	-
2	0.50	0.590 ± 0.1	0.720 ± 0.1	0.450 ± 0.1	0.670 ± 0.1	0.510 ± 0.1	0.620 ± 0.1	0.480 ± 0.1	0.830 ± 0.1	0.480 ± 0.1	0.510 ± 0.1	0.550 ± 0.1	95.2	94.1	89.4	80.5	90.7
	5.00	4.88 ± 0.1	5.03 ± 0.3	5.12 ± 0.1	4.43 ± 0.1	4.81 ± 0.1	5.35 ± 0.1	4.52 ± 0.1	4.95 ± 0.1	5.35 ± 0.1	5.35 ± 0.1	4.52 ± 0.1	95.2	95.6	102	83.2	95.0
	15.0	14.2 ± 0.2	14.6 ± 0.1	15.5 ± 0.2	14.6 ± 0.1	13.9 ± 0.2	15.4 ± 0.1	16.2 ± 0.1	14.3 ± 0.2	15.4 ± 0.1	15.4 ± 0.1	16.2 ± 0.1	94.3	96.8	104	95.5	92.3
	0.00	ND	LLOQ	ND	LLOQ	ND	-	-	-	-	-						
	0.50	0.640 ± 0.1	0.690 ± 0.1	0.440 ± 0.1	0.740 ± 0.1	0.550 ± 0.1	0.660 ± 0.1	0.730 ± 0.1	0.660 ± 0.1	0.620 ± 0.1	0.620 ± 0.1	0.730 ± 0.1	97.5	88.4	88.5	99.6	94.8
3	5.00	4.78 ± 0.2	4.69 ± 0.1	5.09 ± 0.2	4.68 ± 0.1	4.82 ± 0.1	5.00 ± 0.1	5.06 ± 0.3	5.00 ± 0.1	5.39 ± 0.1	5.06 ± 0.3	5.06 ± 0.3	92.6	94.6	102	92.0	95.2
	15.0	14.2 ± 0.2	15.4 ± 0.2	15.1 ± 0.1	14.3 ± 0.2	14.3 ± 0.1	14.9 ± 0.2	15.9 ± 0.2	14.9 ± 0.2	15.9 ± 0.2	15.9 ± 0.2	15.9 ± 0.1	94.2	102	101	94.7	94.9
	0.00	ND	ND	ND	ND	ND	ND	ND	ND	ND	ND	ND	-	-	-	-	-
	0.50	0.510 ± 0.1	0.520 ± 0.1	0.500 ± 0.1	0.470 ± 0.1	0.500 ± 0.1	0.500 ± 0.1	0.500 ± 0.1	0.550 ± 0.1	0.500 ± 0.1	0.500 ± 0.1	0.550 ± 0.1	101	104	99.0	95.1	100
	5.00	4.69 ± 0.2	4.66 ± 0.2	5.10 ± 0.1	4.74 ± 0.1	5.30 ± 0.1	5.14 ± 0.1	5.05 ± 0.1	5.14 ± 0.1	5.44 ± 0.1	5.05 ± 0.1	5.05 ± 0.1	93.8	93.2	102	94.8	106
Swine meat	15.0	14.6 ± 0.2	14.7 ± 0.1	15.1 ± 0.3	15.2 ± 0.1	15.2 ± 0.6	15.4 ± 0.6	16.1 ± 0.1	15.2 ± 0.6	15.4 ± 0.6	16.1 ± 0.1	14.1 ± 0.3	97.4	98.1	101	102	102
	0.00	ND	ND	ND	ND	ND	ND	ND	ND	ND	ND	ND	-	-	-	-	-
	0.50	0.470 ± 0.1	0.470 ± 0.1	0.500 ± 0.1	0.480 ± 0.1	0.510 ± 0.1	0.550 ± 0.1	0.510 ± 0.1	0.550 ± 0.1	0.510 ± 0.1	0.510 ± 0.1	0.500 ± 0.1	93.0	94.8	100	95.4	102
	5.00	4.75 ± 0.1	4.86 ± 0.1	5.26 ± 0.1	4.74 ± 0.1	5.38 ± 0.1	5.33 ± 0.1	5.50 ± 0.1	5.33 ± 0.1	5.50 ± 0.1	5.50 ± 0.1	5.06 ± 0.2	95.0	97.1	105	101	108
	15.0	15.2 ± 0.2	15.6 ± 0.3	15.9 ± 0.2	15.2 ± 0.1	16.1 ± 0.3	16.1 ± 0.3	16.1 ± 0.1	14.1 ± 0.2	16.1 ± 0.1	16.1 ± 0.1	15.4 ± 0.2	101	90.6	103	106	107
3	0.00	ND	ND	ND	ND	ND	ND	ND	ND	ND	ND	ND	-	-	-	-	-
	0.50	0.470 ± 0.1	0.540 ± 0.1	0.530 ± 0.3	0.550 ± 0.1	0.440 ± 0.1	0.550 ± 0.1	0.540 ± 0.1	0.550 ± 0.1	0.540 ± 0.1	0.540 ± 0.1	0.530 ± 0.1	94.8	107	105	109	87.7
	5.00	5.21 ± 0.1	5.27 ± 0.1	5.08 ± 0.2	5.47 ± 0.1	5.35 ± 0.3	5.68 ± 0.1	5.05 ± 0.1	5.68 ± 0.1	5.05 ± 0.1	5.05 ± 0.1	5.06 ± 0.3	104	105	102	109	107
	15.0	16.1 ± 0.2	15.8 ± 0.3	15.0 ± 0.3	15.0 ± 0.7	16.5 ± 0.2	16.2 ± 0.2	14.9 ± 0.2	16.2 ± 0.2	14.9 ± 0.2	14.9 ± 0.2	15.8 ± 0.6	107	106	100	108	109
	0.00	ND	ND	ND	ND	ND	ND	ND	ND	ND	ND	ND	-	-	-	-	-
Artificial urine	0.50	0.540 ± 0.1	0.500 ± 0.1	0.440 ± 0.1	0.540 ± 0.1	0.50 ± 0.1	0.520 ± 0.1	0.450 ± 0.1	0.520 ± 0.1	0.450 ± 0.1	0.450 ± 0.1	0.550 ± 0.1	108	100	88.8	107	99.4
	5.00	5.01 ± 0.1	5.44 ± 0.1	5.00 ± 0.2	4.48 ± 0.2	5.00 ± 0.1	5.05 ± 0.1	4.83 ± 0.1	5.05 ± 0.1	5.05 ± 0.1	4.83 ± 0.1	4.97 ± 0.3	100	108	100	89.5	99.9
	15.0	15.8 ± 0.3	16.5 ± 0.1	15.5 ± 0.4	14.6 ± 0.5	15.4 ± 0.3	15.5 ± 0.3	14.6 ± 0.1	15.5 ± 0.3	15.5 ± 0.3	14.6 ± 0.1	15.9 ± 0.3	105	110	103	96.2	102
	0.00	ND	ND	ND	ND	ND	ND	ND	ND	ND	ND	ND	-	-	-	-	-
	0.50	0.540 ± 0.1	0.500 ± 0.1	0.440 ± 0.1	0.540 ± 0.1	0.50 ± 0.1	0.520 ± 0.1	0.450 ± 0.1	0.520 ± 0.1	0.450 ± 0.1	0.450 ± 0.1	0.550 ± 0.1	108	100	88.8	107	99.4
Paired two-tail test	t critical = 2.45	2.32	1.68	2.37	1.74	2.02	0.473	0.681	2.31	0.93	1.87	0.252	0.93	1.87	0.252	0.93	1.87
	t-value (5)	2.02	1.68	2.37	1.74	2.02	0.473	0.681	2.31	0.93	1.87	0.252	0.93	1.87	0.252	0.93	1.87
	t-value (15)	1.07	0.473	0.681	2.31	1.07	0.473	0.681	2.31	1.07	0.473	0.681	2.31	1.07	0.473	0.681	2.31

4.1.4 Conclusion

The PdNPs modified BDD electrode was firstly fabricated and proposed for determination of TER, SAL, RAC and CLB after their separation using UHPLC. The proposed UHPLC-ECD system presented the rapid separation and the reproduced analysis of four β -agonists within 11 min. The modified BDD electrode offered excellent repeatability and stability of the electrode surface for continuous detection of these compounds up to 10 times attributed to the excellent anti-fouling capability with satisfactory decreasing current lower than 5% RSD values. As a result, no complicated and time-consuming cleaning steps are needed in this work, compared to the previous study. Additionally, the high stability and reproducibility of this method were observed *via* the inter-day and intra-day spiked samples with %RSD lower than 7%. Furthermore, the developed method was acceptable and reliable comparing with UHPLC-UV method, and it was successfully applied in various samples including swine feed, swine meat, and urine with satisfactory recoveries.



PART II

4.2 A ready-to-use electrochemical origami-like sensor based on molecular imprinting for selective detection of SAL

Atchara Lomae^a , Sudkate Chaiyo^{a,b} , Orawon Chailapakul^a , Weena Siangproh^c , Peter A. Lieberzeit^{d*} and Janjira Panchompoo

^a Electrochemistry and Optical Spectroscopy Center of Excellence, Department of Chemistry, Faculty of Science, Chulalongkorn University, Pathumwan, Bangkok 10330, Thailand

^b The Institute of Biotechnology and Genetic Engineering, Chulalongkorn University, Pathumwan, Bangkok, 10330, Thailand

^c Department of Chemistry, Faculty of Science, Srinakharinwirot University, Sukhumvit 23, Wattana, Bangkok 10110, Thailand

^d University of Vienna, Faculty for Chemistry, Department of Physical Chemistry, 1090, Vienna, Austria

จุฬาลงกรณ์มหาวิทยาลัย
CHULALONGKORN UNIVERSITY

**Corresponding author

*Co-corresponding author

Abstract

Currently, the ready-to-use with a simplified, reliable, inexpensive devices is extremely needed as well as the high selectivity and portable device. Herein, an origami-like electrochemical paper-based analytical device (origami-ePAD) was established for salbutamol (SAL) determination. An enhanced selectivity and sensitivity of origami-ePAD could be acquired from the molecularly imprinted polymer and conducting polymer, utilized as modifier for electrochemical embedment onto screen-printed graphene electrode surface. The polyaniline (PANI) was firstly employed for electrode surface modification to enhance the conducting property of SPGE and assist the embedment of MIP on the electrochemical sensing surface. For the preparation of MIP, the co-electropolymerization of 3-aminophenyl boronic acid (APB) and *o*-phenylenediamine (*o*-PD) in presence of the template molecule (SAL) was performed. Since PAD exhibits the capable of incubating sample, washing, and delivering the reagent, this developed origami-ePAD offers the convenient use through only one drop of running buffer solution in EIS measurement. Using origami-ePADs based MIP/PANI/SPGE under optimized condition, the linearity was found to be in the range of 0.05 – 20 $\mu\text{g mL}^{-1}$ with an excellent LOD of 7.5 ng mL^{-1} . The MIP/PANI/SPGE integrated origami-PAD could be used to measure SAL in a urine sample with satisfactory % recoveries from 88.2 to 101.4%. This established origami-ePAD based MIP/PANI/SPGE sensor offered the numerous advantages of simplicity, and the ability to perform a multiple step in one device only. This proposed sensor could be exceptionally applied in biological sample with good accuracy and great reliability, acquiesced in the obtained results from standard HPLC-UV method.

Keyword; Molecularly imprinted polymer (MIP), Polyaniline (PANI), Salbutamol (SAL), origami-ePADs.

4.2.1 Introduction

The illegal use of salbutamol (SAL), categorized as one of the β_2 -receptor agonists, as growth-promoting and doping agents has become an apparent issue worldwide. Currently, SAL is prevalently used as meat leaning and doping agents as it possesses ergogenic action. Typically, SAL could enhance the muscle mass through the fat level transformation^{169, 170}. Yet, the utilization of SAL for improving athlete performance has still been illegal^{130, 171}. Consequently, the application of SAL is therefore strictly controlled by laws and regulations. According to World Anti-Doping Agency (WADA), the maximum SAL content of 1000 ng mL^{-1} found in urine, has been legally allowed¹⁷². Due to the misuse of SAL, the development of SAL sensor for monitoring and controlling of its usage has extensively received much attention. However, dominant characteristics of the applied sensor such as portability, affordability, simplicity should also be realized.

There are numerous methods for determination of SAL including spectrophotometry^{173, 174}, high-performance liquid chromatography¹⁶⁹, electrochemistry^{175, 176}, aptamer based sensor¹⁷⁷ and EILISA approach¹⁷⁸. Among these techniques, electrochemical approaches could be used as portable sensing systems for SAL determination because of its capability of miniaturization, as well as being inexpensive, rapid, user-friendly and, highly sensitive^{7, 17}. However, the critical challenge of electrochemical strategy is the sensitive measurement of target analyte in complex media, especially in biological and food samples. Recently, researchers have been improved the selectivity of electrochemical method by employing the electrode modification and the uses of the separation technique including HPLC^{179, 180} or UHPLC⁷⁸, as previously reported in the literature. Although these chromatographically integrated electrochemical techniques offer high selectivity and sensitivity, they are some limitation such as time consuming, require complicated and expensive instrumentation, and skilled operators. These limitations making them are

unsuitable for the development of a portable sensor. Due to these selectivity drawbacks, the specific modification of electrochemical sensor surface with recognition system is therefore greatly required.

Molecularly imprinted polymers (MIP) is one of recognition techniques that have attracted growing interest for numerous applications especially in biological areas. This technique has been extensively developed and integrated with electrochemical sensing platforms in order to improve their detection selectivity. The principle of MIP approach is based on “lock and key” mechanism in which the target analytes are captured into the generated cavities with physical and chemical interactions. The MIP preparation is carried out by the polymerization of monomer and cross-linker in the presence of the molecule of interest, called the template. The cavities distribute over the MIPs surface with complementary size, shape, and chemical functionality are then developed after the removal of specific template molecule^{27, 90}. With the aid of electropolymerization procedure, the MIP film directly grows on electrode surface, and its thickness can be simultaneously controlled by changing the polymerization condition.^{26, 181} As relevant features addressed, the MIP-based electrochemical biosensor have consecutively developed for extensive applications supported by many publications¹⁸¹⁻¹⁸⁵. The MIP-based sensor exhibited high stability and selectivity, prominent reusability, and good reproducibility^{185, 186}. So far, Taher Alizadeh and co-workers¹⁴⁰ studied the use of Cu²⁺-mediated imprinted polymer-based carbon paste electrode as sensing platform for SAL determination, and the results revealed that offered high sensitivity of SAL determination with the limit of detection (LOD) of 6.0×10^{-10} M. In addition, another research article published by Decha Dechtrirat et.al,⁸⁵ reported the embedment of MIP recognition layer onto PEDOT: PSS/graphene electrode surface for SAL measurement, and the improved analytical performance of their proposed sensor could be enhanced. Nonetheless, these troublesome of MIP-based platforms persistently require complicated multi-steps sequential process of

removing template, washing and incubation of the template and the analyte, respectively. Moreover, long analysis time is also required to complete the detection step making them inconvenient for the end-users. To eradicate these obstacles, a microfluidic paper-based device (μ PAD) platform for a ready-to-use sensor was created^{35, 187}. The advantage features of μ PADs are attributed to its affordability, ease of fabrication and adaptability in the design of sensor. Also, a small sample volume is needed for completing each measurement. As previously reported by Abdulhadee Yakoh et.al., the highly adaptable design of μ PADs has been investigated, and developed sensor could be used for the electrochemical detection either stopped flow and flow system. By employing this developed sensing platform, multiple steps of experiment could be combined, and the analysis time could subsequently be reduced^{9, 38, 188, 189}.

Herein, we demonstrated the ready-to-use MIP-based electrochemical impedance sensor with origami and sliding PAD design for the determination of SAL. In this present work, the sliding PAD consisted of three removal channels for loading sample, washing, and detection. All these steps could be finished by sliding the movable PAD sequentially with each introduction of the sample solution and a carrier buffer. In addition, the developed PAD was firstly merged with MIP-based polyaniline modified screen-printed graphene electrode (MIP/PANI/SPGE) to create the electrochemical sensor. This proposed strategy offered high selectivity and sensitivity, as well as providing simplicity in the detection. Moreover, this created sensing platform could be successfully applied to examine SAL in urine sample with satisfactory results, indicating that the proposed sensor could be used as an alternative tool for measuring SAL in complex biological samples with high selectivity.

4.2.2. Experimental

4.2.2.1 Materials and equipment.

All commercial chemicals and reagents utilized in this study were analytical grade and used as received without further purification. Salbutamol sulfate, clenbuterol hydrochloride, ractopamine, phosphate buffered saline (PBS) and potassium ferricyanide were purchased from Sigma Aldrich (St. Louis, MO, USA). The monomer and cross-linker which are 3-aminophenylboronic acid hemisulfate salt and *o*-phenylenediamine (*o*-PD), orderly, were acquired from Sigma Aldrich (St. Louis, MO, USA). Aniline was purchased from AppliChem (Darmstadt, Germany). Potassium hexacyanoferrate(III), $[K_3Fe(CN)_6]$ and potassium hexacyanoferrate(II), $[K_4Fe(CN)_6]$ were purchased from Sigma Aldrich (St. Louis, MO, USA). Acetic acid, sodium acetate, sulfuric acid and perchloric acid were purchased from Merck (Darmstadt, Germany). All solutions were freshly prepared in ultrapure water produced by a Milli-Q system (18.2 M Ω cm) from Millipore. The PVC used as electrode substrate was obtained from Deecraft (Bangkok, Thailand). The conductive ink-material for manufacturing screen-printed electrode including graphene and Ag/AgCl ink were purchased from Serve science (Bangkok, Thailand) and Gwent group/Sun Chemical (Pontypool, U.K.), respectively. For manufacturing the sliding paper-based device (Sliding-PADs) and holding paper-based devices (holding-PAD), Whatman No.4 chromatography paper was used as substrate material and acquired from Fisher Scientific (PA). The hydrophobic and hydrophilic areas on PAD were created by a Xerox ColorQube 8570 (CT) wax printer. The surface morphology of the modified electrode was verified by a Scanning Electron Microscope and Energy Dispersive X-ray Spectrometer (SEM-EDS) (IT-500HR) (JEOL Ltd., Japan). The characterization of MIP was performed by cyclic voltammetry (CV) and electrochemical impedance spectroscopy (EIS). All electrochemical measurements were carried out using a potentiostat from PlamSens.

4.2.2.2 Preparation of polyaniline modified screen-printed graphene electrode (PANI/SPGE).

Polyaniline film was coated on SPGE surface using a cyclic voltammetry as previously described¹⁹⁰. For electropolymerization procedure, the potential sweep was scanned from -0.2 and 0.9 V (versus Ag/AgCl) with a scan rate of 50 mVs⁻¹ for 20 cycles in 1 M HClO₄ containing of 3 mM aniline.

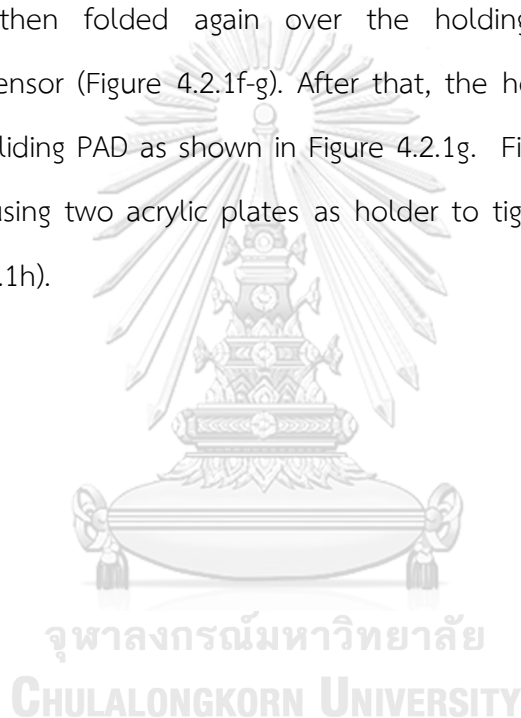
4.2.2.3 Preparation of imprinted and non-imprinted electrode.

The MIP film was electrochemically embedded onto the PANI/SPGE using cyclic voltammetry according to the previous report⁸⁵. The experiment was carried out by employing the sweeping potential ranging from 0 to 1.2 V (vs Ag/AgCl) with a scan rate of 50 mVs⁻¹ for 20 cycles in a mixture solution comprising 5 mM aminophenylboronic acid, 5 mM *o*-PD and 2.5 mM salbutamol sulfate dissolved in 200 mM acetate buffer. After the polymerizing step, the template molecule was then removed by immersing the modified PANI/SPGE in a 0.1 M H₂SO₄ for 7 min. The according electrode was thoroughly rinsed with excess amount of Milli-water in order to extract any loose binding SAL molecules on electrode surface. For comparison, a non-imprinted electrode was also prepared using the same procedure, except that the template molecule (SAL) was excluded from the experiment.

4.2.2.4 Fabrication of the origami-ePAD.

The origami-ePAD consisted of two main parts: the buffer holding and the sequential sliding compartments. All device designs were created by employing Adobe Illustrator CC (Adobe System, USA). A wax pattern was printed onto Whatman grade 4 chromatography paper using a wax-printing technique (Wax-printer, Xerox ColorQube 8570, Japan). After that, the printed paper was subsequently placed in an oven at 160 °C for 1 min to melt the printed wax in order to generate the wax barrier on PAD. Next, the hydrophilic zone in sample loading channel was punctured to create the sample zone on sliding-PAD. To assemble solution surplus, blotting paper was

attached along the bottom-side of sliding-PAD. Before devices assembling, the small holes for fluid flow in washing step were created around WE of the MIP based PANI/SPGE (Figure 4.2.1a). Next, the punched double-side adhesive tape was directly stuck over the electrode, creating retraining solution channel (Figure 4.2.1b). After that, this established electrode was then attached onto the holding-PAD (Figure 4.2.1c). To assemble devices, the sliding-PAD was placed over the holding-PAD, followed by fold of sensor channel over the sliding PADs as shown in Figure 4.2.1e. The upper side of sliding-PAD was then folded again over the holding-PADs to sandwich the electrochemical sensor (Figure 4.2.1f-g). After that, the holding buffer channel was flipped over the sliding PAD as shown in Figure 4.2.1g. Finally, the established PAD was sandwiched using two acrylic plates as holder to tighten the origami ePAD by magnet (Figure 4.2.1h).



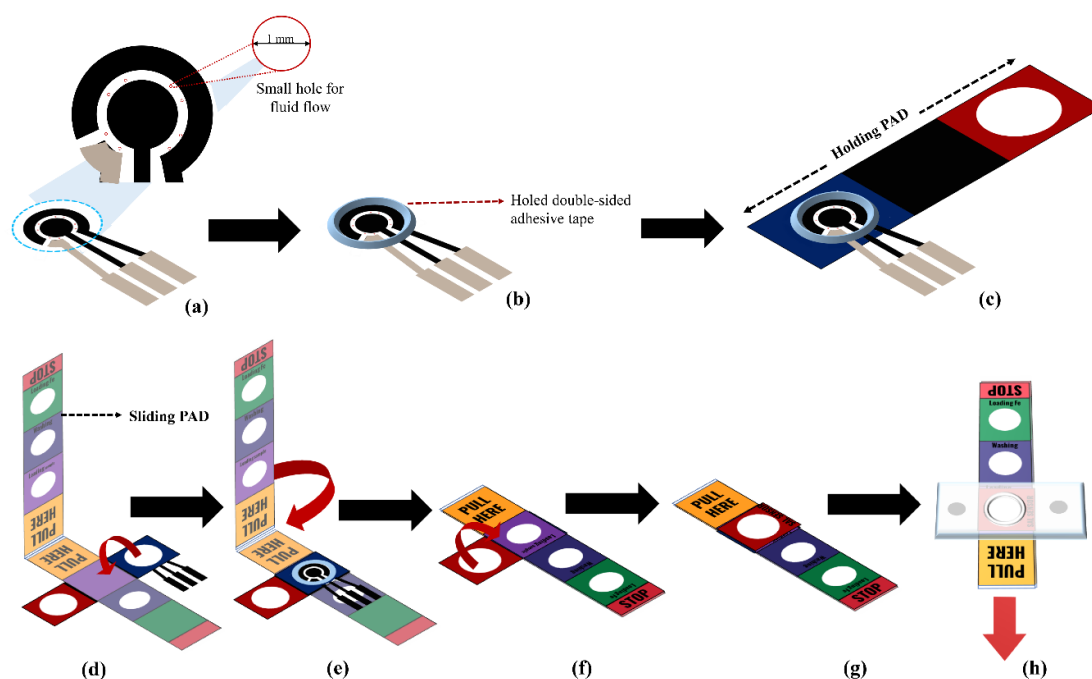


Figure 4.2.1 Schematic illustration of the fabrication of the origami-ePAD based MIP/PANI/SPGE device as follows: (a) the small holes were created around WE, (b) the holed double-side adhesive tape was stuck over the electrode. (c) the constructed electrode was then attached onto the holding PADs. For sliding-PADs manufacture, (d) the holding PADs was firstly placed beneath sliding PADs. Then (e) the sensing channel contained MIP modified electrode was flipped over the sliding PADs, followed by the fold of upper-side of sliding-PAD over electrode sensor. After that, the (f) the holding channel was flipped again over the sliding PADs. The established device was shown in (g). Finally, (h) the attained device was sandwiched between two acrylic plates and tightened by the magnet.

4.2.2.5 Measurement of SAL using the origami-like electrochemical paper-based analytical device (origami-ePAD).

To measure SAL using the developed origami-ePAD modified with MIP, SAL standard or sample solution was directly added on the “sample loading” channel and then incubated for 7 min to allow binding between SAL and its complementary cavities on MIP. Next, the sliding PAD was slipped to the “washing” channel, followed by the addition of running buffer solution onto the solution reservoir. After this step, the running buffer, carrying all residue and non-binding SAL, straightforwardly flowed to the electrode surface and the absorbent pad attached at the bottom-side of the sliding PAD, respectively. For the detection step, the sliding PAD was slipped towards the reagent reservoir, stored the $[\text{Fe}(\text{CN})_6]^{3-/4-}$ solution as electroactive probe. Additionally, the stopped mobility of solution was designated by the wax barrier channel opposite to the reagent reservoir. In this work, electrochemical impedance spectroscopy (EIS) was employed in the detection since it provides simplified operation and high sensitivity.

4.2.2.6 Preparation of real sample.

Artificial urine purchased from Carolina lot 37260601 (York Road, Burlington) was prepared in PBS buffer (pH 7.4). The samples were spiked with various concentration of standard SAL. Finally, the recoveries were thoroughly calculated and compared to demonstrate the efficiency and applicability of this proposed sensor.

4.2.3. Results and discussion

4.2.3.1 Characterization of the MIP modified PANI/SPGE

In this work, the characterization of the sequential modification electrode of SPGE, polymeric film generated from polyaniline modified SPGE (PANI/SPGE) and MIP film produced from aminophenylboronic-co-o-PD modified PANI/SPGE, was carried out by EIS technique. EIS has been typically used to confirm the achieving modification of electrochemical sensor surface. The basis of this technique relies on the electrode's

capability to resist the flow of electron transfer at its interface. As depicted in the Nyquist plot (Figure 4.2.2a), at the SPGE, the small semicircle diameters (R_{ct}) of Nyquist plot was observed (1.76 k Ω) indicating that the electron could be directly transferred toward electrode surface without any hindrance. However, after modifying with PANI, a comprehensive decrease in R_{ct} value was observed (0.80 k Ω) indicating the greater conducting property of PANI/SPGE in comparison to the bare SPGE. Additionally, when the cross-linker and analyte template were polymerized onto the PANI/SPGE, the R_{ct} value further increased to 333.4 k Ω , confirming the successful fabrication of the MIP layer on the electrode surface. Nonetheless, after extracting the template molecule, the surface with specific cavities noticeably decreased in the R_{ct} response, suggesting the improved electron-transfer capability at the electrode interface. This achieved result might be generated cavities distributing on the entire surface could enhance the electro-active surface area of the modified sensor, resulting in the lower responsive R_{ct} . Finally, the R_{ct} value was found to increase again after the incubating step. This result revealed the forbidden electron transfer between redox probe and interfacial of electrode sensor attributing to the binding between SAL and specific cavities of MIP. Moreover, these results were consistent with the electron transfer rate (K_{et}) calculated from equation 4.2.1.

$$K_{et} = \frac{RT}{n_2 F_2 R_{ct} A C} \quad (4.2.1)$$

Where R is the ideal gas constant (JK⁻¹ mol⁻¹), T is temperature (K), n is a number of electron transfer, F is the faraday constant, R_{ct} value is obtained from Nyquist plot, A is the geometrical area of the electrode surface (cm²), and C redox is the concentration of [Fe(CN)₆]^{3-/4-} solution (10 mM).

Additionally, the change of electrode surface was thoroughly characterized using cyclic voltammetry. As show in Figure 4.2.2b, after polymerization of MIP, the current response of 10 mM redox probe ($\text{Fe}(\text{CN})_6^{3-/4-}$) was lower than that PANI/SPGE and SPGE. These might be attributed to the higher insulating property of the MIP polymeric film embedded on the electrode surface, resulting in the low penetration of electron toward interfacial electrode. After the template molecule was removed, the modified electrode with MIP cavities possessed the higher current response of the redox signal compared to the MIP/PANI/SPGE. After that the current response rapidly decreased once again after incubating SAL owing to rebinding of target molecule in MIP cavities. The obtained EIS and CV results confirmed that the deposition of PANI and MIP could be achieved.



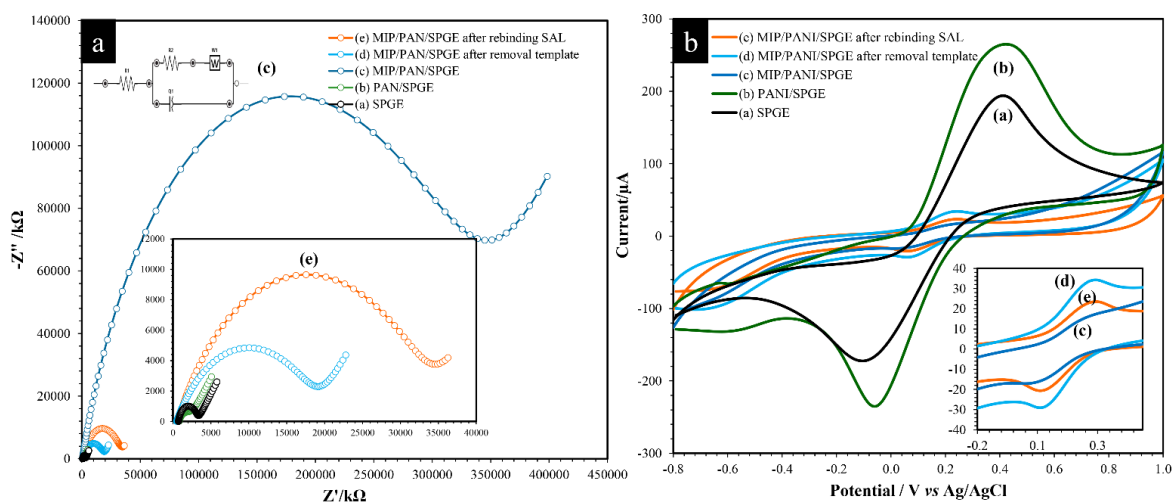


Figure 4.2.2 The characterization of MIP/PANI/SPGE sensor in the step-by-step modification for the SAL determination by (a) EIS technique and its data was obtained for the equivalent circuit including solution resistance (R_1), charge transfer resistance (R_2), constant Phase Element (Q) and warburg element (W), and (b) CV of 10 mM $[\text{Fe}(\text{CN})_6]^{3-/4-}$ in absent and present of $10 \mu\text{g mL}^{-1}$ of SAL with potential scan from -0.8 – 1.0 V vs Ag/AgCl and scan rate of 100 mVs^{-1} .

Table 4.2.1 The R_{ct} and K_{et} values of different electrodes.

Electrode	$R_{ct} / \text{k}\Omega$	$K_{et} \times 10^{-5} \text{ cm s}^{-1}$
SPGE	1.76	9.2
PANI/SPGE	0.806	20
MIP/PANI/SPGE	333.4	0.048
MIP/PANI/SPGE after template removal	18.7	0.86
MIP/PANI/SPGE after rebinding SAL	33.4	0.48

4.2.3.2 Optimization of influence parameters for SAL determination using the MIP/PANI/SPGE.

Importantly, the sensitivity of EIS response could be affected by the concentrations of aminophenylboronic, *o*-PD and PANI. Thus, these factors were optimized using EIS technique as follows:

4.2.3.2.1 Effect of aniline concentration on PANI thickness

According to rich amine groups on the PANI's backbone and its conductive property^{191, 192}, the PANI was therefore considered as polymeric material to modify electrode surface. This incident might be attributed to the dipole induce dipole or hydrogen bond between functional groups in both co-monomers including -OH and -NH₂ and backbone of PANI¹⁹¹. The polymeric PANI was simultaneously synthesized and deposited on the electrode surface via electropolymerization process. Therefore, the concentration of aniline and number of CV scan for creating the PANI film were optimized. The concentration of aniline was firstly investigated in the range of 1- 10 mM. The R_{ct} response of redox probe after rebinding SAL subtracted the R_{ct} response of redox probe after removal template was reported as ΔR_{ct} . In this case, the difference in ΔR_{ct} response was expected in order to acquire the highly sensitive sensor. As displayed in Figure 4.2.3a, the lowest ΔR_{ct} response was observed at 1 mM aniline. A possible explanation could be that PANI incompletely covered the whole electrode surface, resulting in the low efficiency of MIP formation. However, the highest ΔR_{ct} response was obtained when 3 mM of aniline was employed in the polymerizing step. It indicated that the entire surface sensor was covered by the polymeric PANI film, allowing more MIP to adsorb on the electrode surface. Nonetheless, the ΔR_{ct} value abruptly decreased and became constant when high concentration (more than 3 mM) of aniline was applied. The high aniline concentration used might cause the branch polymer¹⁹³ which could obstruct the deposition of the MIP polymeric film.

Moreover, the thickness of polymeric film covering the electrode surface should also be evaluated since it could affect the measurement. Regarding the electrochemical polymerization, the polymeric thickness can be simply controlled by varying number of cycles in cyclic voltammetry^{34, 194}. The number of CV cycles was investigated in the range from 5 to 30 cycles, and it was found that the ΔR_{ct} value gradually increased with increasing the number of CV scans from 5 to 20 cycles (Figure 4.2.3b). This signal increment could be attributed to the progressive deposition of MIP on PANI film during the polymerization process. However, the ΔR_{ct} value immediately decreased when 30 cycles of CV scan were employed. This result suggested that the higher thickness film could be generated, resulting in the low electron-transfer capability of the redox probe. Therefore, it could be concluded that 3 mM of aniline and 20 cycles of CV scans were the optimal conditions for this system. Thus, these parameters were selected for further experiments.

4.2.3.2.2 Effect of MIP-template formation

To target the SAL, the APB containing -OH and -NH₂ functional groups⁸⁵, offering H-bond acceptor against SAL molecule was employed as functional monomer. However, the only use of aminophenylboronic acid and SAL for producing MIP, being undesirable binding impedimentary. Thus, the *o*-PD presenting low affinity against template molecule was co-polymerized with APB and template molecule to suppress this non-specific binding. The molar ratio of monomer to template importantly affects the efficiency toward SAL determination such as sensitivity and response time that was assessed. The MIP, prepared in different [APB]: [SAL] ratio of 1:2, 1:1, 2:1, 4:1 and 8:1, was embedded in optimizing PANI used for electrode modification as displayed in Figure 4.2.3c. It could be seen in Figure 4.2.3c that the ΔR_{ct} value increased with increasing the molar ratio from 1:2 to 2:1, indicating an enlargement of MIP cavities against SAL molecule. However, the decrease in ΔR_{ct} value in any excess concentrations of APM (at 4:1 and 8:1 molar ratio of AMP against SAL) could be

observed. This result indicated that the MIP cavities could be covered by excess polymeric-AMP consequently affected the decrease in effective cavities. Thus, APB: SAL molar ratio of 2:1 was therefore selected as the optimal condition to fabricate an effective MIP layer. These results were consistent with those obtained from the computational simulation reported by Dechtrirat et.al⁸⁵, suggesting that one template molecule can be stable with two surrounding APB monomers via the H-bonding.

Beside suppressing non-specific binding, *o*-PD also has the capability to form rigid polymer via binding with another nearby APB. Hence, the molar ratio between APM and *o*-PD which could significantly affect the selectivity and capacity of MIP binding was next investigated and the obtained results were as shown in Figure 4.2.3d. The [APB]: [*o*-PD] ratios of 2:1, 1:1, 1:2, 1:3, 1:4 and 1:6 were used for preparing MIP in this optimizing step. The ΔR_{ct} response of SAL on the MIP modified PANI/SPGE was then compared. In the presence of lowest molar ratio of *o*-PD, the lowest ΔR_{ct} was obtained. This result could be explained by the uncertain mechanical property of the MIP cavities owing to uncompleted creation⁹¹. However, the obtained results exhibited that the ΔR_{ct} responses gradually increased with increasing the molar ratio (Figure 4.2.3d) and reached a maximum current at [APB]: [*o*-PD] ratio of 1:1. After higher concentration, the ΔR_{ct} responses then reached a plateau, and as a result, it could be presumed that the high concentration of *o*-PD against APB could reduce the recognized moiety per unit of MIPs via overabundantly strong MIP formation. Thereby, the *o*-PD: APB: SAL molar ratio of 2: 2 :1 was considered for effective polymerization of MIP.

4.2.3.2.3 Effect of MIP thickness

In this study, the MIP thickness could be simply controlled by changing the number of CV scan during the electrochemical polymerization as described above. The ΔR_{ct} values of SAL on the MIP modified PANI/SPGE were utterly examined in different number of CV scans from 5 to 30 cycles. Figure 4.2.3e shows that the ΔR_{ct} response

reached a maximum value with 20 cycles of scan, which might be due to an enhancement of the specifically recognized cavities during the polymerization process. However, these obtained ΔR_{ct} values suddenly decreased after increasing number of scan cycles (more than 30 cycles) were applied. The thickness of MIP affects the presence of the recognized sites on the modified sensor. Herein, the proper thickness of MIP could be achieved by using 20 cycles of electrochemical polymerization.



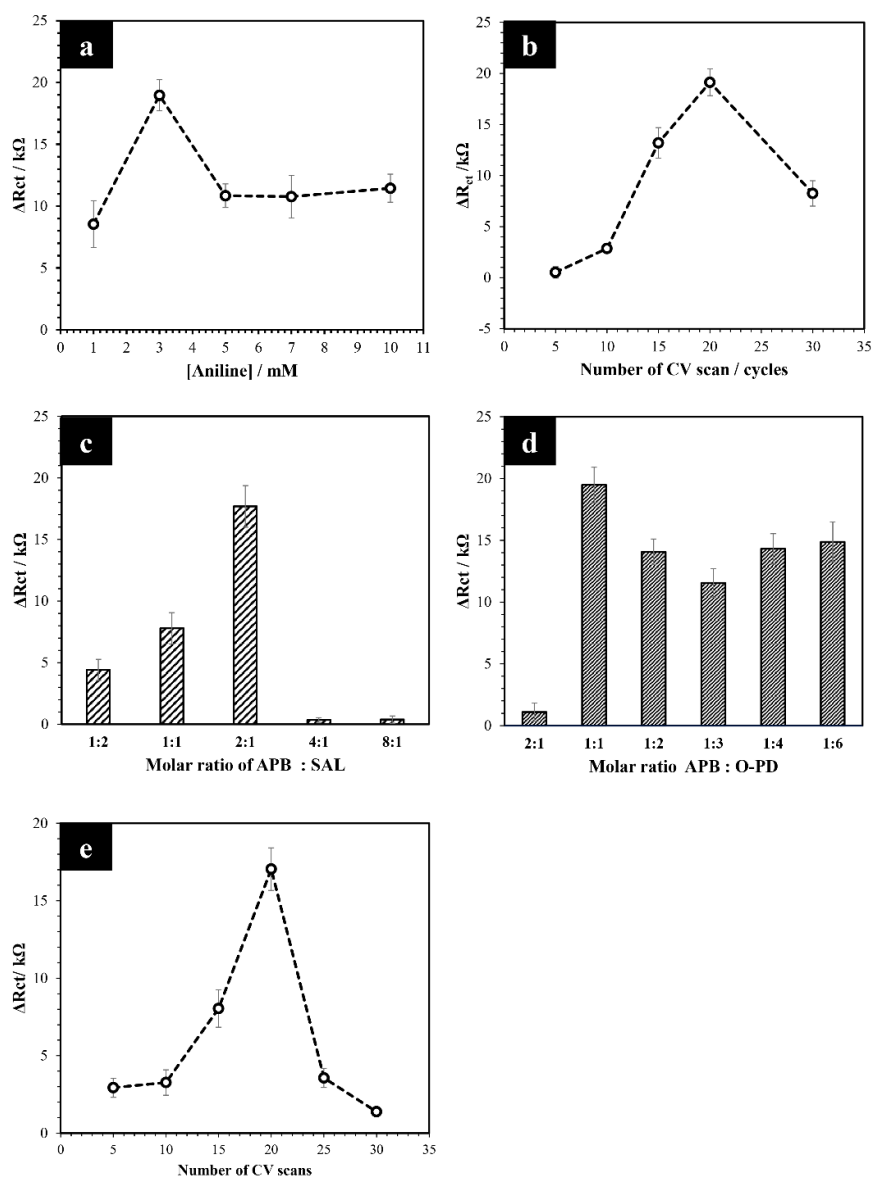


Figure 4.2.3 The effects of (a) aniline concentration, (b) number of CV scans in aniline polymerization step, (c) the molar ratio between monomer and target analyte, (d) the molar ratio between monomer and cross-linker and (e) number of CV scans in MIP polymerization step, these parameters were investigated using EIS techniques for determination of $10 \mu\text{g mL}^{-1}$ SAL. All experimental results were obtained from the mean of three repetitive measurements.

4.2.3.3 Optimization of influent parameters for electrochemically SAL detection using sliding PADs based MIP/PAN/SPGE.

For SAL detection employing EIS technique, the mass transfer including diffusion, migration, and convection, significantly affected on electrochemical dynamic behavior of electrochemical species as reconcile the Nernst-Planck equation¹⁹⁵. These mass transfer should be eliminated in practical electrochemical system for proper resistance response. Particularly, the convection from porous media of paper substrate was importantly affected to the flow rate and fluid motion in paper-based devices. Herein, the sliding PADs was specifically designed to circumvent this convection effect in detection step. As illustrated in figure 4.2.4, there are three steps for SAL analysis as follows: (1) simple loading step, the wax-barrier channel is specially built in bottom side of sliding PADs, resulting in stopping mobility of the sample solution for rebinding SAL within MIP cavities, (2) washing step, the hydrophilic channel was created in both sides of sliding PADs for delivery the non-binding molecule straightforward the waste collector, (3) reagent loading and EIS detection step, the wax-barrier channel is also built in bottom side of sliding PADs for stopping mobility of solution, called stopped-flow, during EIS measurement. To confirm the stopped flow concept, the cyclic voltammetry was used for considered the $\text{Fe}(\text{CN})_6^{3-/4-}$ behavior. As shown in Figure 4.2.5a the cyclic voltammetry of $\text{Fe}(\text{CN})_6^{3-/4-}$ from 4 uninterrupted cycles of CV exhibited high reproducibility. This evidence obviously demonstrated that the proposed device was achieved in stopped fluid motion. Thus, it could be deduced that the design of sliding PADs proffers an efficiency for electrochemical detection, requiring stationary solution system.

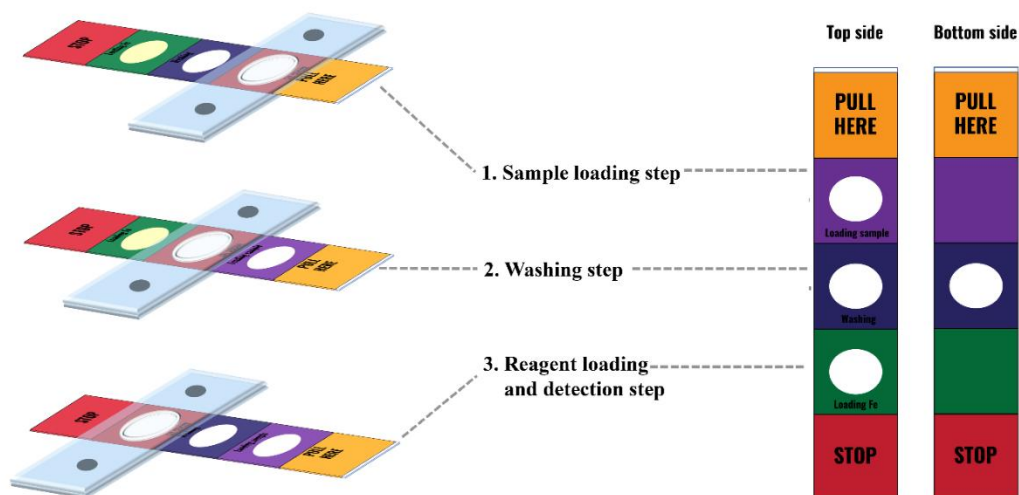


Figure 4.2.4 Schematic illustration of sequential sliding-step for SAL determination.

4.2.3.3.1 Influence of incubation time for SAL detection using sliding PADs based MIP/PANI/SPGE.

In addition, the crucial parameter for SAL detection using sliding PADs based MIP/PANI/SPGE is incubation time for rebinding between SAL and specific cavities of MIP. For incubated sample in sliding PADs device, the wax barrier placing on opposite side of sample reservoir in sliding PADs device as shown in Fig.1 was generated. The rebinding time was assessed in the range of 1 to 20 min. The Figure 4.2.5b displays the increasing ΔR_{ct} with increase of rebinding time and reaches the maximum response after incubation time over 7 min due to enhancing the binding capability of SAL toward specific cavities in MIP. And then the ΔR_{ct} remains constant after incubation time up to 7 min because of saturated SAL binding capability. Therefore, the 7 min incubation time was chosen previous to electrochemical determination of SAL.

4.2.3.3.2 Influence of $\text{Fe}(\text{CN})_6^{3-/4-}$ concentration for SAL detection using sliding PADs based MIP/PAN/SPGE.

In this study, SAL determination was measured indirectly from the impeded electron transfer of $\text{Fe}(\text{CN})_6^{3-/4-}$ on the interfacial surface. Then the concentration of redox probe was investigated for improved sensitivity of the proposed assay. The different concentration of redox probe in the range of 0.5 to 10 mM was dropped on reagent reservoir in sliding PADs and their EIS response were compared. Figure 4.2.5c shows that ΔR_{ct} gradually increased and reached the maximum ΔR_{ct} when using the concentration of redox probe up to 3 mM. After that, the saturated ΔR_{ct} was produced after using the concentration over 3 mM. In this case, the 10 mM $\text{Fe}(\text{CN})_6^{3-/4-}$ was established for SAL measurement by considering the persistence and degradability of redox probe as well as the stability of the proposed device.

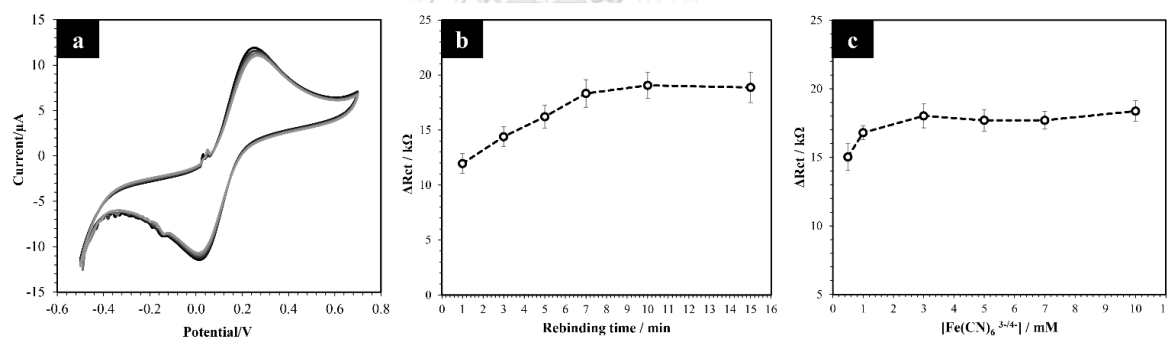


Figure 4.2.5 (a) The Cyclic voltammogram of 10 mM $\text{Fe}(\text{CN})_6^{3-/4-}$ with scan rate 100 mV s^{-1} and continuous four repetitive measurements. The changing ΔR_{ct} response of $10 \mu\text{g mL}^{-1}$ with (b) varied rebinding time in the range of 1 to 15 min and (c) different electroactive species concentration from 0.5 to 10 mM.

4.2.3.4 Analytical figures of merit

The efficiency of sliding PADs based MIP/PAN/SPGE for SAL determination was evaluated under optimized condition. For this purpose, the concentration of SAL was employed in the range of 0.05 to 15 $\mu\text{g mL}^{-1}$. Figure 4.2.6 shows the change of ΔR_{ct} respect to SAL concentration. The increasing ΔR_{ct} is directly proportional with the SAL concentration according to the equation $\Delta R_{\text{ct}} = 3.7303 \log [\text{SAL}] + 14.89$ with a correlation coefficient (R^2) of 0.9925. This proposed approach provided the limit of detection (LOD) of 7.50 ng mL^{-1} , calculated by 3 times of the standard deviation of the blank and slope of the calibration plot (3.7303), referred as the sensitivity. All the experiments were obtained from the mean of 3 times replicates. Compared with the other modified electrode in Table 2, the MIP/PANI/SPGE sensor combined with sliding PADs device offered more sensitivity with a lower detection limit.

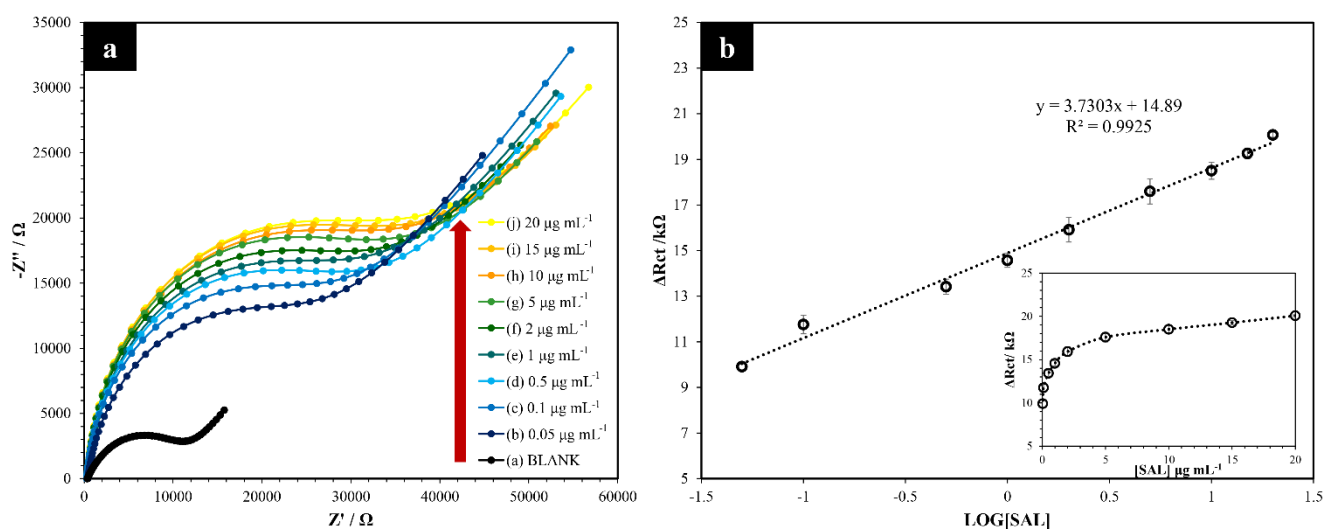


Figure 4.2.6 (a) The R_{ct} response of various SAL concentration in the range of 0.05 to 20 $\mu\text{g mL}^{-1}$ using MIP/PANI/SPGE accompanying with sliding PADs. (b) The linear calibration plot of SAL concentration (inset picture) and its logarithm against the changing ΔR_{ct} response.

Table 4.2.2 The comparison the analytical performance for SAL determination using different electrode.

Electrode	Linear range ($\mu\text{g mL}^{-1}$)	LOD ($\mu\text{g mL}^{-1}$)	References
Pd NPs/BDD	0.2 – 2.0	0.02	78
Poly taurine/ZrO ₂ /GCE	1.20 – 52.6	0.005	196
Chitosan-MWCNT/GCE	0.12 - 9.57	0.02	197
Poly(amino sulfonic acid)/GCE	0.48 – 24.0	0.14	198
MIP/PANI/SPGE	0.05 - 20	0.0075	This work

4.2.3.5 Reproducibility, Selectivity and Stability of the sliding-PADs based electrochemical detection.

For practical sliding-PADs based MIP/PANI/SPGE device, the reproducibility is the crucial factor for evaluation of constructed device. To assess this reproducibility, the five electrodes were used for detecting SAL with different three concentration of 0.05, 1 and 10 $\mu\text{g mL}^{-1}$. The acceptable relative standard deviation (%RSD) in the range of 2.9 to 6.8 % was obtained, implying that the sliding-PADs based MIP/PANI/SPGE offered excellent fabrication reproducibility.

To evaluate the selectivity of proposed system, the change in EIS response (ΔR_{ct}) of the proposed MIP sensor toward TER, RAC and PHE which structurally related to SAL was studied. The obtained ΔR_{ct} of molecular imprinted polymer (MIP) and molecular non-imprinted polymer modified electrode integrated sliding-PADs was compared as shown in Figure 4.2.7. The low ΔR_{ct} of NIP modified electrode was observed due to non-specific adsorption on polymeric surface whereas the superior change in the EIS response (ΔR_{ct}) of MIP modified electrode toward SAL was noticed

than the others. This high selectivity could be occurring from complimentary binding site between imprinted cavities and the functional group of SAL structure. However, TER having similar hydroxy-amine side chain motif to SAL provided higher ΔR_{ct} than RAC and PHE attributing to partial binding of its functional moiety to imprinted cavity. While the RAC is markedly too large and PHE is considerably too small than imprinted cavity. The non-binding molecule of RAC and PHE could be eliminated in washing step resulting in lower ΔR_{ct} . Additionally, the higher ΔR_{ct} of SAL using MIP modified electrode than using NIP modified electrode implied that the response was only obtained from specific binding of SAL moiety and MIP cavities.

Additionally, the stability of sliding PADs based MIP/PANI/SPGE sensor was investigated. The removed template of MIP/PANI/SPGE was prepared by the same procedure and stored desiccator for 2 weeks. As displayed in Figure 4.2.10, the EIS response remained stable for 2 weeks with the normalized response of 99.46% from the initial EIS response value and %RSD after 14 days storage time of the proposed sensor was significantly found to be 1.22% (less than 5%). This result demonstrated that this proposed sensor exhibited good stability up to 2 weeks.

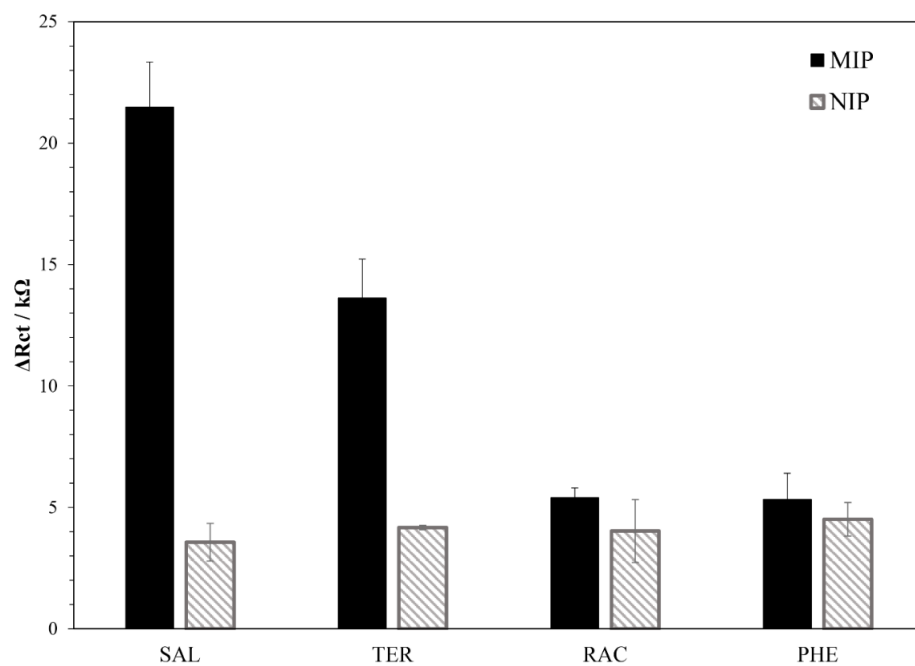


Figure 4.2.7 The selectivity test of other structurally related to SAL including TER, RAC and PHE by comparison of MIP and NIP based electrochemical sensor.

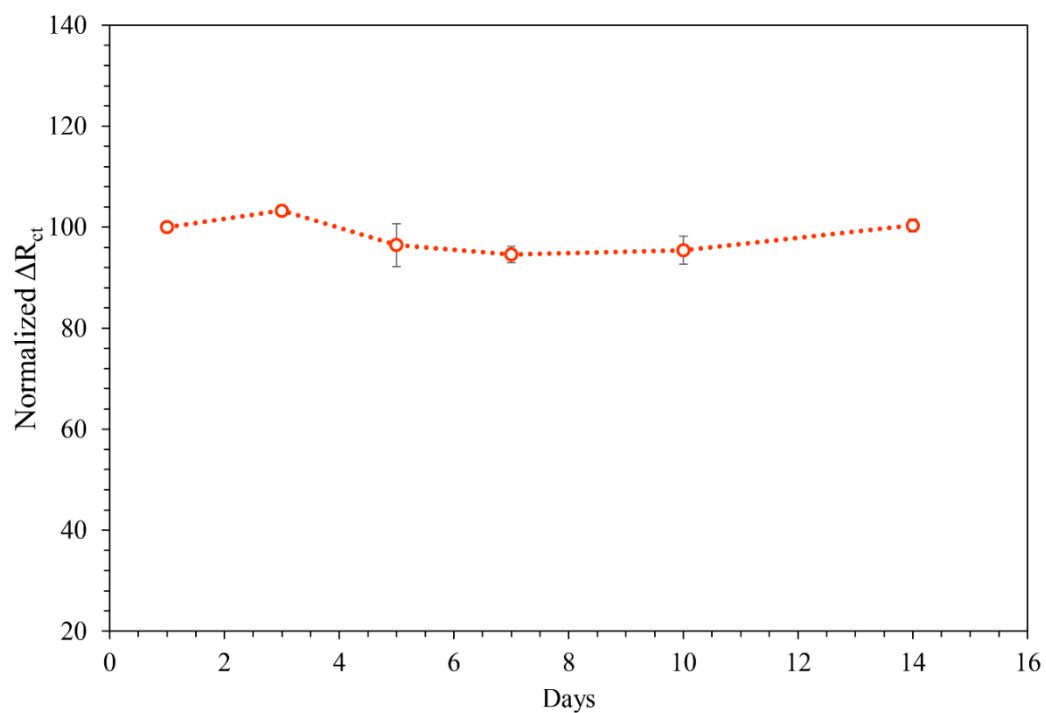


Figure 4.2.8 The storage stability of the sliding PADs based MIP/PANI/SPGE.

4.2.3.6 Determination of SAL in urine sample.

The proposed device was employed for SAL determination in urine sample in order to investigating its efficiency. The known amounts of SAL were added in urine sample (spike method) for recovery analysis. As summarized in Table 4.2.3, the % recovery and %RSDs were found to be in the ranges of 88.2 – 101.4 % and 2.3 – 9.0 %, respectively. Additionally, the reliability of this proposed system was investigated by using HPLC-UV method as a standard method for validation. The compared %recovery and %RSD were shown in Table 4.2.3. The calculated t-values of two different method was found to be 0.31, being significantly lower than the critical t-critical value (3.18) at the 95% confidence interval. It indicated that the achieved results from the proposed method and HPLC-UV were no significant difference. Thus, It was deduced that the developed sliding PADs based MIP/PANI/SPGE exhibited the great reliability and high performance for real sample application.

Table 4.2.3 Determination of SAL in urine sample. The recovery and RSD were obtained from the mean of three measurements.

Sample	Spiked $\mu\text{g mL}^{-1}$	Found		Recovery (%)		RSD (%)	
		$\mu\text{g mL}^{-1}$					
		Sliding PADs	HPLC-UV	Sliding PADs	HPLC-UV	Sliding PADs	HPLC-UV
	0.0	ND	ND	-	-	-	-
Urine	0.20	0.22	0.19	110.0	94.1	6.3	8.0
	3.0	2.9	2.7	97.7	91.6	9.0	5.6
	12	12.2	11.5	101.4	95.5	2.3	2.2

ND = not detectable

4.2.4 Conclusion

MIP based electrochemical sensor integrated with sliding-PADs for SAL determination was attained fabrication. In this case, a MIP was carried out by electropolymerization of aminophenylboronic acid and *o*-phenylenediamine accompanying with the template molecule. The MIP was embedded on the PANI/SPGE, used for assisting the uniform MIP adsorption on electrode surface and improving the sensitivity of the proposed sensor. For end-user convenience, the paper-based was designed, called sliding-PADs, assisting in delivery sample and reagent in one drop only of running buffer. Under the optimized condition, the sliding PADs based MIP/PANI/SPGE presents its momentous efficiency with LOD of 7.5 ng mL^{-1} and wide linearity in the range of $0.05 - 20 \text{ ng mL}^{-1}$. Additionally, the established sensor also offered significant selectivity, high reproducibility, and satisfying stability. Moreover, the proposed sensor was achieving applied in real samples with significant % recovery in the range of $97.7 - 110.0 \%$ without the requirement of complicated step and time-consuming and the result is agreeable with the obtained result from standard HPLC-UV method. This is the evidence proving that the established sensor has the potential and reliability to monitoring and controlling the misuse of SAL. Besides that, the MIP based electrochemical platform can be facilely make practical use for various application in hereafter.

PART III**4.3 Synergistically catalytic activity of trimetallic CuNiAu alloy modified screen-printed graphene-based electrochemical sensor towards simultaneous determination of norepinephrine and serotonin**

Atchara Lomae^a, Sakda Jampasa^{a,b}, Kanokwan Charoenkitamorn^d, Weena Siangproh^c, Orawon Chailapakul^{a*}, and Janjira Panchompoo^{a**}

^a Electrochemistry and Optical Spectroscopy Center of Excellence (EOSCE), Department of Chemistry, Faculty of Science, Chulalongkorn University, 254 Phayathai Road, Pathumwan, Bangkok 10330, THAILAND

^b The Institute of Biotechnology and Genetic Engineering, Chulalongkorn University, Patumwan, Bangkok, 10330, Thailand

^c Department of Chemistry, Faculty of Science, Srinakharinwirot University, Sukhumvit, Wattana, Bangkok 10110, THAILAND

^d Department of Chemistry, Faculty of Science, Silpakorn University, Nakorn Pathom 73000, Thailand

** Corresponding author

* Co-corresponding author

Abstract

A trimetallic alloy consisting of Cu, Ni, and Au nanoparticles with superior synergistic activity towards the electrocatalytic oxidation of monoamine neurotransmitters was first fabricated by a facile one-step electrodeposition approach. Generally, the trimetallic alloy-based electrochemical sensor could be simply obtained by co-electrodeposition of Cu, Ni, and Au nanoclusters onto a screen-printed graphene electrode (SPGE). The resulting trimetallic CuNiAu composite modified SPGE (CuNiAu/SPGE) was characterized by field emission scanning electron microscopy (FE-SEM), energy dispersive X-ray spectroscopy (EDS), and X-ray photoelectron spectroscopy (XPS). In addition, the electrochemical behaviors of the proposed CuNiAu/SPGE sensor were thoroughly investigated by cyclic voltammetry (CV), square wave voltammetry (SWV), and electrochemical impedance spectroscopy (EIS). The results showed that the trimetallic CuNiAu composite immobilized on the SPGE exhibited excellent electrocatalytic activity towards the oxidation of norepinephrine (NE) and serotonin (also known as 5-hydroxytryptamine; 5-HT) with high sensitivity and enhanced selectivity, compared to its monometallic and bimetallic counterparts. The superior performance of the trimetallic catalyst in electroanalysis was potentially due to the synergistically catalytic effect of ternary Cu-Ni-Au alloy. The simultaneous determination of NE and 5-HT using the developed CuNiAu/SPGE could then be performed by SWV, exhibiting two well-defined and well-separated corresponding anodic peaks. Under the optimum experimental conditions, the linearities for NE and 5-HT were found to be in the wide ranges of 1–40 μM and 5–70 μM , with limits of detection (LODs) of 0.19 μM and 0.18 μM , respectively. Moreover, the CuNiAu/SPGE sensor was successfully applied to measure NE and 5-HT in serum samples, with good reproducibility and satisfactory recoveries ranging from 92.6–108.8 %.

Keywords: CuNiAu alloy; synergistic effect; electro-catalytic property; norepinephrine; serotonin.

4.3.1 Introduction

Neurotransmitters are biochemical signaling substances in the nervous system that transmit messages from nerve cells (neurons) to target cells (e.g. other neurons, muscle or gland cells), allowing cells to communicate. Typically, they play an important role in behavioral and physiological functions in human. For example, norepinephrine (NE) and serotonin (also known as 5-hydroxytryptamine; 5-HT) are two monoamine neurotransmitters in the central nervous system that primarily participate in the regulation of sleep, mood and pleasure^{199, 200} and also play a major role in stress and depression²⁰¹. The altered levels of NE and 5-HT in human body are directly related to several diseases including arrhythmia, heart failure, Parkinson's, Alzheimer's, and depression^{202, 203}. Therefore, the quantitative analysis of these neurotransmitters in biological samples is indeed necessary to monitor risk factors for those diseases. As a result, the development of analytical methods and sensing devices with high sensitivity, excellent selectivity, good reliability, and fast analysis for simultaneous determination of NE and 5-HT has attracted more attention in recent years. Generally, there are several methods developed for detection of NE and 5-HT including gas chromatography (GC)²⁰⁴, high performance liquid chromatography (HPLC)^{205, 206}, and electrochemical techniques, fluorimetry^{207, 208}, and electrochemical techniques²⁰⁹⁻²¹¹. Among these various methods, electrochemistry seems to have highly promising advantages in terms of simplicity, high sensitivity, fast analysis time, cost effectiveness, and capability of miniaturization.

However, the determination of NE and 5-HT employing the electrochemical techniques for biological application have been quite challenged for 3 reasons: (1) The oxidation potential of NE is close to that of 5-HT^{212, 213} resulting in an undistinguishable signal of both substances. (2) The common biological interferences such as ascorbic acid (AA) and uric acid (UA) provide the same oxidation potential with NE and 5-HT^{214, 215} that are limited their applications. (3) The reusability and reproducibility of

electrochemical sensor have been limited due to the absorbing property of these compounds on electrode surface ²¹⁶⁻²¹⁸. Therefore, the surface modification of the electrochemical sensor becomes more urgent. As previous research, much attention has been devoted to utilizing chemical and metallic materials as the modifiers on the surface of the electrode, especially nanoparticles or nanocomposites. Various materials such as eriochrome cyanide R (ECR)²¹⁹, cetyltrimethylammonium bromide (CTAB) immobilized SnO₂²²⁰, N,P-doped molybdenum carbide@carbon/Prussian blue/graphite felt composite²²¹, graphene/cobalt tetrasulfonated phthalocyanine ²²² and nafion/polyaniline/zeolitic imidazolate ²²³ have been applied as the modifiers for the detection of neurotransmitter. Despite these materials provided high selectivity toward phenolic compounds in the present of electrochemically interfering species, their synthesis and modification steps were still complicated and time-consuming. As a result, noble metals such as gold (Au) ²²⁴⁻²²⁶, platinum (Pt) ²²⁷⁻²³⁰, palladium (Pd) ⁷⁸, copper (Cu) ²³¹⁻²³³, and copper oxide (CuO) ²³⁴ have been presented as attractive materials to assist electrochemical procedure with an exceptional performance of their excellent electrocatalytic properties and simple modification procedure. In addition, the bimetallic and trimetallic, especially Au-based bimetallic and trimetallic, have been extensively studied for the detection of various substances, for examples, AuPt nanoparticles modified BDD electrode³⁴ and AuAg nanoparticles modified RGO/GCE for glucose measurement ²³⁵, AuAg bimetallic modified GCE ²³⁶ and CuAu nanowire for detection of H₂O₂ ²³⁷, AuCu bimetallic modified GCE for arsenic (III) sensor ²³⁸, AuCu alloy over foil electrode for CO₂ reduction ²³⁹, PtCuAu nanoparticles modified RGO/GCE toward formic acid oxidation ²⁴⁰, Au/PtPd nanoparticles for cancer cell sensing ²⁴¹ and AuPt alloy nanostructure and ²⁴²,PtAuAg trimetallic nanodendrite structure regarding to methanol oxidation ²⁴³. These bimetallic and trimetallic materials offer superior catalytic performance in comparison with individual metal.

In this research, we interest in the development of electrochemical sensor for the disguisable determination of NE and 5-HT. To approach this propose, we decide to utilization of Cu, Au and Ni as material for modified electrode. Since Au admitted as catalytic activity toward phenolic compound and Cu known as catalytic performance of -NH₂ functional group which existed in NE and 5-HT structures. Considering Ni nanoparticles could easily be alloy with other metal such as CuNi²⁴⁴⁻²⁴⁶, NiMn²⁴⁷, and NiCo²⁴⁸, affording better electrocatalytic property toward the oxidation reaction of organic containing -OH and -NH₂ functional group²⁴⁹⁻²⁵¹ involving the electron transfer mediated of Ni²⁺/Ni³⁺ surface²⁵². The strategy of CuNiAu modified carried out by electrodeposition process could distinguish the oxidation peak of both target analyses resulting in synergistic property of CuNiAu, providing better kinetic oxidation of NE than 5-HT. And then the individual and bimetallic modified electrode were investigated comparing with the proposed sensor in order to justify its synergistic catalysis of CuNiAu. Moreover, the SEM, EDS and XPS techniques were employed for characterization and structural investigating.

4.3.2 Experimental methods

4.3.2.1 Material and apparatus.

Analytical grade chemicals without any further purification were used in this work. All solution was prepared using Milli-Q water from Millipore (R_z 18.2 MΩ at 25 °C). Copper (II) sulfate (CuSO₄), potassium chloride (KCl), and magnesium chloride (MgCl₂) were purchased from Merck (Darmstadt, Germany). Nickel (II) sulfate (NiSO₄), sodium sulfate (Na₂SO₄), sodium chloride (NaCl), and sulfuric acid (H₂SO₄) were bought from Carlo Erba reagent (Chaussée du Vexin, France). Potassium Tetrachloroaurate (III) *n*-Hydrate (K[AuCl₄]·*n*H₂O) was purchased from Wako Pure Chemical Industries (Chuo-Ku, Osaka, Japan). Norepinephrine-(+)-butartrate salt, serotonin hydrochloride, tyrosine, phosphate buffered saline tables, and lyophilized albumin human serum

were obtain from Sigma Aldrich (St.Louis,MO,USA). Ascobic acid (AA) and D-(+)-Glucose anhydrous (Glu) were bought from Carlo Erba reagent (Chaussée du Vexin, France). Uric acid was purchased from Wako Pure Chemical Industries (Chuo-Ku, Osaka, Japan).

The electrochemical measurement was performed using a PlamSens 4 (Metrohm, Switzerland) and controlled with PlamSens 4.6 software. The three-electrode system consist of silver/silver chloride (Ag/AgCl) ink (Gwent Electronic materials Ltd., UK) was used as reference electrode (RE) and graphene ink (Gwent Electronic materials Ltd., UK) was employed as working electrode (WE) and counter electrode (CE)

4.3.2.2 Fabrication of the trimetallic CuNiAu modified screen-printed graphene electrode.

The pattern of electrode and wax barrier were designed (Figure 4.3.1) by Adobe illustrator software (Adobe Systems, Inc.). The wax pattern was printed on a polyvinyl chloride (PVC) sheet with 0.15 mm of thickness (Dee-craft Co. Ltd., Bangkok, Thailand) through a solid-wax printer (Xerox Color Qube 8570, Japan) for limiting the sample zone. The in-house screen-printed electrodes were fabricated via screen-printed method using Ag/AgCl as the reference electrode and conductive pads, and graphene ink as the working and counter electrodes. After screen-printed in each step, the printed electrode was allowed to dry in the oven at 55 °C for 1 hr. For the electrode modification, the mixture solution of Cu (II): Ni (II): Au (III) (1:50:1 mole ratio) was prepared in 0.2 M Na₂SO₄. 100 μL of mixture solution was introduced on the electrode surface and consequently modified electrode via electrodeposition method by holding a constant potential at -1.0 V for 200 sec.

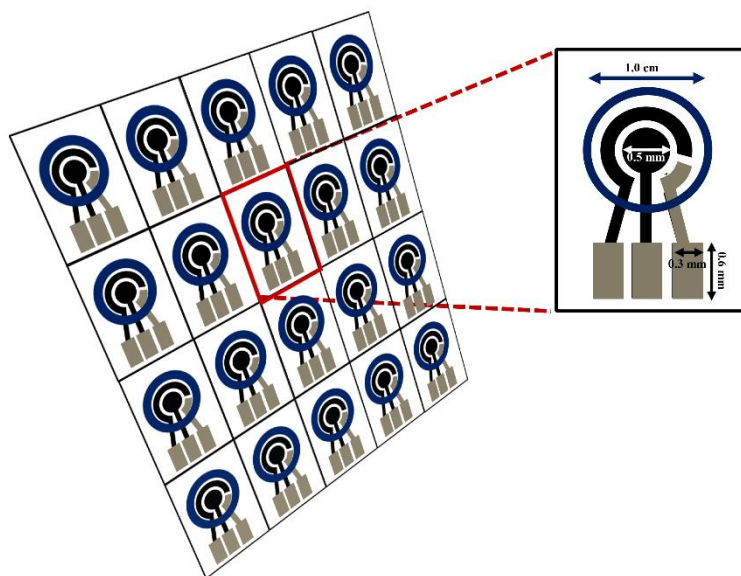


Figure 4.3.1 Schematic illustration of designed electrode and wax barrier platform on PVC substrate.

4.3.2.3 Characterization of CuNiAu modified SPGE surface

4.3.2.3.1 Electrochemical characterization.

The electrochemical behaviors of the analytes and the resistance of both trimetallic CuNiAu modified electrode and unmodified electrode were investigated by Cyclic voltammetry (CV) and the electrochemical impedance spectroscopy (EIS), respectively.

4.3.2.3.2 Morphological characterization.

The morphological processing of CuNiAu composites were obtained using the scanning electron microscopy (SEM) and energy dispersive X-ray spectrometer (EDS) using JSM-IT500HR model (JEOL, (U.K.) Ltd., England). The valence state and elemental compositions of the trimetallic CuNiAu were studied via X-ray photoelectron spectroscopy (XPS) using Kratos, Axis Supra model with an Al source (1486.6 eV) at 15 kV (40 mA).

4.3.2.3.4 Electrochemical measurement

The determination of norepinephrine (NE) and serotonin (5-HT) were carried out in 0.1 M PBS buffer pH 7.4 using square wave voltammetry (SWV). The mixture solution of NE and 5-HT (100 μL) was drop onto three-system electrode. Then, SWV was scanned from 0.0 to 0.6 V vs Ag/AgCl with a step potential (E_{step}) of 0.3 mV, an amplitude of 75 mV, and a frequency of 35 Hz.

4.3.2.3.5 Sample analysis

The human serum was prepared by dissolving the lyophilized albumin human serum (100 mg mL⁻¹) with ultra-high purity water as a stock solution. Then, the precipitation of protein in the serum was carried out by TCA method⁵⁵. Briefly, 250 μL of 10% (W/V) TCA was added in mixture solution containing 200 μL of stock human serum solution and different concentration of standard NE and 5-HT. After that ultra-high purity water was added for adjustable volume of the mixture to 2 mL followed by mixing with vortexing for 5 min. The obtained solution was centrifuged at 6000 rpm (Cole-Parmer, USA) for 10 min. The supernatants were transferred to another microtube for further analysis.

4.3.3. Results and discussion

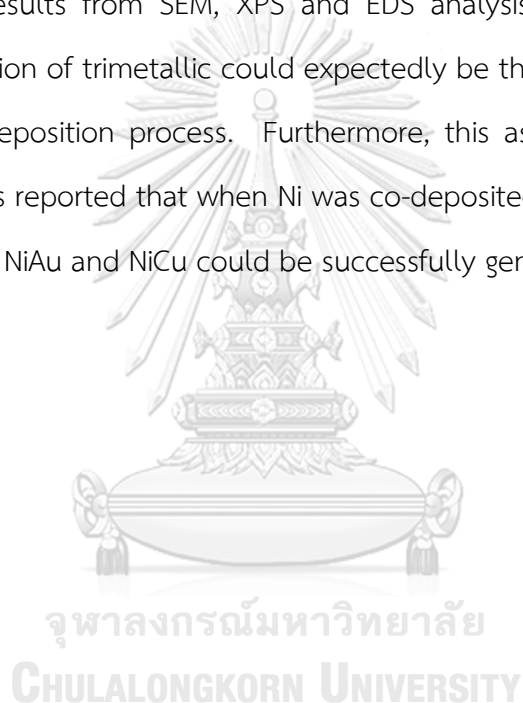
4.3.3.1 Characterization of trimetallic CuNiAu/SPGE and bare SPGE

To verify the feasible construction of CuNiAu trimetallic nanoparticles, the numerous characterization techniques were utilized including SEM, EDS and XPS. The first technique for study the morphological surface is SEM, The SEM images were shown in Fig. 4.3.2 (a-f). Comparing the SEM images of bare SPGE and CuNiAu/SPGE at 20,000 magnification, As shown in the Figure 4.3.2a, the graphene sheet distinctively emerged on the surface of bare SPGE. Meanwhile the cluster of trimetallic evenly dispersed across graphene surface onto the CuNiAu/SPGE as shown in Figure 4.3.2b. Additionally, the constructing trimetallic of CuNiAu nanoparticle via one-step electrodeposition of the Cu(II), Ni(II), and Au(II) mixture solution led to the aggregation of composited clusters

on bare graphene surface (Figure. 4.3.2b) resulting in increasing electroactive area. Moreover, the morphological structures of Cu/SPGE, Ni/SPGE, Au/SPGE, and CuNiAu/SPGE were systemically investigated through the SEM at the magnification of 45,000 as displayed in Figure 4.3.2c, d, e and f, orderly. The results indicated that the trimetallic clusters of CuNiAu were uniformly dispersed on the surface whereas the monometallic clusters of Cu/SPGE, Ni/SPGE, and Au/SPGE showed less dispersion. The homogeneous dispersion of CuNiAu trimetallic on SPGE might be attributing to the alloy composition of trimetallic confirmed by EDS and XPS discussed later. According to electrodeposition process, the amounts of deposited nanoparticles directly related to peculiarity of electrokinetic activity. As shown in Figure 4.3.3, Ni ion difficult deposition on the electrode surface comparison with Cu and Au. The reduction potential of Ni(II) was obtained of -0.19 V vs Ag/AgCl meanwhile the reduction potential of Cu (II) was found to be -0.50 V vs Ag/AgCl and Au(III) was obtain two reduction peak of -0.11 V vs Ag/AgCl and -0.44 V vs Ag/AgCl for Au^{3+} to Au^+ and Au^+ to Au^0 , respectively. Although the reduction potential of Ni (II) is lower than the reduction potential of Cu (II) and Au (III), considering the reducing current of Cu and Au higher than Ni attributed to facily electrokinetic reduction of Cu and Au.

Then, the X-ray photoelectron spectroscopy (XPS) was employed in order to verify the element composition of trimetallic CuNiAu on electrode surface. The XPS profiles (Figure 4.3.2 (g-l)) showed the chemical state of the elements on electrode surface including C, O, Cu, and Au whereas Ni could not be detectable with the XPS analysis probably be the less amount of Ni nanoparticle on modified SPGE. The CuAu alloy could be apparently observed at the XPS profile of Au element (Figure 4.3.2g) at peak energy of 84.21 ($4f_{7/2}$) and 87.88 ($4f_{5/2}$) eV with mass percentage of 31.81 and 23.85, respectively, indicating that CuAu alloy was the major component of the modified material. Meanwhile, the XPS profile of Cu majority (Figure 4.3.2h) presented the characteristic of CuO with the mass percentage of 32.69 and 16.34 for Cu

configuration $2p_{3/2}$ (peak energy at 935.16 eV) and $2p_{1/2}$ (peak energy at 955.06 eV), respectively. Additionally, the minority of characteristic composition of CuAu could be observed at 932.49 ($2p_{3/2}$) and 952.34 ($2p_{1/2}$) eV with the mass percentage of 8.18 and 4.09, respectively. Despite Ni element was non-detectable using the XPS analysis, the uniform dispersion of the constituting Ni element was clearly noticed through the EDS element analysis as shown in Figure 4.3.2j-k as well as the distribution of Cu and Au. The % mass of Cu, Ni and Au was found to be 8.25, 0.79 and 0.16, respectively. Considering the results from SEM, XPS and EDS analysis were evidence that the element composition of trimetallic could be expectedly be the CuNiAu alloys form after one-step electrodeposition process. Furthermore, this assumption is agreeable to several researchers reported that when Ni was co-deposited with either Au or Cu, the bimetallic alloy of NiAu and NiCu could be successfully generated^{99, 253-255}.



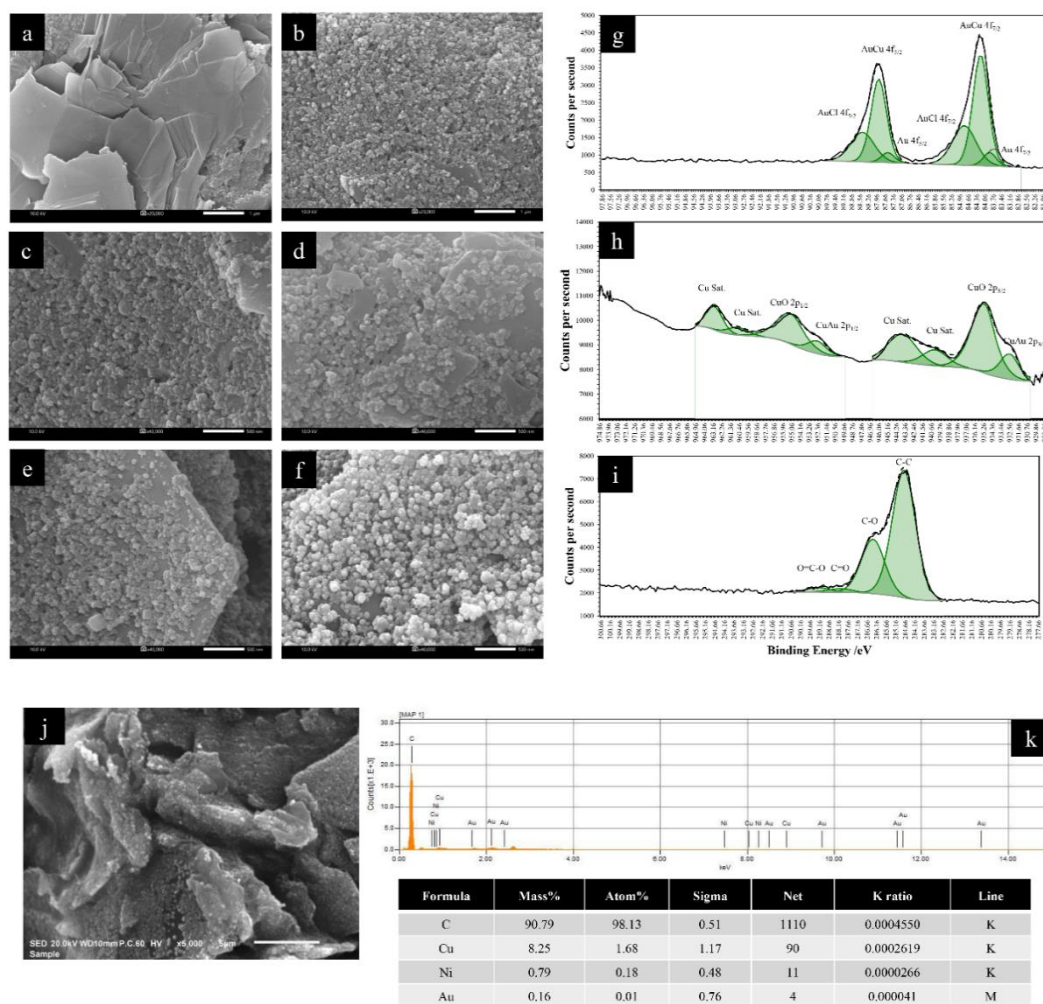


Figure 4.3.2 FE-SEM image with 20,000 magnification of (a) bare graphene, (b) CuNiAu/SPGE and FE-SEM image with 40,000 magnification of (c) Ni/SPGE, (d) Cu/SPGE, (e) Au/SPGE and (f) CuNiAu/SPGE, orderly. XPS spectra of (g) Au, (h) Cu and (i) graphene, respectively. EDS element analysis of CuNiAu/SPGE (j-k) EDS element analysis.

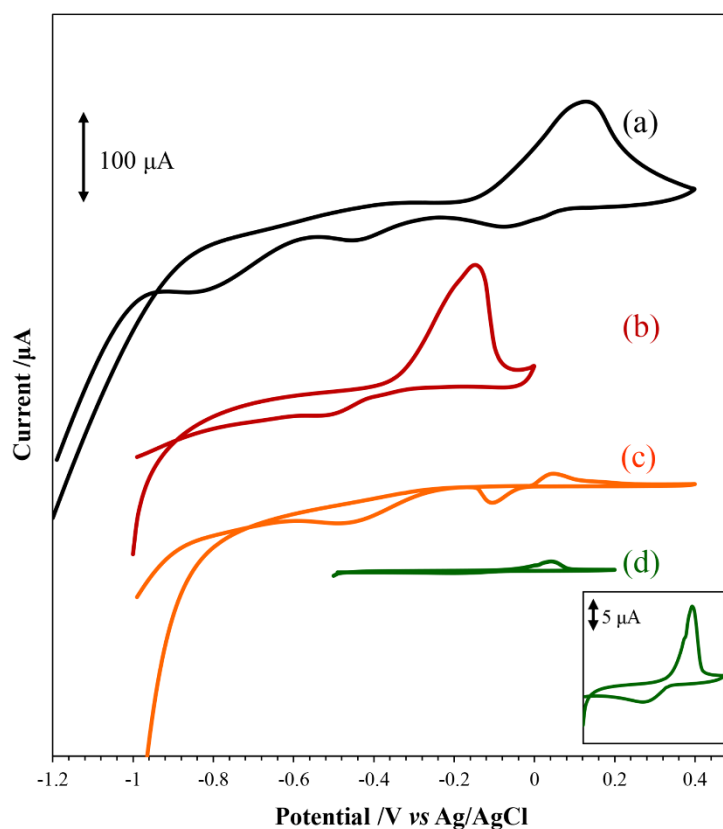


Figure 4.3.3 The CV of (a) CuNiAu (molar ratio 2:100:2), (b) 5 mM of Cu(II), (c) 5 mM of Au (III) and (d) 5 mM of Ni(II) in 0.2 M Na₂SO₄ on SPGE was scan from 0.0 V to 1.0 V vs Ag/AgCl at 100 mVs⁻¹ of scan rate. The inset figure; the zooming in figure of CV of 5 mM Ni (II).

4.3.3.2 Electrochemical performance of the modified electrodes

The electrochemical behavior of the modification at SPGE was investigated using 0.1 M KCl containing 5 mM [Fe(CN)₆]^{3-/4-}, an electroactive redox probe for evaluating the kinetic barrier of the modified electrode, for verifying the electrochemical performance of the modification. As shown in Fig. 4.3.4A, the difference between the anodic peak potential and cathodic peak potential, called peak-to-peak separation “ ΔE_p ” of 1.056, 0.670, 0.979, 0.819, and 0.649 V was observed on SPGE, Au/SPGE, Cu/SPGE, Ni/SPGE, and CuNiAu/SPGE, respectively. The lowest ΔE_p of CuNiAu/SPGE obviously indicated the excellent reversible charge transfer of

electroactive redox probe on the CuNiAu/SPGE. The improvement of electrocatalytic activity on trimetallic can be ascribed to the synergistic effect of alloying Au with unoccupied 3d orbitals of transition metals (Cu and Ni) ²⁵⁶. In this study the concentration of Cu, Ni and Au was controlled at molar ratio of 2:100:2, orderly, for modification step. The anodic peak currents were 0.067 V, 0.110 V, 0.083 V, 0.114 V and 0.127 V vs Ag/AgCl for SPGE, Au/SPGE, Cu/SPGE, Ni/SPGE and CuNiAu/SPGE, respectively. According to the higher molar ratio of Ni in modification step, the higher current responses was observed at the Ni/SPGE comparing with Cu/SPGE and Au/SPGE. Additionally, The CuNiAu/SPGE also produced higher current responses comparison with the others as presented in Figure 4.3.4A. The ΔE_p and current response results demonstrated that the CuNiAu/SPGE produced excellent electrocatalytic activity attributing to enhancement of electron transfer kinetic and increasing electroactive area.

In order to monitor the alteration of electrochemical surface properties of modified electrode, the electrochemical impedance spectroscopy (EIS) was employed. Within the conducting metal film modified electrode, the impedance behavior consisted of four components: the electrolyte resistance (R_s), the interfacial electron transfer resistance (R_{ct}), the capacitance (C_1) and the Warburg impedance introduced by the diffusion of ions (W_1) as well as the equivalent circuit as shown in Figure 4.3.4B. The semicircle in Nyquist plot could interpret to combination of R_1 and R_2 as show in equation 4.3.1 ²⁵⁷.

$$Z'(\omega) = R_s + R_{ct} \quad (4.3.1)$$

As shown in the Fig. 4.3.4B the large semicircle with the high charge transfer resistance (R_2) of 4.258 m Ω for SPGE could be observed. After electrodeposition of the Cu (II) and Ni(II) onto SPGE, the dramatically increasing of R_{ct} could be noticed to 4.990 ,and 5.066 m Ω , respectively, arise from poor electron transfer kinetic of Ni/SPGE and

Cu/SPGE. In otherworld, the R_2 was decreased to 1.711 and 3.588 m Ω after modified SPGE with the Au and trimetallic composite, respectively. These results coincided with ΔE_p of CV results for SPGE, Cu/SPGE and Ni/SPGE. Although the CV result indicating the CuNiAu/SPGE have the electron transfer kinetic higher Au/SPGE. The EIS result exhibited more R_{ct} of CuNiAu/SPGE provide Au/SPGE might be attributing to higher thickness of trimetallic film than Au film on electrode surface. The thickness affects to the resistance of system including electrolyte resistance and charge transfer resistance. Furthermore, the synergistic effect of trimetallic CuNiAu exhibiting good electrocatalytic properties could be considered thoughtfully from the lowest ΔE_p . It implied that electron transfer was facilitated, and higher oxidation peak current was obtained as well. Hence the CuNiAu/SPGE could provide a good electrochemical sensing for simultaneous determination of NE and 5-HT.

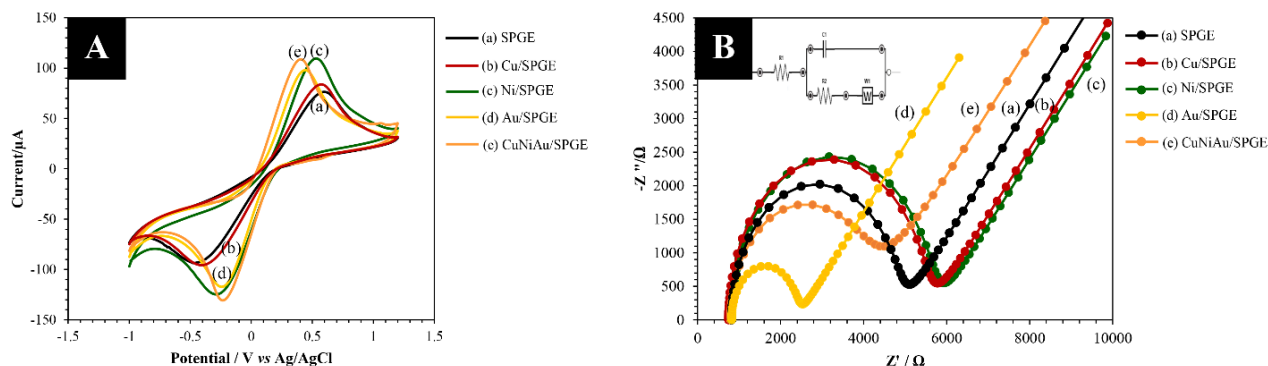


Figure 4.3.4 (A) The CV of 5 mM $[\text{Fe}(\text{CN})_6]^{3-/4-}$ in 0.1 M KCl solution at different electrode as follows Ni/SPGE (a; green line), SPGE (b; black line), Au/SPGE (c; yellow line), CuNiAu/SPGE (d; light orange line) and Cu/SPGE (e; red line) was performed from -1.0 V to 1.0 V vs Ag/AgCl at 100 mVs^{-1} of scan rate. (B) Nyquist plot of Ni/SPGE (a; green line), Cu/SPGE (b; red line), Au/SPGE (c; yellow line), CuNiAu/SPGE (d; light orange line), and SPGE (e; black line) in the present of 5 mM $[\text{Fe}(\text{CN})_6]^{3-/4-}$ in 0.1 M KCl solution. Inset: equivalent circuit applied to model EIS data, R_1 : the electrolyte solution

resistance; C_1 : the capacitance phase angle element; R_2 : the interfacial electron transfer resistance; W_1 : the Warburg impedance introduced by diffusion of ions.

4.3.3.3 Electrocatalytic activity toward the oxidation of NE and 5-HT at CuNiAu/SPGE

The oxidation of NE and 5-HT at unmodified SPGE, mono-metallic, bimetallic and trimetallic modified SPGE was investigated using cyclic voltammetry. The unmodified SPGE (Figure 4.3.5a) and mono-metallic modified electrode as follow; Cu/SPGE (Figure 4.3.5b), Ni/SPGE (Figure 4.3.5c) and Au/SPGE (Figure 4.3.5d) could not distinguish the oxidation peak between NE and 5-HT in the potential range from 0.0 to 1.0 V vs Ag/AgCl. The bimetallic modified electrode was then examined. As shown in result of NiAu/SPGE (Figure 4.3.5e) and CuNi/SPGE (Figure 4.3.5d), the overlap oxidation peak of the target analytes was observed, whereas the CuAu/SPGE (Figure 4.3.5g) could discriminate the oxidation peak of NE from the oxidation peak of 5-HT due to the synergistically catalytic property of CuAu alloy^{238, 240, 255}. The separated oxidation peak of NE and 5-HT at 0.21 and 0.37 V vs Ag/AgCl, respectively, were noticed at CuAu/SPGE. Compared to unmodified SPGE, the potentials of NE and 5-HT were shift to less positive potential on CuAu/SPGE. Since the CuAu alloy might be assisted in faster kinetic electron transfer of diol group of NE structure and phenolic group of 5-HT structure. Same as CuAu/SPGE, the distinguishable oxidation peak of NE and 5-HT was obtained on trimetallic CuNiAu/SPGE (Figure 4.3.5h) but the trimetallic modified electrode provide higher sensitivity of NE determination around 2-fold than CuAu/SPGE as show in Figure 4.3.5o. The current response of NE and 5-HT were found to be $4.02 \pm 0.93 \mu\text{A}$ and $3.08 \pm 0.16 \mu\text{A}$ at CuAu/SPGE and $7.01 \pm 1.09 \mu\text{A}$ and $3.36 \pm 0.37 \mu\text{A}$ at CuNiAu/SPGE, respectively. It demonstrated that the existence of Ni could improve the kinetic electron transfer forward the oxidation of NE due to the synergistic property of CuNiAu alloy.

Additionally, the single electrodeposition of CuNiAu and sequent electrodeposition of Au/Cu/Ni/SPGE (Figure 4.3.5i), Ni/Cu/Au/SPGE (Figure 4.3.5j), Cu/Au/Ni/SPGE (Figure 4.3.5k), Au/Ni/Cu/SPGE (Figure 4.3.5l), Ni/Au/Cu/SPGE (Figure 4.3.5m) and Cu/Ni/Au/SPGE (Figure 4.3.5n) were compared for study the effect of the modification electrode. As the result shown in Figure 4.3.5(i-n) the sequent electrodeposition of precursor ion could not distinguish the oxidation peak of NE and 5-HT. With these results can conclude that the catalytic performance of the electrode depended on the nanostructure form of the trimetallic alloy. Considered the electrocatalytic activity of CuNiAu/SPGE via single electrodeposition step, the discriminated oxidation peak of NE and 5-HT would be attributed to superior synergistically electrocatalytic activity of CuNiAu alloy toward the oxidation of NE resulting in the shift of the oxidation potential to a less positive potential led to distinguishable peak of NE from the oxidation peak of 5-HT. Unlike the sequent electrodeposition of individual metallic, the nanocatalytic layer of each metallic was generated individually, the synergistic property could not be observed at this stage. These results evidenced that the CuNiAu/SPGE via single electrodeposition step of had excellent electrocatalytic activity toward the oxidation of NE resulting in synergistic property of alloy form. According to synergistically electrocatalytic property of CuNiAu alloy, the oxidation peak of NE was achieved in distinguishable separation from the oxidation peak of 5-HT. Therefore, this proposed electrode was suitable for simultaneous determination of NE and 5-HT.

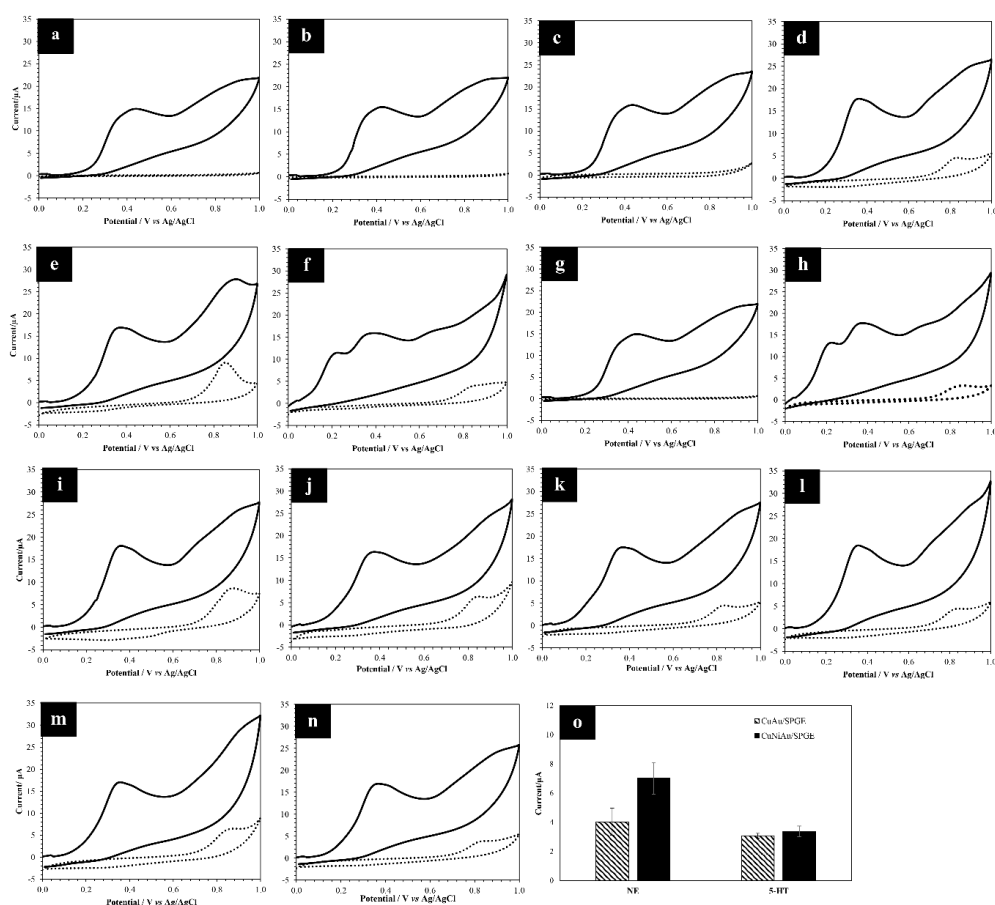


Figure 4.3.5 The CV of 25 μM NE and 50 μM 5-HT in 0.1 M PBS buffer pH 7.4 at different modified electrode as follows (a) SPGE, (b) Cu/SPGE, (c) Ni/SPGE, (d) Au/SPGE, (e) NiAu/SPGE, (f) CuAu/SPGE, (g) CuNi/SPGE, (h) CuNiAu/SPGE, (i) Au/Cu/Ni/SPGE, (j) Ni/Cu/Au/SPGE, (k) Cu/Au/Ni/SPGE, (l) Au/Ni/Cu/SPGE, (m) Ni/Au/Cu/SPGE and (n) Cu/Ni/Au/SPGE was scan from 0.0 V to 1.0 V vs Ag/AgCl at 100 mVs^{-1} of scan rate. (o) The comparing bar chart of NE and 5-HT current response at CuAu/SPGE and CuNiAu/SPGE.

4.3.3.4 Optimization of parameters

As the previous discussion, the trimetallic CuNiAu alloy provided the superior electrocatalytic oxidation of NE and 5-HT. Here, the optimization of trimetallic

deposition on electrode surface was systematically investigated including the electrodeposition potential, the electrodeposition time, and the molar ratio of Cu, Ni and Au precursors, significantly affecting to the catalytic property of the trimetallic modified electrode. The optimizations of electrodeposition parameters were described below.

4.3.3.4.1 Effect of electrodeposition parameters

To acquire the highest electrocatalytic activity of modified electrode, the parameters relating to the electrode modification were investigated including electrodeposition potential and electrodeposition time. The electrodeposition potential of CuNiAu solution at -1.2, -1.1, -1.0, -0.9 and -0.8 V vs Ag/AgCl was studied. The SWV voltammograms of 25 μM NE and 50 μM 5-HT with different electrodeposition potential was reported coexisting with the plot of current response of these compounds against electrodeposition potential as illustrated in Figure 4.3.6a and Figure 4.3.6b, respectively. As previously discussion, the Ni ion plays important role in assisting of Cu and Au deposition. However, Ni deposition step onto electrode surface should occur at high negative electrodeposition ^{258, 259}. Therefore, the increasing electrodeposition potential from -0.8 to -1.0 V vs Ag/AgCl lead to increasing NE current response, which can be resulted from the increasing amount of CuNiAu alloy nanoparticle on electrode surface. The poor Ni deposited composition at electrode surface at low negative potential (-0.8 V vs Ag/AgCl) resulting in the poor deposition efficiency of trimetallic alloy at electrode surface which can prove by SEM image (Figure 4.3.7a). On the other hand, the increased electrodeposition potential from -0.8 to -1.0 V vs Ag/AgCl resulting from gradually decreased of the 5-HT current response. This phenomenon may be attributed to the increasing amount of Ni composition in trimetallic alloy enhancing the composition of CuAu in trimetallic alloy as well at electrode surface, affirmed by the SEM image (Figure 4.3.7b). The increasing of CuNiAu composition in trimetallic alloy perform the good electrocatalytic activity of

NE oxidation reaction. Thus, the increasing of NE current response may be interfered the 5-HT in reduction of current response. For the high negative electrodeposition potential of -1.2 V vs Ag/AgCl , the oxidative current of NE and 5-HT was dramatically decreased relating to aggregate of large trimetallic onto electrode surface, which harmonized with obtained SEM result (Figure 4.3.7c). Consequentially, the electrocatalytic activity was reduced. Additionally, the SEM image at -1.0 V vs Ag/AgCl of electrodeposition potential displays well disperse of trimetallic CuNiAu on electrode surface. Considering the best electrocatalytic property of trimetallic CuNiAu modified SPGE electrode, the electrodeposition potential of -1.0 V vs Ag/AgCl was chosen for electrode modification.

Beside the electrodeposition potential, the electrodeposition time, affecting the electrodeposition efficiency of trimetallic CuNiAu, was next considered. The varied electrodeposition time from 60 to 400 second was investigated. Similarly, the plot between current response of $25\ \mu\text{M}$ of NE and $50\ \mu\text{M}$ of 5-HT against the electrodeposition time was reported accompanying with SWV voltammograms (Figure 4.3.7d and Figure 4.3.7c, respectively). The NE current response was increased relating to the increase of electrodeposition time from 60 to 200 second, whereas the 5-HT current response is slightly reduced, which may be attributed to the deposition efficiency of Ni as well as the effect of electrodeposition potential. At short period time of electrodeposition step may be led to low deposition efficiency of Ni cluster at electrode surface resulting in poor deposition efficiency of CuAu. This obtained result agrees with the SEM image at electrodeposition time of 60 second (Figure 4.3.7d), exhibiting poor distribution of trimetallic CuNiAu at SPGE surface. Even though the increasing composition of Ni when using the deposition time of 400 second could be enhancing the NE current response, this phenomenon interrupted the 5-HT detection in the decreasing its responses due to incompletely separated baseline of NE and 5-HT. Another reason of the decreasing NE and 5-HT response with the enhancement

of the deposition time is the aggregation of trimetallic electrode surface as shown in SEM image (Figure 4.3.7f). With this reason the electrodeposition time at 200 sec was selected as optimal condition due to uniform distributions of nanocluster and high current response.

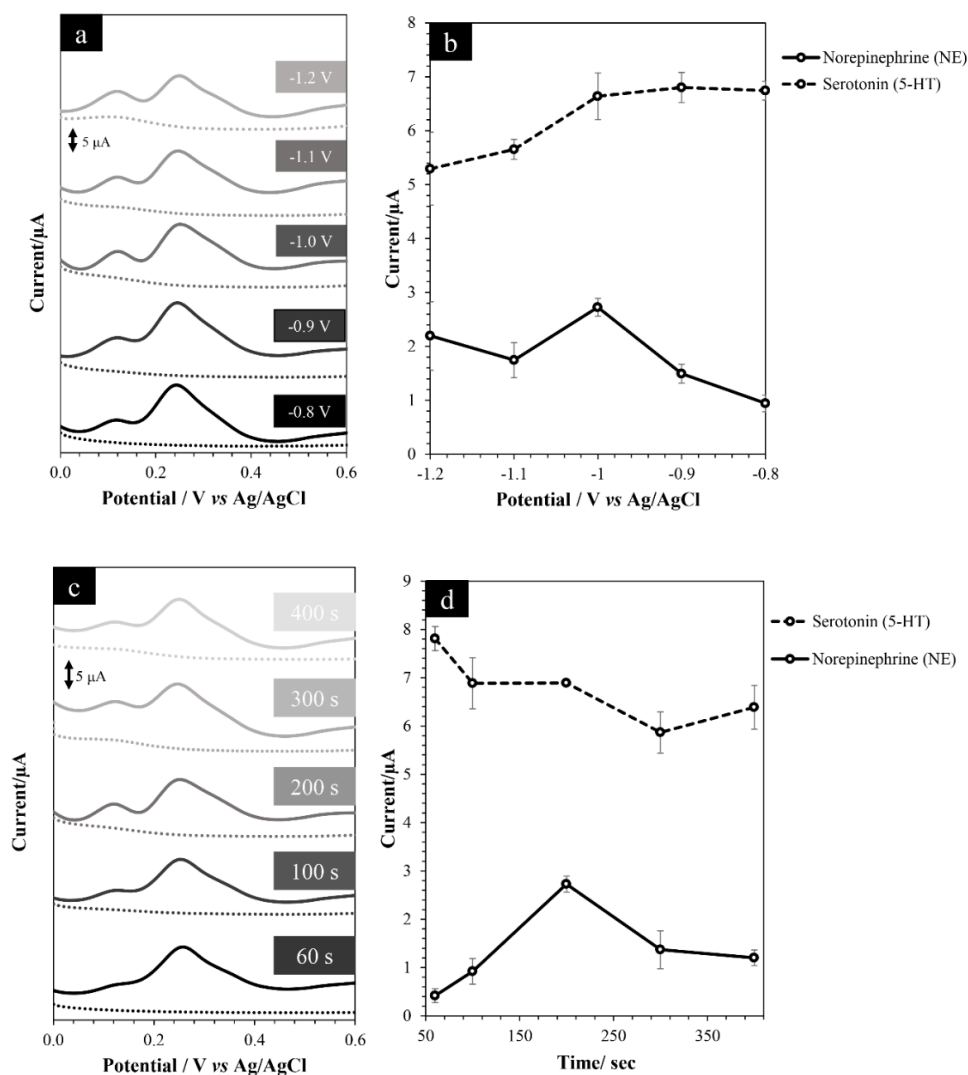


Figure 4.3.6 (a) The SWV voltammogram of 25 μM NE and 50 μM 5-HT at the different electrodeposition potential performed from 0.0 V to 0.6 V vs Ag/AgCl with E_{step} of 0.4 mV, amplitude of 50 mV and frequency of 35 Hz. (b) The relative plot between current response of 25 μM NE and 50 μM 5-HT and electrodeposition potential. (c) The SWV voltammogram of 25 μM NE and 50 μM 5-HT at the different electrodeposition time scanned from 0.0 V to 0.6 V vs Ag/AgCl with E_{step} of 0.4 mV and

frequency of 35 Hz. (e) The relative plot between current response of 25 μM NE and 50 μM 5-HT and electrodeposition time. The SWV voltammogram and current response values are representative of three measurements.

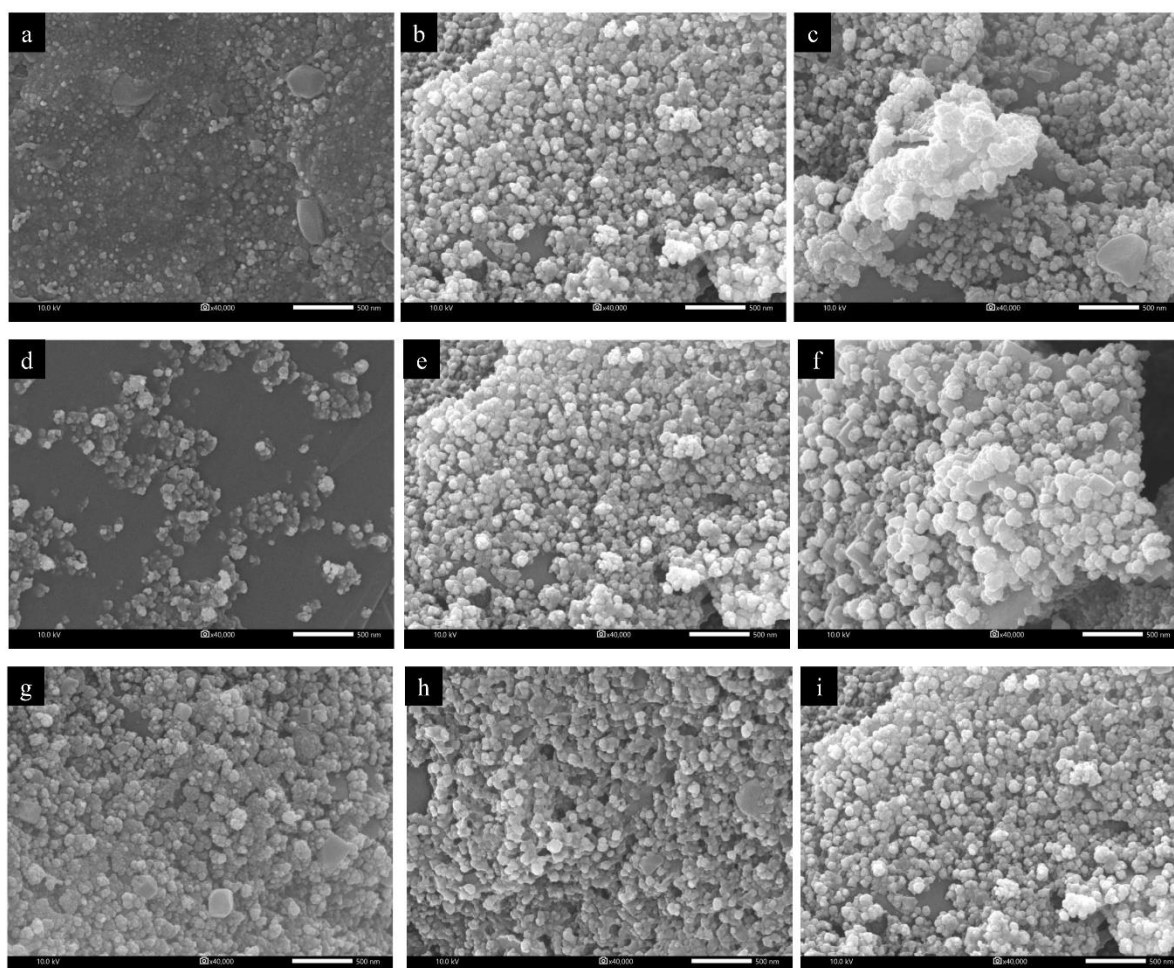


Figure 4.3.7 SEM image of 40,000 magnification of different electrodeposition potential of modified electrode procedure at (a) -0.8 V, (b) -1.0 V and (c) -1.2 V vs Ag/AgCl and various electrodeposition time of (d) 60 s, (e) 200 s and (f) 400 s. Additionally, SEM image of various molar ratio of Cu:Ni:Au was investigated for morphology study of (g) 1:100:1, (h) 1:100:2 and (i) 2:100:2

4.3.3.4.2 The effect of ion precursor ratio

In order to acquire the highly catalytic property of the modified electrode, the molar ratio of Cu(II), Ni(II), and Au(II) precursor were systematically investigated. The relationship between the current response and molar ratio of the metal precursor were recorded. The molar ratio of Ni(II) was study from 10-fold to 300-fold of molar ratio of Cu(II) and Au(II) meanwhile the molar ratio of Cu and Au ion was maintaining at 1-fold. As shown in the Figure 4.3.8a the current response of both 5-HT and NE increased with the increasing of the molar ratio of Ni ion from 10-fold to 100-fold, respected to the molar ratio of Cu and Au ion (when fix the concentration of Cu and Au at 0.2 mM), due to the enhancement of catalytic property of CuNiAu alloy. Now, the actual mechanism of Ni is not clear. From the observation of Yen et al. and Darabdhara et al. for NiCu²⁶⁰ and NiAu²⁶¹ alloy, orderly, the amount of Cu and Au increased upon increasing the content of Ni. With this notice, the Ni might be assisting the deposited of Cu and Au on the electrode surface resulting in highly synergistically catalytic property of trimetallic. Nerveless, higher amount of Ni ion than 100-fold might cause the overabundant CuAu alloy cluster on electrode surface. Consequently, the current response decreases due to decreasing of electroactive area. Considering the sensitivity of both 5-HT and NE, the 100-fold molar ratio of Ni was selected for next study. Then the molar ratio of Au precursor was investigated from 1-fold to 6-fold as shown in Figure. 4.3.8b. The background current coming from the PBS measurement was increasingly emerged when increased the molar ratio of Au amount. This increasing of background may be resulting in the electrocatalytic property of Au on PBS buffer when the amount of Au increased on the electrode surface (Figure 4.3.8e). Therefore, the 2-fold of molar ratio of Au was selected for optimal condition, compromising with both the aspect of sensitive NE and 5-HT measurement and low background current. Subsequently, the molar ratio of Cu was examined from 1- to 6-fold as illustrated in Figure 4.3.8c. The increasing of the molar ratio of Cu led to the enhancement of the

5-HT response whereas the current response of NE reduced when increasing molar ratio of Cu. The reduction of NE may be attributed to degradation of alloy property by the replacement of CuAu alloy with CuNPs at higher molar ratio of Cu (II) than Au (III). Therefore, the 2-fold molar ratio of Cu was selected for the modification of electrode. As a result, the appropriately molar ratio of Cu (II): Ni (II): Au (II) was 2: 100: 2 for highly catalytic efficiency of NE and 5-HT determination.

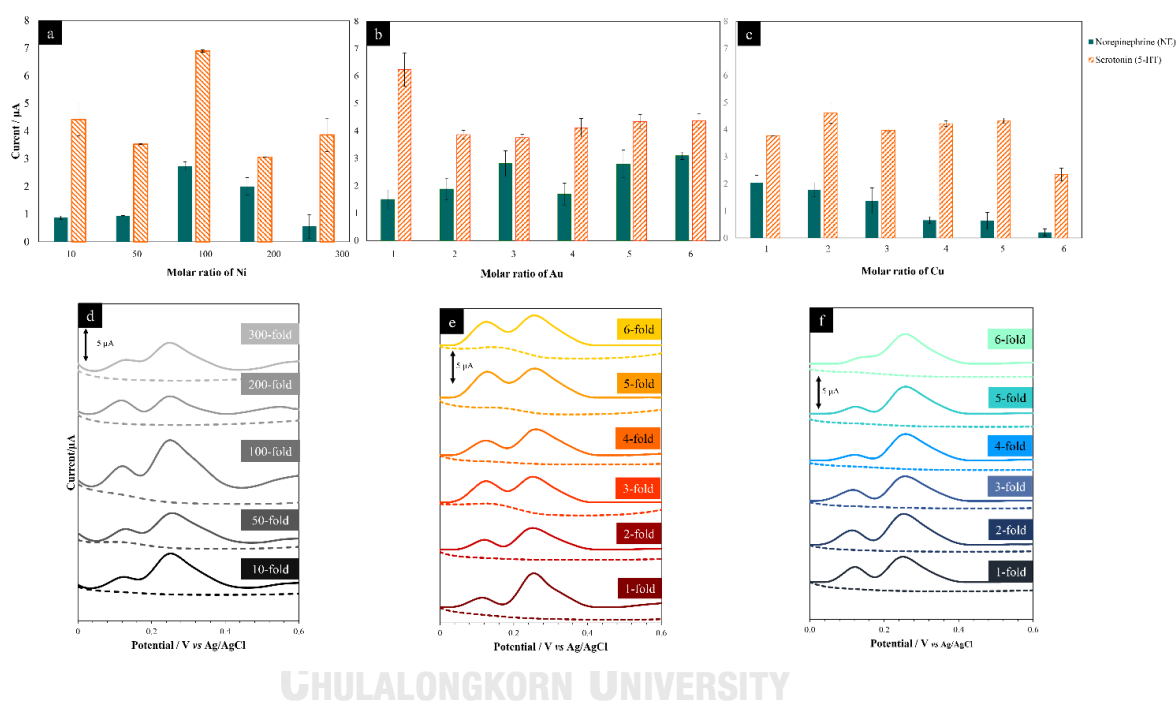


Figure 4.3.8 Molar ratio of metal precursors effect accompanied with the SWV voltammogram of (a and d) various molar ratio of Ni was studied at 10, 50, 100, 200 and 300 fold comparing with molar ratio of Cu and Au (fixed at 1-fold of molar ratio), (b and e) different molar ratio of Au was examined from 1, 2, 3, 4, 5, and 6 fold while the molar ratio of Ni and Cu was kept at 100 and 1, orderly, of molar ratio, (c and f) the molar ratio of Cu was varied from 1, 2, 3, 4, 5, and 6 fold, meanwhile the molar ratio of Ni and Au was kept at 100 and 2 fold, orderly, of molar ratio.

4.3.3.4.3. The effect of pH on the separated oxidation peak of NE and 5-HT

The pH was an important affected parameter on the electrochemical behavior of NE and 5-HT²⁶² as well as the separation efficiency of these compounds. Herein, the SWV measurement was utilized for examination of oxidative behavior of NE and 5-HT at CuNiAu/SPGE over pH range of 0.1 M PBS buffer from 6.0 to 9.0 as shown in Figure 4.3.9a. Because pH was not only affected to the oxidation of NE and 5-HT but also affected to the existing background current, the relationship between S/N ratio and pH value was reported as illustrated in Figure 4.3.9b. The S/N ratio of both NE and 5-HT directly proportional with the increase of pH. The maximum response was observed at pH 7.4 and the current response decreased when pH value was raised to 9. Considering to peak potential, the oxidation peak potential of 5-HT at pH value 6.0, 7.0, 7.4, 8.0 and 9.0 was found to be 0.34 ± 0.01 , 0.27 ± 0.02 , 0.28 ± 0.01 , 0.26 ± 0.02 , and 0.24 ± 0.03 , respectively. The increasing pH from 6.0 to 7.4, which was lower than the pKa of 5-HT (pKa : 9.8²¹⁹) and NE (pKa : 8.58²¹⁹), resulted in the promoting of the protonated form ($-NH_3^+$) of NE and 5-HT. Consequently, the oxidation of 5-HT was facilitated causing the shift of the oxidation peak potential to less positive. The NE peak potential was obtained at 0.10 ± 0.01 , 0.10 ± 0.01 , 0.12 ± 0.01 , 0.13 ± 0.01 and 0.11 ± 0.01 of pH value 6.0, 7.0, 7.4, 8.0 and 9.0, respectively. At the pH values from 6.0 to 8.0, the difficult oxidation process of NE resulted the shift of the oxidation peak potential in more positive potential and then the peak potential shifted to less positive potential at pH 9. With the well-defined peak and sensitivity aspect, the 7.4 pH value of 0.1 M PBS buffer was chosen for NE and 5-HT measurement.

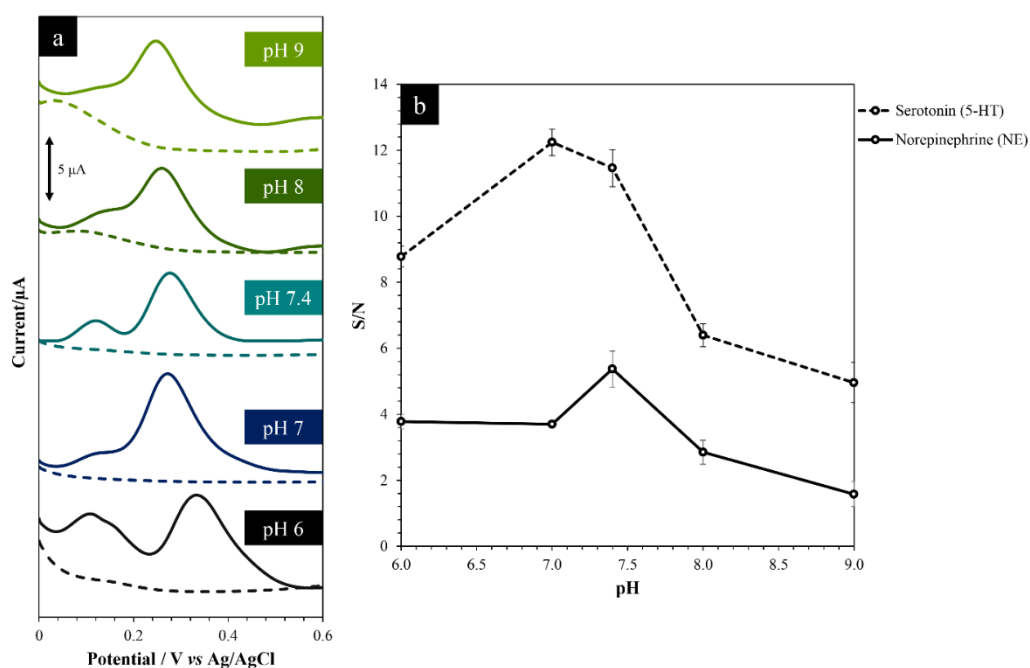


Figure 4.3.9 (a) The SWV voltammograms of 25 μM NE and 50 μM 5-HT at the pH range 6.0 to 9.0 were performed from 0.0 V to 0.6 V vs Ag/AgCl with E_{step} of 0.4 mV, amplitude of 50 mV and frequency of 35 Hz. (b) The relationship between S/N and pH. The SWV voltammograms are representative of three repeated measurements.

4.3.3.4.4 The effect of SWV parameter

According to SWV technique influential separation through different electron transfer kinetic²⁶³ of NE and 5-HT at CuNiAu/SPGE, the parameters of SWV including step potential, amplitude, and frequency were inspected. The potential step (E_{step}) strongly influent on the electron transfers kinetic was firstly investigated in the range of 0.1, 0.2, 0.3, 0.4, 0.5, 0.6 mV s⁻¹ with analysis time of 4.45, 2.22, 1.35, 1.11, 0.57, 0.65 min, respectively (Figure 4.3.10a). As the clearly observed in Figure 4.3.10d, the SWV voltammogram exhibited the completely separated peak between NE and 5-HT at lowest E_{step} . And then the gradually combined peak (like shoulder peak) was noticed at high E_{step} due to incompletely electron transfer kinetic of NE from too fast of scan rate. Additionally, the background current was noticeably emerged with high E_{step} which

might be coming from the AuNPs peeling. Therefore, the S/N ratio was reported. Consideration of the peak separation and analysis time, E_{step} of 0.3 mV was chosen as optimized condition. In this SWV technique, the sensitivity is acquired from the change in potential amplitude (E_{amp}) and frequency²⁶⁴. The varied E_{amp} in the range from 25 - 125 mV (Figure 4.3.10b) and frequency from 20- 85 Hz (Figure 4.3.10c) were investigated. Despite the increasing E_{amp} and frequency provided the high peak current, the background current was highly emerged as well as shown in Figure 4.3.10 e and f, orderly. For the demand of high sensitivity and symmetry peak in electrochemical analysis, the E_{amp} of 75 mV and frequency of 50 Hz were selected as optimized condition for further experiment.



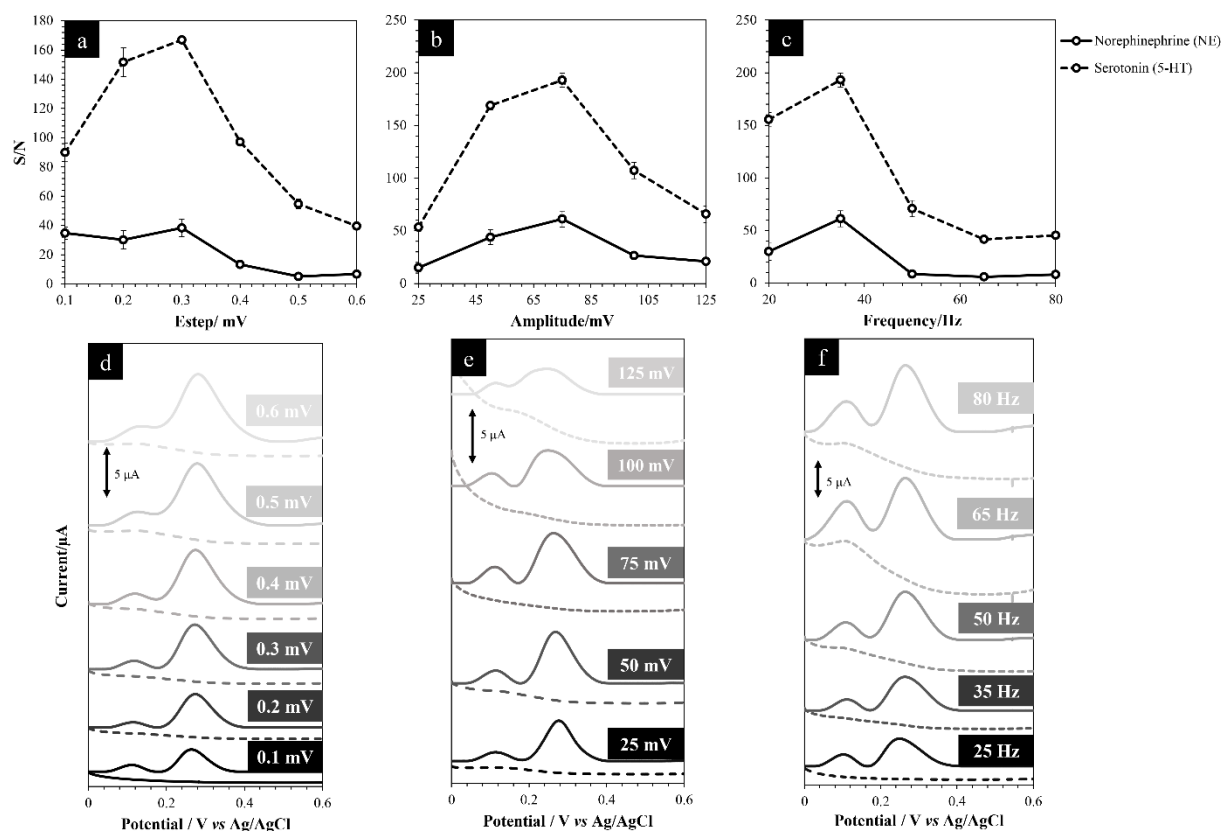


Figure 4.3.10 The plot of SWV parameters between S/N and (a) E_{step} , (b) amplitude, (c) frequency of 25 μ M NE and 50 μ M 5-HT in 0.1 M PBS buffer pH 7.4. The SWV voltammogram of various (d) E_{step} , (e) amplitude and (f) frequency against with potential. The SWV voltammograms are representative of three repetition.

4.3.3.5 Analytical figure of merit

4.3.3.5.1. Individual determination of NE and 5-HT using CuNiAu/SPGE

In order to evaluate the performance of CuNiAu/SPGE sensor for simultaneous determination of NE and 5-HT, the individual determinations of NE and 5-HT were carried out by gradual changing the concentration of one species, whereas the concentration of other species was kept constant. As shown in Figure 4.3.11, When the concentration of NE was increased, its current response increased and no significant changing of the current of 5-HT at fixed concentration (the %RSD of 5-HT was found to be 6.99 %) was observed. Meanwhile, the similar result was obtained when fixed

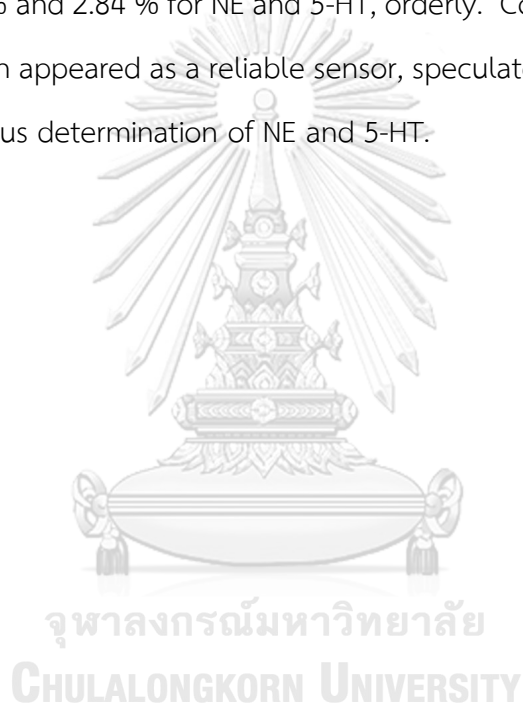
the concentration of NE (the %RSD of NE was found to be 7.75 %) and varied concentration of 5-HT. Therefore, the results confirmed that both compounds did not affect each other. The oxidation peak current of NE was proportional increased with the increase of concentration in a range of 0.1 – 40 μM with a linear regressive equation of $I_{pa} (\mu\text{A}) = 0.1243 C (\mu\text{M}) - 0.0472$, and a linear regression (R^2) of 0.9912 while fixed the concentration of 5-HT at 30 μM as illustrated in Figure 4.3.11a. Similarly, as show in Figure 4.3.11b the oxidation peak current of 5-HT was linearly increased with increasing the concentration in a range of 2.5 – 70 μM with $I_{pa} (\mu\text{A}) = 0.1275C (\mu\text{M}) - 0.3758$ of linear regressive equation ($R^2 = 0.9973$) accomplished by remaining the concentration of NE at 25 μM . These results demonstrated that CuNiAu/SPGE could be employed for the simultaneous determination of NE and 5-HT without interfering with each other.

4.3.3.5.2 Simultaneous determination of NE and 5-HT using CuNiAu/SPGE

Simultaneous changing concentration of both NE and 5-HT was performed in order to evaluate the efficiency of proposed sensor. Under optimized condition, the analytical performance of utilizing CuNiAu/SPGE was investigated by continuous increasing the concentration of NE and 5-HT in the range of 1- 40 μM and 5-70 μM , respectively, as shown in Figure 4.3.11c. The linear regressive equation of NE and 5-HT were found to be $I_{pa} (\mu\text{A}) = 0.1094 C (\mu\text{M}) + 0.4065$ ($R^2 = 0.9929$) and $I_{pa} (\mu\text{A}) = 0.1154 C (\mu\text{M}) + 0.2376$ ($R^2 = 0.9907$), respectively. The limit of detections (calculated from $3SD_{\text{blank}}/\text{slope}$) were found to be 0.19 μM for NE and 0.18 μM for 5-HT, meanwhile the limit of quantitation (calculated from $10SD_{\text{blank}}/\text{slope}$) of the simultaneous determination NE and 5-HT were found to be 0.64 and 0.61 μM , respectively. The analytical performance of CuNiAu/SPGE was compared with previous literatures as displays in Table.4.3.1. Although the proposed sensor for simultaneous determination of NE and 5-HT offers the insignificant improvement of the linearity and the LOD

compared to the other modified electrodes. The CuNiAu modified SPGE is straightforward modification via electrodeposition method of CuNiAu mixing solution. With this process, the synergistic CuNiAu alloy was firstly employed for simultaneous determination of NE and 5-HT.

Additionally, the reproducibility and the repeatability were evaluated regarding the reliability of the proposed. The reproducibility of 25 μM of NE and 50 μM of 5-HT was performed on different seven electrodes. The %RSDs of seven electrodes were found to be 5.68 % and 2.84 % for NE and 5-HT, orderly. Consequently, the proposed electrode has been appeared as a reliable sensor, speculated as an alternative sensor for the simultaneous determination of NE and 5-HT.



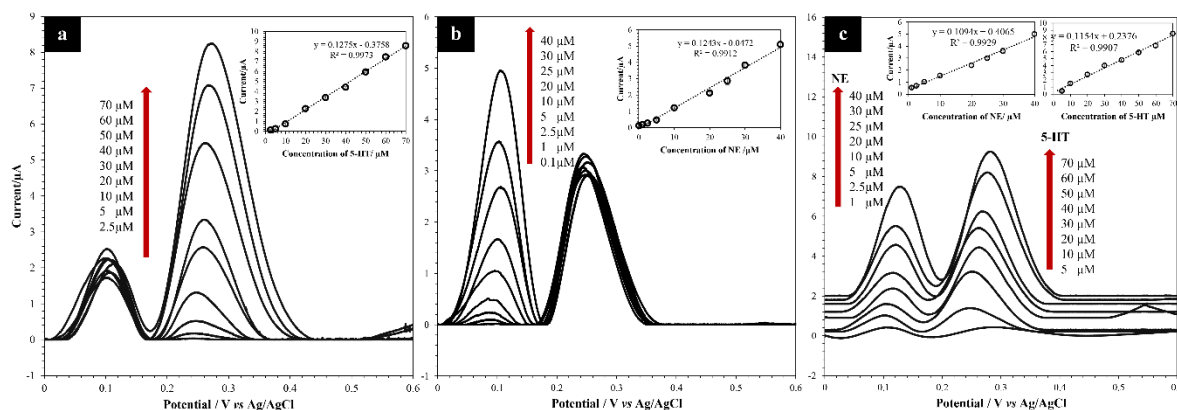


Figure 4.3.11 Individual test for (a) different concentration of 5-HT in the presence of 25 μM of NE in 0.1M PBS buffer (pH 7.4). 5-HT concentration are: 2.5, 5, 10, 20, 30, 40, 50, 60 and 70 μM, (b) different concentration of NE in the presence of 30 μM of 5-HT in 0.1M PBS buffer (pH 7.4). NE concentration are: 0.1, 1, 2.5, 5, 10, 20, 25, 30 and 40 μM and (c) different concentration of NE and 5-HT in 0.1M PBS buffer (pH 7.4). NE concentration are: 1, 2.5, 5, 10, 20, 25, 30 and 40 μM. Meanwhile 5-HT concentration are 5, 10, 20, 30, 40, 50, 60, and 70. Inset picture: the relationship between concentration of the target analyte and the current response coexisting with the linear regressive equation.

Table 4.3.1 Comparison of the linear range and detection sample obtained at the CuNiAu/SPGE for simultaneous determination of NE and 5-HT with others.

Modified electrode	NE		5-HT		References
	Linear range (μM)	LOD (μM)	Linear range (μM)	LOD (μM)	
CNT-IE	-	-	1.00-15.00	0.20	265
5-HTP/GCE	-	-	5.00-35.00	1.70	266
PAA-MWCNTs/SPCE	0.00-10.00	0.13	-	-	267
DDP-CNT/CPE	0.10-38.00	0.07	-	-	268
Eriochrome cyanine R/GCE	2.00-50.00	1.50	0.05-5.00	0.05	219
MWNTs-ZnO/chitosan/SPE	1.00-30.00	0.20	0.10-1.00	0.01	269
CuNiAu/SPGE	1.00-40.00	0.19	5.00-70.00	0.18	This work

4.3.3.6 Interference study

The influences of various species existing in human serum on the determination of NE and 5-HT were evaluated in order to extend the validity of the proposed sensor. The investigative interferences were the common ions in serum (Cl^- , K^+ , and Mg^{2+}), biological molecules (glucose, L-glycine, and tyrosine), and common electroactive species (uric acid (UA) and ascorbic acid (AA)). The interfering effect was examined by mixing those interfering substances at the found concentration in human serum with

25 μM NE and 50 μM 5-HT followed by the measurement with proposed electrode via SWV technique. As the result shown in Figure 4.3.12, AA was major interfering species while the others did not obviously affect to the measurement of NE and 5-HT utilizing CuNiAu/SPGE. The broad oxidation peak of AA was obtained at 0.13 V vs Ag/AgCl nearby the oxidation peak of NE resulting in an unusual higher current response of NE. Similarly, the oxidation peak of 5-HT was moderately increasing via broad peak of AA (Figure 4.3.13). According the dominant interfering effect of AA, the elimination of this interference was manipulated before the measurement by oxidized AA with Cu^{2+} to produce dehydroascorbic acid which is oxidized forms of ascorbic acid²⁷⁰ which could not affect the oxidation of the target analytes. Due to influential interference of AA for determination of NE and 5-HT, the removal interfering AA was investigated. According the previous report^{270, 271}, the Cu (II) acting as reducing agent could oxidize AA to dehydroascorbic acid. With this perspective, the stepwise of this procedure was testified. Afterward the mixed solution of 0.2 mM Cu (II) and 0.1 mM AA in 0.1 M PBS buffer was tested and the nonexistent oxidation peak of AA was obtained. And then the 0.2 mM Cu (II) solution was added in the mixture of 25 μM NE, 50 μM 5-HT and 0.1 mM AA in 0.1 M PBS buffer pH 7.4. The current response after eliminated AA provide reachable standard solution measurement. The current response of NE and 5-HT after removal AA are 2.61 ± 0.19 and 5.73 ± 0.37 , respectively and the current response of standard NE and 5-HT are 2.71 ± 0.03 and 5.96 ± 0.11 , respectively. The result indicating that this procedure of removal AA oxidized with Cu (II) was succeeded resulting in accomplished determination of NE and 5-HT in real sample.

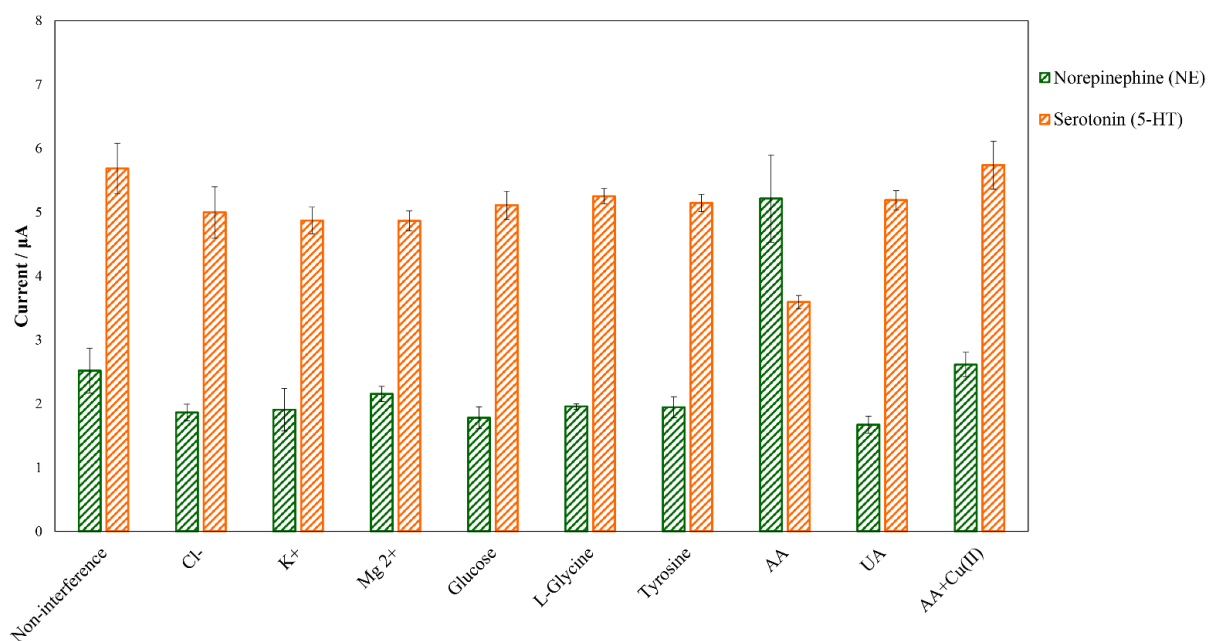


Figure 4.3.12 The common interfering species in serum were studied by mixed various interference with standard solution of 25 μM NE and 50 μM 5-HT in 0.1 M PBS buffer pH 7.4. The interfering species as follows 0.05 M of Cl⁻, K⁺ and Mg²⁺, 1 mM of glucose, L-glycine and tyrosine, and 0.1 mM of ascorbic acid (AA) and uric acid (UA) were investigated.

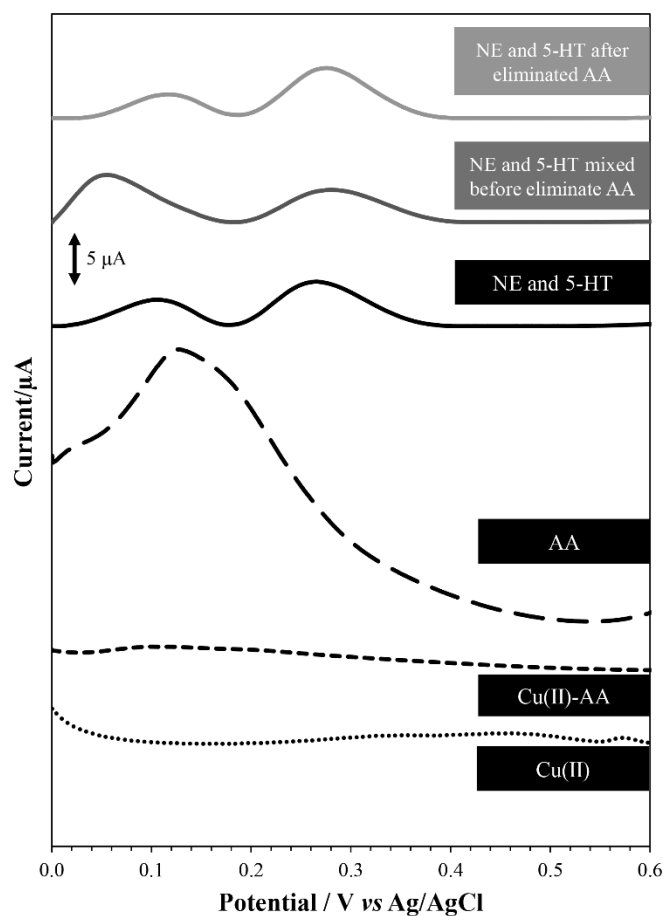


Figure 4.3.13 The SWV voltammograms of sequentially eliminated AA. All SWV voltammograms are representative of three repetitive experiments.

4.3.3.7 Simultaneous determination of NE and 5-HT in the artificial serum

The feasibility of CuNiAu/SPGE for real sample analysis was investigated using spike method. The three concentrations of spike standard solution were studied at 2, 20, and 30 μM for NE, and at 6, 40 and 60 μM for 5-HT. Additionally, the standard addition was employed for recovery study of real sample analysis. The linear regressive equations of standard addition method for NE and 5-HT were $I_{pa} (\mu\text{A}) = 0.107 C (\mu\text{M}) + 0.4477$ ($R^2 = 0.9621$) and $I_{pa} (\mu\text{A}) = 0.0954 C (\mu\text{M}) + 0.4662$ ($R^2 = 0.9687$), respectively. Afterward, the acceptable recoveries of NE and 5-HT were found to be 100.9 ± 3.5 to 108.8 ± 3.6 and 92.55 ± 1.4 to 108.3 ± 3.6 , respectively. Hence, the

proposed electrode could be accomplished utilization for the determination of NE and 5-HT in artificial serum with satisfiable recovery as mentioned above.

4.3.4 Conclusion

In summary, the trimetallic CuNiAu alloy was simply synthesized by a one-step electrodeposition onto SPGE surface, to obtain the CuNiAu/SPGE sensing platform for simultaneous determination of NE and 5-HT. This proposed CuNiAu/SPGE sensor exhibited excellent electrocatalytic activity towards the oxidation of NE and 5-HT in which the two corresponding anodic peaks could be clearly distinguished from each other, compared with the bare SPGE, Cu/SPGE, Au/SPGE, and Ni/SPGE sensors that possessed low selectivity as they could not provide the well-separated oxidation peaks for NE and 5-HT. Moreover, the electrochemical deposition of Cu-Ni-Au alloys onto the electrode surface was studied using two methods including the single-bath and the stepwise processes which typically affected the electrocatalytic properties of the resulting modified electrodes. The results showed that the trimetallic alloy electrodeposited from the single-bath process (CuNiAu) demonstrated the highest electrocatalytic activity, compared to that obtained from the stepwise electrodeposition (Cu/Ni/Au). The enhanced electrocatalytic activity of the trimetallic CuNiAu composite would be potentially due to the synergistic effect between Cu, Ni, and Au nanoparticles. Although the developed electrochemical sensor could not tolerate AA interference, AA could be simply eliminated from the system by oxidation reaction using Cu^{2+} prior to the measurement. Subsequently, the quantitative determination of NE and 5-H at the CuNiAu/SPGE was thoroughly examined by SWV, and the satisfied linearities and LODs could be achieved. Moreover, the developed CuNiAu/SPGE sensor was then applied to simultaneously detect NE and 5-HT in serum samples with good reproducibility and excellent recoveries, highlighting that the

CuNiAu/SPGE has a potential to be used as a sensitive and selective sensor for NE and 5-HT in complex biological samples.



CHAPTER 5

CONCLUSIONS AND FUTURE PERSPECTIVE

The purpose of this dissertation is to develop the analytical sensing devices for quantitative analysis. The results distinctly demonstrated that the developed sensors offered the remarkable performance for diverse applications in pharmaceutical, food control and clinical areas. Typically, the developed analytical sensors were categorized regarding the detection techniques which were either colorimetry or electrochemistry. Their sensing performances and applications could be summarized as follows:

CHAPTER 3: The development of integrated platforms for colorimetric sensor and its application. The transparency based colorimetric sensor was developed for SAL measurement in pharmaceutical application. This proposed sensing device exhibited the noticeable color change of the reagent from light pink to orangish color when the analyte was present in the system. This change of color was based on the well-known redox reaction between KMnO_4 acting as the strongly oxidizing agent and the reducing analyte (SAL). This developed colorimetric sensor offered the beneficial advantages of fast analysis, simple operation and interpretation, and suitability for on-site application.

CHAPTER 4: The development of integrated platforms for electrochemical sensor and its application. The new electrochemical sensors were developed with the improvement in selectivity towards the oxidation of compounds with almost similar chemical structures whose anodic peaks would be overlapping. The electrochemical system was integrated to the separation platform, the polymeric film recognition unit, and the electrocatalytic nanomaterial-based electrode. In the first section, the PdNPs/BDD electrode was integrated with the UHPLC platform in order to enhance the selectivity for the detection of four β -agonists. Next (in the second section), the electrochemical sensor was combined to the MIP recognition system for the selective extraction of the target analyte (SAL) from other interferences. In the final section, the synergistically electrocatalytic activity of trimetallic composite modified

SPGE was investigated, and the developed sensor was then used for simultaneous determination of 5-HT and NE, with enhanced sensitivity and selectivity. Overall, the improvement in selectivity of the developed electrochemical sensors could be successfully achieved. These selective electrochemical sensors could then be further applied in complex applications.

5.1 Future Perspective

The miniaturized and portable sensors have recently received great interest. As reported in the literature, the wifi cloud-based portable potentiostat and the smartphone-based detection have been extensively developed and used as electrochemical sensing and colorimetric sensing tools with user friendly interface. According to the advancement of technology, the electrochemical and colorimetric methods could be further developed in great compatibility with the accessible and portable sensors, which would be easy to operate as an end-user. Therefore, the further development of analytical sensors would offer new opportunities to the resource-limited areas and the promising applications, especially in doping control process and point-of-care (POC) testing, could be potentially achieved.

REFERENCES

1. Jedlińska, K.; Strus, M.; Baś, B., A new electrochemical sensor with the Refreshable Silver Liquid Amalgam Film multi-Electrode for sensitive voltammetric determination of vitamin K2 (menaquinone). *Electrochimica Acta* 2018, 265, 355-363.
2. Khaleghi, F.; Arab, Z.; Gupta, V. K.; Ganjali, M. R.; Norouzi, P.; Atar, N.; Yola, M. L., Fabrication of novel electrochemical sensor for determination of vitamin C in the presence of vitamin B9 in food and pharmaceutical samples. *Journal of Molecular Liquids* 2016, 221, 666-672.
3. Charoenkitamorn, K.; Chaiyo, S.; Chailapakul, O.; Siangproh, W., Low-cost and disposable sensors for the simultaneous determination of coenzyme Q10 and α -lipoic acid using manganese (IV) oxide-modified screen-printed graphene electrodes. *Analytica Chimica Acta* 2018, 1004, 22-31.
4. Kotlarek, D.; Vorobii, M.; Ogieglo, W.; Knoll, W.; Rodriguez-Emmenegger, C.; Dostálek, J., Compact Grating-Coupled Biosensor for the Analysis of Thrombin. *ACS Sensors* 2019, 4 (8), 2109-2116.
5. Yang, Y.; Gao, F.; Cai, X.; Yuan, X.; He, S.; Gao, F.; Guo, H.; Wang, Q., β -Cyclodextrin functionalized graphene as a highly conductive and multi-site platform for DNA immobilization and ultrasensitive sensing detection. *Biosensors and Bioelectronics* 2015, 74, 447-453.
6. Tanwar, S.; Lu, H.-Y.; Magi, E.; Ho, J.-a. A., A 2,4-dinitrophenylhydrazine/kojic acid derivative as a simple colorimetric probe for determination of cupric ions in water. *Sensors and Actuators B: Chemical* 2014, 203, 204-208.
7. Mishra, R. K.; Sempionatto, J. R.; Li, Z.; Brown, C.; Galdino, N. M.; Shah, R.; Liu, S.; Hubble, L. J.; Bagot, K.; Tapert, S.; Wang, J., Simultaneous detection of salivary Δ^9 -tetrahydrocannabinol and alcohol using a Wearable Electrochemical Ring Sensor. *Talanta* 2020, 211, 120757.

8. Chaiyo, S.; Siangproh, W.; Apilux, A.; Chailapakul, O., Highly selective and sensitive paper-based colorimetric sensor using thiosulfate catalytic etching of silver nanoplates for trace determination of copper ions. *Analytica Chimica Acta* 2015, 866, 75-83.
9. Jampasa, S.; Pummoree, J.; Siangproh, W.; Khongchareonporn, N.; Ngamrojanavanich, N.; Chailapakul, O.; Chaiyo, S., "Signal-On" electrochemical biosensor based on a competitive immunoassay format for the sensitive determination of oxytetracycline. *Sensors and Actuators B: Chemical* 2020, 320, 128389.
10. Dong, R.-E.; Kang, P.; Xu, X.-L.; Cai, L.-X.; Guo, Z., Cation-exchange strategy for a colorimetric paper sensor: Belt-like ZnSe nanoframes toward visual determination of heavy metal ions. *Sensors and Actuators B: Chemical* 2020, 312, 128013.
11. Guo, Z.; Niu, Q.; Li, T.; Wang, E., Highly chemoselective colorimetric/fluorometric dual-channel sensor with fast response and good reversibility for the selective and sensitive detection of Cu²⁺. *Tetrahedron* 2019, 75 (30), 3982-3992.
12. Vyas, G.; Bhatt, S.; Si, M. K.; Jindani, S.; Suresh, E.; Ganguly, B.; Paul, P., Colorimetric dual sensor for Cu(II) and tyrosine and its application as paper strips for detection in water and human saliva as real samples. *Spectrochimica Acta Part A: Molecular and Biomolecular Spectroscopy* 2020, 230, 118052.
13. Hosu, O.; Lettieri, M.; Papara, N.; Ravalli, A.; Sandulescu, R.; Cristea, C.; Marrazza, G., Colorimetric multienzymatic smart sensors for hydrogen peroxide, glucose and catechol screening analysis. *Talanta* 2019, 204, 525-532.
14. Li, R.; Zhen, M.; Guan, M.; Chen, D.; Zhang, G.; Ge, J.; Gong, P.; Wang, C.; Shu, C., A novel glucose colorimetric sensor based on intrinsic peroxidase-like activity of C60-carboxyfullerenes. *Biosensors and Bioelectronics* 2013, 47, 502-507.
15. Chen, P.; Zhao, A.; Wang, J.; He, Q.; Sun, H.; Wang, D.; Sun, M.; Guo, H., In-situ monitoring reversible redox reaction and circulating detection of nitrite via an ultrasensitive magnetic Au@Ag SERS substrate. *Sensors and Actuators B: Chemical* 2018, 256, 107-116.

16. Liu, Q.; Chen, P.; Xu, Z.; Chen, M.; Ding, Y.; Yue, K.; Xu, J., A facile strategy to prepare porphyrin functionalized ZnS nanoparticles and their peroxidase-like catalytic activity for colorimetric sensor of hydrogen peroxide and glucose. *Sensors and Actuators B: Chemical* 2017, 251, 339-348.
17. Yin, J.; Gao, W.; Zhang, Z.; Mai, Y.; Luan, A.; Jin, H.; Jian, J.; Jin, Q., Batch microfabrication of highly integrated silicon-based electrochemical sensor and performance evaluation via nitrite water contaminant determination. *Electrochimica Acta* 2020, 335, 135660.
18. Charoenkitamorn, K.; Chailapakul, O.; Siangproh, W., Development of gold nanoparticles modified screen-printed carbon electrode for the analysis of thiram, disulfiram and their derivative in food using ultra-high performance liquid chromatography. *Talanta* 2015, 132, 416-423.
19. Kajornkavinkul, S.; Punrat, E.; Siangproh, W.; Rodthongkum, N.; Praphairaksit, N.; Chailapakul, O., Graphene/polyvinylpyrrolidone/polyaniline nanocomposite-modified electrode for simultaneous determination of parabens by high performance liquid chromatography. *Talanta* 2016, 148, 655-660.
20. Yang, X.; Kirsch, J.; Fergus, J.; Simonian, A., Modeling analysis of electrode fouling during electrolysis of phenolic compounds. *Electrochimica Acta* 2013, 94, 259-268.
21. Wang, J.; Jiang, M.; Lu, F., Electrochemical quartz crystal microbalance investigation of surface fouling due to phenol oxidation. *Journal of Electroanalytical Chemistry* 1998, 444 (1), 127-132.
22. Goyal, R. N.; Oyama, M.; Singh, S. P., Fast determination of salbutamol, abused by athletes for doping, in pharmaceuticals and human biological fluids by square wave voltammetry. *Journal of Electroanalytical Chemistry* 2007, 611 (1), 140-148.
23. Quintino, M. S. M.; Angnes, L., Bia-amperometric quantification of salbutamol in pharmaceutical products. *Talanta* 2004, 62 (2), 231-236.

24. Fischer, A. E.; Show, Y.; Swain, G. M., Electrochemical Performance of Diamond Thin-Film Electrodes from Different Commercial Sources. *Analytical Chemistry* 2004, 76 (9), 2553-2560.
25. Pecková, K.; Musilová, J.; Barek, J., Boron-doped diamond film electrodes-new tool for voltammetric determination of organic substances. *Critical Reviews in Analytical Chemistry* 2009, 39 (3), 148-172.
26. Motia, S.; Bouchikhi, B.; Llobet, E.; El Bari, N., Synthesis and characterization of a highly sensitive and selective electrochemical sensor based on molecularly imprinted polymer with gold nanoparticles modified screen-printed electrode for glycerol determination in wastewater. *Talanta* 2020, 216, 120953.
27. Panahi, Y.; Motaharian, A.; Hosseini, M. R. M.; Mehrpour, O., High sensitive and selective nano-molecularly imprinted polymer based electrochemical sensor for midazolam drug detection in pharmaceutical formulation and human urine samples. *Sensors and Actuators B: Chemical* 2018, 273, 1579-1586.
28. Yücebaş, B. B.; Yaman, Y. T.; Bolat, G.; Özgür, E.; Uzun, L.; Abaci, S., Molecular imprinted polymer based electrochemical sensor for selective detection of paraben. *Sensors and Actuators B: Chemical* 2020, 305, 127368.
29. Lin, X.; Ni, Y.; Li, S.; Kokot, S., A novel method for simultaneous analysis of three β 2-agonists in foods with the use of a gold-nanoparticle modified glassy carbon electrode and chemometrics. *Analyst* 2012, 137 (9), 2086-2094.
30. Ostrom, C. K.; Chen, A., Synthesis and Electrochemical Study of Pd-Based Trimetallic Nanoparticles for Enhanced Hydrogen Storage. *The Journal of Physical Chemistry C* 2013, 117 (40), 20456-20464.
31. Wanjala, B. N.; Loukrakpam, R.; Luo, J.; Njoki, P. N.; Mott, D.; Zhong, C.-J.; Shao, M.; Protsailo, L.; Kawamura, T., Thermal Treatment of PtNiCo Electrocatalysts: Effects of Nanoscale Strain and Structure on the Activity and Stability for the Oxygen Reduction Reaction. *The Journal of Physical Chemistry C* 2010, 114 (41), 17580-17590.

32. Zhang, H.; Okumura, M.; Toshima, N., Stable Dispersions of PVP-Protected Au/Pt/Ag Trimetallic Nanoparticles as Highly Active Colloidal Catalysts for Aerobic Glucose Oxidation. *The Journal of Physical Chemistry C* 2011, 115 (30), 14883-14891.
33. Lin, L.; Weng, S.; Zheng, Y.; Liu, X.; Ying, S.; Chen, F.; You, D., Bimetallic PtAu alloy nanomaterials for nonenzymatic selective glucose sensing at low potential. *Journal of Electroanalytical Chemistry* 2020, 865, 114147.
34. Nantaphol, S.; Watanabe, T.; Nomura, N.; Siangproh, W.; Chailapakul, O.; Einaga, Y., Bimetallic Pt–Au nanocatalysts electrochemically deposited on boron-doped diamond electrodes for nonenzymatic glucose detection. *Biosensors and Bioelectronics* 2017, 98, 76-82.
35. Charoenkitamorn, K.; Chotsuwan, C.; Chaiyo, S.; Siangproh, W.; Chailapakul, O., A new ready-to-use gel-based electrolyte for paraquat sensor. *Sensors and Actuators B: Chemical* 2020, 315, 128089.
36. Pinyorosphatum, C.; Rattanarat, P.; Chaiyo, S.; Siangproh, W.; Chailapakul, O., Colorimetric sensor for determination of phosphate ions using anti-aggregation of 2-mercaptoethanesulfonate-modified silver nanoplates and europium ions. *Sensors and Actuators B: Chemical* 2019, 290, 226-232.
37. Pungjunun, K.; Nantaphol, S.; Praphairaksit, N.; Siangproh, W.; Chaiyo, S.; Chailapakul, O., Enhanced sensitivity and separation for simultaneous determination of tin and lead using paper-based sensors combined with a portable potentiostat. *Sensors and Actuators B: Chemical* 2020, 318, 128241.
38. Srisomwat, C.; Teengam, P.; Chuaypen, N.; Tangkijvanich, P.; Vilaivan, T.; Chailapakul, O., Pop-up paper electrochemical device for label-free hepatitis B virus DNA detection. *Sensors and Actuators B: Chemical* 2020, 316, 128077.
39. Kunpatee, K.; Traipop, S.; Chailapakul, O.; Chuanuwatanakul, S., Simultaneous determination of ascorbic acid, dopamine, and uric acid using graphene quantum dots/ionic liquid modified screen-printed carbon electrode. *Sensors and Actuators B: Chemical* 2020, 314, 128059.

40. Duenchay, P.; Chailapakul, O.; Siangproh, W., A Transparency Sheet-Based Colorimetric Device for Simple Determination of Calcium Ions Using Induced Aggregation of Modified Gold Nanoparticles. *Int J Mol Sci* 2019, 20 (12), 2954.
41. Carrilho, E.; Martinez, A. W.; Whitesides, G. M., Understanding Wax Printing: A Simple Micropatterning Process for Paper-Based Microfluidics. *Analytical Chemistry* 2009, 81 (16), 7091-7095.
42. Dungchai, W.; Chailapakul, O.; Henry, C. S., Electrochemical Detection for Paper-Based Microfluidics. *Analytical Chemistry* 2009, 81 (14), 5821-5826.
43. Prabhu, A.; Giri Nandagopal, M. S.; Peralam Yegneswaran, P.; Singhal, H. R.; Mani, N. K., Inkjet printing of paraffin on paper allows low-cost point-of-care diagnostics for pathogenic fungi. *Cellulose* 2020.
44. Sameenoi, Y.; Nongkai, P. N.; Nouanthavong, S.; Henry, C. S.; Nacapricha, D., One-step polymer screen-printing for microfluidic paper-based analytical device (μ PAD) fabrication. *Analyst* 2014, 139 (24), 6580-6588.
45. Kishimoto, T.; Matsuoka, T.; Imamura, S.; Mizuno, K., A novel colorimetric assay for the determination of lysophosphatidic acid in plasma using an enzymatic cycling method. *Clinica Chimica Acta* 2003, 333 (1), 59-67.
46. Park, H.-R.; Ahn, H.-J.; Kim, S.-H.; Lee, C.-H.; Byun, M.-W.; Lee, G.-W., Determination of the phytic acid levels in infant foods using different analytical methods. *Food Control* 2006, 17 (9), 727-732.
47. Murray, E.; Nesterenko, E. P.; McCaul, M.; Morrin, A.; Diamond, D.; Moore, B., A colorimetric method for use within portable test kits for nitrate determination in various water matrices. *Analytical Methods* 2017, 9 (4), 680-687.
48. Amourizi, F.; Dashtian, K.; Ghaedi, M., Developing a new colorimetric bioassay for iodide determination based on gold supported iridium peroxidase catalyts. *New Journal of Chemistry* 2020, 44 (14), 5588-5597.
49. Venugopalan, R.; Ideker, R., Chapter II.5.10 - Bioelectrodes. In *Biomaterials Science (Third Edition)*, Ratner, B. D.; Hoffman, A. S.; Schoen, F. J.; Lemons, J. E., Eds. Academic Press: 2013; pp 957-966.
50. Kevin Li, S.; Hao, J.; Liddell, M., Chapter 11 - Electrotransport Across Membranes in Biological Media: Electrokinetic Theories and Applications in Drug Delivery. In *Transport*

in Biological Media, Becker, S. M.; Kuznetsov, A. V., Eds. Elsevier: Boston, 2013; pp 417-454.

51. Oberacher, H.; Pitterl F Fau - Erb, R.; Erb R Fau - Plattner, S.; Plattner, S., Mass spectrometric methods for monitoring redox processes in electrochemical cells. (1098-2787 (Electronic)).

52. Irigoyen Otamendi, J. Fabrication and Characterization of Multilayered Assemblies based on Polyelectrolytes and Hybrid Systems with Carbon Nanomaterials for Applications in Nanofiltration and as Smart Surfaces. 2016.

53. Rezaei, B.; Irannejad, N., Chapter 2 - Electrochemical detection techniques in biosensor applications. In *Electrochemical Biosensors*, Ensafi, A. A., Ed. Elsevier: 2019; pp 11-43.

54. Forster, R. J.; Walsh, D. A., VOLTAMMETRY | Overview. In *Encyclopedia of Analytical Science (Second Edition)*, Worsfold, P.; Townshend, A.; Poole, C., Eds. Elsevier: Oxford, 2005; pp 181-188.

55. Ruecha, N.; Rangkupan, R.; Rodthongkum, N.; Chailapakul, O., Novel paper-based cholesterol biosensor using graphene/polyvinylpyrrolidone/polyaniline nanocomposite. *Biosensors and Bioelectronics* 2014, 52, 13-19.

56. Hui, C.-y.; Kan, C.-w.; Mak, C.-l.; Chau, K.-h., Flexible Energy Storage System—An Introductory Review of Textile-Based Flexible Supercapacitors. *Processes* 2019, 7 (12).

57. Simões, F. R.; Xavier, M. G., 6 - Electrochemical Sensors. In *Nanoscience and its Applications*, Da Róz, A. L.; Ferreira, M.; de Lima Leite, F.; Oliveira, O. N., Eds. William Andrew Publishing: 2017; pp 155-178.

58. Differential Pluse Voltammetry. <https://www.ukessays.com/essays/chemistry/differential-pulse-voltammetry-8008.php>.

59. Scott, K., 2 - Electrochemical principles and characterization of bioelectrochemical systems. In *Microbial Electrochemical and Fuel Cells*, Scott, K.; Yu, E. H., Eds. Woodhead Publishing: Boston, 2016; pp 29-66.

60. Mirceski, V.; Skrzypek, S.; Stojanov, L., Square-wave voltammetry. *ChemTexts* 2018, 4 (4), 17.

61. Adeloju, S. B., AMPEROMETRY. In *Encyclopedia of Analytical Science (Second Edition)*, Worsfold, P.; Townshend, A.; Poole, C., Eds. Elsevier: Oxford, 2005; pp 70-79.

62. Schöning, M. J.; Krause, R.; Block, K.; Musahmeh, M.; Mulchandani, A.; Wang, J., A dual amperometric/potentiometric FIA-based biosensor for the distinctive detection of organophosphorus pesticides. *Sensors and Actuators B: Chemical* 2003, 95 (1), 291-296.
63. Zavolskova, M. D.; Nikitina, V. N.; Maksimova, E. D.; Karyakina, E. E.; Karyakin, A. A., Constant Potential Amperometric Flow-Injection Analysis of Ions and Neutral Molecules Transduced by Electroactive (Conductive) Polymers. *Analytical Chemistry* 2019, 91 (12), 7495-7499.
64. Islam, M. A.; Koreshkova, A. N.; Gupta, V.; Lewis, T.; Macka, M.; Paull, B.; Mahbub, P., Fast pulsed amperometric waveform for miniaturised flow-through electrochemical detection: Application in monitoring graphene oxide reduction. *Electrochimica Acta* 2019, 328, 135087.
65. Randviir, E. P.; Banks, C. E., Electrochemical impedance spectroscopy: an overview of bioanalytical applications. *Analytical Methods* 2013, 5 (5), 1098-1115.
66. Faulkner, A. J. B. a. L. R., *Electrochemical methods : Fundamentals and Application*. JOHN WILEY & SONS, INC: New York.
67. Guy, O. J.; Walker, K.-A. D., Chapter 4 - Graphene Functionalization for Biosensor Applications. In *Silicon Carbide Biotechnology (Second Edition)*, Sadow, S. E., Ed. Elsevier: 2016; pp 85-141.
68. He, Y.; Lin, H.; Guo, Z.; Zhang, W.; Li, H.; Huang, W., Recent developments and advances in boron-doped diamond electrodes for electrochemical oxidation of organic pollutants. *Separation and Purification Technology* 2019, 212, 802-821.
69. Macpherson, J. V., A practical guide to using boron doped diamond in electrochemical research. *Physical Chemistry Chemical Physics* 2015, 17 (5), 2935-2949.
70. Vihagthakur, Boron Doped Diamond Electrode Market Insights. Setember 13, 2019 ed.
71. Cinti, S.; Arduini, F., Graphene-based screen-printed electrochemical (bio)sensors and their applications: Efforts and criticisms. *Biosensors and Bioelectronics* 2017, 89, 107-122.
72. Le, L. T.; Ervin, M. H.; Qiu, H.; Fuchs, B. E.; Lee, W. Y., Graphene supercapacitor electrodes fabricated by inkjet printing and thermal reduction of graphene oxide. *Electrochemistry Communications* 2011, 13 (4), 355-358.

73. Alonso-Lomillo, M. A.; Domínguez-Renedo, O.; Arcos-Martínez, M. J., Screen-printed biosensors in microbiology; a review. *Talanta* 2010, 82 (5), 1629-1636.
74. Ping, J.; Wu, J.; Wang, Y.; Ying, Y., Simultaneous determination of ascorbic acid, dopamine and uric acid using high-performance screen-printed graphene electrode. *Biosensors and Bioelectronics* 2012, 34 (1), 70-76.
75. Tan, X.; Hu, Q.; Wu, J.; Li, X.; Li, P.; Yu, H.; Li, X.; Lei, F., Electrochemical sensor based on molecularly imprinted polymer reduced graphene oxide and gold nanoparticles modified electrode for detection of carbofuran. *Sensors and Actuators B: Chemical* 2015, 220, 216-221.
76. Hu, G.; Ma, Y.; Guo, Y.; Shao, S., Electrocatalytic oxidation and simultaneous determination of uric acid and ascorbic acid on the gold nanoparticles-modified glassy carbon electrode. *Electrochimica Acta* 2008, 53 (22), 6610-6615.
77. Ma, Z.; Wang, Q.; Gao, N.; Li, H., Electrochemical detection of clenbuterol with gold-nanoparticles-modified porous boron-doped diamond electrode. *Microchemical Journal* 2020, 157, 104911.
78. Lomae, A.; Nantaphol, S.; Kondo, T.; Chailapakul, O.; Siangproh, W.; Panchompoo, J., Simultaneous determination of β -agonists by UHPLC coupled with electrochemical detection based on palladium nanoparticles modified BDD electrode. *Journal of Electroanalytical Chemistry* 2019, 840, 439-448.
79. Kuroki, H.; Tamaki, T.; Matsumoto, M.; Arai, M.; Kubobuchi, K.; Imai, H.; Yamaguchi, T., Platinum-Iron-Nickel Trimetallic Catalyst with Superlattice Structure for Enhanced Oxygen Reduction Activity and Durability. *Industrial & Engineering Chemistry Research* 2016, 55 (44), 11458-11466.
80. Eid, K.; Wang, H.; Malgras, V.; Alothman, Z. A.; Yamauchi, Y.; Wang, L., Trimetallic PtPdRu Dendritic Nanocages with Three-Dimensional Electrocatalytic Surfaces. *The Journal of Physical Chemistry C* 2015, 119 (34), 19947-19953.
81. Wang, P.; Zhang, Y.; Shi, R.; Wang, Z., Shape-Controlled Synthesis of Trimetallic PtPdCu Nanocrystals and Their Electrocatalytic Properties. *ACS Applied Energy Materials* 2019, 2 (4), 2515-2523.

82. Chen, Z.; Rao, D.; Zhang, J.; Liu, Y.; Wang, Y.; Liu, C.; Hu, W.; Deng, Y., Highly Active and CO-Tolerant Trimetallic NiPtPd Hollow Nanocrystals as Electrocatalysts for Methanol Electro-oxidation Reaction. *ACS Applied Energy Materials* 2019, 2 (7), 4763-4773.
83. Punrat, E.; Maksuk, C.; Chuanuwatanakul, S.; Wonsawat, W.; Chailapakul, O., Polyaniline/graphene quantum dot-modified screen-printed carbon electrode for the rapid determination of Cr(VI) using stopped-flow analysis coupled with voltammetric technique. *Talanta* 2016, 150, 198-205.
84. Promphet, N.; Rattanarat, P.; Rangkupan, R.; Chailapakul, O.; Rodthongkum, N., An electrochemical sensor based on graphene/polyaniline/polystyrene nanoporous fibers modified electrode for simultaneous determination of lead and cadmium. *Sensors and Actuators B: Chemical* 2015, 207, 526-534.
85. Dechtrirat, D.; Sookcharoenpinyo, B.; Prajongtat, P.; Sriprachuabwong, C.; Sanguankiat, A.; Tuantranont, A.; Hannongbua, S., An electrochemical MIP sensor for selective detection of salbutamol based on a graphene/PEDOT:PSS modified screen printed carbon electrode. *RSC Advances* 2018, 8 (1), 206-212.
86. Dhand, C.; Das, M.; Datta, M.; Malhotra, B. D., Recent advances in polyaniline based biosensors. *Biosensors and Bioelectronics* 2011, 26 (6), 2811-2821.
87. Liu, F.-J., Electrodeposition of manganese dioxide in three-dimensional poly(3,4-ethylenedioxythiophene)-poly(styrene sulfonic acid)-polyaniline for supercapacitor. *Journal of Power Sources* 2008, 182 (1), 383-388.
88. Chen, L.; Su, Z.; He, X.; Liu, Y.; Qin, C.; Zhou, Y.; Li, Z.; Wang, L.; Xie, Q.; Yao, S., Square wave anodic stripping voltammetric determination of Cd and Pb ions at a Bi/Nafion/thiolated polyaniline/glassy carbon electrode. *Electrochemistry Communications* 2012, 15 (1), 34-37.
89. Mujahid, A.; Dickert, F. L., 5 - Molecularly Imprinted Polymers: Principle, Design, and Enzyme-Like Catalysis. In *Molecularly Imprinted Catalysts*, Li, S.; Cao, S.; Piletsky, S. A.; Turner, A. P. F., Eds. Elsevier: Amsterdam, 2016; pp 79-101.
90. Lu, X.; Zhou, G.; Zhang, J.; Xie, W.; Yang, Y.; Zeng, Y.; Zhang, Z.; Wang, H.; Li, L., Highly Sensitive Determination of 2,4,6-Trichlorophenol by Using a Novel SiO₂@MIPIL Fluorescence Sensor with a Double Recognition Functional Monomer. *ACS Sensors* 2020, 5 (5), 1445-1454.

91. Chen, L.; Wang, X.; Lu, W.; Wu, X.; Li, J., Molecular imprinting: perspectives and applications. *Chemical Society Reviews* 2016, 45 (8), 2137-2211.
92. Napporn, T. W.; Holade, Y.; Kokoh, B.; Mitsushima, S.; Mayer, K.; Eichberger, B.; Hacker, V., Chapter 9 - Electrochemical Measurement Methods and Characterization on the Cell Level. In *Fuel Cells and Hydrogen*, Hacker, V.; Mitsushima, S., Eds. Elsevier: 2018; pp 175-214.
93. Honeychurch, K. C., 13 - Printed thick-film biosensors. In *Printed Films*, Prudenziati, M.; Hormadaly, J., Eds. Woodhead Publishing: 2012; pp 366-409.
94. Brown, A. W. a. P. R., *High Performance Liquid Chromatography & Capillary Electrophoresis: Principles and Practices*. W.B. Saunders Company: USA.
95. van Deemter, J. J.; Zuiderweg, F. J.; Klinkenberg, A., Longitudinal diffusion and resistance to mass transfer as causes of nonideality in chromatography. *Chemical Engineering Science* 1995, 50 (24), 3869-3882.
96. Bélanger, J. M. R.; Jocelyn Paré, J. R.; Sigouin, M., Chapter 2 High performance liquid chromatography (HPLC): Principles and applications. In *Techniques and Instrumentation in Analytical Chemistry*, Paré, J. R. J.; Bélanger, J. M. R., Eds. Elsevier: 1997; Vol. 18, pp 37-59.
97. Leandro, C. C.; Hancock, P.; Fussell, R. J.; Keely, B. J., Comparison of ultra-performance liquid chromatography and high-performance liquid chromatography for the determination of priority pesticides in baby foods by tandem quadrupole mass spectrometry. *Journal of Chromatography A* 2006, 1103 (1), 94-101.
98. Chen, D.; Yang, M.; Zheng, N.; Xie, N.; Liu, D.; Xie, C.; Yao, D., A novel aptasensor for electrochemical detection of ractopamine, clenbuterol, salbutamol, phenylethanolamine and procaterol. *Biosensors and Bioelectronics* 2016, 80 (Supplement C), 525-531.
99. Guo, X. C.; Wang, H. H.; Chen, X. J.; Xia, Z. Y.; Kang, W. Y.; Zhou, W. H., One step electrodeposition of graphene-au nanocomposites for highly sensitive electrochemical detection of salbutamol. *International Journal of Electrochemical Science* 2017, 12 (2), 861-875.
100. Blanca, J.; Muñoz, P.; Morgado, M.; Méndez, N.; Aranda, A.; Reuvers, T.; Hooghuis, H., Determination of clenbuterol, ractopamine and zilpaterol in liver and urine

by liquid chromatography tandem mass spectrometry. *Analytica Chimica Acta* 2005, 529 (1), 199-205.

101. Bourdillon, P. D.; Dawson, J. R.; Foale, R. A.; Timmis, A. D.; Poole-Wilson, P. A.; Sutton, G. C., Salbutamol in treatment of heart failure. *British Heart Journal* 1980, 43 (2), 206-210.

102. Ventura, R.; Ramírez, R.; Monfort, N.; Segura, J., Ultrapformance liquid chromatography tandem mass spectrometric method for direct quantification of salbutamol in urine samples in doping control. *Journal of Pharmaceutical and Biomedical Analysis* 2009, 50 (5), 886-890.

103. Karuwan, C.; Wisitsoraat, A.; Maturos, T.; Phokharatkul, D.; Sappat, A.; Jaruwongrunsee, K.; Lomas, T.; Tuantranont, A., Flow injection based microfluidic device with carbon nanotube electrode for rapid salbutamol detection. *Talanta* 2009, 79 (4), 995-1000.

104. Huclová, J.; Šatinský, D.; Sklenářová, H.; Karlíček, R., Determination of salbutamol using on-line solid-phase extraction and sequential injection analysis. Comparison of chemiluminescence and fluorescence detection. *Analytical and Bioanalytical Chemistry* 2003, 376 (4), 448-454.

105. Li, M.; Zhang, Y.; Xue, Y.; Hong, X.; Cui, Y.; Liu, Z.; Du, D., Simultaneous determination of β_2 -agonists clenbuterol and salbutamol in water and swine feed samples by dual-labeled time-resolved fluorimmunoassay. *Food Control* 2017, 73 (Part B), 1039-1044.

106. Li, C.; Wu, Y.-L.; Yang, T.; Zhang, Y.; Huang-Fu, W.-G., Simultaneous determination of clenbuterol, salbutamol and ractopamine in milk by reversed-phase liquid chromatography tandem mass spectrometry with isotope dilution. *Journal of Chromatography A* 2010, 1217 (50), 7873-7877.

107. Yan, H.; Wang, R.; Han, Y.; Liu, S., Screening, recognition and quantitation of salbutamol residues in ham sausages by molecularly imprinted solid phase extraction coupled with high-performance liquid chromatography-ultraviolet detection. *Journal of Chromatography B* 2012, 900 (Supplement C), 18-23.

108. Domínguez-Romero, J. C.; García-Reyes, J. F.; Martínez-Romero, R.; Martínez-Lara, E.; Del Moral-Leal, M. L.; Molina-Díaz, A., Detection of main urinary metabolites of

- β -agonists clenbuterol, salbutamol and terbutaline by liquid chromatography high resolution mass spectrometry. *Journal of Chromatography B* 2013, 923 (Supplement C), 128-135.
109. Wang, W.; Zhang, Y.; Wang, J.; Shi, X.; Ye, J., Determination of β -agonists in pig feed, pig urine and pig liver using capillary electrophoresis with electrochemical detection. *Meat Science* 2010, 85 (2), 302-305.
110. Chen, Q.; Fan, L.-Y.; Zhang, W.; Cao, C.-X., Separation and determination of abused drugs clenbuterol and salbutamol from complex extractants in swine feed by capillary zone electrophoresis with simple pretreatment. *Talanta* 2008, 76 (2), 282-287.
111. Sheu, S.-Y.; Lei, Y.-C.; Tai, Y.-T.; Chang, T.-H.; Kuo, T.-F., Screening of salbutamol residues in swine meat and animal feed by an enzyme immunoassay in Taiwan. *Analytica Chimica Acta* 2009, 654 (2), 148-153.
112. Wang, M. Y.; Zhu, W.; Ma, L.; Ma, J. J.; Zhang, D. E.; Tong, Z. W.; Chen, J., Enhanced simultaneous detection of ractopamine and salbutamol – Via electrochemical-facial deposition of MnO₂ nanoflowers onto 3D RGO/Ni foam templates. *Biosensors and Bioelectronics* 2016, 78 (Supplement C), 259-266.
113. Lin, X.; Ni, Y.; Kokot, S., A novel electrochemical sensor for the analysis of β -agonists: The poly(acid chrome blue K)/graphene oxide-nafion/glassy carbon electrode. *Journal of Hazardous Materials* 2013, 260 (Supplement C), 508-517.
114. He, P.; Shen, L.; Liu, R.; Luo, Z.; Li, Z., Direct Detection of β -Agonists by Use of Gold Nanoparticle-Based Colorimetric Assays. *Analytical Chemistry* 2011, 83 (18), 6988-6995.
115. Zhou, Y.; Wang, P.; Su, X.; Zhao, H.; He, Y., Colorimetric detection of ractopamine and salbutamol using gold nanoparticles functionalized with melamine as a probe. *Talanta* 2013, 112 (Supplement C), 20-25.
116. Xiang, X.; Zhang, Z.; Shi, J. B.; Huang, F. H., Paper-based analytical device with colorimetric assay application to the determination of phenolic acids and recognition of Fe³⁺. *Rsc Advances* 2015, 5 (4), 2615-2619.
117. Hossain, S. M. Z.; Brennan, J. D., β -Galactosidase-Based Colorimetric Paper Sensor for Determination of Heavy Metals. *Analytical Chemistry* 2011, 83 (22), 8772-8778.

118. Liu, S.; Su, W.; Ding, X., A Review on Microfluidic Paper-Based Analytical Devices for Glucose Detection. *Sensors (Basel, Switzerland)* 2016, 16 (12), 2086.
119. Martinez, A. W.; Phillips, S. T.; Butte, M. J.; Whitesides, G. M., Patterned Paper as a Platform for Inexpensive, Low Volume, Portable Bioassays. *Angewandte Chemie (International ed. in English)* 2007, 46 (8), 1318-1320.
120. Martinez, A. W.; Phillips, S. T.; Whitesides, G. M.; Carrilho, E., Diagnostics for the Developing World: Microfluidic Paper-Based Analytical Devices. *Analytical Chemistry* 2010, 82 (1), 3-10.
121. Ruecha, N.; Rodthongkum, N.; Cate, D. M.; Volckens, J.; Chailapakul, O.; Henry, C. S., Sensitive electrochemical sensor using a graphene–polyaniline nanocomposite for simultaneous detection of Zn(II), Cd(II), and Pb(II). *Analytica Chimica Acta* 2015, 874 (Supplement C), 40-48.
122. Lu, Y.; Shi, W. W.; Jiang, L.; Qin, J. H.; Lin, B. C., Rapid prototyping of paper-based microfluidics with wax for low-cost, portable bioassay. *Electrophoresis* 2009, 30 (9), 1497-1500.
123. Rattanarat, P.; Dungchai, W.; Cate, D.; Volckens, J.; Chailapakul, O.; Henry, C. S., Multilayer Paper-Based Device for Colorimetric and Electrochemical Quantification of Metals. *Analytical Chemistry* 2014, 86 (7), 3555-3562.
124. Sirichai, S.; Khanatharana, P., Rapid analysis of clenbuterol, salbutamol, procaterol, and fenoterol in pharmaceuticals and human urine by capillary electrophoresis. *Talanta* 2008, 76 (5), 1194-1198.
125. Dol, I.; Knochen, M., Flow-injection spectrophotometric determination of salbutamol with 4-aminoantipyrine. *Talanta* 2004, 64 (5), 1233-1236.
126. Skoog, D. A., *Fundamentals of analytical chemistry*. 9th Ed. ed.; Cengage - Brooks/Cole: Belmont, CA, 2012.
127. Hassan, R.; Dahy, A. R.; Ibrahim, S.; Zaafarany, I.; Fawzy, A., Oxidation of Some Macromolecules. Kinetics and Mechanism of Oxidation of Methyl Cellulose Polysaccharide by Permanganate Ion in Acid Perchlorate Solutions. *Industrial & Engineering Chemistry Research* 2012, 51 (15), 5424-5432.

128. Chen, D.; Yang, M.; Zheng, N.; Xie, N.; Liu, D.; Xie, C.; Yao, D., A novel aptasensor for electrochemical detection of ractopamine, clenbuterol, salbutamol, phenylethanolamine and procaterol. *Biosensors and Bioelectronics* 2016, 80, 525-531.
129. Cheng, J.; Su, X.-O.; Han, C.; Wang, S.; Wang, P.; Zhang, S.; Xie, J., Ultrasensitive detection of salbutamol in animal urine by immunomagnetic bead treatment coupling with surface-enhanced Raman spectroscopy. *Sensors and Actuators B: Chemical* 2018, 255, 2329-2338.
130. Philipson, L. H., β -Agonists and metabolism. *Journal of Allergy and Clinical Immunology* 2002, 110 (6, Supplement), S313-S317.
131. Hooijerink, H.; Schilt, R.; Haasnoot, W.; Courtheijn, D., Determination of clenbuterol in urine of calves by high-performance liquid chromatography with in series ultraviolet and electrochemical detection. *Journal of Pharmaceutical and Biomedical Analysis* 1991, 9 (6), 485-492.
132. Agency, W. A.-D., Prohibited list. 2018.
133. Liu, N.; Su, P.; Gao, Z.; Zhu, M.; Yang, Z.; Pan, X.; Fang, Y.; Chao, F., Simultaneous detection for three kinds of veterinary drugs: Chloramphenicol, clenbuterol and 17-beta-estradiol by high-throughput suspension array technology. *Analytica Chimica Acta* 2009, 632 (1), 128-134.
134. Ricks, C. A.; Dalrymple, R. H.; Baker, P. K.; Ingle, D. L., Use of a β -Agonist to Alter Fat and Muscle Deposition in Steers¹. *Journal of Animal Science* 1984, 59 (5), 1247-1255.
135. Li, M.; Zhang, Y.; Xue, Y.; Hong, X.; Cui, Y.; Liu, Z.; Du, D., Simultaneous determination of β_2 -agonists clenbuterol and salbutamol in water and swine feed samples by dual-labeled time-resolved fluoroimmunoassay. *Food Control* 2017, 73, 1039-1044.
136. Chan, S. H.; Lee, W.; Asmawi, M. Z.; Tan, S. C., Chiral liquid chromatography–mass spectrometry (LC–MS/MS) method development for the detection of salbutamol in urine samples. *Journal of Chromatography B* 2016, 1025, 83-91.
137. Churchwell, M. I.; Twaddle, N. C.; Meeker, L. R.; Doerge, D. R., Improving LC–MS sensitivity through increases in chromatographic performance: Comparisons of UPLC–ES/MS/MS to HPLC–ES/MS/MS. *Journal of Chromatography B* 2005, 825 (2), 134-143.

138. Lin, L. A.; Tomlinson, J. A.; Duane Satzger, R., Detection of clenbuterol in bovine retinal tissue by high-performance liquid chromatography with electrochemical detection. *Journal of Chromatography A* 1997, 762 (1), 275-280.
139. Karuwan, C.; Sriprachuabwong, C.; Wisitsoraat, A.; Phokharatkul, D.; Sritongkham, P.; Tuantranont, A., Inkjet-printed graphene-poly(3,4-ethylenedioxythiophene):poly(styrene-sulfonate) modified on screen printed carbon electrode for electrochemical sensing of salbutamol. *Sensors and Actuators B: Chemical* 2012, 161 (1), 549-555.
140. Alizadeh, T.; Fard, L. A., Synthesis of Cu²⁺-mediated nano-sized salbutamol-imprinted polymer and its use for indirect recognition of ultra-trace levels of salbutamol. *Analytica Chimica Acta* 2013, 769, 100-107.
141. Liu, Z.; Zhou, Y.; Wang, Y.; Cheng, Q.; Wu, K., Enhanced oxidation and detection of toxic ractopamine using carbon nanotube film-modified electrode. *Electrochimica Acta* 2012, 74, 139-144.
142. Shen, L.; Li, Z.; He, P., Electrochemical behavior of β_2 -agonists at graphite nanosheet modified electrodes. *Electrochemistry Communications* 2010, 12 (7), 876-881.
143. Yilmaz, N.; Özkan, S. A.; Uslu, B.; Şentürk, Z.; Biryol, İ., Determination of terbutaline based on oxidation by voltammetry¹ Presented at the Fifth International Symposium on Pharmaceutical Science, June 1997, Ankara, Turkey.¹ *Journal of Pharmaceutical and Biomedical Analysis* 1998, 17 (2), 349-355.
144. Felix, F. S.; Daniel, D.; Matos, J. R.; Lucio do Lago, C.; Angnes, L., Fast analysis of terbutaline in pharmaceuticals using multi-walled nanotubes modified electrodes from recordable compact disc. *Analytica Chimica Acta* 2016, 928, 32-38.
145. Wu, C.; Sun, D.; Li, Q.; Wu, K., Electrochemical sensor for toxic ractopamine and clenbuterol based on the enhancement effect of graphene oxide. *Sensors and Actuators B: Chemical* 2012, 168, 178-184.
146. Bo, B.; Zhu, X.; Miao, P.; Pei, D.; Jiang, B.; Lou, Y.; Shu, Y.; Li, G., An electrochemical biosensor for clenbuterol detection and pharmacokinetics investigation. *Talanta* 2013, 113, 36-40.

147. Pecková, K.; Musilová, J.; Barek, J., Boron-Doped Diamond Film Electrodes—New Tool for Voltammetric Determination of Organic Substances. *Critical Reviews in Analytical Chemistry* 2009, 39 (3), 148-172.
148. Wilson, R. E.; Stoianov, I.; O'Hare, D., Biofouling and in situ electrochemical cleaning of a boron-doped diamond free chlorine sensor. *Electrochemistry Communications* 2016, 71, 79-83.
149. Nantaphol, S.; Channon, R. B.; Kondo, T.; Siangproh, W.; Chailapakul, O.; Henry, C. S., Boron Doped Diamond Paste Electrodes for Microfluidic Paper-Based Analytical Devices. *Analytical Chemistry* 2017, 89 (7), 4100-4107.
150. Souza, G. A.; Pimentel, D. M.; Lima, A. B.; Guedes, T. J.; Arantes, L. C.; de Oliveira, A. C.; Sousa, R. M. F.; Muñoz, R. A. A.; dos Santos, W. T. P., Electrochemical sensing of NBOMes and other new psychoactive substances in blotting paper by square-wave voltammetry on a boron-doped diamond electrode. *Analytical Methods* 2018, 10 (20), 2411-2418.
151. Kiran, R.; Scorsone, E.; Mailley, P.; Bergonzo, P., Quasi-Real Time Quantification of Uric Acid in Urine Using Boron Doped Diamond Microelectrode with in Situ Cleaning. *Analytical Chemistry* 2012, 84 (23), 10207-10213.
152. Wu, W.; Bai, L.; Liu, X.; Tang, Z.; Gu, Z., Nanograss array boron-doped diamond electrode for enhanced electron transfer from *Shewanella loihica* PV-4. *Electrochemistry Communications* 2011, 13 (8), 872-874.
153. Wang, M.; Kang, M.; Guo, C.; Fang, S.; He, L.; Jia, C.; Zhang, G.; Bai, B.; Zong, W.; Zhang, Z., Electrochemical biosensor based on Cu/Cu₂O nanocrystals and reduced graphene oxide nanocomposite for sensitively detecting ractopamine. *Electrochimica Acta* 2015, 182, 668-675.
154. Zhang, Z.; Zhang, Y.; Song, R.; Wang, M.; Yan, F.; He, L.; Feng, X.; Fang, S.; Zhao, J.; Zhang, H., Manganese(II) phosphate nanoflowers as electrochemical biosensors for the high-sensitivity detection of ractopamine. *Sensors and Actuators B: Chemical* 2015, 211, 310-317.
155. Wang, H.; Zhang, Y.; Li, H.; Du, B.; Ma, H.; Wu, D.; Wei, Q., A silver-palladium alloy nanoparticle-based electrochemical biosensor for simultaneous detection of ractopamine, clenbuterol and salbutamol. *Biosensors and Bioelectronics* 2013, 49, 14-19.

156. Huang, J.; Liu, Y.; Hou, H.; You, T., Simultaneous electrochemical determination of dopamine, uric acid and ascorbic acid using palladium nanoparticle-loaded carbon nanofibers modified electrode. *Biosensors and Bioelectronics* 2008, 24 (4), 632-637.
157. Wang, X.; Wu, M.; Tang, W.; Zhu, Y.; Wang, L.; Wang, Q.; He, P.; Fang, Y., Simultaneous electrochemical determination of ascorbic acid, dopamine and uric acid using a palladium nanoparticle/graphene/chitosan modified electrode. *Journal of Electroanalytical Chemistry* 2013, 695, 10-16.
158. Thiagarajan, S.; Yang, R.-F.; Chen, S.-M., Palladium nanoparticles modified electrode for the selective detection of catecholamine neurotransmitters in presence of ascorbic acid. *Bioelectrochemistry* 2009, 75 (2), 163-169.
159. Atta, N. F.; El-Kady, M. F., Poly(3-methylthiophene)/palladium sub-micro-modified sensor electrode. Part II: Voltammetric and EIS studies, and analysis of catecholamine neurotransmitters, ascorbic acid and acetaminophen. *Talanta* 2009, 79 (3), 639-647.
160. Szunerits, S.; Boukherroub, R., Investigation of the electrocatalytic activity of boron-doped diamond electrodes modified with palladium or gold nanoparticles for oxygen reduction reaction in basic medium. *Comptes Rendus Chimie* 2008, 11 (9), 1004-1009.
161. Zhou, Y.; Wang, P.; Su, X.; Zhao, H.; He, Y., Colorimetric detection of ractopamine and salbutamol using gold nanoparticles functionalized with melamine as a probe. *Talanta* 2013, 112, 20-25.
162. DrugBank Terbutaline. <https://www.drugbank.ca/drugs/DB00871>.
163. Information, N. C. f. B. PubChem Compound Summary for CLD 2083, Salbutamol. <https://pubchem.ncbi.nlm.nih.gov/compound/2083>.
164. Information, N. C. f. B. PubChem Compound Summary for CID 56052, Ractopamine. <https://pubchem.ncbi.nlm.nih.gov/compound/56052>.
165. DrugBank Clenbuterol. <https://www.drugbank.ca/drugs/DB01407>.
166. Zhao, Y.; Zhan, L.; Tian, J.; Nie, S.; Ning, Z., Enhanced electrocatalytic oxidation of methanol on Pd/polypyrrole-graphene in alkaline medium. *Electrochimica Acta* 2011, 56 (5), 1967-1972.

167. Watanabe, M.; Motoo, S., Electrocatalysis by ad-atoms: Part I. Enhancement of the oxidation of methanol on platinum and palladium by gold ad-atoms. *Journal of Electroanalytical Chemistry and Interfacial Electrochemistry* 1975, 60 (3), 259-266.
168. Tang, H.; Chen, J.; Nie, L.; Yao, S.; Kuang, Y., Electrochemical oxidation of glutathione at well-aligned carbon nanotube array electrode. *Electrochimica Acta* 2006, 51 (15), 3046-3051.
169. Li, L.; Li, L.; Jin, Y.; Shuang, Y.; Wang, H., Preparation of a teicoplanin-bonded chiral stationary phase for simultaneous determination of clenbuterol and salbutamol enantiomers in meat by LC-MS/MS. *Microchemical Journal* 2020, 157, 104925.
170. Yakoh, A.; Chaiyo, S.; Siangproh, W.; Chailapakul, O., 3D Capillary-Driven Paper-Based Sequential Microfluidic Device for Electrochemical Sensing Applications. *ACS Sensors* 2019, 4 (5), 1211-1221.
171. Pozzoli, C.; Bertini, S.; Poli, E.; Placenza, G.; Menozzi, A., Relaxing effects of clenbuterol, ritodrine, salbutamol and fenoterol on the contractions of horse isolated bronchi induced by different stimuli. *Research in Veterinary Science* 2020, 128, 43-48.
172. agency, W. a.-d., Prohibited at all time 2020.
173. Othman, N.; Asaad, A., Spectrophotometric Determination of Salbutamol Sulphate by Coupling with Diazotized 5-Amino-2-chlorobenzotrifluoride-Application to Pharmaceutical Preparations. 2018, 25, 38-49.
174. Šatinský, D.; Karlíček, R.; Svoboda, A. n., Using on-line solid phase extraction for flow-injection spectrophotometric determination of salbutamol. *Analytica Chimica Acta* 2002, 455 (1), 103-109.
175. Lin, K.-C.; Hong, C.-P.; Chen, S.-M., Simultaneous determination for toxic ractopamine and salbutamol in pork sample using hybrid carbon nanotubes. *Sensors and Actuators B: Chemical* 2013, 177, 428-436.
176. Wei, Y.; Zhang, Q.; Shao, C.; Li, C.; Zhang, L.; Li, X., Voltammetric determination of salbutamol on a glassy carbon electrode coated with a nanomaterial thin film. *Journal of Analytical Chemistry* 2010, 65, 398-403.
177. Gao, J.; Chang, Z.; Tian, R.; Li, P.; Ahmad, F.; Jia, X.; Liang, Q.; Zhao, X., Reversible and site-specific immobilization of β_2 -adrenergic receptor by aptamer-

directed method for receptor-drug interaction analysis. *Journal of Chromatography A* 2020, 1622, 461091.

178. He, H.; Sun, T.; Liu, W.; Xu, Z.; Han, Z.; Zhao, L.; Wu, X.; Ning, B.; Bai, J., Highly sensitive detection of salbutamol by ALP-mediated plasmonic ELISA based on controlled growth of AgNPs. *Microchemical Journal* 2020, 156, 104804.

179. Koole, A.; Bosman, J.; Franke, J. P.; de Zeeuw, R. A., Multiresidue analysis of β 2-agonists in human and calf urine using multimodal solid-phase extraction and high-performance liquid chromatography with electrochemical detection. *Journal of Chromatography B: Biomedical Sciences and Applications* 1999, 726 (1), 149-156.

180. Oosterhuis, B.; Van Boxtel, C. J., Determination of salbutamol in human plasma with bimodal high-performance liquid chromatography and a rotated disc amperometric detector. *Journal of Chromatography B: Biomedical Sciences and Applications* 1982, 232 (2), 327-334.

181. Motaharian, A.; Hosseini, M. R. M.; Naseri, K., Determination of psychotropic drug chlorpromazine using screen printed carbon electrodes modified with novel MIP-MWCNTs nano-composite prepared by suspension polymerization method. *Sensors and Actuators B: Chemical* 2019, 288, 356-362.

182. Jafari, S.; Dehghani, M.; Nasirizadeh, N.; Azimzadeh, M., An azithromycin electrochemical sensor based on an aniline MIP film electropolymerized on a gold nano urchins/graphene oxide modified glassy carbon electrode. *Journal of Electroanalytical Chemistry* 2018, 829, 27-34.

183. da Silva, H.; Pacheco, J. G.; McS Magalhães, J.; Viswanathan, S.; Delerue-Matos, C., MIP-graphene-modified glassy carbon electrode for the determination of trimethoprim. *Biosensors and Bioelectronics* 2014, 52, 56-61.

184. Ma, Y.; Shen, X.-L.; Wang, H.-S.; Tao, J.; Huang, J.-Z.; Zeng, Q.; Wang, L.-S., MIPs-graphene nanoplatelets-MWCNTs modified glassy carbon electrode for the determination of cardiac troponin I. *Analytical Biochemistry* 2017, 520, 9-15.

185. Roushani, M.; Rahmati, Z.; Hoseini, S. J.; Hashemi Fath, R., Impedimetric ultrasensitive detection of chloramphenicol based on aptamer MIP using a glassy carbon electrode modified by 3-ampy-RGO and silver nanoparticle. *Colloids and Surfaces B: Biointerfaces* 2019, 183, 110451.

186. Ji, J.; Zhou, Z.; Zhao, X.; Sun, J.; Sun, X., Electrochemical sensor based on molecularly imprinted film at Au nanoparticles-carbon nanotubes modified electrode for determination of cholesterol. *Biosensors and Bioelectronics* 2015, 66, 590-595.
187. Bradbury, D. W.; Azimi, M.; Diaz, A. J.; Pan, A. A.; Falktoft, C. H.; Wu, B. M.; Kamei, D. T., Automation of Biomarker Preconcentration, Capture, and Nanozyme Signal Enhancement on Paper-Based Devices. *Analytical Chemistry* 2019, 91 (18), 12046-12054.
188. Jahanshahi-Anbuhi, S.; Pennings, K.; Leung, V.; Kannan, B.; Brennan, J. D.; Filipe, C. D. M.; Pelton, R. H., Design Rules for Fluorocarbon-Free Omniphobic Solvent Barriers in Paper-Based Devices. *ACS Applied Materials & Interfaces* 2015, 7 (45), 25434-25440.
189. Santhiago, M.; da Costa, P. G.; Pereira, M. P.; Corrêa, C. C.; de Moraes, V. B.; Bufon, C. C. B., Versatile and Robust Integrated Sensors To Locally Assess Humidity Changes in Fully Enclosed Paper-Based Devices. *ACS Applied Materials & Interfaces* 2018, 10 (41), 35631-35638.
190. Hrichi, H.; Monser, L.; Adhoum, N., A novel electrochemical sensor based on electropolymerized molecularly imprinted poly(aniline-co-anthranilic acid) for sensitive detection of amlodipine. *Journal of Electroanalytical Chemistry* 2017, 805, 133-145.
191. Liu, S.; Ma, Y.; Cui, M.; Luo, X., Enhanced electrochemical biosensing of alpha-fetoprotein based on three-dimensional macroporous conducting polymer polyaniline. *Sensors and Actuators B: Chemical* 2018, 255, 2568-2574.
192. Nasr-Esfahani, P.; Ensafi, A. A.; Rezaei, B., Fabrication of a highly sensitive and selective modified electrode for imidacloprid determination based on designed nanocomposite graphene quantum dots/ionic liquid/multiwall carbon nanotubes/polyaniline. *Sensors and Actuators B: Chemical* 2019, 296, 126682.
193. Yang, H.; Bard, A. J., The application of fast scan cyclic voltammetry. Mechanistic study of the initial stage of electropolymerization of aniline in aqueous solutions. *Journal of Electroanalytical Chemistry* 1992, 339 (1), 423-449.
194. Wei, M.; Geng, X.; Liu, Y.; Long, H.; Du, J., A novel electrochemical sensor based on electropolymerized molecularly imprinted polymer for determination of luteolin. *Journal of Electroanalytical Chemistry* 2019, 842, 184-192.
195. Zhang, J., PEM Fuel Cell Electrocatalysts and Catalyst Layers: Fundamentals and Applications. Springer Science & Business Media: London, 2008.

196. Rajkumar, M.; Li, Y.-S.; Chen, S.-M., Electrochemical detection of toxic ractopamine and salbutamol in pig meat and human urine samples by using poly taurine/zirconia nanoparticles modified electrodes. *Colloids and Surfaces B: Biointerfaces* 2013, 110, 242-247.
197. Cao, Z.; Zhao, Y.-T.; Dai, Y.-M.; Long, S.; Guo, X.-C.; Yang, R.-H., Determination of Salbutamol Sulfate Based on Chitosan Multi-Wall Carbon Nanotubes Film Modified Glassy Carbon Electrode. *Sensor Letters* 2011, 9, 1985-1989.
198. Lijun, L.; Laibo, Y.; Hao, C.; Qifeng, C.; Fengmin, W.; Tian, C.; Xiaoyong, Z.; Hongxing, K.; Jianling, W., The Determination of Salbutamol Sulfat Based on a Flow-Injection Coupling Irreversible Biamperometry at Poly(aminosulfonic acid)-Modified Glassy Carbon Electrode. *Analytical Letters* 2007, 40 (17), 3290-3308.
199. Imeri, L.; Mancina, M.; Bianchi, S.; Opp, M. R., 5-hydroxytryptophan, but not l-tryptophan, alters sleep and brain temperature in rats. *Neuroscience* 1999, 95 (2), 445-452.
200. Lin, M. T.; Tsay, H. J.; Su, W. H.; Chueh, F. Y., Changes in extracellular serotonin in rat hypothalamus affect thermoregulatory function. *American Journal of Physiology-Regulatory, Integrative and Comparative Physiology* 1998, 274 (5), R1260-R1267.
201. D. Voet, J. G. V., *Biochemistry*. Wiley, New York 1995, 2nd ed.
202. Rommelfanger, K. S.; Weinschenker, D., Norepinephrine: The redheaded stepchild of Parkinson's disease. *Biochemical Pharmacology* 2007, 74 (2), 177-190.
203. Carney, R. M.; Freedland, K. E.; Veith, R. C.; Cryer, P. E.; Skala, J. A.; Lynch, T.; Jaffe, A. S., Major depression, heart rate, and plasma norepinephrine in patients with coronary heart disease. *Biological Psychiatry* 1999, 45 (4), 458-463.
204. Naccarato, A.; Gionfriddo, E.; Sindona, G.; Tagarelli, A., Development of a simple and rapid solid phase microextraction-gas chromatography-triple quadrupole mass spectrometry method for the analysis of dopamine, serotonin and norepinephrine in human urine. *Analytica Chimica Acta* 2014, 810, 17-24.
205. González, R. R.; Fernández, R. F.; Vidal, J. L. M.; Frenich, A. G.; Pérez, M. L. G., Development and validation of an ultra-high performance liquid chromatography-tandem mass-spectrometry (UHPLC-MS/MS) method for the simultaneous determination of neurotransmitters in rat brain samples. *Journal of Neuroscience Methods* 2011, 198 (2), 187-194.

206. Ji, C.; Li, W.; Ren, X.-d.; El-Kattan, A. F.; Kozak, R.; Fountain, S.; Lepsy, C., Diethylation Labeling Combined with UPLC/MS/MS for Simultaneous Determination of a Panel of Monoamine Neurotransmitters in Rat Prefrontal Cortex Microdialysates. *Analytical Chemistry* 2008, 80 (23), 9195-9203.
207. Yoshitake, T.; Fujino, K.; Kehr, J.; Ishida, J.; Nohta, H.; Yamaguchi, M., Simultaneous determination of norepinephrine, serotonin, and 5-hydroxyindole-3-acetic acid in microdialysis samples from rat brain by microbore column liquid chromatography with fluorescence detection following derivatization with benzylamine. *Analytical Biochemistry* 2003, 312 (2), 125-133.
208. De Benedetto, G. E.; Fico, D.; Pennetta, A.; Malitesta, C.; Nicolardi, G.; Lofrumento, D. D.; De Nuccio, F.; La Pesa, V., A rapid and simple method for the determination of 3,4 - dihydroxyphenylacetic acid, norepinephrine, dopamine, and serotonin in mouse brain homogenate by HPLC with fluorimetric detection. *Journal of Pharmaceutical and Biomedical Analysis* 2014, 98, 266-270.
209. Yao, H.; Li, S.; Tang, Y.; Chen, Y.; Chen, Y.; Lin, X., Selective oxidation of serotonin and norepinephrine over eriochrome cyanine R film modified glassy carbon electrode. *Electrochimica Acta* 2009, 54, 4607-4612.
210. Mazloum-Ardakani, M.; Khoshroo, A., High sensitive sensor based on functionalized carbon nanotube/ionic liquid nanocomposite for simultaneous determination of norepinephrine and serotonin. *Journal of Electroanalytical Chemistry* 2014, 717-718, 17-23.
211. Wang, Y.; Wang, S.; Tao, L.; Min, Q.; Xiang, J.; Wang, Q.; Xie, J.; Yue, Y.; Wu, S.; Li, X.; Ding, H., A disposable electrochemical sensor for simultaneous determination of norepinephrine and serotonin in rat cerebrospinal fluid based on MWNTs-ZnO/chitosan composites modified screen-printed electrode. *Biosensors and Bioelectronics* 2015, 65.
212. Van Schoors, J.; Lens, C.; Maes, K.; Michotte, Y.; Smolders, I.; Van Eeckhaut, A., Reassessment of the antioxidative mixture for the challenging electrochemical determination of dopamine, noradrenaline and serotonin in microdialysis samples. *Journal of Chromatography B* 2015, 998-999, 63-71.

213. Yu, Y.; Guo, M.; Yuan, M.; Liu, W.; Hu, J., Nickel nanoparticle-modified electrode for ultra-sensitive electrochemical detection of insulin. *Biosensors and Bioelectronics* 2016, 77, 215-219.
214. Kim, S. K.; Kim, D.; Jeon, S., Electrochemical determination of serotonin on glassy carbon electrode modified with various graphene nanomaterials. *Sensors and Actuators B: Chemical* 2012, 174, 285-291.
215. Liu, A.-L.; Zhang, S.-B.; Chen, W.; Lin, X.-H.; Xia, X.-H., Simultaneous voltammetric determination of norepinephrine, ascorbic acid and uric acid on polycalconcarboxylic acid modified glassy carbon electrode. *Biosensors and Bioelectronics* 2008, 23 (10), 1488-1495.
216. Jackson, B. P.; Dietz, S. M.; Wightman, R. M., Fast-scan cyclic voltammetry of 5-hydroxytryptamine. *Analytical Chemistry* 1995, 67 (6), 1115-1120.
217. Swamy, B. E. K.; Venton, B. J., Carbon nanotube-modified microelectrodes for simultaneous detection of dopamine and serotonin in vivo. *Analyst* 2007, 132 (9), 876-884.
218. Amal Raj, M.; Abraham John, S., Graphene layer modified glassy carbon electrode for the determination of norepinephrine and theophylline in pharmaceutical formulations. *Analytical Methods* 2014, 6 (7), 2181-2188.
219. Yao, H.; Li, S.; Tang, Y.; Chen, Y.; Chen, Y.; Lin, X., Selective oxidation of serotonin and norepinephrine over eriochrome cyanine R film modified glassy carbon electrode. *Electrochimica Acta* 2009, 54 (20), 4607-4612.
220. Lavanya, N.; Sekar, C., Electrochemical sensor for simultaneous determination of epinephrine and norepinephrine based on cetyltrimethylammonium bromide assisted SnO₂ nanoparticles. *Journal of Electroanalytical Chemistry* 2017, 801, 503-510.
221. Yang, S.; Zhao, J.; Tricard, S.; Yu, L.; Fang, J., A sensitive and selective electrochemical sensor based on N, P-Doped molybdenum Carbide@Carbon/Prussian blue/graphite felt composite electrode for the detection of dopamine. *Analytica Chimica Acta* 2020, 1094, 80-89.
222. Diab, N.; Morales, D. M.; Andronescu, C.; Masoud, M.; Schuhmann, W., A sensitive and selective graphene/cobalt tetrasulfonated phthalocyanine sensor for detection of dopamine. *Sensors and Actuators B: Chemical* 2019, 285, 17-23.

223. Yuan, Y.; Xia, J.; Zhang, F.; Wang, Z.; Liu, Q., Nafion/polyaniline/Zeolitic Imidazolate Framework-8 nanocomposite sensor for the electrochemical determination of dopamine. *Journal of Electroanalytical Chemistry* 2018, 824, 147-152.
224. Mena, M. L.; Yáñez-Sedeño, P.; Pingarrón, J. M., A comparison of different strategies for the construction of amperometric enzyme biosensors using gold nanoparticle-modified electrodes. *Analytical Biochemistry* 2005, 336 (1), 20-27.
225. Dai, X.; Nekrassova, O.; Hyde, M. E.; Compton, R. G., Anodic Stripping Voltammetry of Arsenic(III) Using Gold Nanoparticle-Modified Electrodes. *Analytical Chemistry* 2004, 76 (19), 5924-5929.
226. Liu, S.-f.; Li, X.-h.; Li, Y.-c.; Li, Y.-f.; Li, J.-r.; Jiang, L., The influence of gold nanoparticle modified electrode on the structure of mercaptopropionic acid self-assembly monolayer. *Electrochimica Acta* 2005, 51 (3), 427-431.
227. Huang, Y.; Wen, Q.; Jiang, J.-H.; Shen, G.-L.; Yu, R.-Q., A novel electrochemical immunosensor based on hydrogen evolution inhibition by enzymatic copper deposition on platinum nanoparticle-modified electrode. *Biosensors and Bioelectronics* 2008, 24 (4), 600-605.
228. Dai, X.; Compton, R. G., Detection of As(III) via oxidation to As(V) using platinum nanoparticle modified glassy carbon electrodes: arsenic detection without interference from copper. *Analyst* 2006, 131 (4), 516-521.
229. Yang, J.; Zhang, R.; Xu, Y.; He, P.; Fang, Y., Direct electrochemistry study of glucose oxidase on Pt nanoparticle-modified aligned carbon nanotubes electrode by the assistance of chitosan-CdS and its biosensing for glucose. *Electrochemistry Communications* 2008, 10 (12), 1889-1892.
230. Chakraborty, S.; Retna Raj, C., Pt nanoparticle-based highly sensitive platform for the enzyme-free amperometric sensing of H₂O₂. *Biosensors and Bioelectronics* 2009, 24 (11), 3264-3268.
231. Manoj, D.; Saravanan, R.; Santhanalakshmi, J.; Agarwal, S.; Gupta, V. K.; Boukherroub, R., Towards green synthesis of monodisperse Cu nanoparticles: An efficient and high sensitive electrochemical nitrite sensor. *Sensors and Actuators B: Chemical* 2018, 266, 873-882.

232. Luo, J.; Jiang, S.; Zhang, H.; Jiang, J.; Liu, X., A novel non-enzymatic glucose sensor based on Cu nanoparticle modified graphene sheets electrode. *Analytica Chimica Acta* 2012, 709, 47-53.
233. Ulubay, Ş.; Dursun, Z., Cu nanoparticles incorporated polypyrrole modified GCE for sensitive simultaneous determination of dopamine and uric acid. *Talanta* 2010, 80 (3), 1461-1466.
234. Jiang, L.-C.; Zhang, W.-D., A highly sensitive nonenzymatic glucose sensor based on CuO nanoparticles-modified carbon nanotube electrode. *Biosensors and Bioelectronics* 2010, 25 (6), 1402-1407.
235. Shi, Q.; Diao, G.; Mu, S., The electrocatalytic oxidation of glucose on the bimetallic Au-Ag particles-modified reduced graphene oxide electrodes in alkaline solutions. *Electrochimica Acta* 2014, 133, 335-346.
236. Tsai, T.-H.; Thiagarajan, S.; Chen, S.-M., Green synthesized Au–Ag bimetallic nanoparticles modified electrodes for the amperometric detection of hydrogen peroxide. *Journal of Applied Electrochemistry* 2010, 40 (12), 2071-2076.
237. Wang, N.; Han, Y.; Xu, Y.; Gao, C.; Cao, X., Detection of H₂O₂ at the Nanomolar Level by Electrode Modified with Ultrathin AuCu Nanowires. *Analytical Chemistry* 2015, 87 (1), 457-463.
238. Yang, M.; Guo, Z.; Li, L.-N.; Huang, Y.-Y.; Liu, J.-H.; Zhou, Q.; Chen, X.; Huang, X.-J., Electrochemical determination of arsenic(III) with ultra-high anti-interference performance using Au–Cu bimetallic nanoparticles. *Sensors and Actuators B: Chemical* 2016, 231, 70-78.
239. Andrews, E.; Fang, Y.; Flake, J., Electrochemical reduction of CO₂ at CuAu nanoparticles: size and alloy effects. *Journal of Applied Electrochemistry* 2018, 48 (4), 435-441.
240. Zhang, K.; Wang, H.; Wang, C.; Yang, B.; Ren, F.; Yang, P.; Du, Y., Facile fabrication of PtCuAu nanoparticles modified reduced graphene oxide with high electrocatalytic activity toward formic acid oxidation. *Colloids and Surfaces A: Physicochemical and Engineering Aspects* 2015, 467, 211-215.
241. Ge, S.; Zhang, Y.; Zhang, L.; Liang, L.; Liu, H.; Yan, M.; Huang, J.; Yu, J., Ultrasensitive electrochemical cancer cells sensor based on trimetallic dendritic Au@PtPd

nanoparticles for signal amplification on lab-on-paper device. *Sensors and Actuators B: Chemical* 2015, 220, 665-672.

242. Manivannan, S.; Seo, Y.; Kim, K., Electrodeposition of AuPt Alloy Nanostructures on a Biotemplate with Hierarchically Assembled M13 Virus Film Used for Methanol Oxidation Reaction. *J. Electrochem. Sci. Technol* 2019, 10 (3), 284-293.

243. Huan, T. N.; Shinde, D. V.; Kim, S.; Han, S.-H.; Artero, V.; Chung, H., Forest of Pt–Au–Ag tri-metallic nanodendrites as an efficient electrocatalyst for methanol oxidation reaction. *RSC Advances* 2015, 5 (9), 6940-6944.

244. Danaee, I.; Jafarian, M.; Forouzandeh, F.; Gopal, F.; Mahjani, M. G., Electrocatalytic oxidation of methanol on Ni and NiCu alloy modified glassy carbon electrode. *International Journal of Hydrogen Energy* 2008, 33 (16), 4367-4376.

245. Jafarian, M.; Forouzandeh, F.; Danaee, I.; Gopal, F.; Mahjani, M. G., Electrocatalytic oxidation of glucose on Ni and NiCu alloy modified glassy carbon electrode. *Journal of Solid State Electrochemistry* 2009, 13 (8), 1171-1179.

246. He, W.; Ding, Y.; Ji, L.; Zhang, X.; Yang, F., A high performance sensor based on bimetallic NiCu nanoparticles for the simultaneous determination of five species of biomolecules. *Sensors & Actuators: B. Chemical* 2017, 241, 956.

247. Danaee, I.; Jafarian, M.; Mirzapoor, A.; Gopal, F.; Mahjani, M. G., Electrooxidation of methanol on NiMn alloy modified graphite electrode. *Electrochimica Acta* 2010, 55 (6), 2093-2100.

248. Asgari, M.; Maragheh, M. G.; Davarkhah, R.; Lohrasbi, E.; Golikand, A. N., Electrocatalytic oxidation of methanol on the nickel–cobalt modified glassy carbon electrode in alkaline medium. *Electrochimica Acta* 2012, 59, 284-289.

249. Fleischmann, M.; Korinek, K.; Pletcher, D., The kinetics and mechanism of the oxidation of amines and alcohols at oxide-covered nickel, silver, copper, and cobalt electrodes. *Journal of the Chemical Society, Perkin Transactions 2* 1972, (10), 1396-1403.

250. Revenga-Parra, M.; García, T.; Lorenzo, E.; Pariente, F., Electrocatalytic oxidation of methanol and other short chain aliphatic alcohols on glassy carbon electrodes modified with conductive films derived from NiII-(N,N'-bis(2,5-dihydroxybenzylidene)-1,2-diaminobenzene). *Sensors and Actuators B: Chemical* 2008, 130 (2), 730-738.

251. Majdi, S.; Jabbari, A.; Heli, H.; Moosavi-Movahedi, A. A., Electrocatalytic oxidation of some amino acids on a nickel–curcumin complex modified glassy carbon electrode. *Electrochimica Acta* 2007, 52 (14), 4622-4629.
252. Danaee, I.; Jafarian, M.; Forouzandeh, F.; Gobal, F.; Mahjani, M. G., Impedance spectroscopy analysis of glucose electro-oxidation on Ni-modified glassy carbon electrode. *Electrochimica Acta* 2008, 53 (22), 6602-6609.
253. Danaee, I.; Jafarian, M.; Forouzandeh, F.; Gobal, F.; Mahjani, M. G., Electrocatalytic oxidation of methanol on Ni and NiCu alloy modified glassy carbon electrode. *International Journal of Hydrogen Energy* 2008, 33, 4376.
254. Li, S.; Yue, S.; Yu, C.; Chen, Y.; Yuan, D.; Yu, Q., A label-free immunosensor for the detection of nuclear matrix protein-2 2 based on a chrysanthemum-like Co-MOFs/CuAu NWs nanocomposite. *Analyst* 2019, 144 (2), 649-655.
255. Huang, S.-S.; Liu, L.; Mei, L.-P.; Zhou, J.-Y.; Guo, F.-Y.; Wang, A.-J.; Feng, J.-J., Electrochemical sensor for nitrite using a glassy carbon electrode modified with gold-copper nanochain networks. *Analytical Sciences Based on Micro- and Nanomaterials* 2016, 183, 797.
256. He, P.; Wang, X.; Liu, Y.; Liu, X.; Yi, L., Comparison of electrocatalytic activity of carbon-supported Au–M (M = Fe, Co, Ni, Cu and Zn) bimetallic nanoparticles for direct borohydride fuel cells. *International Journal of Hydrogen Energy* 2012, 37 (16), 11984-11993.
257. Park, S.-M.; Yoo, J.-S., Peer Reviewed: Electrochemical Impedance Spectroscopy for Better Electrochemical Measurements. *Analytical Chemistry* 2003, 75 (21), 455 A-461 A.
258. Hutton, L. A.; Vidotti, M.; Patel, A. N.; Newton, M. E.; Unwin, P. R.; Macpherson, J. V., Electrodeposition of Nickel Hydroxide Nanoparticles on Boron-Doped Diamond Electrodes for Oxidative Electrocatalysis. *The Journal of Physical Chemistry C* 2011, 115 (5), 1649-1658.
259. Salimi, A.; Noorbakhash, A.; Sharifi, E.; Semnani, A., Highly sensitive sensor for picomolar detection of insulin at physiological pH, using GC electrode modified with guanine and electrodeposited nickel oxide nanoparticles. *Biosensors and Bioelectronics* 2008, 24 (4), 792-798.

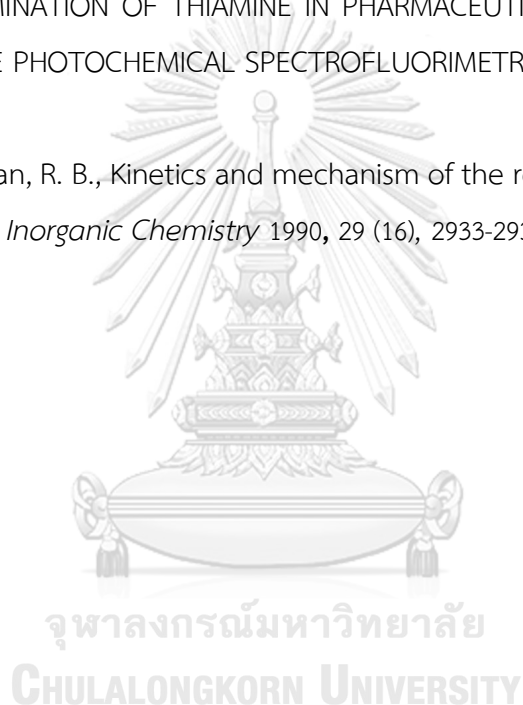
260. Yun, Y. S.; Park, D. S.; Yi, J., Effect of nickel on catalytic behaviour of bimetallic Cu–Ni catalyst supported on mesoporous alumina for the hydrogenolysis of glycerol to 1,2-propanediol. *Catalysis Science & Technology* 2014, 4 (9), 3191-3202.
261. Darabdhara, G.; Das, M. R.; Amin, M. A.; Mersal, G. A. M.; Mostafa, N. Y.; Abd El-Rehim, S. S.; Szunerits, S.; Boukherroub, R., AuNi alloy nanoparticles supported on reduced graphene oxide as highly efficient electrocatalysts for hydrogen evolution and oxygen reduction reactions. *International Journal of Hydrogen Energy* 2018, 43 (3), 1424-1438.
262. Nantaphol, S.; Kava, A. A.; Channon, R. B.; Kondo, T.; Siangproh, W.; Chailapakul, O.; Henry, C. S., Janus electrochemistry: Simultaneous electrochemical detection at multiple working conditions in a paper-based analytical device. *Analytica Chimica Acta* 2019, 1056, 88-95.
263. Dauphin-Ducharme, P.; Arroyo-Currás, N.; Kurnik, M.; Ortega, G.; Li, H.; Plaxco, K. W., Simulation-Based Approach to Determining Electron Transfer Rates Using Square-Wave Voltammetry. *Langmuir* 2017, 33 (18), 4407-4413.
264. Crowley, K.; Cassidy, J., Trace Analysis of Lead at a Nafion-Modified Electrode Using Square-Wave Anodic Stripping Voltammetry. *Electroanalysis* 2002, 14 (15-16), 1077-1082.
265. Wang, Z.-h.; Liang, Q.-l.; Wang, Y.-m.; Luo, G.-a., Carbon nanotube-intercalated graphite electrodes for simultaneous determination of dopamine and serotonin in the presence of ascorbic acid. *Journal of Electroanalytical Chemistry* 2003, 540, 129-134.
266. Jin, G.-P.; Lin, X.-Q.; Gong, J.-m., Novel choline and acetylcholine modified glassy carbon electrodes for simultaneous determination of dopamine, serotonin and ascorbic acid. *Journal of Electroanalytical Chemistry* 2004, 569 (1), 135-142.
267. Huang, S.-H.; Liao, H.-H.; Chen, D.-H., Simultaneous determination of norepinephrine, uric acid, and ascorbic acid at a screen printed carbon electrode modified with polyacrylic acid-coated multi-wall carbon nanotubes. *Biosensors and Bioelectronics* 2010, 25 (10), 2351-2355.
268. Mazloum-Ardakani, M.; Beitollahi, H.; Amini, M. K.; Mirkhalaf, F.; Mirjalili, B.-F., A highly sensitive nanostructure-based electrochemical sensor for electrocatalytic

determination of norepinephrine in the presence of acetaminophen and tryptophan. *Biosensors and Bioelectronics* 2011, 26 (5), 2102-2106.

269. Wang, Y.; Wang, S.; Tao, L.; Min, Q.; Xiang, J.; Wang, Q.; Xie, J.; Yue, Y.; Wu, S.; Li, X.; Ding, H., A disposable electrochemical sensor for simultaneous determination of norepinephrine and serotonin in rat cerebrospinal fluid based on MWNTs-ZnO/chitosan composites modified screen-printed electrode. *Biosensors and Bioelectronics* 2015, 65, 31-38.

270. Zhu, H.; He, Q.; Fang, Q.; Chen, H., ELIMINATION OF ASCORBIC ACID INTERFERENCE WITH THE DETERMINATION OF THIAMINE IN PHARMACEUTICAL PREPARATION BY FLOW INJECTION ON-LINE PHOTOCHEMICAL SPECTROFLUORIMETRY. *Analytical Letters* 2002, 35 (4), 707-720.

271. Xu, J.; Jordan, R. B., Kinetics and mechanism of the reaction of aqueous copper(II) with ascorbic acid. *Inorganic Chemistry* 1990, 29 (16), 2933-2936.





จุฬาลงกรณ์มหาวิทยาลัย
CHULALONGKORN UNIVERSITY

VITA

NAME	Atchara Lomae
DATE OF BIRTH	2 July 1991
PLACE OF BIRTH	Narathiwat
INSTITUTIONS ATTENDED	Chulalongkorn University
HOME ADDRESS	41/1, Muno Subdistrict, Sungai Kolok District, Narathiwat, THAILAND 96120
PUBLICATION	<p>1. Atchara Lomae, Siriwan Nanyaphol, Takeshi Kondo, Orawon Chailapakul, Weena Siangproh, Janjira Panchompoo "Simultaneous determination of β-agonists by UHPLC coupled with electrochemical detection based on palladium nanoparticles modified BDD electrode" J. Electroanal. 2019, 840,439-448.</p> <p>2. Jeerakit Thangphatthananarungruang, Atchara Lomae, Orawon Chailapakul, Sudkate Chaiyo, Weena Siangproh "A Low-cost Paper-based Diamond Electrode for trace Copper Analysis at On-site Environmental Area" Electroanalysis 2020, 32, 1 –8.</p> <p>3. Atchara Lomaea , Sudkate Chaiyoo, Orawon Chailapakula , Weena Siangproh, and Janjira Panchompoo "Development of transparency-based analytical device for facile colorimetric determination of salbutamol" Analytica Chimica Acta, (Submitted), 2020.</p>
AWARD RECEIVED	Outstanding poster presentation, Flow Analysis XIV, 2018